THERMODYNAMICS LABORATORY

AEROSPACE AND MECHANICAL ENGINEERING DEPARTMENT

FACULTY OF APPLIED SCIENCES

UNIVERSITY OF LIÈGE

CONTRIBUTIONS TO THE DEVELOPMENT OF A SINGLE ROOM VENTILATION UNIT WITH HEAT RECOVERY

CONFIDENTIAL

A Thesis

Submitted to the Faculty of Applied Sciences

of the

University of Liège

By

Samuel GENDEBIEN

In Partial Fulfillment of the Requirements for the Degree

Of

Doctor of Applied Sciences

Liège, October 2014

To my family,

ABSTRACT

The present thesis contributes to the knowledge, characterization and development of single room ventilation with heat recovery (SRVHR) systems dedicated to the residential sector. Investigation focuses on both the thermal and hydraulic aspects of such units. Thus, a large part of the thesis focuses particularly on air-to-air heat exchangers dedicated to SRVHR systems.

Impacts of the operating conditions (dry, partially wet and frosting conditions) on the performance are investigated. The thesis relies on the results of experimental and modeling studies carried out on several polystyrene air-to-air heat exchangers. An experimental apparatus was built in order to characterize the thermal and hydraulic performance of air-to-air heat exchanger under various operating conditions. The first developed model includes prediction of thermal and hydraulic performances in dry conditions but also in totally and partially wet conditions. The developed model is based on a moving boundary model ("two zones" heat exchanger model) initially dedicated to cooling coil. The validation of the developed model is first realized on a cooling coil experimental data set and then on experimental results collected on an air-to-air heat exchanger. In order to characterize the behavior under frosting conditions, the moving boundary model is later improved by taking into account the frost growth (three zones heat exchanger model). This dynamic model allows to determine the heat transfer rate as well as the pressure drop evolution due to the presence of frost. Once again, validation of this developed dynamic model is carried out by means of experimental results collected on an air-to-air heat exchanger. Strategies under frosting conditions are presented and compared by using a newly defined factor of energy performance.

In the frame of the design of heat exchanger dedicated to SRVHR unit, a methodology in order to choose the best geometry parameters for the heat recovery exchanger is proposed. This methodology is based on the optimization of the overall coefficient of performance of the unit. This corresponds to the best trade-off between hydraulic and thermal performance and involves numerical and experimental investigations. An innovative method in the field of air-to-air heat exchanger was developed. It consists in determining the evolution of pressure drop as a function of flow rate on a sample composed of only two "corrugated" plates. Those plates have been quickly fabricated thanks to a rapid prototyping process. Finally, the so-called optimized heat exchanger was manufactured and tested by means of the developed test rig. A deep study of the core of the heat exchanger was realized. This investigation permits to highlight some manufacturer defects, which were verified by comparison with the predictions of a new heat exchanger simulation model.

A whole newly developed SRVHR unit (composed of fans, filters, heat exchanger) is also experimentally characterized. The main characteristic of the investigated device is its possible integration into windows ledge, which makes it particularly suitable for housing retrofitting. In the performance assessment of this unit, both thermal and hydraulic performances of the unit have been investigated. First, each single component of the unit (fans, filters, heat exchanger) has been tested separately. It has been decided to use a technique, called pressure compensated box method, in order to determine the flow rate delivered by the device. Initially, this method is dedicated to measure flow rate delivered by fan coil units. Fan performance curves have also been experimentally determined for various rotational speeds. Tests in climatic chamber have been carried out to determine the performance of the overall device. Once the whole performance of the device has been characterized, a performance map was established. The perfect knowledge of the device performance (on the contrary to centralized system which depends on the ducting characteristics) allows us to compare the system to several types of ventilation in terms of primary energy, CO_2 emissions and energy costs by means of the Heating Degree Day (HDD) method, given a specific climate.

THESIS CONTENT

Chapter I   **General introduction**
1. Introduction
2. Energy context
3. Ventilation
4. Balanced single room ventilation with heat recovery
5. Market trends
6. Objectives of the thesis
7. Organization of the manuscript
8. References

Chapter II   **Development of a ventilation heat recovery exchanger simulation model**
1. Introduction
2. Simulation of the ventilation heat recovery
3. Heat recovery exchanger test bench description
4. Experimental investigations on the studied heat recovery exchanger: testing conditions and measured performance
5. Calibration and validation of the model
6. Parametric studies
7. Comparison with discretized models
8. Conclusions
9. References

Chapter III   **Development steps of a heat exchanger dedicated to single room ventilation**
1. Introduction
2. Main characteristics of the developed heat exchanger
3. Optimization of the heat exchanger geometry
4. CFD analysis
5. Rapid prototyping testing method
6. Characterization of the final heat exchanger
7. Conclusions
8. References

Chapter IV   **Investigations of strategies under frosting conditions**
1. Introduction
2. Heat exchanger model under frosting conditions
3. Experimental investigations
4. Strategies under frosting conditions
5. Conclusions
6. References

NOMENCLATURE

A: area [m^2]

Aspect: ratio to the minimum to the maximum length

of the duct [-]

AU : global heat transfer coefficient [W/K]

CFD : Computational Fluid Dynamic

COP : Coefficient Of Performance

cp : heat capacity [J/kg-K]

$\dot{C}$:capacity flow rate [W/K]

C$_r$: heat capacity ratio [-]

D : diameter [m] or vapor diffusivity in air [m²/s]

DNu: entrance region term for the Nusselt

determination [-]

DNurat : Prantl effect term for the Nusselt

determination [-]

e : thickness [m]

f : friction factor [-]

FS: full scale

G : mass flux or mass velocity [kg/m^2-s]

h : specific enthalpy [J/kg]

h: convective heat transfer [W/m^2-K]

h$_m$: mass transfer coefficient [kg/m²-s]

h$_w$: enthalpy of vaporization of water [J/kg]

H: height of the exchanger [m]

HR: Heat Recovery

j : Colburn factor [-]

k: conductivity [W/m-K]

Greek letters

ΔP : differential pressure [Pa]

ΔT : temperature difference [K]

ε : effectiveness [-] / porosity [-]

θ: enlargement factor [-]

ρ : density[kg/m^3]

ν : kinematic viscosity [m^2/s]

τ : tortuosity [-]

Subscripts

A: corresponding to the part A of the

heat exchanger

a : air

amb : ambient

B: corresponding to the part B of the

heat exchanger

bnd: boundary

C: corresponding to the part C of the

heat exchanger

cond: condensate

d: density/densification

dp: dewpoint

dry : relative to the dry regime

ex : exhaust from the heat exchanger

fresh : fresh

f: fictitious/frost

fd: fully developed

L: length of the exchanger [m]

Le: Lewis number [-]

L_{mean} : mean distance [m]

m.v.: measured value

$\dot{M}$: Mass flow rate [kg/s]

Nu : Nusselt number [-]

n.m.: not measured

P : pressure [Pa]

prop: ratio between a part and

the total surface of the HX [-]

$\dot{Q}$: heat transfer rate [W]

R: thermal resistance [K/W]

Re : Reynolds number [-]

RH : relative humidity [%]

SEM : Semi Empirical Model

SRVHR: Single Room Ventilation with Heat Recovery

T : temperature [°C]

v : velocity [m/s]

$\dot{V}$: Volumetric flow rate [m³/h]

W: width of the exchanger [m]

w : humidity ratio [kg/kg]

x: thickness [m]

x_{plus}: dimensionless length for a hydrodynamically

developing internal flow [-]

x_{star}: dimensionless length for a thermally

developing internal flow [-]

Y: dry part of the exchanger [-]

g: growth

h : hydraulic

H: uniform heat flux

hx : heat exchanger

in: inlet

ind : indoor

lat: latent

meas: measured

new: new (result of an algorithm run)

mod: from the model

s: frost surface

sen: sensible

su : supply to the heat exchanger

surf: surface

tot: total

w : wall

wb: wet bulb

wet: relative to the wet regime

CHAPTER I: INTRODUCTION

CHAPTER I : INTRODUCTION

1 INTRODUCTION

The first part of this introduction chapter first consists of a very **short overview** on the current **energy context**.

Improving building energy efficiency (especially for existing buildings) represents an attractive solution to reduce a significant contribution to the overall energy consumption. This can be realized by improving insulation and airtightness of buildings. However, it is important to maintain adequate ventilation flow rate in order to ensure **Indoor Air Quality** (IAQ).

As a result, **efficient ventilation technologies** are developed to couple in an effective way low **energy consumption and good IAQ**.

In this context, a concept of independent ventilation per room with heat recovery integrated in window ledge was developed. In technical and scientific literature, this kind of unit is called **single room ventilation with heat recovery** <u>or</u> **aerating windows with heat recovery** <u>or also</u> **room based ventilation with heat recovery.**

The present thesis focuses on the **development steps and performance characterization** of this specific device. A large part of the present work focuses on the **heat exchanger** (modeling and experimental investigations) which is considered as one of the key components of the unit. Behavior of such heat exchangers is deeply investigated for **different operating conditions**.

Single room ventilation with heat recovery consists in a **mechanical pulsing and extracting ventilation per individual room with heat recovery**, as schematically represented in Figure I-1:
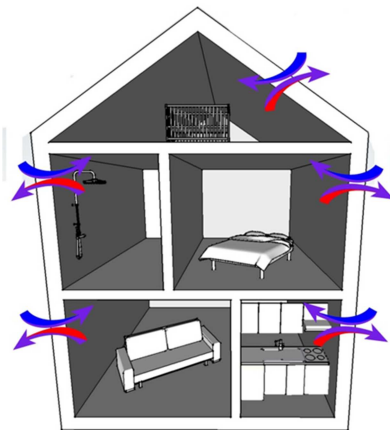
Figure I-1: Concept of Single Room Ventilation with Heat Recovery

This kind of system is particularly **suitable in the frame of the renovation of a residential building** involving windows replacement.

After highlighting the importance of (heat recovery) ventilation in the current context, some details/features about the device are already given in this introduction. A qualitative **comparison** with traditional **centralized heat recovery** ventilation is also realized in this chapter.

Finally, **objectives** and the **organization of the thesis** (chapter by chapter) are presented.

2 ENERGY CONTEXT

Nowadays, with the increasing costs of energy and the growing concern about human impact on climate, important efforts are deployed to reduce our actual energy consumption. World final energy consumption has drastically increased from 1971 to 2009, as it can be observed in Figure I-2 (a). More precisely, World final energy consumption has almost doubled.

(a)   (b)
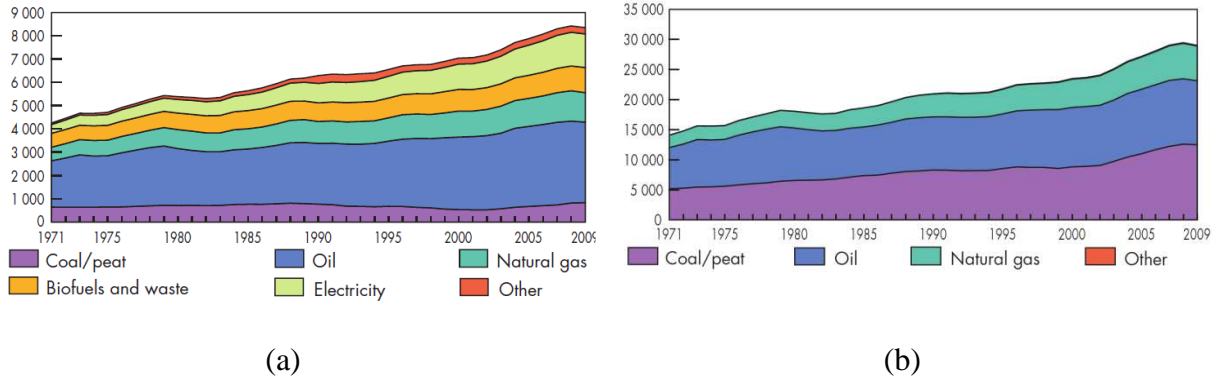
Figure I-2 : Evolution from 1971 to 2009 of World total final consumption by fuel (Mtoe) (a) and World CO2 emissions in Mt (b) (IEA, 2011)

As a matter of fact, world CO2 emissions and world final energy consumption are deeply linked and follow the same evolution (from 15640 Mt of CO2 in 1973 to 28999 Mt of CO2 in 2009). Mainly due to the growing scarcity of the World energy resources (and many other reasons such as speculation, economic crisis, emerging countries…), energy prices are increasing. Evolution of the natural gas import prices for different IEA countries is given in Figure I-3.
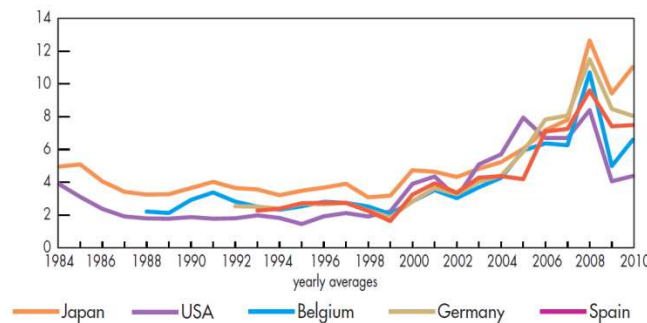
Figure I-3 : Natural gas import prices in US dollars/MBtu (IEA, 2011)

According to IEA (2008), the building sector accounts for almost 40% of the final energy used in the World, as shown in *Figure I-4*. More precisely, the energy consumption related to the residential sector accounts for almost the third of the final energy consumption. This highly justifies the efforts to improve the energy efficiency of this sector.
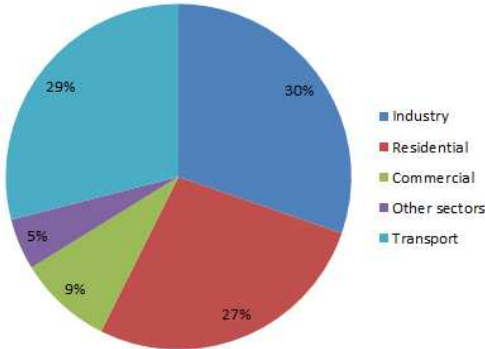
Figure I-4 : Energy consumption in different sectors - Share of final end use in % (IEA (2008))

In 2011, IEA published its « Technology Roadmap for Energy-efficient Buildings ». It is proposed a reduction of energy consumption of global building sector by 1509 Mtoe in 2050 in comparison with baseline scenario. Residential sector accounts for 63% of these energy savings.

The major part of energy used in residential buildings is due to space heating as shown in Figure I-5. Differences can be observed between different countries, especially in terms of total (not normalized) energy use.
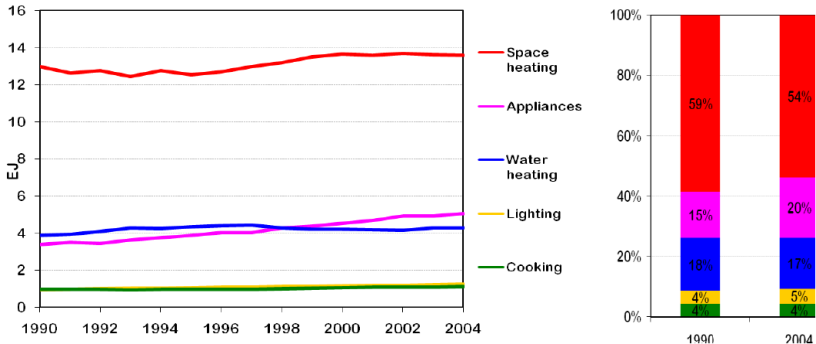
Figure I-5: Aggregated subdivision of energy consumption in residential buildings for different countries (IEA (2008))

Energy consumption due to appliances has been rising since 1990. This fact can be partly explained by the growing use of electrical equipment in residential buildings (computer, cell phone chargers, washing machines, etc…). In 2004, the third source of energy used concerns the domestic hot water supply. Energy dedicated to lighting and cooking stays relatively stable and represents a smaller part of energy consumption (less than 10%).

As a result, it can be stated that the higher the building energy efficiency (with a high insulation level) the larger the relative part dedicated to domestic hot water and ventilation.

In Europe, in 2004, buildings consumption accounted for 40% of the total energy demand, among which the residential sector represented a share of over 70%, as reported by Perez-Lombard et al. (2008).

As shown in Figure I-6, European energy consumption share in terms of final energy is quite similar to the World consumption in 2009. Once again, the energy consumption related to the residential buildings accounts for 27% of the total energy use.
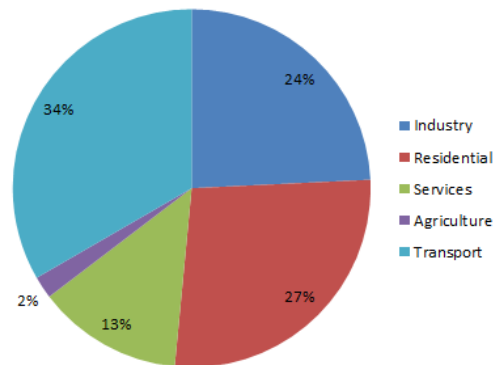
Figure I-6 : European final energy consumption per sector (Eurostat (2011))

In 2002, the Energy Performance of Buildings Directive (EPBD) was adopted by Europe as a commitment to reduce energy impact of the building sector.

In 2008, the European Union adopted the Climate and Energy Package, a range of measures to fight against climate change. The proposal includes the 20-20-20 targets for 2020:

- Reduce EU greenhouse gas emissions by 20% from 1990 levels;
- Improve the EU's energy efficiency by 20%.
- Reach 20% of renewable energy in the total EU energy consumption.

In 2011, European Commission adopted the Energy Roadmap 2050. EU is committed to reduce greenhouse gas emissions by 80-95% below 1990 by 2050. This roadmap could be divided in two main parts: higher energy efficiency and higher share of renewable energy sources.

Higher energy efficiency involves:

- More stringent minimum requirements for energy efficiency of appliances and buildings;
- nZEB should become the norm (recast EPBD 2010/31/EU) for all new building occupied or owned by public authorities in 2019 and for all new buildings in 2021;
- High renovation rates of existing buildings;
- Smart meter in buildings: occupants will get more information on their own consumption profiles.

As a conclusion, residential sector accounts for a large part of the energy consumption in Europe and all over the World. The residential buildings sector offers a large potential of reduction of energy consumption and therefore CO_2 emissions. As a result, many measures are nowadays adopted in order to reduce its impact.

3 VENTILATION

This chapter aims to explain some general concepts related to ventilation. Importance of ventilation on occupant's health is also presented. In order to better categorize the device investigated in the frame of this thesis, a classification depending on the type of ventilation systems (A, B, C D) with or without heat recovery is proposed.

3.1 Definitions

One can distinguish ventilation and infiltration as two ways of air exchange from outside and air contained in a building. Following definitions are proposed by the Fundamentals of ASHRAE (2009):

*"**Air exchange** of outdoor air with air already in a building can be divided into two broad classifications: **ventilation** and **infiltration**.*

- *- **Ventilation** is intentional introduction of air from the outside into a building; it is further subdivided into natural and mechanical ventilation:*

  - *• **Natural ventilation** is the flow of air through open windows, doors, grilles, and other planned building envelope penetrations, and it is driven by natural and/or artificially produced pressure differentials.*

  - *• **Mechanical** (or **forced**) ventilation is the intentional movement of air into and out of a building using fans and intake and exhaust vents.*

- *- **Infiltration** is the flow of outdoor air into a building through cracks and other unintentional openings and through the normal use of exterior doors for entrance and egress. Infiltration is also known as **air leakage** into a building. **Exfiltration** is leakage of indoor air out of a building through similar types of openings. Like natural ventilation, infiltration and exfiltration are driven by natural and/or artificial pressure differences."*

The main objective of the ventilation is to remove or dilute polluted/contaminated air and to introduce fresh air throughout the building in order to maintain a good indoor air quality and thermal comfort for the occupants. Liddament (1996) provides an overview of the IAQ in relation to:

- Sources of pollutants;
- Metabolism and Health;
- Odour;
- Sick Buildings Symptoms;
- Comfort;
- Reducing pollutant concentration.

3.2 Ventilation and Indoor Air Quality (IAQ)

According to several sources (U.S. environmental Protection Agency (1989) and Jenkins et al. (1992)), it is stated that on average, people spend most of their time indoor (approximately 90% of time spent indoor). Brasche and Bischof (2005) shows that the overall mean time spent at home is 15.7 h/day in Germany. Similar results have been obtained for the United States (15.6 h/day) as well as for Canada (15.8 h/day), according to Leech. et al. (2002).

As a result, Indoor Air Quality became a major concern over the last decade and ventilation became a key topic for researchers. It is estimated that in 2008 the annual burden of disease related to inadequate IAQ is 2 million disability adjusted life years in EU27. This problem has also been identified by the World Health Organisation (Braubach et al. (2011)).

Recently, the European HealthVent project aims at *"developing a guide for heath-based ventilation dedicated non-industrial buildings in Europe (offices, homes, schools, nursery and day cares centers) by taking into account health and energy impacts of the ventilation"*. In the frame of this project, a scientific literature review (on the relation between health and ventilation) has been carried out by Carrer et al. (2012) (Work Package 4 of the Health Vent project).

In this context, the Lawrence Berkeley National Laboratory (LBNL) also proposes an Indoor Air Quality Scientific Findings Resource Bank (IAQ-SFRB). The aim of this data bank is to provide/collect information about the effects of IAQ (and ventilation) on people's health and work performance.

From the collected data, it can be observed a direct link between ventilation rates and:

- Office Work Performance;
- School Performance;
- Respiratory illness;
- Absence in Offices and School;
- Sick Building Syndromes (SBS);
- Health in homes.

An example of paper (among others) describing the direct correlation between ventilation flow rates and SBS is the one written by Fisk et al. (2009).

3.3 Types of ventilation

Ventilation can be completely natural, completely mechanical or hybrid.
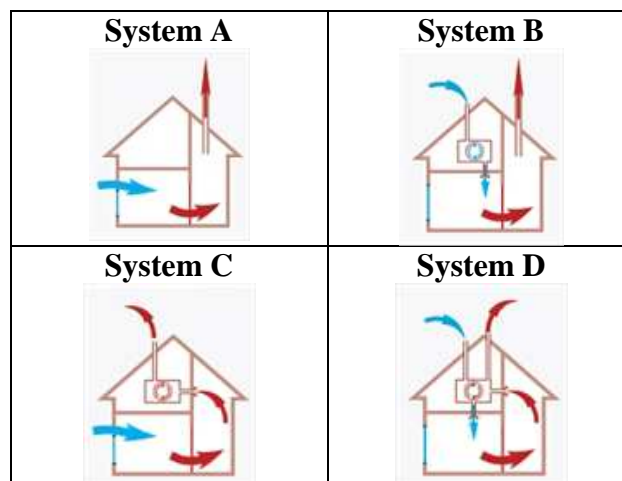
Figure I-7 : Type of ventilation

According to NBN D50-001, residential ventilation can be divided into four categories, schematically represented in Figure I-7:

- **System A** : natural ventilation;
- **System B**: mechanically supplied ventilation;
- **System C**: mechanical extracting ventilation;
- **System D**: mechanically supplied and extracting ventilation. It is important to mention that most of the dwellings (especially for buildings constructed before 1970) are not equipped with a proper ventilation system. Air change is only ensured by infiltration/exfiltration and airing.

Ecolot (2012) proposes an estimation of the ventilation systems stock per type for EU27 in 2003. This is represented in Figure I-8. As it can be, in 2003, most of the European dwellings are not equipped with a proper ventilation system and a negligible part (0.3%) of the ventilation stock corresponds to System D. It is also interesting to notice that only a quarter of the ventilation stock corresponds to system A.
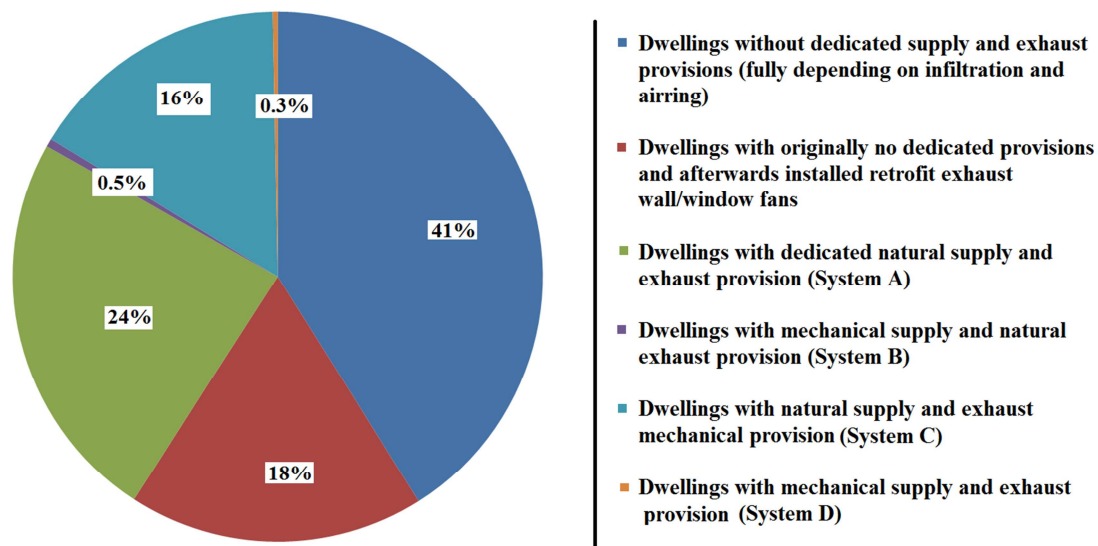
Figure I-8: Ventilation systems repartition for EU 27 (Ecolot (2012))

3.4 Regulations/policies on ventilation in housing

3.4.1 European level

As already specified, Europe adopted in 2002 the Energy Performance of Buildings Directive but this barely mentions ventilation requirements.

Currently, a common Standard in terms of ventilation flow rates for housing for European countries does not exist. Dimitroulopoulou (2012) recently released a review of Standards for European residential dwellings. It can be observed non-homogeneities between countries in terms of required flow rates per specific room (and for the whole building) as well as in terms of unity for determined flow rates (some Standards specifies the flow rates in m³/h-m², in h^{-1} or in m³/h-pers).

However, ventilation flow rates to be considered for designing ventilation systems in the absence of national regulations are specified by EN 15251 (see Table I-1). This Standard also specifies ventilation recommended when the building is not occupied. This standard does not prescribe a methodology for the design, but provides the parameters for the design of buildings, heating, cooling, ventilation and lighting. It defines how the different categories of criteria for indoor environment can be used, but

does not require the criteria to use. It also specifies methods for long-term evaluation of the indoor environment obtained.

Table I-1: Ventilation flow rates for housing during occupancy hours according to EN 15251

Category	Air renewal		Living room, Bedroom, essentially pulsed fresh air		Extracted air (m³/h)		
	m³/h-m²	vol/h	l/s-pers	m³/h-m²	Kitchen	Bathroom	WC
I	1.76	0.7	10	5.04	100.8	72	50.4
II	1.51	0.6	7	3.6	72	54	36
III	1.26	0.5	4	2.16	50.4	36	25.2

Category I, II and III corresponds respectively to:

- A high expected level that is recommended for spaces occupied by very sensitive and fragile persons with special requirements such as handicapped, sick, very young children and the elderly;
- A normal level expected to be used for new buildings and renovations;
- An acceptable moderate level expected which can be used in existing buildings.

During vacancy period, the minimal flow rate recommended by the Standard is comprised between 0.18 and 0.36 m³/h-m².

3.4.2 Belgium level

NBN D50-001 is the Belgian standard concerning the ventilation systems for new housing and heavily retrofitted buildings. This Standard specifies the flow rate dedicated to each room of housing, as reported in Table I-2.

Table I-2: Flow rates according to the NBN D50-001

	Living room	Bedroom	Kitchen Bathroom Laundry	WC	Corridor, Living and night hall
Nominal flow rate of ventilation	3.6 m³/h-m² <u>Min:</u> 75 m³/h <u>Max:</u> 150m³/h	3.6 m³/h-m² <u>Min:</u> 25 m³/h <u>Max:</u> 36m³/h-pers	3.6 m³/h-m² <u>Min:</u> 50 m³/h <u>Max:</u> 75m³/h	25 m³/h	3.6 m³/h-m²

The NBN D50-001 standard mentions that the flow rate indicated in Table I-2 can only be met by supplying and exhausting air through mechanical ventilation for each room. Indeed, the standard mentions this case as "the most complete case and rarely met in practice". It is then proposed to only extract or only supply flow rate, depending on the type of the room.

Concerning mechanical ventilation (systems B, C and D), vitiated air is usually extracted from wet rooms such as bathroom, kitchen and fresh air is supplied into dry rooms such as living room and bedroom.

3.5 Single room ventilation with heat recovery: device positioning

Given the growing interest to reduce energy penalty due to ventilation, a large number of heat recovery technologies have been developed in the last decades as reported by Mardiana-Idayu and Riffat (2012). According to Shurliff (1988), *"Any device that removes (extracts, recovers, salvages) heat from one airstream and delivers it to another airstream is called an air-to-air heat exchanger"*. One can distinguish sensible heat and enthalpy (sensible and latent heats) recovery exchanger.

Mardiana and Riffat (2013) also recently propose a review on physical (size, heat transfer area, fans, ducting, materials and structures) and performance (heat and mass transfer, ε-NTU method, effects of airflow, temperature moisture and pressure drop) parameters of heat recovery for building applications.

In Figure I-9, a division of the ventilation systems (with or without heat recovery) in order to better categorize the possible systems for single room ventilation with heat recovery is proposed:
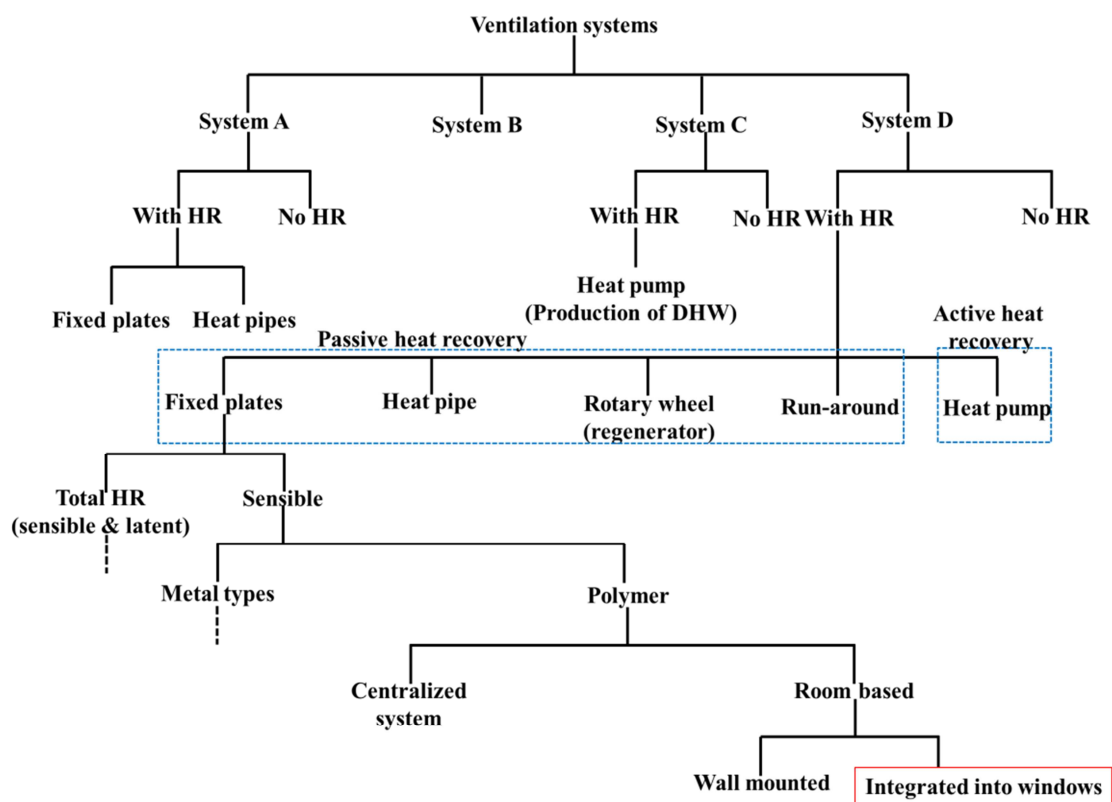
Figure I-9: Product positioning

The device investigated in the frame of this thesis (framed in red in Figure I-9) can be classified as a **room based system D (mechanical supply and exhaust) with (passive) heat recovery**. In contrary to wall mounted device which implies the creation of two ducts (one dedicated to the fresh air and another dedicated to the return air) leading through the external wall (as shown in Figure I-10), the system is supposed to be integrated in **windows ledge** which makes it particularly suitable for renovation, and more specifically for renovation that implies windows replacement.
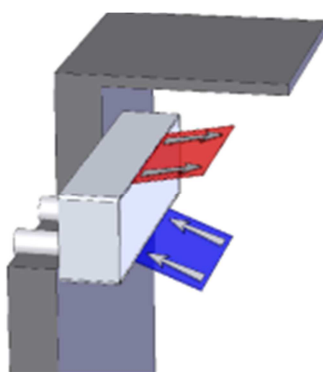
Figure I-10: Wall mounted SRVHR

Heat exchanger is made in **polystyrene** (as detailed in Chapter III) and only recovers **sensible heat** (no mass transfer) in contrary to enthalpy exchangers investigated by Nasif (2008), Zhang (1999, 2000, 2002) and Zhou (2006).

4   BALANCED SINGLE ROOM VENTILATION WITH HEAT RECOVERY

4.1   Interest

As seen in the previous sections, it is obvious that improvement of building's efficiency represents an attractive solution to reduce a large part of energy consumption (and thus to reduce energy bills). As referred by the Trias Energetica, introduced by Lysen (1996), "*the most sustainable energy is saved energy*".
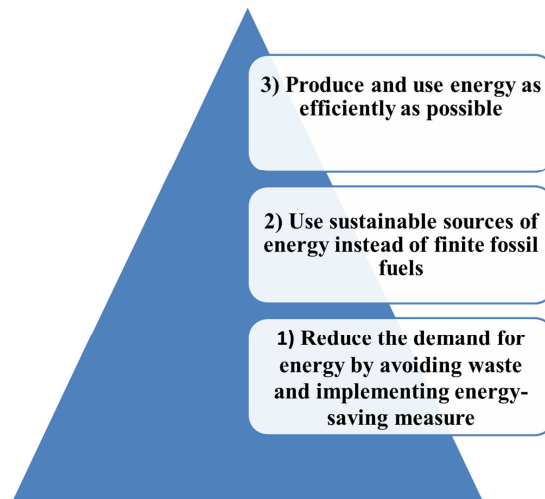
Figure I-11 : Trias Energetica concept

From this fact, the best way to make a building climate friendly is first to improve its shell.

The two most common actions that are undertaken in the field of renovation of existing houses are the improvement of the thermal insulation and improvement of air tightness. This represents a high potential for the reduction of energy consumption (Gendebien (2011)) but also a possible degradation of the indoor air quality due to reduction of air renewal related to insufficient infiltration/exfiltration ventilation flow rate. This phenomenon was first observed during the 70's petrol crisis that led people to tighten their building envelope. As a result, many humidity and mold problems have been observed in Belgium dwellings, as deplored by DGTRE (1998). This was the first general awareness of the importance of the ventilation.

Nowadays, the baseline rate concerning retrofitting for the European countries is set to 1% by different studies carried out for Europe (Eurima (2012) and BPIE (2011)), as well as for a study conducted in Norway (Norwegian University of Science and Technology (2011)). SPF Economie (2013) gives a number of 30000 dwellings per year since 2003 in Belgium, which corresponds to a rate of 0.6% per year. However, this number corresponds to the heavy retrofits that require building permits. Roof insulation or windows retrofitting do not require such permits, and their rate is unknown with precision.

In Belgium, for Brussels Region (IBSA (2013)), the number of retrofit grants awarded for the years 2002 to 2010 is given in Figure 3. These grants gather all type of renovations, whether it requires a permit or not. One can see a significant increase in the retrofit rate after 2007. In 2012, the number of dwellings was 509433 according to the Belgian "*Institut national des statistiques*" - INS (2014). Therefore, the retrofit rate ranged from 0.45 to 0.8% per year.

Since 37% of the Belgian building stock was built before 1945, it can be assumed that a natural trend to the increase in retrofitting will take place by 2030, with a retrofit rate of 0.8% per year (analogy with Brussels region).

In combination with the desire to maintain good air indoor quality (as explained in previous Section), these building envelope improvements have the effect of increasing ventilation's contribution to energy consumption. From this fact, it can be stated that the more improvement of the envelope will be a growing interest in future years, the more ventilation will become an important concern.
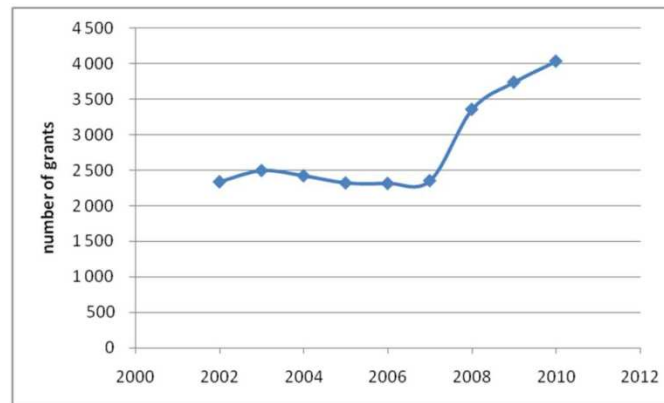
Figure I-12: Evolution of the number of grants for renovation in Brussels IBSA (2013)

According to Roulet et al. (2001), more than 50% of the total energy losses can be due to ventilation, in building with a high thermal insulation. Liddament and Orme (1998) show that infiltration and ventilation highly impact the energy use in buildings by estimating that 36% of space conditioning energy is due to total air change. According to Simonson (2005), it is estimated that the ventilation flow rate constitutes between 20 and 50% of the heating energy load.

Previous facts highly justify efforts to develop efficient ventilation device (particularly suitable in the frame of a renovation) such as the one investigated in the frame of this thesis.

4.2 Centralized ventilation versus balanced single room ventilation unit with heat recovery

The aim of this section is to offer a qualitative comparison between traditional centralized and single room ventilation with heat recovery systems. These two systems are represented in Figure I-13. As already specified, the principle of heat recovery ventilation is well-known, but most of already commercialized units are centralized (Ecodesign Lot 10 (2012)), which involves air extracting and air pulsing ducts through the house.

Some **advantages** of single room ventilation are listed by Manz et al. (2000):

- *Local ventilation units do not need any ducting within the dwelling and are therefore very suitable for retrofitting use*.

- *Independent ventilation per room is possible with optimal adjustment to local needs*.

- *Local room ventilation allows quick removal of pollutants from a source-room, before they mix up with the air in other rooms as might happen with central dwelling ventilation*.

- *A direct sound transmission from room to room through the ventilation system cannot occur*.

Centralized unit
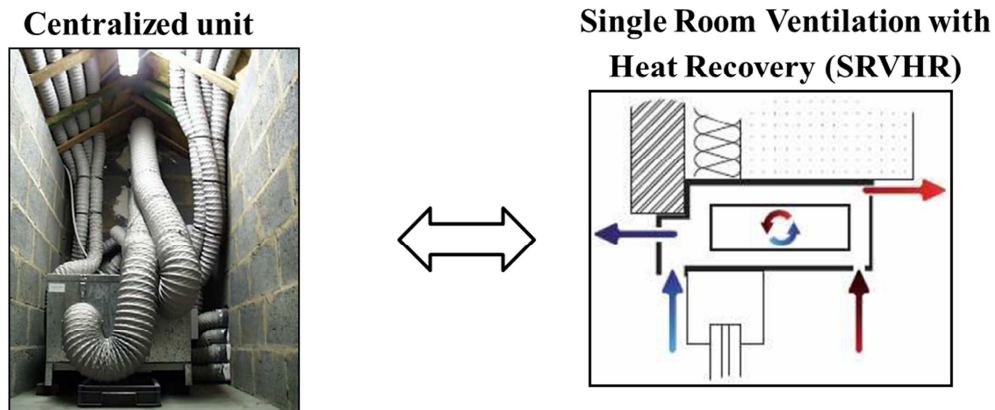
Single Room Ventilation with Heat Recovery (SRVHR)

Figure I-13: Centralized unit vs SRVHR

Others **advantages** can be added to this list:

- Avoiding ducts means **shortening the hydraulic circuits**, and hence the pressure drops related to the passage of air flows through them. From this fact, the specific fan power (SFP) can be reduced.

- Given their placement in habitable rooms and the **accessibility of each component**, the maintenance of the system (particularly, the filters replacement) is easier and cheaper than in centralized heat recovery ventilation systems.

- As referred by Wouters and Van den Bossche (2005), possible problems of installed centralized ventilation systems are **leaking air ducts**. According to Andersson (2013), "many studies have identified defective ventilation and insufficient air flow as a mean reason for occurrence of sick building… Duct systems accounts for a large fraction of the energy use in a building. This is further increased with a leaky duct system." These potential issues are **avoided** in single room units.

- **Dust accumulation** in ducting can lead to a performance degradation of the installation due to a rising of the pressure drop (Anon (2000)). Moreover, the indoor air quality can decrease due to a **contamination** of air flow rate by particles, micro-organisms or volatile organic compounds (Barbat and Feldmann (2010)). Once again, these problems **are avoided** in single room ventilation units.

- It should also be noticed that recent studies (Laverge (2011), Maripuu (2011)) investigated the potential of **demand controlled ventilation** (DCV), which could be particularly suitable with balanced single room ventilation.

- One of the major advantages of the single room ventilation with heat recovery is the opportunity to **well balance** the flow coming from the outdoor environment and the flow coming from the indoor environment during the manufacturing phase of the unit. This could be realized by means of a **calibration** consisting in an adjustment of the electrical power supplied to each of the fans to reach the requirement in terms of flow rates. This calibration can be achieved for all of the commercialized units, contrary to centralized units that require an adjustment of the exhaust and supply flow rates in situ. So, in terms of **practical**

installation, the single room ventilation seems particularly easy compared to centralized systems.

The main intrinsic **drawbacks** of Single Room Ventilation with Heat Recovery are that devices are installed directly in the rooms. Thus, it is necessary to take care of the **aesthetic** and **acoustical** aspects of the device. Moreover, the **miniaturization**, as well as the **multiplicity** of the units inside the houses, can lead to additional losses (such as current converter losses, as an example).

4.3 Challenges

All of the previous given characteristics imply a considerable challenge: **developing a competitive heat recovery ventilation system despite of a small available volume by taking care of the aesthetic and acoustic aspects**.

As for every heat recovery ventilation system, the developed device faces a trade-off between a high thermal effectiveness and a related rise of pressure drops inducing a degradation of the global performance of the unit due to a higher energy use for the fan. Greater attention is also paid to **hydraulic performance** than in centralized systems since they are directly related to the **noise generated** by the fans.

As an example, in Belgium, according to the NBN S01-400-1, acoustic requirements for each type of local are summarized in Table I-3:

Table I-3: Requirement in terms of acoustic comfort according to the Belgian norm NBN S01-400-1 for mechanical ventilation

Local	Normal acoustic comfort level	Superior acoustic comfort level
Bathroom, toilets	≤ 35 dB	≤ 30 dB
Kitchen	≤ 35 dB	≤ 30 dB
Living room	≤ 30 dB	≤ 27 dB
Bedroom	≤ 27 dB	≤ 25 dB

The World Health Organization recommends two values in the report "Guideline values for community noise in specific environments" (1999): respectively, 35 dB for living rooms and 30 dB inside bedrooms.

4.4 Specificity of the developed device

Starting from the observation that most of the time, building retrofitting implies windows replacement (Schwenzfeier et al. (2009)) and given the growing interest for renovation in Europe as seen in previous Section, a device where **double flow ventilation is achieved through the integration of the unit into windows ledges** was developed, as shown in Figure I-14.

Thanks to this concept, the windows replacement would also permit to ensure mechanical ventilation with heat recovery, and thus a good Indoor Air Quality.
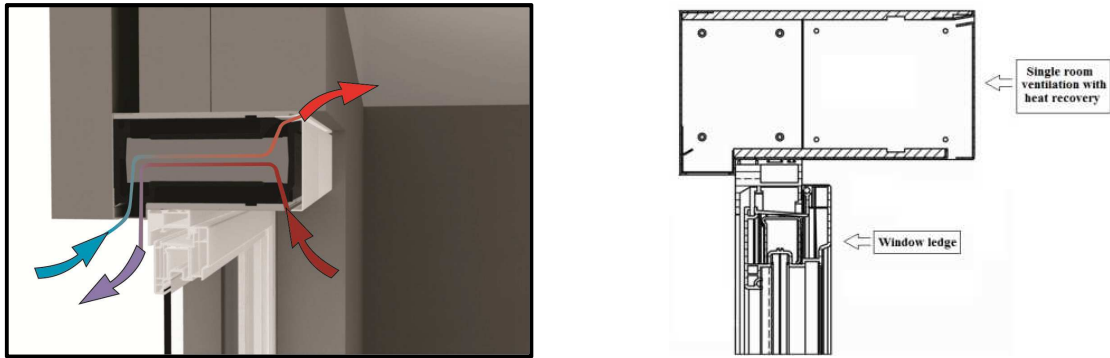
Figure I-14: Schematic representation of the developed device

The developed single room ventilation unit with heat recovery mostly consists in a parallelepiped box containing:

- **two DC fans** (an extracting one and a pulsing one);
- **two filters** (for both fresh and indoor air flow rate);
- an **AC/DC** current converter;
- an **electronic fan control**;
- a **set of sensors** (CO_2, humidity, presence sensors, depending on the device);
- a **heat recovery exchanger** considered as the key component of the unit.

Characteristics (geometry, performances, type of filters,…) of the first generation of developed devices are detailed in Chapter V.

5 MARKET TRENDS

The aim of this present section is first to present the characteristics of the ideal single room ventilation with heat recovery. Then, performances of some devices recently released on the market will be presented.

5.1 The ideal single room ventilation with heat recovery

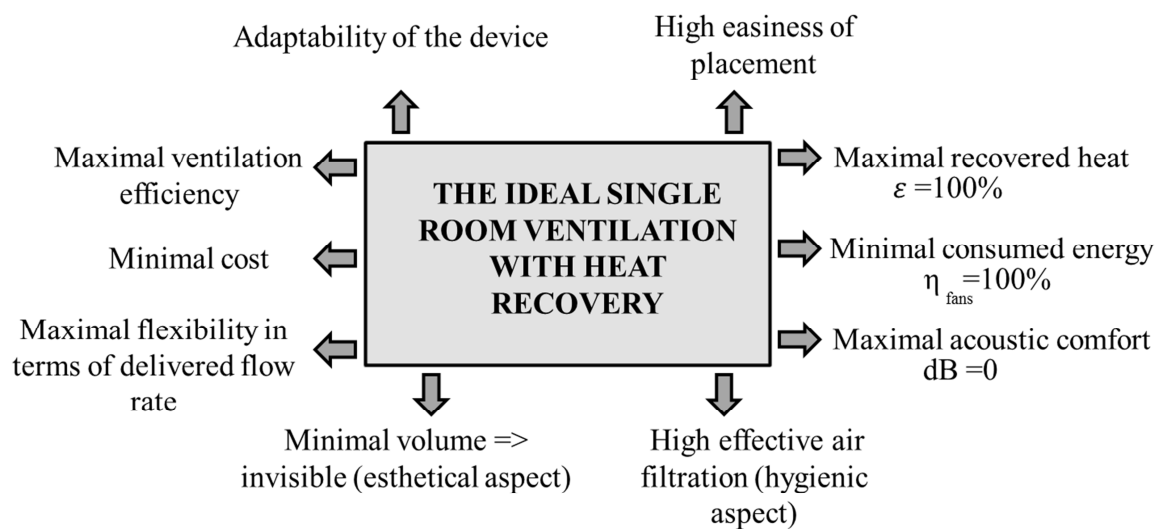Before launching the development phase of any products, it is common to define what would have been the ideal device. By definition, the perfect product is a fictitious ideal device with a set of performance targets impossible to reach practically. The aim of any constructor is obviously to build a device as close as the perfect defined one for all of the parameters.

In the case of single room ventilation with heat recovery, what would be the ideal device features? Response to this question is summarized in Figure I-15:

Adaptability of the device   High easiness of placement

Maximal ventilation efficiency   **THE IDEAL SINGLE ROOM VENTILATION WITH HEAT RECOVERY**   Maximal recovered heat $\varepsilon = 100\%$

Minimal cost   Minimal consumed energy $\eta_{fans} = 100\%$

Maximal flexibility in terms of delivered flow rate   Maximal acoustic comfort $dB = 0$

Minimal volume => invisible (esthetical aspect)   High effective air filtration (hygienic aspect)

Figure I-15: The "ideal" single room ventilation with heat recovery

Obviously, the real final device results in a trade-off between all the features of the device. As an example, an effective filtration raises the consumed energy or a small volume implies a poor heat exchanger efficiency.
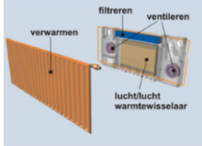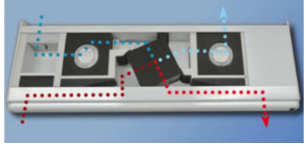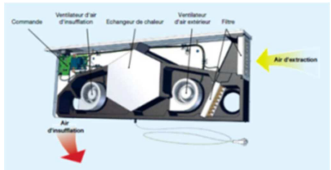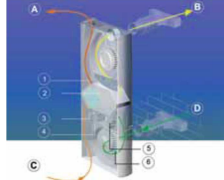
One advantage resulting from the definition of the perfect device is to establish a hierarchy of the performance targets to be met by the real developed device. This hierarchy can be based on subjective, economical or legal issues. In the frame of the thesis, it will be proposed an approach to determine the best trade-off between hydraulic and thermal performance of the device.

5.2 Off-the-shelf devices

The present section shows a technical state of the art by presenting a non-exhaustive list of some devices very recently released on the market. It is important to notice that most of these products have been commercialized after 2009.

Even if there are only a few products on the market (less than ten to our best knowledge), that trend confirms the growing interest for room based ventilation with heat recovery, especially these last few years.

Table I-4 : Benchmarking

Brand	Model	Installation	Flow rate	Power	ε	Product
Aldes	Ventileo	Below the windows ledge	20 m³/h	3.5W per fan	65%	
Climarad	Climarad	Coupled to the heating system (radiator)	20 m³/h: 3W 40 m³/h : 5W 60 m³/h: 9W 80 m³/h : 15,5W 100m³/h : 25,5W 125 m³/h : 42W Standby: < 1,0 W		85% (max.)	
HöHbauer	AirPur Modul	Coupled to the shutter	11-45 m³/h	n.a.	69-84%	
Schüco	Vento therm	Integrated into the window ledge	15 m³/h: 5W 30 m³/h :13W		45% 40%	
Siegina	Aeromat vt	Upon the window	42 m³/h (max.)	n.a.	62% (max.)	
Storkair Zehnder	Duett	Coupled to the heating system	0-100 m³/h (max.)	< 0.4 W/m³h	80% (max.)	
Brink	Advance	Wall mounted	0-75 m³/h (max.)	n.a.	90% at 20m³/h	
Paul	Ventos 50 DC	Wall mounted	40-120 m³/h	11 to 62W	83% at 40 m³/h	

5.3 Ventilation market segment

Differences can be observed between zones of Europe in terms of ventilation market. Balanced mechanical ventilation with heat recovery seems to be more popular in the Northern part of Europe such as Finland: 100% of new buildings are equipped with mechanical ventilation, as reported by Kurnitski (2008). Simple exhaust ventilation is more widespread in medium climate such as France, as specified by Durier (2008). In the Southern part, infiltration and airing seems to remain the most common way of ventilating.

Figure I-16 shows the repartition of mechanical ventilation sales in 2003 according to Ecolot (2012). It can be observed that the major part of the market is due to like for like replacement market.

Major part of the market concerning the room based mechanical ventilation with heat recovery concerns obviously the renovation market. Given the rise of renovation due to new policies and incentives (see Section 4), a growth of this market for the future years is expected.
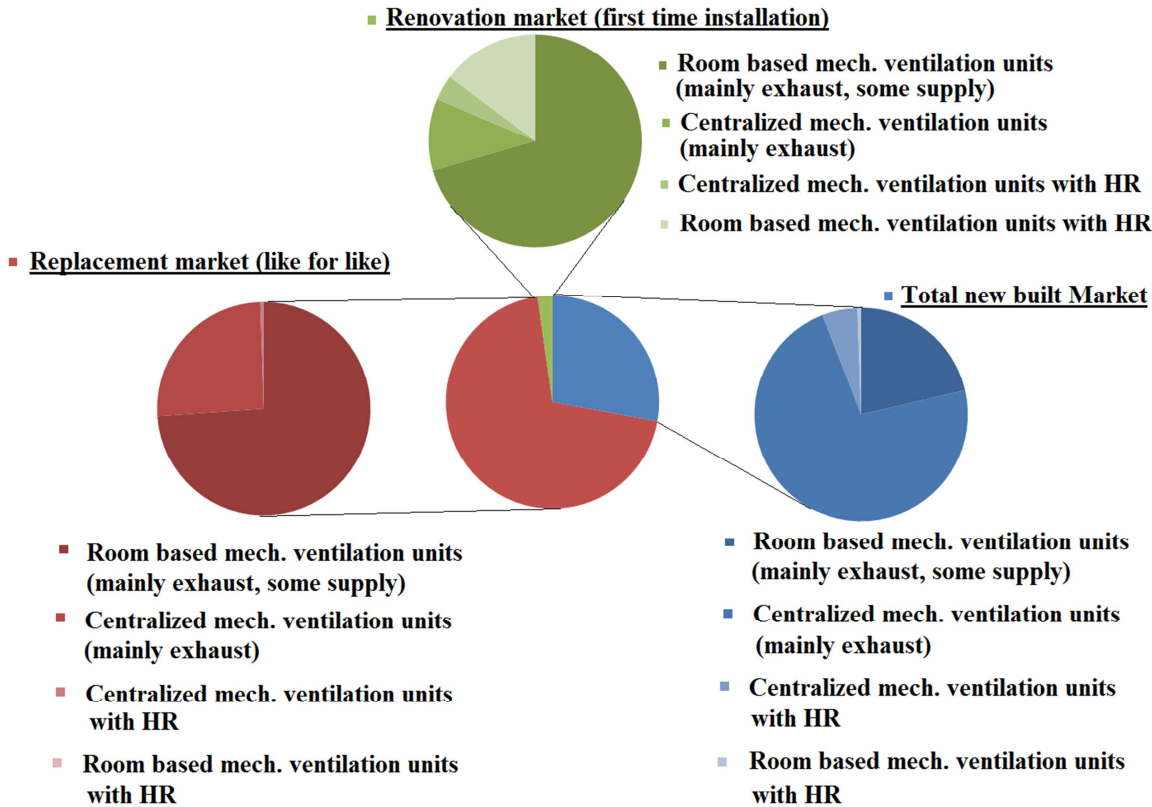
Figure I-16 : Ventilation market segment in 2003 (Ecolot design (2012))

5.4 Past annual sales and forecast for mechanical heat recovery ventilation

As referred by Fehrm et al. (2002), heat recovery ventilation dedicated to residential building started in the late seventies in Sweden. Heat recovery ventilation has now acquired a status of efficient ventilation strategies, especially for low or net zero energy buildings (Handel (2011)).

As shown in Figure I-17, a strong growth of the market concerning the mechanical heat recovery ventilation is expected. Ecodesign Lot 10 (2012) estimates a potential market of approximately

938000 mechanical heat recovery units to be met in 2025 in the EU 27, with an explosion of sales in the medium climate market.
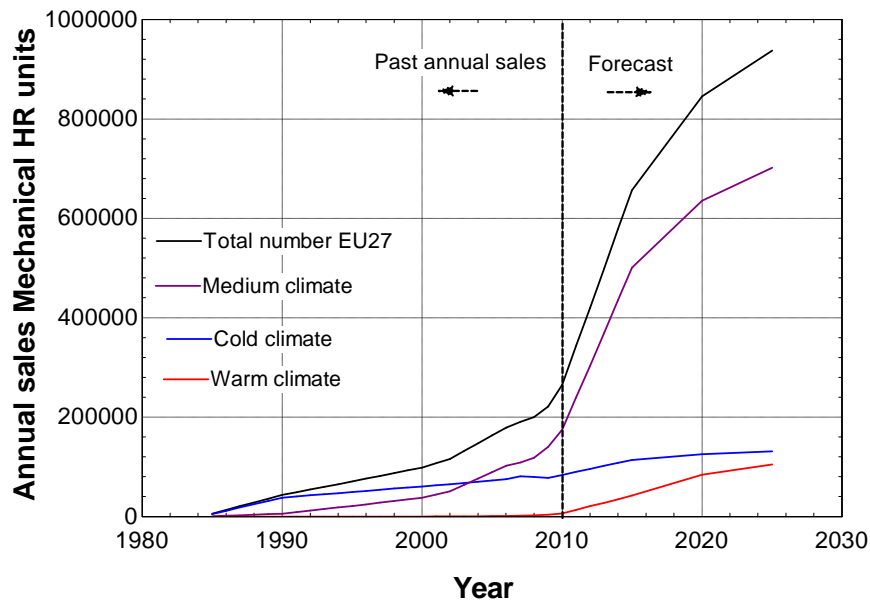
Figure I-17 : EU27 Forecast and Market trends (Ecolot design (2012))

As reported by Wouters et al. (2008), this trend is already observed in Belgium (in the frame of the Walloon project "Construire avec l'énergie") with an increasing of the share of the balanced mechanical ventilation systems.

This is also confirmed by Seppanen (2012) that showed an important changement in the ventilation market in Belgium:

-   Before 2007, only 0.68% of buildings are equipped with mechanical ventilation systems;
-   5% of buildings constructed during years 2007 and 2008 are equipped with mechanical ventilation systems;
-   40% of buildings constructed after 2008 are equipped with mechanical ventilation systems.

6   NOMENCLATURE

Nomenclature used in the frame of the thesis is given in Figure I-18:

- **-** Supply and exhaust corresponds to the inlet and the outlet of the heat exchanger;
- **-** Indoor and fresh air side corresponds respectively to the flow coming from the building and the flow entering in the building.
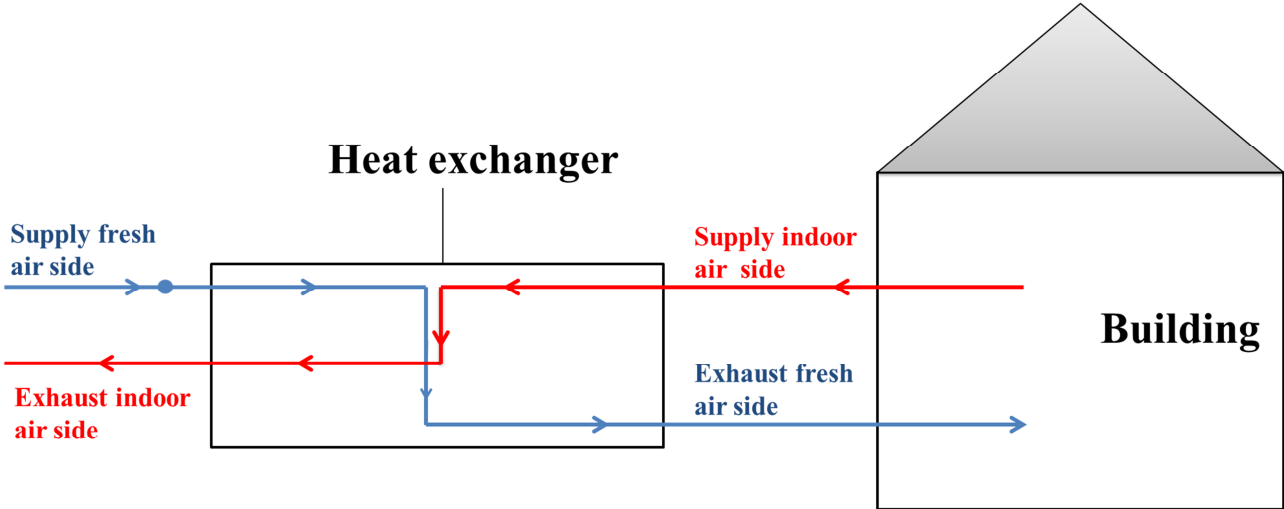
Figure I-18: Used nomenclature

7   OBJECTIVES OF THE THESIS

This thesis aims at contributing to the state of scientific and technical knowledge on the development and the characterization of mechanical heat recovery ventilation and more precisely Single Room Ventilation with Heat Recovery (SRVHR) by developing new and improving existing methods (both experimental and numerical). A large part of the thesis focuses on air-to-air heat recovery exchanger which is often considered as one of the key components of the device. Most of the work was carried out in the frame of the *Green +* project launched in 2009 and which aimed to develop an integrated single room ventilation unit with heat recovery.

The <u>first objective</u> of the thesis is to develop models able to simulate the behavior of air-to-air heat recovery exchanger in **various operating conditions**: dry, partially wet and frosting conditions. The aim of those models is to evaluate the impact of various operating conditions on the overall performance of the unit. This first objective also includes the performance determination of **polystyrene** heat exchangers presenting **different geometries**. In their review, T'joen et al. (2009) indicate that polymer matrix seems promising for use in the design and construction of heat exchangers for ventilation applications. However, only a few experimental investigations have been carried out on polymer based heat exchanger, in the scientific literature (Kragh et al. (2008) and Fernandez et al. (2010)).

The <u>second objective</u> of the thesis consists of proposing a methodology in order to choose the best geometry parameters for a heat exchanger dedicated to SRVHR unit. This approach consists of choosing **the best trade-off between hydraulic and thermal performance** by means of an optimization of the coefficient of performance of the unit.

The <u>third objective</u> of the thesis is to propose an **approach in order to experimentally characterize** a newly developed whole SRVHR unit that could be integrated in windows ledge. A distinction is made between experimental investigations during and after the development steps of the unit.

The <u>final objective</u> consists in **comparing the seasonal energy performance** of the unit with other ventilation systems (A, B, C and D), given a specific climate.

8 ORGANIZATION OF THE MANUSCRIPT

The thesis is organized as follow:

- **The second chapter** focuses on the development and experimental validation of a model of air-to-air heat exchanger dedicated to domestic mechanical heat recovery ventilation. The proposed model describes dry and partially wet regimes. The first part of the chapter presents a semi-empirical model based on the physical characteristics of the heat recovery device and relying on empirical correlations available in the literature for the convective heat transfer coefficients and the friction factor. In the case of partially wet regime, a moving boundary model is applied in order to predict sensible and latent heat transfer rates. The second part of the chapter describes the experimental investigation conducted on an off-the-shelf heat exchanger presenting triangular channel in the central part. Experimental data are used to tune correlations for the determination of the convective heat transfer coefficient and the friction factor. A validation of the proposed simulation model of the ventilation heat recovery exchanger in partially wet conditions is then realized. Finally, examples of use of the developed model are presented.

- **The third chapter** first proposes a definition of the coefficient of performance (COP) of single room ventilation with heat recovery. Starting from this definition, a methodology to determine the best trade-off between hydraulic and thermal performance for the heat exchanger (given a specific geometry) is proposed. The optimization of the COP is not the only parameter to take into account in the development process of the device. Indeed, due its position in living rooms, the sound generated by the device is also one major parameter. Thus, great attention is paid to hydraulic performance. In this context, an innovative method is proposed in the frame of the development step of the device: measuring the hydraulic performance of a proposed geometry by means of two rapid prototyped plates. Investigations carried out by means of these rapid prototyped plates are detailed. Finally, the so-called optimized heat exchanger has been manufactured, experimentally tested and analyzed.

- **The fourth chapter** proposes a dynamic simulation model of the heat exchanger under frosting conditions. A description of the frost formation is added and the heat exchanger is now divided in three zones: dry, wet and frosting. The presence of a frost layer has significant impact on hydraulic and energy performances. That is one of the reasons why the study of the frost formation in single room ventilation heat exchanger is so important, especially in cold climates. The numerical model is validated through experimental investigations. Then, several strategies under frosting conditions are presented. Advantages and drawbacks of each method in terms of practical implementation are also discussed. A method of evaluation based on the determination of an "energy" factor is proposed in order to compare the different strategies.

- **The fifth chapter** first presents the features of the developed single room ventilation with heat recovery unit. Then, the experimental investigations carried out on the several components of the final unit are presented. Each of them has first been tested separately during the development step of the unit. Then, experimental investigations are carried out on the entire final unit in climatic chamber. Thanks to these experimental results, a performance map of the unit is established. This performance map allows to evaluate the potential of the use of the device compared to other systems. A comparison of the unit with those of other ventilation systems by means of the Heating Degree Day (HDD) method is realized. This latter allows to

show some trends at a regional/national scale. Moreover, this method allows comparing two heat recovery ventilation systems by only one single equation involving the heat exchanger efficiency and the Specific Fan Power (SFP).

- **<u>The last chapter</u>** concerns the conclusions and the perspectives related to this work. Some recommendations concerning the device are also given.

9   REFERENCES

Andersson, J., 2013. *Swedish experience with airtight ductwork.* REHVA Journal - January 2013

Anon. 2000. *Nettoyer et décontaminer les gaines de climatisation*, L'entrepreneur, juin/juillet 2000, N° 164, pp. 42-43 Buildings Performance Institute Europe, (BPIE). 2011.

ASHRAE. 2009. *Handbook – Fundamentals*. SI Edition. 2009.

Barbat, M., Feldmann, 2010. *Besoins et méthodes de nettoyage des conduits d'air en France.* AIVC. Ventilation Information Paper n° 34. Juillet 2010.

Berglund B, Lindvall T, Schwela DH, editors. *Guidelines for Community Noise.* Geneva: World Health Organization; 1999.

Brasche, S., Bischof, W. 2005. *Daily time spent indoors in German homes – Baseline data for the assessment of indoor exposure of German occupants.* Int. J. Hyg. Environ.-Health 208 (2005) 247-253

Braubach, M., Jacobs, D., Ormandy, D. 2011. *Environmental burden of disease associated with inadequate housing. A method guide to the quantification of health effects of selected housing risks in the WHO European Region.* Summary report. WHO, 2011.

Carrer et al. 2012. *Health and ventilation : review of the scientific litterature.* HealthVent project. Report Word Package 4. 2012.

DGTRE. 1998. *La ventilation des logements.* Document written by «La Direction Générale des Technologies de la Recherche et de l'Energie » du ministère de la Région Wallonne.

Dimitripoulo, C., 2012. *Ventilation in European dwellings: A review*. Building and environment 47 (2012) 109-125

Durier, F. 2008. Trends in the French building ventilation market and drivers for changes. In: AIVC editor, editor.

Ecolot design. 2012. Supplements to Preparatory Study on Residential Ventilation LOT 10. 2012. Fachinstitut Gebäude-Klima e.V.

EN13779. 2007. *Ventilation for non-residential buildings – Performance requirements for ventilation and room conditioning systems.* European Standard written by European Committee for Standardization

EN 15251. 2007. *Indoor environmental input parameters for design and assessment of energy performance of buildings addressing indoor air quality, thermal environment, lighting and acoustics.* European Standard written by European Committee for Standardization

EURIMA, Ecofys. *Renovation tracks for Europe up to 2050.* 2012.

Eurostat, 2011. *Europe in figures- Eurostat year book 2011.* http://www.epp.eurostat.ec.europa.eu

Fehrm M, Reiners W., Matthias Ungemach, M. 2002. *Exhaust air heat recovery in buildings.* International Journal of Refrigeration 25 (2002) 439–449

Fernandez-Seara , J., Diz, R., Uhia, F., Dopazo, A., Ferro, M., 2010. *Experimental analysis of an air-to-air recovery unit for balanced ventilation systems in residential building.* Energy conversion and management (2010)

Fisk, W., Mirer, A., Mendell, M. 2009. *Quantitative relationship of sick building syndrome symptoms with ventilation rates.* Indoor Air Journal. Volume 19, 2009.

Gendebien, S. 2011. *Economic and environmental impacts of several retrofit options for residential buildings (Bottom up approach).* Master thesis. HEC/ULG. http://orbi.ulg.ac.be/handle/2268/133961

Green + project. 2014. Website: http://www.labothap.ulg.ac.be/cmsms/index.php?page=green

Handel, C., 2011. *Ventilation with heat recovery is a necessity in « nearly zero » energy buildings.* REHVA Journal – May 2011.

IBSA. 2013. Institut Bruxellois de Statistique et d'Analyse.
https://monitoringdesquartiers.irisnet.be/

International Energy Agency. 2011. *Key World energy statistics*.

International Energy Agency. 2008. *Energy efficiency requirements in building codes, energy efficiency policies for new buildings*.

Institut National des statistiques. INS 2014. *Le parc de bâtiment.*
http://statbel.fgov.be/fr/statistiques/chiffres/economie/construction_industrie/parc/

Jenkins, P., Phillips, T., Mulberg, E., Hui, S. 1992. Activity patterns of Californians: Use of and proximity to indoor pollutant sources. Atmospheric Environment. Part A. General Topics Volume 26, Issue 12, August 1992, Pages 2141–2148

Kragh, J., Rose, J., Nielsen, T.R., Svendsen, S. 2008. *New counter flow heat exchanger designed for ventilation systems in cold climate.* Energy and buildings 39, (2008), 1151-8

Kurnitski, J., Seppanen, OA. Trends and drivers in the Finnish ventilation and AC market. In: AIVC editor. Ventilation information papers. Brussels: AIVC 2008.

Laverge J., Van den Bossche, N., Heijmans, N., Janssens, A. 2011. *Energy saving potential and repercussions on indoor air quality of demand controlled residential ventilation strategies.* Building and environment 46 (2011) 1497-1503

Lawrence Berkeley National Laboratory (LBNL). *Indoor Air Quality. Scientific Findings Resource Bank.* Website: http://www.iaqscience.lbl.gov/sfrb.html

Leech, J.A., Nelson, W.C., Burnett, R.T., Aaron, S., Raizenne, M.E., 2002. *It's about time: a comparison of Canadian and American time-activity patterns.* J. Expo. Anal. Environ. Epidemiol. 12, 427–432.

Liddament, MW. 1996. *A guide to energy efficient ventilation.* Air infiltration and Ventilation Centre, ISBN 0 946075 85 9; 1996

Liddament M.W., Orme, M., 1998. *Energy and ventilation.* Applied Thermal Engineering 18 (1998) 1101-1109

Chapter I: Introduction

Manz. H., Huber, H., Schalin A., Weber, A., Ferrazzini M., Studer, M., 2000. *Performance characterization of single room ventilation unit with recuperative or regenerative heat recovery.* Energy and building 31 (2000) 37-47

Maripuu, M-L, 2011. *Demand controlled ventilation (DCV) for better IAQ and energy efficiency.* REHVA journal. March 2011

NBN S01-400-1. *Norme nationale belge. Critères de l'isolation acoustique pour les immeubles d'habitation.* Janvier 2008.

Norwegian University of Science and Technology. *The effect of renovation and reconstruction on overall energy consumption and material throughput in the Norwegian residential building.* 2011.

Lysen. 1996. *The trias Energica: Solar energy Strategies for Developing Countries.* Eurosun Conference, Freiburg, 16-19 Sept 1996.

Mardiana-Idayu, A., Riffat, S.B., 2012. *Review on heat recovery technologies for building applications.* Renewable and Sustainable Energy Reviews 16 (2012) 1241– 1255

Marianu, A. and Riffat, S.B. 2013. Review on physical and performance parameters of heat recovery systems for building applications. Renewable and Sustainable Energy Reviews 28 (2013) 174-190

Nasif S., M., (2008). *Analysis and modeling of membrane heat recovery exchanger in HVAC energy recovery systems.* Ph.D., School of Mechanical and Manufacturing Engineering, The University of New South Wales, Sydney-Australia

NBN D50-001. 1991. Belgian Standard. *Ventilation systems for housing.* October 1991.Institut Belge de Normalisation (NBN).

Pérez-Lombard, L., Ortiz, J. and Pout, C. 2008. *A review on buildings energy consumption information.* Energy and building, vol. 40, pp. 394-398, 2008.

Roulet, C.-A.,. Heidt F.D, Foradini F., Pibiri M.-C. 2001. *Real heat recovery with air handling units*, Energy and Buildings 33 (2001) 495–502.

Seppanen, O. 2012. *Existing buildings, building codes, ventilation standards and ventilation in Europe.* Final Report. Word Package 5 of the HealthVent project. REHVA.

Simonson, C., 2005. *Energy consumption and ventilation performance of a naturally ventilated ecological house in a cold climate.* Energy and buildings 37 (2005) 23-35

Schwenzfeier, L., Akoua, J-J., Bianchina, M., Buseyne, S., Limoges, D., and Morel, R. 2009. *Use of compact balanced single room ventilation units with heat recovery in existing dwellings.* Proceedings of the 2009 AIVC Conference, Berlin.

SPF Economie (2013). http://economie.fgov.be/fr/.

T'Joen, C., Park, Y., Wang, Q., Sommers, A., Han, X., Jacobi, A. 2009. *A review on polymer heat exchangers for HVAC & R applications.* International Journal of Refrigeration, 32 (2009), pp. 763- 779

U.S. Environmental Protection Agency. 1989. Report to Congress on indoor air quality: Volume 2. EPA/400/1-89/001C. Washington, DC.

Wouters, P., Van den Bossche, P. 2005. *Ventilation system quality for dwellings: a pragmatic approach.* AIVC 26th conference - Brussels, Belgium, 21-23 September 2005 - pp 187

Wouters, P., Heijmans, N., Delmotte, C., Van den Bossche, P., Wuyts, D. 2008. *Trends in the Belgian building ventilation market and drivers for change.* AIVC. Ventilation Information Paper n° 18. May 2008.

Zhang, L. Z., and Jiang, Y., 1999. *Heat and Mass Transfer in a Membrane-Based Energy Recovery Ventilator.* J. Membr. Sci., 163, pp. 29–38.

Zhang, L. Z., Jiang, Y., and Zhang, Y. P., 2000. *Membrane-Based Humidity Pump: Performance and Limitations*, J. Membr. Sci., 171, pp. 207–216.

Zhang, L.Z. and Niu J.L., 2002. *Effectiveness Correlations for Heat and Moisture Transfer Processes in an Enthalpy Exchanger With Membrane Cores.* J. Heat Transfer, Vol. 124, Issue 5, 2002

Zhou Y.P., Whu J.Y., Wang R.Z., 2006. *Performance of energy recovery ventilator with various weathers and temperature set-points.* Energy and Buildings, Vol.39, No.12

CHAPTER II:

DEVELOPMENT OF A VENTILATION HEAT RECOVERY EXCHANGER SIMULATION MODEL

CHAPTER II: DEVELOPMENT OF A VENTILATION HEAT RECOVERY EXCHANGER SIMULATION MODEL

1   INTRODUCTION

This chapter focuses on the development of a **simulation model** of an air-to-air heat exchanger dedicated to heat **recovery ventilation**. Numerical and experimental investigations on an off-the-shelf heat exchanger have been carried out in a **"reverse engineering"** objective, in order to validate some assumptions/correlations useful in the design step of the heat recovery exchanger dedicated to single room ventilation unit (see Chapter 3).

While such exchangers have been on the market for many years, only a few experimental and modeling works are presented in technical and scientific literature. Adamski (2009) carried out experimental studies and developed correlations on a longitudinal flow spiral recuperator, but did not investigate the wet regime. Fernandez-Seara et al. (2011) experimentally studied an air-to-air heat recovery device for balanced ventilation but did not develop a thermal and hydraulic performance prediction model. Kragh et al. (2008) also experimentally investigated a new counter-flow heat exchanger but focused more precisely on the freezing issue.

A thermoeconomic investigation was carried out by Söylemez (2000) in order to optimize heat recovery exchanger size. Adamski (2008, 2010) also estimated the financial effect due to the use of heat recovery ventilation instead of a simple ventilation system.

The **studied air-to-air heat exchanger in this chapter** is **really similar** to the system developed in the frame of this thesis in its form (polystyrene heat exchanger), its volume, its flow configuration (quasi counter-flow configuration) and its purpose (dedicated to single room ventilation unit).

Accurate and robust simulation models, able to predict the behavior in **dry and partially wet regimes**, are needed when designing/ sizing a ventilation heat recovery exchanger and evaluating its thermal and hydraulic performance. Quantification of the condensate flow rate (and thus the latent heat transfer rate) is also an important issue in the design process of such systems mainly in order to size the condensate evacuation system.

Such models are also convenient to better predict the seasonal performance of the heat exchanger by taking into account the **latent part of the heat transfer rate**. This can be done by integrating the system model into an hourly based **building energy simulation model**. These models can also be used to investigate some strategies to avoid **freezing** in the heat exchanger.

A **numerically robust** and **computationally efficient model** of a ventilation heat recovery exchanger is proposed. It is derived from several existing cooling coil models. Partially wet regime operation is modeled through a moving boundary approach that allows for the possibility to distinguish the portion of the heat exchanger where water condensation appears. This new moving boundary model is first **successfully validated** by means of an experimental **cooling coil data set**. The model is also quantitatively compared to different stand-alone methods. As already mentioned by Morisot (2000), application of a cooling coil model to describe a ventilation heat recovery exchanger is not a new idea. However, to the authors' best knowledge, there **is no extensive experimental validation of such models in the scientific literature**.

In order to gather performance points with a view to calibrating and **validating the model for air-to-air application**, an experimental study was conducted. A **test rig** was designed in such a way to reproduce a large range of operating conditions of the heat exchanger. Measured performance points are thoroughly detailed in this chapter. Contrary to Rose et al. (2008) who partially assessed their 1D heat exchanger model by comparing experimental and simulation results through only one single

experimental point, a **detailed validation of the model in dry and partially wet conditions** is presented in the present chapter. Nielsen et al. (2009) used the same model to investigate a few strategies for defrosting in cold climate.

After a short presentation of the investigated heat exchanger, the first part of the chapter presents a semi-empirical model based on the physical characteristics of the off-the-shelf heat recovery device and relying on empirical correlations available in the literature for the **convective heat transfer coefficients**. In the case of partially wet regime, a moving boundary model is applied in order to predict sensible and latent heat transfer rates. The **moving boundary** model is presented and validated thanks to **cooling coil data set**. A model developed with friction factor coefficients estimated by correlations from the literature is also presented in order to predict the **hydraulic performance** in dry conditions.

The second part of the chapter describes the **experimental investigation** conducted on the off-the-shelf heat exchanger. Experimental data are used to tune correlations for the determination of the convective heat transfer coefficient and **validate the proposed simulation model** of the ventilation heat recovery exchanger in partially wet conditions. It will be shown that the model developed to determine the hydraulic performance with existing correlations for the friction factor coefficient does not require a calibration.

Finally, examples of use of the developed model are presented, which includes **coupling the model with a building simulation model**, a study of the **influence of the humidity** on the evolution of the latent and sensible heat transfer rates and **strategies to avoid freezing in the heat exchanger**.

2 SIMULATION MODEL OF THE VENTILATION HEAT RECOVERY

2.1 Presentation of the investigated device

The investigated ventilation air-to-air heat recovery exchanger is actually dedicated to residential building and more precisely to single room ventilation. It is made of several corrugated plates in synthetic material, as shown in Figure II-1.
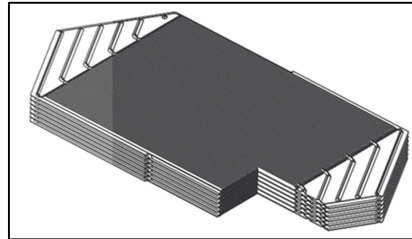
Figure II-1: Polystyrene heat exchanger

The central (main) region of the heat exchanger is in counter-current arrangement and is composed of parallel triangular ducts as shown in Figure II-2.
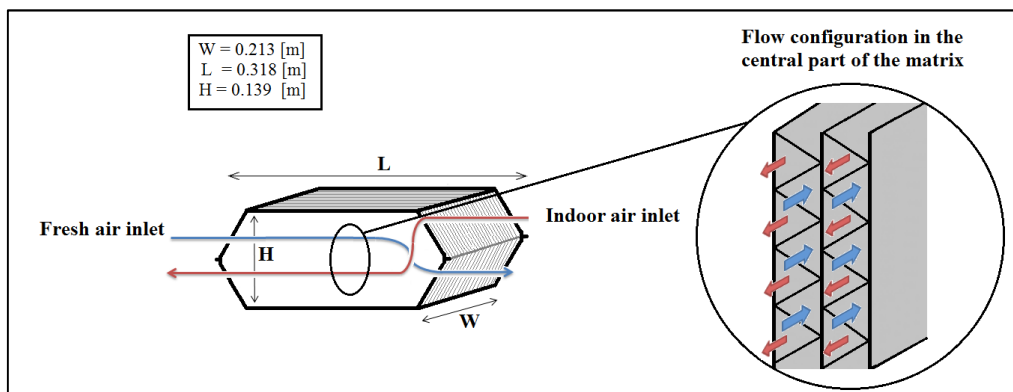
Figure II-2: Schematic representation of the studied exchanger

The inlet and outlet regions of the heat exchanger are in cross-flow arrangement and are composed of channels with rectangular cross-sections. Flow configuration inside the heat exchanger is schematically represented in Figure II-3.
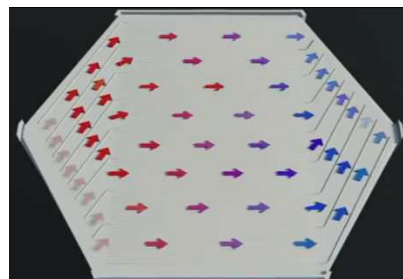
Figure II-3: Flow configuration inside the heat exchanger

The air flows operating range investigated in the present study (for both indoor and fresh air streams) has been chosen between 30 and 100 m³/h. It should be noticed that the study employs the same ratio of maximum to minimum air flow rate as the one presented by Fernandez et al. (2011).

2.2 Development steps

Development of the semi-empirical **thermal model** is achieved with the following steps:

- The thermal effectiveness in dry regime is determined: the heat exchanger is divided in three parts (as explained in section 2.3). Determination of the effectiveness requires the knowledge of the heat transfer convective coefficients that are estimated by correlations for indoor and fresh air flows. Selection of these correlations is also justified below.

- A moving boundary model is used to predict sensible and latent heat transfer rates in partially wet conditions (section 2.4).

- Finally, a solving procedure able to determine the heat exchanger operation regime is presented in section 2.5.

The **hydraulic performance model** is based on the same approach as the thermal performance model:

- The pressure drop is calculated by dividing the heat exchanger in three parts, as explained in section 2.6.

- Determination of the hydraulic performance requires the knowledge of the friction factor value that is determined by correlations for both sides. Selection of these correlations is also justified in section 2.6.

2.3 Thermal performance prediction in dry conditions

The developed model is based on the classical ε-NTU method. The model relies on the method exposed by Nasif et al. (2005) by dividing the heat exchanger into several zones (three in our study case), as shown in Figure II-4.
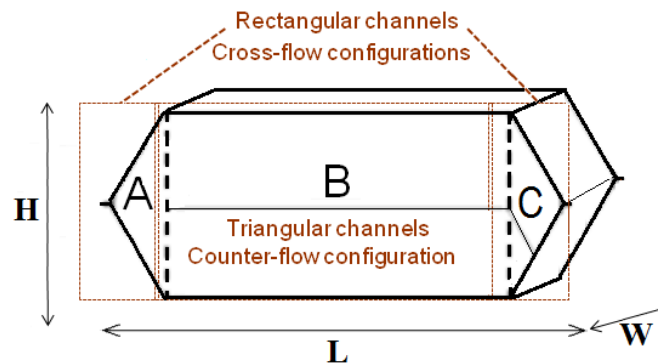
Figure II-4: Parts of the heat exchanger and mean distance considered

This division is employed because the geometries of the different zones are different. The passage channels of the parts A and C have a rectangular cross-section while the passage channels of the part B have a triangular cross-section. Moreover, the configurations are in counterflow arrangement in part B and in crossflow arrangement in parts A and C.

Effectiveness is determined for each parts of the exchanger in a classical way. As an example, effectiveness of part A is determined by the Ɛ-NTU method. The minimal and maximal capacity flow rates are given by Equations II-1 and II-2, where $\dot{C}_{ind}$ and $\dot{C}_{fresh}$ are the indoor and fresh air capacity flow rates in [W/K] respectively:

$$\dot{C}_{min} = \min\left(\dot{C}_{ind}; \dot{C}_{fresh}\right) \qquad \text{II-1}$$

$$\dot{C}_{max} = \max(\dot{C}_{ind}; \dot{C}_{fresh}) \qquad \text{II-2}$$

C_r [-] is the heat capacity ratio and is defined by Equation II-3 :

$$C_r = \frac{\dot{C}_{min}}{\dot{C}_{max}} \qquad \text{II-3}$$

The convective heat transfer coefficient h in [W/m²-K] for both sides of the equivalent heat exchanger is approximated by the weighted average of the value of each region:

$$h = h_A \cdot prop_A + h_B \cdot prop_B + h_C \cdot prop_C \qquad \text{II-4}$$

Fractions $prop_A$, $prop_B$ and $prop_C$ correspond respectively to the ratio of the heat transfer areas of each zone A, B and C to the total heat transfer area of the heat exchanger. Numerical values of these fractions for the currently investigated heat exchanger are given in Table II-1. The sum of these fractions is equal to one.

Table II-1 : Heat transfer area ratio

Zone	prop [%]
A = C	2.8%
B	94.4%

Heat transfer resistances R_{ind}, R_{fresh} and R_w in [K/W] are expressed as functions of the convective heat transfer coefficients h_{ind} and h_{fresh} in [W/m²-K] and the conductivity of the material plates k_w in [W/m-K], by means of Equations II-5, II-6 and II-7:

$$R_{ind} = \frac{1}{A_{hx} \cdot h_{ind}} \qquad \text{II-5}$$

$$R_{fresh} = \frac{1}{A_{hx} \cdot h_{fresh}} \qquad \text{II-6}$$

$$R_w = \frac{e_{plate}}{A_{hx} \cdot k_w} \qquad \text{II-7}$$

The overall heat transfer conductance AU in [W/K] is given by Equations II-8:

$$AU = \frac{1}{R_{ind} + R_{fresh} + R_w} \qquad \text{II-8}$$

For part A and C of the heat exchanger with a crossflow configuration, its effectiveness is given by the commonly-used Equation II-9, given in Incropera and DeWitt (2002):

$$\varepsilon_A = 1 - exp\left[\frac{NTU^{0.22}}{C_r} \cdot \left(exp[-C_r \cdot NTU^{0.78}] - 1\right)\right] \qquad \text{II-9}$$

With NTU, the number of transfer unit [-]:

$$NTU = \frac{AU}{\dot{C}_{min}} \qquad \text{II-10}$$

For the part B of the heat exchanger, the effectiveness is also given by Equation II-11 (Incropera and De Witt (2002)):

$$\varepsilon_B = \frac{1 - exp[-NTU(1 - C_r)]}{1 - C_r \, exp[-NTU(1 - C_r)]} \qquad \text{II-11}$$

As suggested by Nasif et al. (2005), the entire heat exchanger effectiveness ε corresponds to the weighted average of effectiveness of each region (Equation II-12):

$$\varepsilon = \varepsilon_A \cdot prop_A + \varepsilon_B \cdot prop_B + \varepsilon_C \cdot prop_C \qquad \text{II-12}$$

The proposed method based on a weighted average value for the convective heat transfer coefficient has been compared to a discretized model method. This latter consists in dividing the heat exchanger into discrete elements (parts A, B and C in our cases). Due to the high relative value of $prop_B$, the difference between these two methods is insignificant (difference of less than 0.75% in terms of effectiveness in dry regime). The weighted average model has been selected because it allows an easier implementation of the moving boundary model than the discretized model.

The Reynolds number Re [-] is required to determine the regime in the heat exchanger. Definition of the Reynolds number is given by Equation II-13:

$$\text{Re} = \frac{v \cdot D_h}{\nu} \qquad \text{II-13}$$

with:

- v in [m/s], the mean velocity of the air through the matrix;
- D_h in [m], the hydraulic diameter of channels of the matrix. This latter corresponds to the ration between four times the cross sectional area and the wetted perimeter of the cross section;
- ν in [m^2/s], the kinematic viscosity of air.

The hydraulic diameter is equal to 3.9 mm for part A and C and 1.6 mm for part B. For a maximum flow rate of 100 m^3/h, the velocity for part A and C is 3.6 m/s and 2.1 m/s for part B. These considerations involve a Reynolds Number of 960 for part A and C and 230 for part B. The Reynolds number is always less than 1000, in this study and as a result, the correlations selected for the present model are valid only for the laminar regime.

Regarding the calculation of the Nusselt and the Colburn numbers (required to estimate the convective heat transfer coefficients), two different correlations are applied: one for the rectangular channels (part A and C) and one for the triangular channels (part B).

The Nusselt correlation used for the part A and C is the one provided for a uniform heat flux in the library of EES software (2013) and described by Nellis and Klein (2009).

Wall temperature (approximated by the mean temperature between hot and cold fluid) is assumed to be constant through parallel flow exchangers. In contrary, uniform heat flux is assumed to be constant

in counter flow heat exchanger (temperature difference is anywhere the same), as represented in Figure II-5.
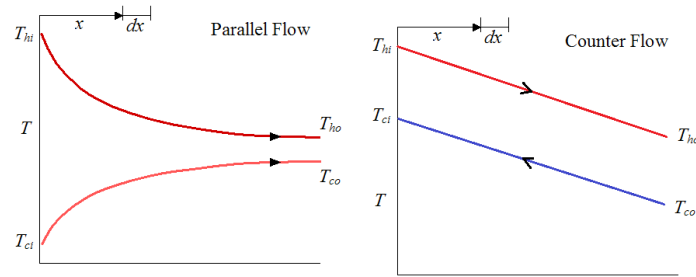
Figure II-5 : Temperature evolution in a parallel and counter flow heat exchanger

In cross flow configuration (as in part A and C), the correlation choice is not so obvious since the 2D temperature evolution inside the heat exchanger, as represented in Figure II-6.

Figure II-6 : Temperature evolution in a parallel and counter flow heat exchanger

For parts A and B, correlations for a uniform heat flux were arbitrarily preferred since the major part of the heat exchanger (part B) is in counter flow configuration. Due to the small relative part of section A and C, it is important to notice that the influence of the correlation selected for these sections is quite negligible (less than 0.4% in term of effectiveness).
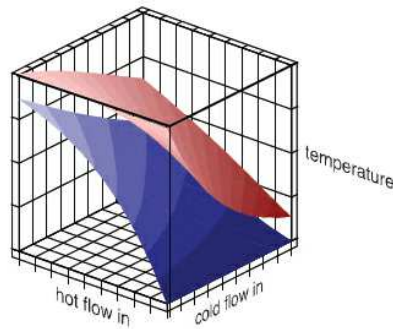
Hesselgreaves (2001) distinguishes the fully developed and the developing laminar flows (entrance region effect). The heat transfer parameters in developing flow are dependent on the Prandtl number, unlike the fully developed case where there is no dependence on Prandtl number.

The Nusselt number for a constant heat flux (Nu_H) is determined by adding the entrance region effect (DNu_H) and the Prandtl number effect terms (*DNurat*) to the fully developed Nusselt number that is exposed to a uniform flux ($Nu_{H,fd}$), as shown in Equation II-14:

$$\mathrm{Nu}_H = \mathrm{Nu}_{H,fd} + DNurat \cdot DNu_H \qquad\qquad \text{II-14}$$

The constant heat flux correlation for Nusselt hydrodynamically and thermally fully developed that is exposed to a uniform heat flux $Nu_{H;fd}$, is provided by Shah and London (1978) through Equation II-15:

$$Nu_{H,fd} = 8.235 \cdot (1 - 2.0421 \cdot Aspect + 3.0853 \cdot Aspect^2 - 2.4765 \cdot Aspect^3 \qquad \text{II-15}$$
$$+ 1.0578 \cdot Aspect^4 + 0.1861 \cdot Aspect^5)$$

'Aspect' corresponds to the ratio of the minimum to maximum dimensions of the duct.

For rectangular section ducts, for simultaneously developing velocity and temperature boundary layer which are more likely to be characteristics of real situations the Nusselt numbers for Prandtl number equal to 0.72 are given by the data of Wibulswas (1966). Two intermediate calculation parameters A_H and B_H are used to determine the entrance region effect term DNu_H, given by Equations II-16, II-17 and II-18:

$$A_H = 0.113636994 + 0.712134212 \cdot Aspect - 0.392104717 \cdot Aspect^2 \qquad \text{II-16}$$

$$B_H = \begin{cases} 0.9403 + Aspect \cdot (0.6994 - 0.9403)/0.25 & if\ (Aspect < 0.25) \\ 0.77413 - 0.35036 \cdot Aspect + 0.1985 \cdot Aspect^2 & if\ (Aspect \geq 0.25) \end{cases} \qquad \text{II-17}$$

$$DNu_H = A_H \cdot exp^{(-B_H \ \cdot \ lnx_{star})} \qquad \text{II-18}$$

The dimensionless thermal length appropriate for a thermally developing flow x_{star} is defined by Equation II-19:

$$x_{star} = \frac{L/D_h}{(Re \cdot Pr)} = \frac{1}{Gz} \qquad \text{II-19}$$

The dimensionless length x_{star} is also referred as the inverse of the Graetz number.

The Prandtl number effect is taken into account by interpolating a table of data for a square duct (Aspect = 1) provided by Kakaç et al. (1987). The Prandtl number effect term DNurat is estimated by Equation II-20:

$$DNurat = \begin{cases} 0.6847 + 0.3153 \ \cdot exp^{(-1.2654459 \ \cdot (ln(Pr) - ln(0.72))} & if\ (Pr > 0.72) \\ 1.68 - 0.68 \ \cdot \ exp^{(0.32 \ \cdot (ln\ (Pr) - l\,n(0.72)))} & if\ (Pr \leq 0.72) \end{cases} \qquad \text{II-20}$$

If the length of the duct is infinite and the Prandtl number is equal to 0.72, the calculated Nusselt is equal to the fully developed one.

The convective heat transfer h in [W/m²-K] coefficient for part A and C is determined by Equation II-II-21:

$$h_a = \frac{Nu_H \ \cdot \ k_a}{D_{h,a}} \qquad \text{II-21}$$

Concerning the part B, the Colburn values proposed by Kays and London (1984) and provided in the library of EES software (2013) were used as shown in Figure II-7. This correlation is dedicated to matrices composed of isosceles triangular flow passages.
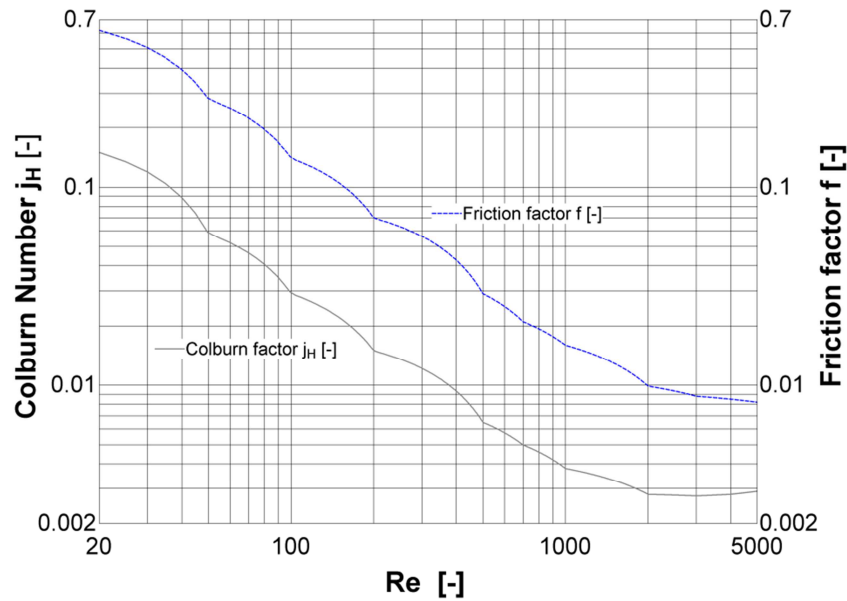
Figure II-7: Interpolation of data provided by Nellis and Klein (2009) for the Colburn and friction factor number

The relation between the convective heat transfer coefficient h in [W/m^2- K] and the non-dimensional Colburn factor $j_{H;a}$ is given by Equation II-22:

$$h_a = \frac{G_a \cdot j_{H,a} \cdot cp_a}{Pr_a^{2/3}}$$

II-22

As explained in Section 5.2, these latter correlations (and hence the value of the Colburn factor) will be calibrated by means of experimental results in dry regime.

2.4 Thermal performance in wet/partially wet regime

2.4.1 Investigated regimes

In heat recovery devices, three regimes can be defined (if the frost formation is not taken into account):

- **Totally dry regime:** no water condensation occurs in the heat exchanger;

- **Totally wet regime:** condensation appears directly at the inlet of the heat exchanger (the inlet surface temperature is inferior to the dew point temperature);

- **Partially wet regime:** condensation occurs in the heat recovery device but not directly (there are a dry and a wet parts of the heat exchanger).

A schematic representation of the partially wet regime is given in Figure II-8. The two parts of the heat recovery device can be observed: the dry zone and the wet zone. At the boundary between these two parts, the wall surface temperature equals to the dew point temperature of the cooling air at the heat exchanger supply.
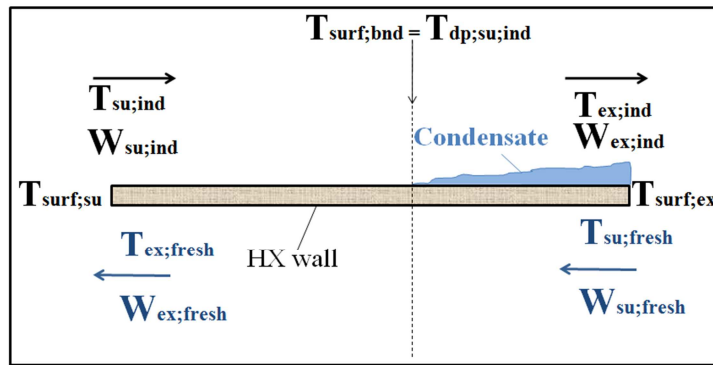
Figure II-8: Schematic representation of the partially wet regime

Due to similarities in terms of regime, it was decided to apply a cooling coil model to our heat recovery exchanger, as previously suggested by Morisot (2000).

2.4.2   Development of a new cooling coil model applicable to heat recovery

The literature proposes a large number of cooling coil models. Two kinds of cooling coil models can be identified: **detailed** and **simplified** ones.

The **detailed** models are often discretized in a finite number of sections called control volumes. These models are generally quite complex and involve a good knowledge of the geometry. Wang and Hihara (2003) proposed a method that aims to simplify the calculation in each control volume and distinguish the three cooling regimes (totally wet, partially wet and totally dry). Wang et al. (2007) proposed to decouple the sensible and the latent heat transfer modes assuming a constant value of the sensible heat ratio (ratio between the sensible and the total heat transfer rate), so called SHR, and the saturation curve slope within a small piece of the cooling coil. Both the SHR and the curve slope are determined by an iterative solution of the unknown conditions of the air, coil surface and chilled water.

The **simplified** models use a restricted number of parameters to describe and characterize the cooling coil. Wang et al. (2004) proposed a simple, yet accurate, steady state cooling coil model, involving only three parameters. The model can be employed for real time control and optimization of HVAC systems. This model is also the origin of a dynamic model developed by Jin et al. (2006) which aims to predict the transient cooling coil performance.

The developed simulation model of the heat recovery exchanger is built on the **basis of three "simplified" models** specifically developed to describe the heat and mass transfers in cooling coils. These are the models presented by Lebrun et al. (1990), Brandemuehl et al. (1993) and Morisot et al. (2002).

All of these three models present advantages and drawbacks. The main advantage of models developed by Lebrun et al. (1990) and Morisot et al. (2002) is their simplicity since they rely on Braun's hypothesis to describe the partially wet regime. Braun's hypothesis (1988) considers simultaneously fully dry and fully wet regimes and considers that the regime to be selected (totally wet or totally dry) is the one leading to the maximal cooling capacity [W].

$$\dot{Q}_{tot} = \max(\dot{Q}_{dry}; \ \dot{Q}_{wet}) \qquad\qquad \text{II-23}$$

Braun showed that this approximation generally leads to an error lower than 5% on the prediction of the total energy rate. Lebrun's and Morisot's models show good behavior and performance

predictions, except in the case of cooling coil operation with a SHR close to unity. This is related to the Braun's hypothesis that assumes the coil to be completely dry when the SHR is close to unity.

On the contrary, the Brandemuehl's model (1993) introduces a moving boundary which yields good performance prediction even for SHR close to unity. Also, Morisot's model presents a solution procedure that can be used to quickly identify the regime. This procedure has been considered in the present model and applied to our heat recovery device, as explained in section 2.5.

The model developed in the frame of this thesis describes the partially wet regime in the same way as Brandemuehl et al. (1993). It divides the heat transfer area of the cooling coil into two parts: a totally dry portion and a totally wet portion. These portions are separated by a moving boundary, whose position is determined by means of the surface temperature. In reality, this method requires two interlinked iterations, as illustrated in Figure II-12:

- A first loop iterating on the wet surface area fraction (location of the boundary). The wet surface is delimited by a surface temperature equal to the entering air dewpoint.

- A second loop iterating on the water temperature at boundary for a given wet surface area fraction.

The solving procedure determines the cooling capacity by identifying the dry and the wet parts of the coil in the considered operating conditions. Cooling coil is considered to be locally wet when the surface temperature is equal to or below the supply air dewpoint temperature.

In the totally wet cooling coil model of Brandemuehl et al. (1993), water enthalpies are replaced by "fictitious fluid" enthalpies, defined as the enthalpy of saturated air at the temperature of the water. The difference between the model developed for heat recovery device and the one proposed by Brandemuehl et al. (1993) concerns the description of the totally wet portion of the heat exchanger. Here, in the new developed model, the wet regime is described in the same manner as proposed by Lebrun et al. (1990): a fictitious perfect gas whose enthalpy is fully defined by the actual wet bulb temperature replaces the air. The replacement of the moist air (the indoor one in winter and the fresh one in summer) instead of water (which is present in a cooling coil and not in an air-to-air heat exchanger) by a fictitious fluid is the reason why Lebrun's method to describe the wet part of the heat exchanger was preferred. Indeed, it is directly adaptable and obviously more intuitive and appropriate for an air-to-air exchanger.

The basis equations of the reference model proposed by Lebrun et al. (1990) are given below for a water cooling coil model. The specific heat capacity of the fictitious fluid $cp_{a,fic}$ in [J/kg-K] is given by Equation II-24:

$$cp_{a,fic} = \frac{h_{su,a} - h_{ex,a,wet}}{t_{wb,su,a} - t_{wb,ex,a,wet}} \qquad \text{II-24}$$

The air side thermal resistance of the fictitious fluid $R_{a,fic}$ [K/W] is weight-averaged by the ratio of the specific heat capacity of the air cp_a [J/kg-K] and the specific capacity of the fictitious fluid $cp_{a,fic}$ [J/kg-K]:

$$R_{a,fic} = R_a \; \frac{cp_a}{cp_{a,fic}} \qquad \text{II-25}$$

Knowing the effectiveness in wet regime (on the basis of the convective resistance), the heat transfer rate for the wet regime $\dot{Q}_{wet}$ [W] can be obtained through the two following relationships. The first one (Equation II-26) involves the coil effectiveness $\varepsilon_{coil,wet}$ in wet regime, the wet bulb supply temperature of the moist air $T_{wb,su,a}$ and the supply water temperature $T_{su;w}$. The second one (Equation II-27) involves the supply and exhaust wet bulb of the moist air.

$$\dot{Q}_{wet} = \varepsilon_{coil,wet} \cdot \dot{C}_{min,wet} \cdot (T_{wb,su,a} - T_{su;w})$$
II-26

$$\dot{Q}_{wet} = \dot{C}_{a,fic} \cdot (T_{wb,su,a} - T_{wb,ex,a,wet})$$
II-27

with the capacity flow rate [W/K] of the fictitious fluid given by Equation II-28:

$$\dot{C}_{a,fic} = \dot{M}_a \cdot cp_{a,fic}$$
II-28

As also proposed in the Brandemuehl et al. (1993) model, a fictitious semi-isothermal heat exchanger is considered to determine the outlet air conditions. One of the two fluids supplying this heat exchanger is the air; the other one is a fictitious fluid of infinite capacity flow rate, whose uniform temperature is supposed to correspond to the average temperature of the external surface of the coil, also called "surface" temperature.

2.4.3 Validation of the new developed model through experimental data

Before applying the new developed cooling coil model to our air-to-air heat recovery device, it was decided to validate and compare it to the different stand-alone methods mentioned above: Braun-Lebrun and Morisot models.

Identifications of model parameters

The parameters of the models mentioned above are:

- The air-side heat transfer coefficient in rating conditions,
- The water-side heat transfer coefficient in rating conditions,
- The metal thermal resistance (supposed constant and most of the time neglected).

Two methods are commonly used to identify the values of these parameters:

- Semi-empirical parameter identification using one or several operating points to calibrate the parameters of the simulation model. The use of the operating points is often combined to practical assumptions (e.g. ratio between water-side and metal thermal resistances).
- Deterministic parameter identification relying on empirical correlations based on the geometrical characteristics of the considered coil.

Only the semi-empirical parameter identification method is considered for the cooling model validation. This method has been well described in the case of the Braun-Lebrun model by Lemort et al. (2008) in the frame of IEA-ECBCS Annex 43 project.

Validation of the developed cooling coil model and comparison with stand-alone methods

As already noticed before, three models are investigated:

- Braun-Lebrun model,

-   Morisot model,
-   the new moving boundary model.

The three models have been built and validated in EES (2013) environment. Performance points considered for validating the models come from experimental data collected by Morisot (2002). Except the water flow rate which is almost constant (0.639 kg/s), all the physical quantities are variable. The inlet air temperature is comprised between 17.2 °C and 23.6 °C and the inlet water temperature is comprised between 7.6 °C and 11.3 °C.

The metal thermal resistance was neglected for the three validations. The identified parameters of the three models are:

-   the air-side heat transfer coefficient in rating conditions,
-   the water-side heat transfer coefficient in rating conditions.

Thermal conductance in non-rating conditions is given by Equation II-29:

$$\frac{1}{AU_a} = \frac{1}{AU_{a,n}} \cdot \left[\frac{\dot{M}_{a,n}}{\dot{M}_a} \right]^{0.6} \qquad \text{II-29}$$

The values of the identified model parameters are given in Table II-2:

Table II-2 : Air and water heat transfer coefficients

	Air heat transfer coefficient	Water heat transfer coefficient
"Braun-Lebrun" model	$AU_{a;n}$ = 2000 W/K	$AU_{w;n}$ = 1850 W/K
"Morisot" model	$AU_{a;n}$ = 2415 W/K	$AU_{w;n}$ = 1768 W/K
New Moving boundary model	$AU_{a;n}$ = 2100 W/K	$AU_{w;n}$ = 1900 W/K

The validation is based on four parameters:

-   the total energy exchanged by the water flow and the air stream: $\dot{Q}$
-   the sensible heat ratio: *SHR*
-   the exhaust water temperature: $T_{ex;w;coil}$
-   the exhaust air temperature: $T_{ex;a;coil}$

Braun-Lebrun model

a)   b)
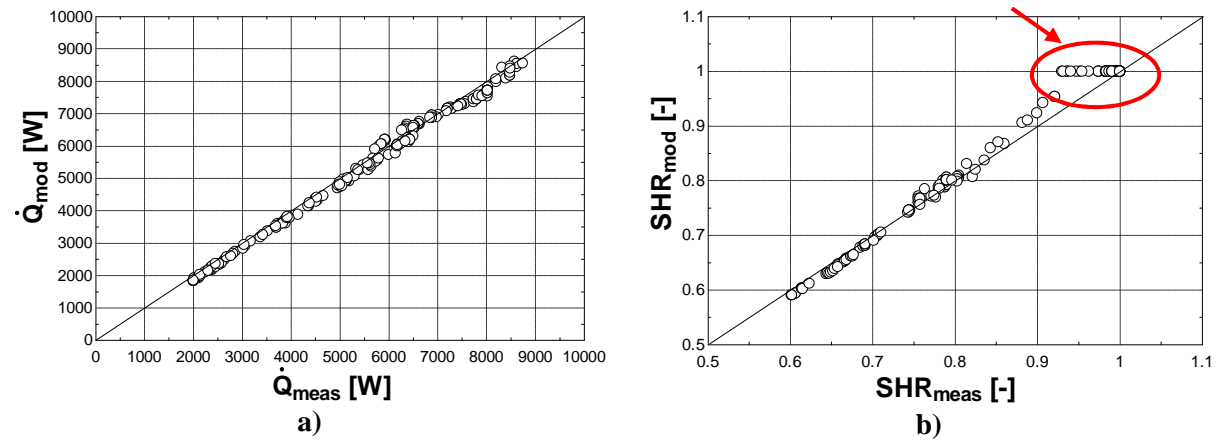
Figure II-9: Comparison of the predictions by the Braun-Lebrun model and the measurement for the cooling capacity a) and SHR b)

Morisot model

b)
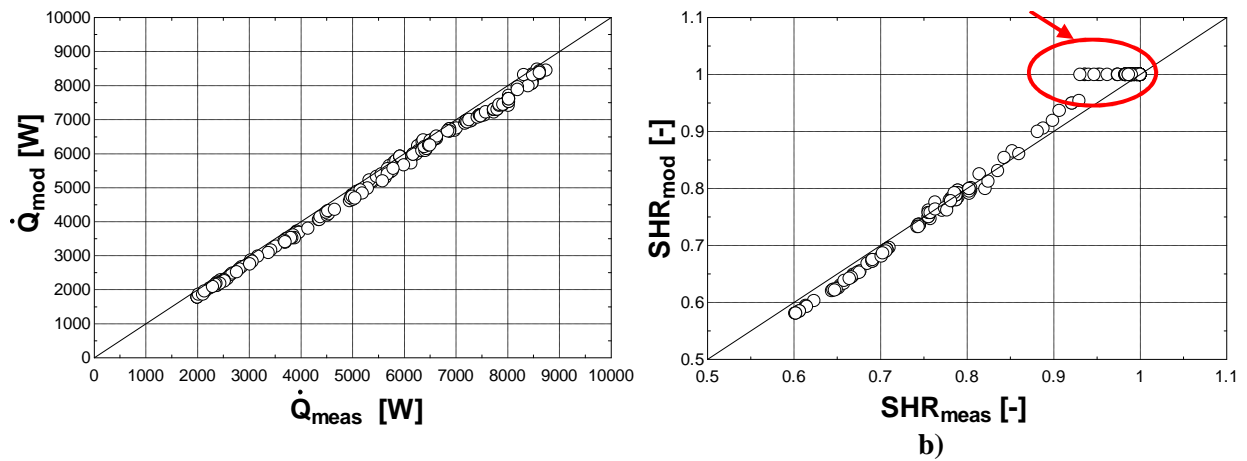
Figure II-10: Comparison of the predictions by the Morisot model and the measurement for the cooling capacity a) and SHR b)

New moving boundary model

a)   b)
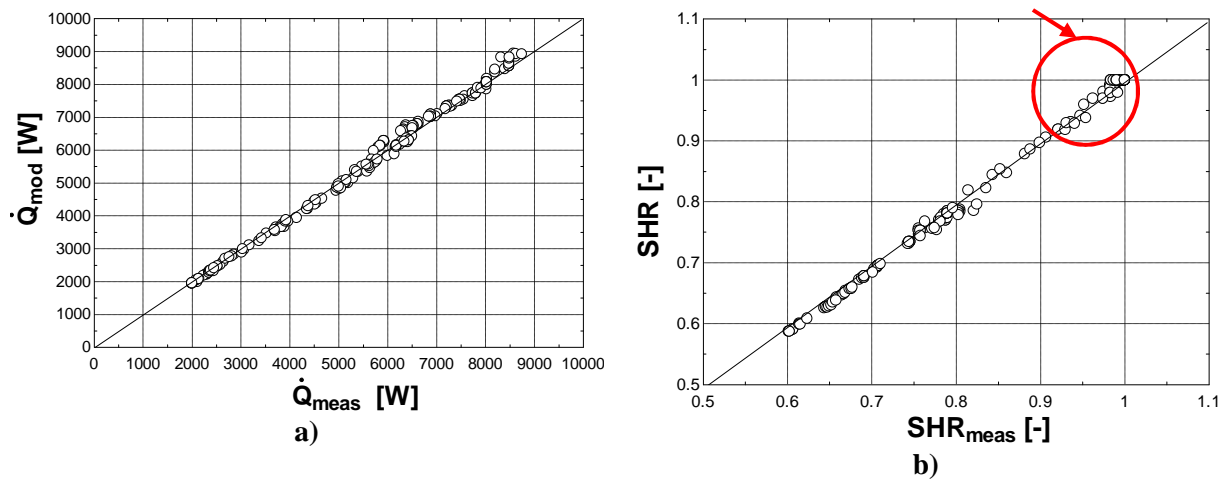
Figure II-11 : Comparison of the predictions by the new moving boundary model and the measurement for the cooling capacity a) and SHR b)

Mean relative errors (for cooling capacity and SHR) and mean absolute errors (for leaving air and water temperature) are given in Table II-3, for the entire data range. It appears that the three models provide satisfying results, in the range of values of the uncertainties on measured energy rate (± 200W) and temperatures (± 0.3K).

Table II-3: Average of absolute value of error and maximal errors for all data range

All data range	Braun-Lebrun		Morisot		Moving boundary	
	AVE	MAX	AVE	MAX	AVE	MAX
Cooling capacity [W] [MRE]	3.5%	8.7%	5.0%	11.7%	2.2%	6.1%
SHR [%] [MRE]	1.3%	7.5%	1.5%	7.4%	1.2%	4.3%
Leaving Air Temp. [K] [MAE]	0.19 K	0.43 K	0.26 K	0.48 K	0.12 K	0.51K
Leaving Water Temp. [K] [MAE]	0.12 K	0.27 K	0.16 K	0.32 K	0.16 K	0.17 K

As shown in Figure II-9 and Figure II-10, the "Braun-Lebrun" and the "Morisot" models have good behavior and performance predictions. The main problem of these two models is that they are not able to represent cooling coil operation for a sensible heat ratio (SHR) around unity. In fact, this problem comes from the Braun's hypothesis: for SHR close to one, Braun's method assumes the coil completely dry. Nevertheless, this approximation does not affect global simulation results. On the contrary, the moving boundary model produces good results even for SHR close to unity, as shown in Figure II-11 and Table II-4. It is one of the main conclusions concerning the new developed model.

Table II-4: Average and maximal errors for measured SHR close to unity
(comprised between 0.9 and 1)

SHR close to unity	Braun-Lebrun		Morisot		Moving boundary	
	AVE	MAX	AVE	MAX	AVE	MAX
Cooling capacity [W] [MRE]	4.2%	8.7%	6.2%	11.7%	2.1%	5.5%
SHR [%] [MRE]	1.3%	7.5%	1.2%	7.4%	0.5%	1.7%
Leaving Air Temp. [K] [MAE]	0.22 K	0.43 K	0.27K	0.48 K	0.13 K	0.32 K
Leaving Water Temp. [K] [MAE]	0.11 K	0.21 K	0.15 K	0.23 K	0.08 K	0.17 K

From this fact, it has been preferred to apply the moving boundary model for our heat recovery device in order to better predict SHR close to unity. Moreover, as explained in Chapter 3, the moving boundary model can be extended to a three-zones heat exchanger model by adding a portion of the heat exchanger where frosting occurs.

2.5 Determination of the regime

In order to allow quicker simulation (especially when coupled to a building simulation model), the determination of the regime (totally dry, totally wet and partially wet) is realized by means of a solving procedure initially developed by Morisot et al. (2002) for cooling coils and presented hereafter.

The implemented solution algorithm, represented in the flow chart given in Figure II-12, includes the following steps:

1. The first step consists in comparing the supply indoor air temperature $T_{su,ind}$ and the supply fresh air temperature $T_{su,fesh}$. If the supply fresh air temperature is lower than the supply indoor temperature, the heat exchanger is supposed to operate in "winter conditions" and in "summer conditions" in the opposite case.

The rest of the description of the solving procedure focuses on the right part of Figure 5 ("winter conditions").

2. The second step consists in comparing the supply indoor air dewpoint temperature $T_{dp,su,ind}$ and the supply fresh air temperature $T_{su,fresh}$.
   Obviously, if the supply fresh air temperature $T_{su,fresh}$ is higher than the supply indoor air dewpoint temperature $T_{dp,su,ind}$, the coil will be in completely dry regime.

   If the supply fresh air temperature $T_{su,fresh}$ is lower than the supply indoor air dewpoint temperature $T_{dp,su,fresh}$, the coil is considered, as a first guess, in a completely wet regime.

3. The third step consists in comparing the supply indoor air dewpoint temperature $T_{dp,su,fresh}$ to the supply cooling coil surface temperature $T_{surf,su}$. Supply surface temperature is determined by Equation II-30:

$$\frac{(T_{wb,su,ind} - T_{surf,su})}{R_{ind,fic}} = \frac{(T_{wb,su,ind} - T_{ex,fresh})}{R_{fresh} + R_w + R_{ind,fic}} \qquad \text{II-30}$$

   If the supply cooling coil surface temperature $T_{surf,su}$ is lower than the supply indoor air dewpoint temperature $T_{dp;su;ind}$, then the cooling coil is completely wet.

4. In the opposite case, the fourth step is to compare the supply indoor air dewpoint temperature $T_{dp,su,ind}$ and the exhaust cooling coil surface temperature $T_{surf,ex}$.

   If the exhaust cooling coil surface temperature $T_{surf,ex}$ is higher than the supply indoor air dewpoint temperature $T_{dp,su,ind}$, then the cooling coil is completely dry.

   In the opposite case, the cooling coil is considered partially wet and the variable boundary model dedicated to partially wet regime is applied.

The "partially wet" model only requires three parameters: convective heat transfer coefficients in dry conditions for indoor and fresh air and conductive heat exchanger wall resistance. Due to its small thickness (2.10^{-4} m), the wall resistance can generally be neglected, even for material such as polystyrene with a low thermal conductivity (around 0.04 W/m-K). As a quantitative example, wall

resistance due to conduction is around 6.5 times lower than the convective heat transfer resistance in the investigated exchanger and taking into account the wall resistance would only decrease the predicted thermal performance by less than 0.6%. The convective heat transfer coefficients are determined by means of correlation, as already discussed in section 2.3.

In the rest of the paper, the supply fresh air temperature is always considered lower than the indoor air temperature (winter conditions). However, the model is still valid when describing the summer conditions.
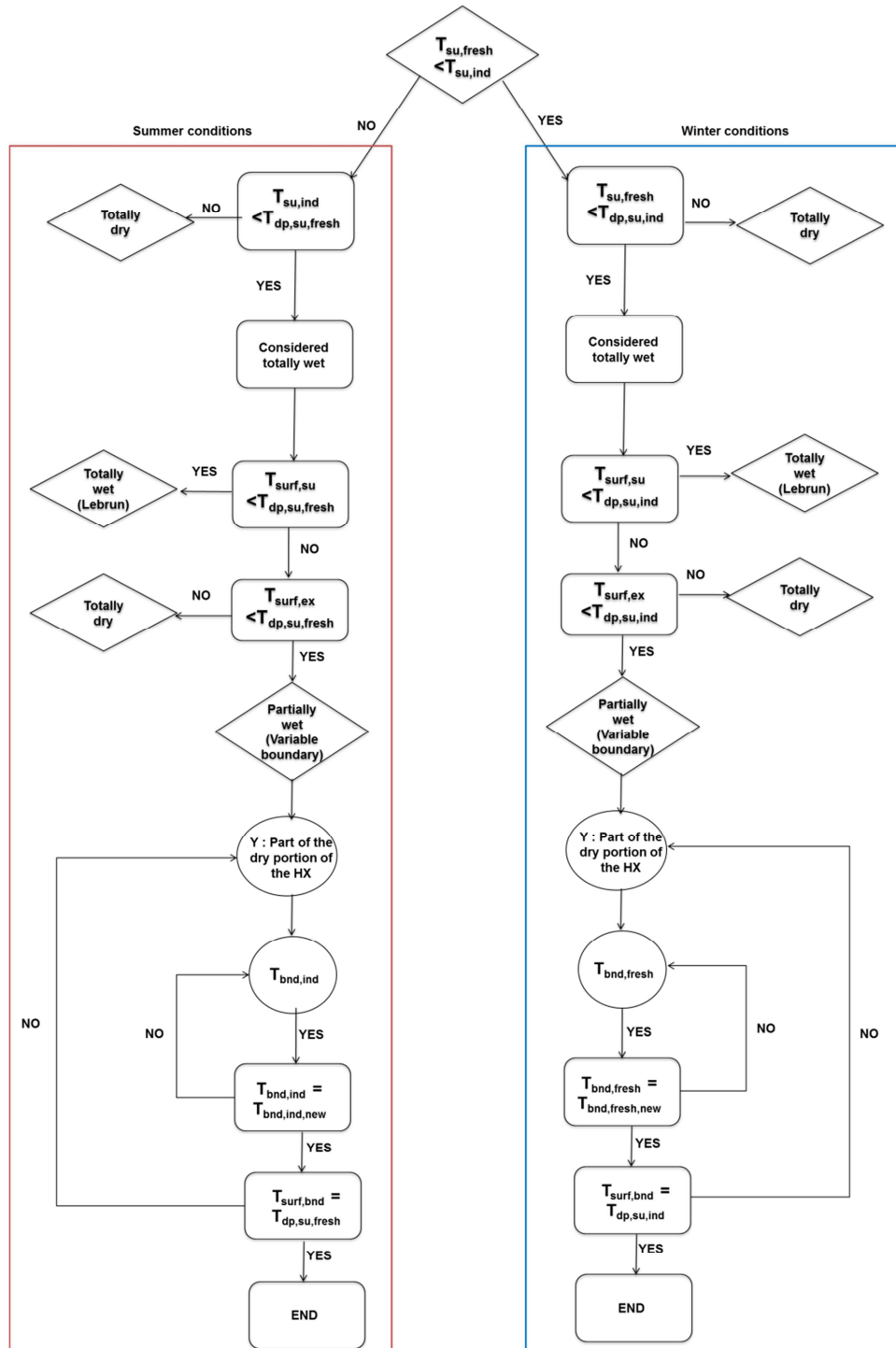

Figure II-12: Solution procedure of the developed model

2.6 Hydraulic performance prediction

The model dedicated to the hydraulic performance prediction applies the same methodology than the one dedicated to the thermal performance since it also divides the heat exchanger into three zones (the reason is that two of them are composed of rectangular channels and one of them is composed of triangular channels). The mean distances considered for each part are represented in Figure II-13. The mean distance considered for the part A and the part C ($L_{mean;A}$ and $L_{mean;c}$) is equal to the half-length of the supply side. The mean distance considered for the part B is equal to the length of the central part of the exchanger.
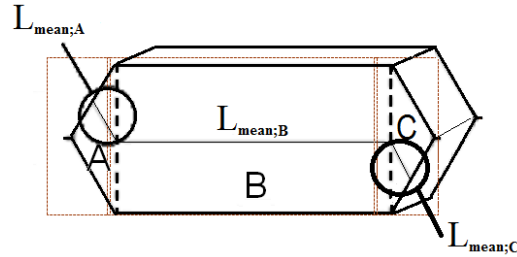

Figure II-13: Mean distance considered for the hydraulic model

As an example, pressure drop in the region A, ΔP_A in [Pa], is determined as a function of the friction factor f_A, the air density ρ_a in [kg/m³], the mean distance considered for the part A $L_{mean,A}$ in [m], the hydraulic diameter $D_{h,a,A}$ in [m] of part A and velocity $v_{a,A}$ in the part A [m/s], as given by Equation II-31:

$$\Delta P_A = \frac{f_A \cdot \rho_a \cdot L_{mean,A} \cdot v_{a,A}^2}{2 \cdot D_{h,a,A}}$$
II-31

The same equation is used for sections B and C of the heat exchanger.

The total pressure drop [Pa] due to friction in the heat exchanger corresponds to the sum of the pressure drops of parts A, B and C:

$$\Delta P = \Delta P_A + \Delta P_B + \Delta P_C$$
II-32

The first step was to develop a model using correlations available from the literature. Two distinct correlations have been used to compute the friction factor: a first one dedicated to the triangular channels (part B) and a second one dedicated to the rectangular channels (parts A and C). As already mentioned, laminar flow correlations are used since the calculated Reynolds is always less than 1000.

According to Nellis and Klein (2009), the fully developed friction factor for rectangular duct is a function of the aspect ratio (ratio of the minimum to the maximum lengths of the duct), according to Equation II-33:

$$f_{fd} = \frac{96}{Re} \cdot (1 - 1.3553 \cdot Aspect + 1.9467 \cdot Aspect^2 - 1.7012 \cdot Aspect^3 + 0.9564 \cdot Aspect^4 + 0.2537 \cdot Aspect^5)$$
II-33

Results of Curr et al. (1972) for a developing laminar flow are approximated by Equation II-34:

$$f = \frac{4}{Re}\left[\frac{3.44}{\sqrt{x_{plus}}} + \frac{\dfrac{1.25}{4 \cdot x_{plus}} + f_{fd} - \dfrac{3.44}{\sqrt{x_{plus}}}}{1 + 0.0021 \cdot x_{plus}}\right] \qquad \text{II-34}$$

where x_{plus} is the dimensionless length for a hydrodynamically developing internal flow defined by Equation II-35:

$$x_{plus} = \frac{L/D_h}{Re} \qquad \text{II-35}$$

Once again, 'Aspect' is based on the geometrical characteristics and is the ratio of the minimum to maximum dimensions of the duct.

Concerning the friction factor dedicated to the part B, the value proposed by Kays and London (1984) and shown in Figure 3 is used. Correlation was experimentally determined for a gas flowing through a matrix composed of isosceles (apex angle varying from 50° to 90°) triangular flow passages.

3   HEAT RECOVERY EXCHANGER TEST BENCH DESCRIPTION

The present section aims at describing the experimental apparatus developed to determine the hydraulic and thermal performance of the analyzed heat exchanger. A schematic representation of the test bench and pictures of its practical achievement are given in Figure II-14.
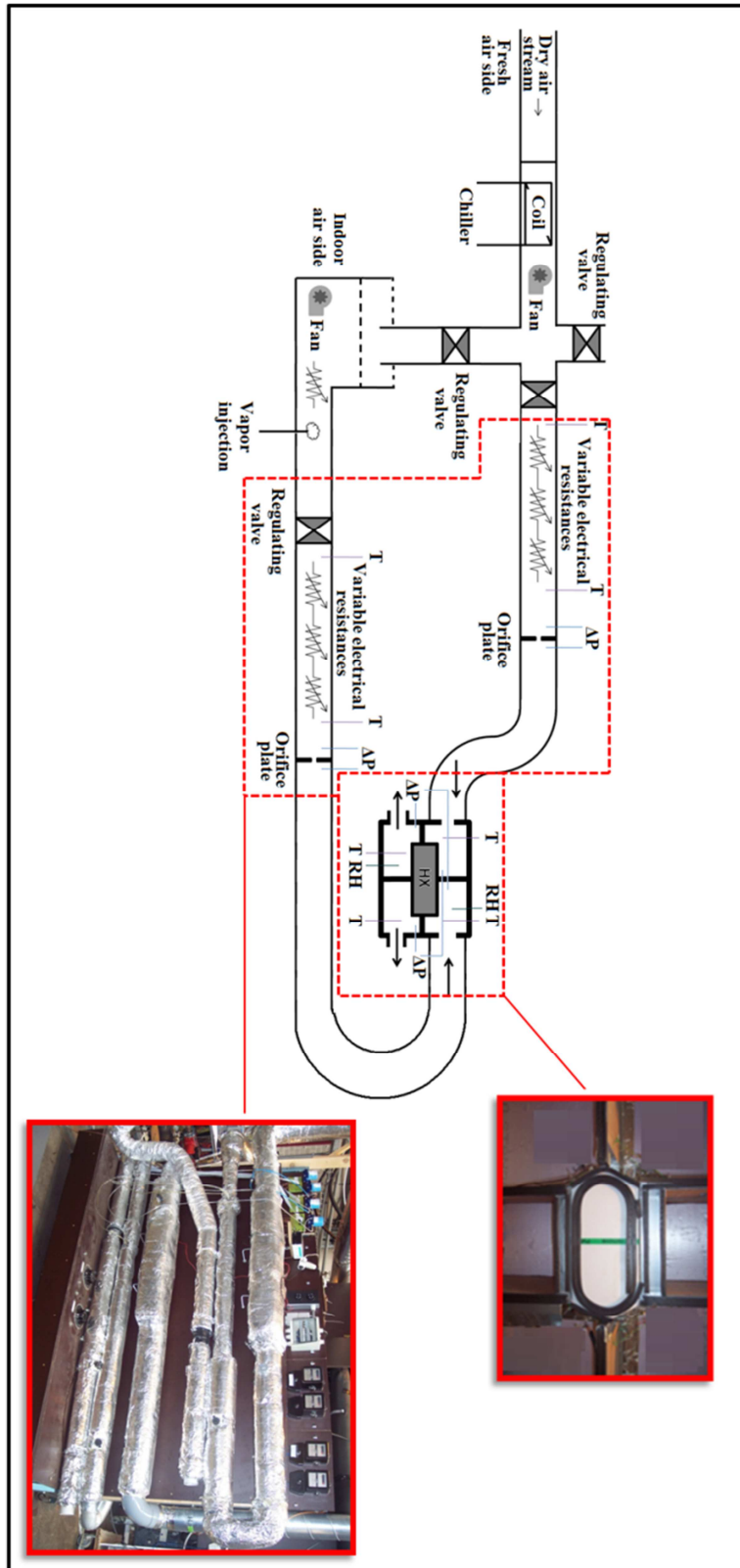

Figure II-14: Schematic representation of the test bench

Fresh air can be cooled down by means of the direct-expansion evaporator of an air-cooled chiller. In order to avoid freezing of the evaporator, the latter is sup-plied with fresh air delivered by an air compressor coupled to an industrial dryer ("Atlas Copco air dryer FD210"), given in Figure II-15.

Figure II-15: Industrial air dryer Atlas Copco FD210

It is possible to control the fresh air temperature at the inlet of the heat exchanger by post-heating the fresh air stream with the use of variable electrical resistances. Ducts containing fresh air flow are insulated by mineral rock of 25 mm thickness.

Indoor air (ambient air) can be cooled down and/or dried by by-passing part of the flow rate exhausting from the evaporator in a mixing box situated at the inlet of the indoor air fan. Here also, it is possible to control with precision the indoor air temperature by means of variable electrical resistances, as represented in Figure II-16.

Figure II-16: Resistances of 900W in series

Humidity is controlled by the use of electrical steam generators supplied with variable electrical power.

The mass flow rate of both fluids (fresh and indoor air) can be adjusted by means of a set of regulating valves and are measured by means of orifice plates, as recommended by ISO 5167 (2003).

Differential pressure 'Schaevitz' sensors dedicated to the air flow rates measurement have an accuracy of ±2.5 Pa. Air temperatures are measured with type T thermocouples with accuracy of ±0.3 K. In the rest of this chapter, the mean supply and exhaust temperature corresponds to the average of respectively two and eight measurements by type T thermocouples.

The differential pressure between the inlet and the outlet of the heat exchanger is measured by means of two distinct differential pressure sensors: one dedicated to the lowest air flow rates with an accuracy of ± 1 Pa with a full-scale value of 100 Pa ('Dimed' sensor) and another one with accuracy of ± 2.5 Pa with a full-scale value of 500 Pa ('Schaevitz' sensor):


Figure II-17: Schaevitz sensor (500 Pa at full scale) and Dimed sensor (100 Pa at full scale)

The relative humidities (RH) at the inlet and at the outlet of the indoor exhaust air stream are measured by means of humidity sensors with an accuracy of ± 2 percent points. These sensors have been calibrated by means of LiCl and NaCl, which permits to create an atmosphere at respectively 11.3% and 70% of relative humidity. Their operating range is comprised between -25°C to 45°C and 0 to 100%.

Figure II-18: 'Status instrument' relative humidity sensor

The heat exchanger is located in a box insulated by 30 mm thick polystyrene in order to reduce heat losses to the atmosphere. In order to ensure a uniform air flow through the heat exchanger, dampers with filters are placed in the box upstream of the heat exchanger, as shown in Figure II-19.
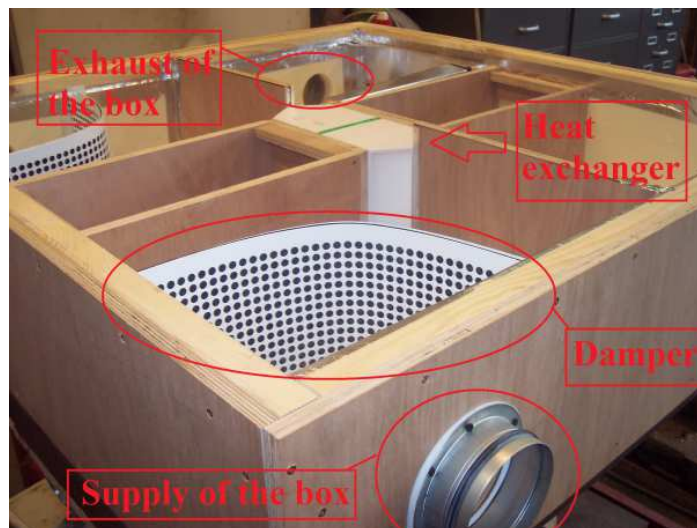
Figure II-19: Heat exchanger box

All the measurements were automatically stored in a PC by means of three data acquisition cards (Solartron Instruments SI 359551), as represented in Figure II-20. The data acquisition unit programmed by the computer receives the signal from the electronic sensors. All the channels are scanned every second.

Figure II-20 : Data acquisition cards (Solartron Instruments SI 359551)

Accuracies of the measurement devices are summarized in Table II-5.

Table II-5 : Accuracy of the measurement devices

Measurements	Accuracy
Type T Thermocouples	+/- 0.5 K
Differential pressure sensors (Full-scale: 500 Pa)	+/-2.5 Pa
Differential pressure sensors (Full-scale: 100 Pa)	+/- 1 Pa
Simultaneous measure of relative humidity and temperature	+/- 2 % +/- 0.4 K

4 EXPERIMENTAL INVESTIGATIONS ON THE STUDIED HEAT RECOVERY EXCHANGER: TESTING CONDITIONS AND MEASURED PERFORMANCE

The present section of the paper presents the experimental investigations carried out by means of the previously presented test bench. Indoor and fresh mass flow rates were equal (well balanced flow rates) as well in dry than in partially wet regimes. This condition was fulfilled by using regulating valves of the test bench.

Four kinds of tests were performed:

- – Measurement of the hydraulic performance in dry regimes,

- – Measurement of the hydraulic performance in wet regimes,

- – Measurement of the thermal performance of the heat exchanger in dry conditions,

- – Measurement of the thermal performance of the heat exchanger in partially wet conditions (which includes the determination of the sensible, latent and total heat transfer rates).

The present section presents the testing conditions relative to each type of experimental tests and some interesting results related to the experimental investigations.

4.1 Hydraulic performance under dry conditions

Concerning the hydraulic performance, the pressure drop was determined for several air flow rates (approximately from 30 to 100 m^3/h). The conditions at the inlet of the heat exchanger for these tests were 24°C and 45% of relative humidity. Each presented result for the several air flow rates concerning the hydraulic performance of the heat exchanger corresponds to a stabilized test of 200 secondes. The matrix is considered to be symmetric given the negligible observed difference in terms of pressure drop if flows are diverted.

4.2 Hydraulic performance under partially wet conditions

Analysis of hydraulic performance under partially wet conditions was realized by carrying out four experimental points. The aim of this investigation was to highlight the influence of condensation on pressure drop. Experimental points corresponded to two volumetric air flow rates and two relative humidities. Supply fresh air temperature was chosen in order to enhance condensation and avoid freezing. Each of the observed pressure drops presents the same evolution and leads to the same conclusions as those drawn by Fernandez et al. [6]. First, there is an increase of the pressure drop which can be attributed to the reduction of the flowing area due to the formation of condensate. Then, pressure drop become nearly stable.

The evolution of pressure for a set of operating conditions is given in Figure II-21.

For an indoor volumetric flow rate of 41 m^3/h, well balanced mass flow rates, a supply indoor air temperature of 18.6°C and a fresh air supply temperature of 1.6°C, the relative increase of pressure drop is equal to 111% for a relative humidity of 100% of the supply indoor air and 46% for a relative humidity of 50%. The difference between these two results can be explained by the fact that condensation appears on a larger surface of the heat exchanger for a higher supply air relative humidity.

For an indoor volumetric flow rate of 80m^3/h, well balanced mass flow rates, an indoor air supply temperature of 18.6°C and a fresh air supply temperature of 1.6°C, the relative increases of pressure

drop are equal to 72% and 20% respectively for a relative humidity of 100% and 50%. The difference between these two results can be explained in the same manner than previously explained.
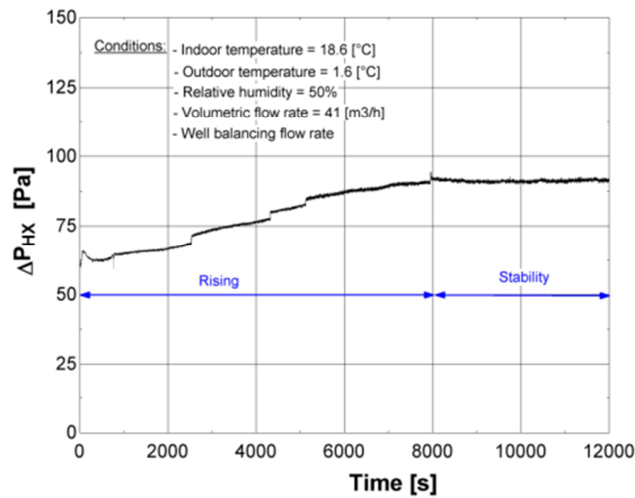

Figure II-21: Pressure drop evolution under partially wet conditions

4.3 Thermal performance under dry conditions

4.3.1 Temperatures

Investigated flow rates are comprised between 30 and 90 m^3/h. Since the flow rates are rather small, the temperature difference at the inlets of the heat exchanger was chosen in a range comprised between 30 to 40 K (between 40 and 50°C for the indoor air at the inlet of the heat exchanger and between 0 and 10°C for the fresh air at the inlet of the heat exchanger). Obviously, these conditions (especially the high virtual indoor temperature) do not correspond to the usual operating conditions of the device but allows minimizing the relative error on the heat transfer measurement.

The results presented in the following part of the paper correspond to the average value of stabilized regimes of 500 sec. An example is given in Figure II-22 and shows the mean temperatures at the inlets and at the outlets of the heat exchanger and the measured orifice plate pressure drop.
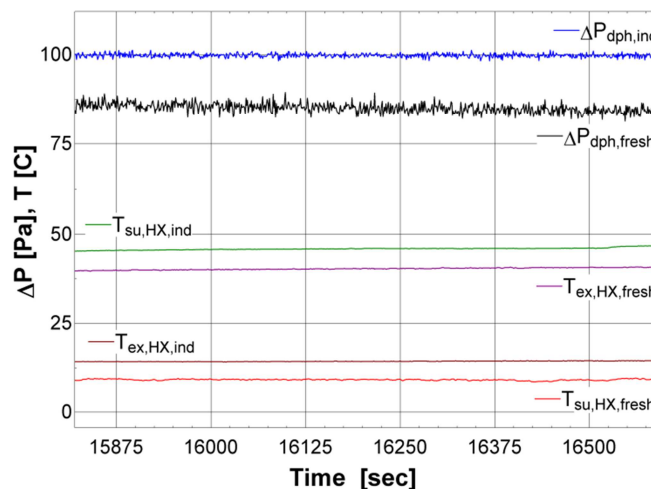

Figure II-22: Example of a stabilized test for a volumetric flow rate of 43 m³/h in the standard condition (25•C and 101325 Pa) for dry regime

The aim of these tests was to determine the performance of the heat exchanger in dry conditions. Part of the dry air coming from the dryer and exhausting from the cooling coil was deviated into the mixing box situated at the inlet of the indoor air pulsing fan (see Figure II-14).

The condition on the dry regime was checked by means of the measurements of the humidities at the inlet and at the outlet of the heat exchanger and was achieved during the whole set of tests.

4.3.2   Balance of heat transfer rates

Heat transfer rates were measured on both the indoor and the fresh air sides and are compared in Figure II-23. The heat transfer rate difference between these two values is always less than 1.5%, which is within the accuracy of the measurements devices. Heat transfer rates $\dot{Q}$ in [W] for each side in dry operation are determined by Equations II-36 and II-37:

$$\dot{Q}_{ind} = \dot{M}_{ind} \cdot cp_{ind} \cdot (T_{su,ind} - T_{ex,ind})$$ II-36

$$\dot{Q}_{fresh} = \dot{M}_{fresh} \cdot cp_{fresh} \cdot (T_{ex,fresh} - T_{su,fresh})$$ II-37
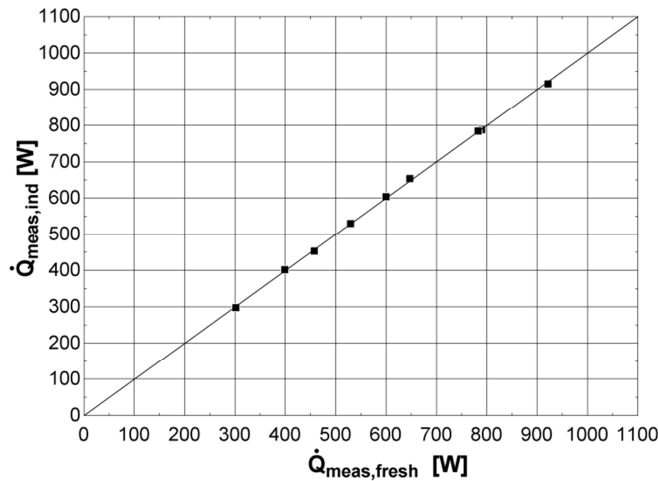
Figure II-23: Balance of heat transfer rates for the dry regime

4.3.3   Measured effectiveness

If the air mass flow rate is converted into a volumetric flow rate in standard condition (25°C and 101325 Pa), the measured effectiveness shown in Figure II-24 is obtained. Horizontal error bars indicate the uncertainty on measurements on the flow rates and vertical error bars indicate the uncertainty on measurements on the effectiveness. The zoom in Figure II-24 permits a better visualization of these uncertainties.
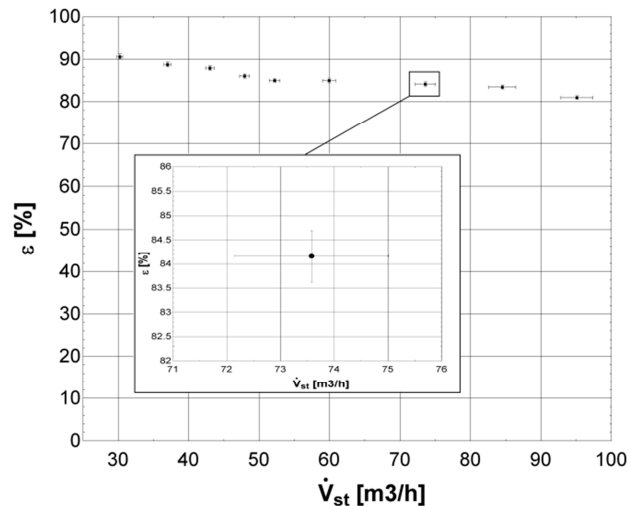
Figure II-24: Measured effectiveness [%] vs. volumetric flow rate [m³/h]

The uncertainty on the measured effectiveness was evaluated using the "Uncertainty propagation" function of the EES Software, which uses the method described in NIST Technical Note 1297 (1994). The purpose of this command is to calculate how the uncertainties in each of the measured variables X_1, X_2, etc propagate into the value of the calculated quantity Y that is a function of one or more variables that are directly measured, i.e., Y = f(X_1, X_2, etc). According to this method, the uncertainty on the calculated quantity U_y can be determined as a function of the uncertainty on the measured variable $U_{x,i}$ by Equation II-38:

$$U_y = \sqrt{\sum_i \left(\frac{\partial Y}{\partial X_i}\right)^2 . U_{x,i}^2}$$

II-38

4.4   Thermal performance under partially wet conditions

4.4.1   Temperature and humidities

Contrary to the previous tests in dry conditions, tests in partially wet conditions were carried out in realistic operating conditions. Temperatures at the inlet of the heat exchanger were respectively comprised between 0 and 5°C for fresh air flow and between 20 and 25°C for the indoor air flow. Inlet relative humidity of the indoor air flow ranged between 45 and 80%.

The value of the inlet fresh air temperature was chosen in order to avoid any risk of freezing and to allow for the partially wet regime. Inlet indoor air temperature and relative humidity representative of inside conditions of a domestic building were imposed.

The results presented in the following part of the paper correspond to the average value of stabilized regime of 500 sec. An example of stabilized test is given in Figure II-25 and shows the mean temperatures at the inlet and at the outlet of the heat exchanger for both fluids. Relative humidities of the indoor air at the inlet and the outlet of the heat exchanger are also given in Figure II-25. It is interesting to stress the fact that the difference between the inlet and the outlet temperatures of the heat exchanger for both air flows are not the same, contrary to the observed case in Figure II-22. This fact can be explained by the appearance of condensation (and thus a part of latent heat transfer rate) on the indoor side of the heat exchanger.
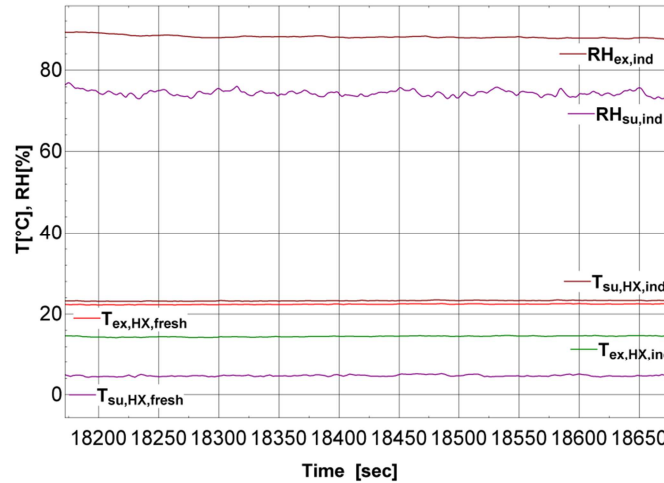
Figure II-25: Example of stabilized tests under partially wet conditions

4.4.2 Balance of the heat transfer rates

Measured heat transfer rates on indoor and fresh air sides are compared in Figure II-26. It can be observed that energy balances on the fresh and indoor air streams agree within a band of ± 15%. Fernandez-Seara (2011) obtained the same range of error on tests realized on the same type of heat recovery exchanger.

These results are considered satisfactory for these kinds of devices, due to the relatively low heat transfer rate and the uncertainties related to the relative humidity sensors. Heat transfer rates $\dot{Q}$ in [W] for each side are determined by the Equations II-39 and II-40:

$$\dot{Q}_{ind} = \dot{M}_{ind} \cdot (h_{su,ind} - h_{ex,ind}) \qquad \text{II-39}$$

where $h_{su,ind}$ and $h_{ex,ind}$ are respectively the enthalpy of the indoor air at the supply and the exhaust of the heat exchanger. These two values are determined by means of the knowledge of the temperature and humidity at those conditions.

$$\dot{Q}_{fresh} = \dot{M}_{fresh} \cdot cp_{fresh} \cdot (T_{ex,fresh} - T_{su,fresh}) \qquad \text{II-40}$$
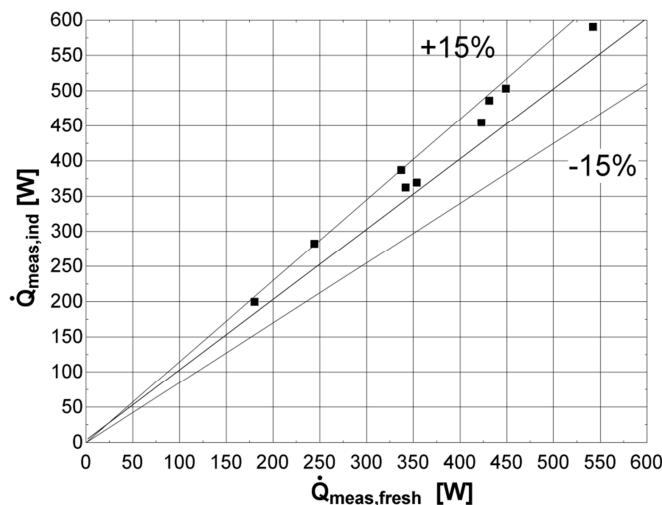

Figure II-26: Heat transfer rates determined from the experimental data through the energy balance on the indoor and fresh air-flow rates

As it can be observed in Figure II-26, heat transfer rate measured on the indoor air side is always larger than the one measured on the fresh air side. This can be explained by the unavoidable saturation of relative humidity sensors in the range of high measured relative humidity. However, measurement of relative humidity at the inlet and the outlet of the heat exchanger is not necessary, as explained in section 5.3.

5   CALIBRATION AND VALIDATION OF THE MODEL

5.1   Hydraulic performance

The comparison between the predictions by the model and the measurements in terms of hydraulic performance is given in Figure II-27.
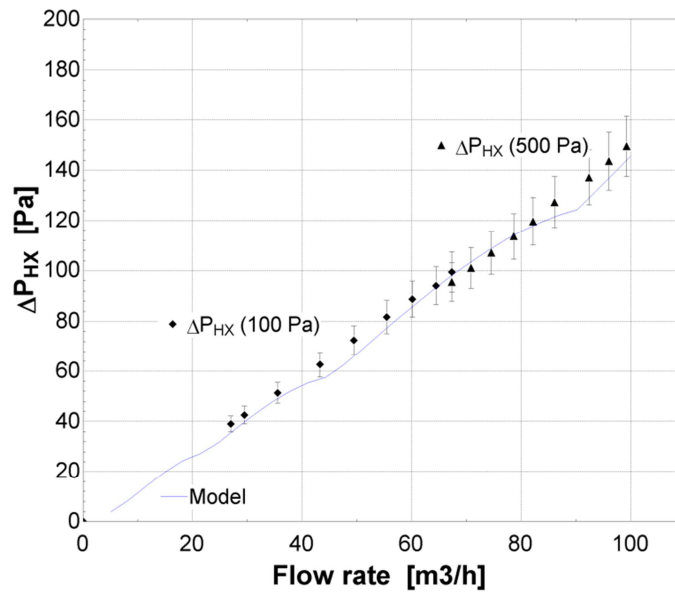
*Figure II-27: Pressure drop through the heat exchanger [Pa] vs. volumetric flow rate [m³/h]*

The full line in Figure II-27 represents the simulation results from the model. The mean deviation between the prediction by the model and the measurement is 4.6% and the maximum deviation is less than 7%.

Considering the uncertainty on the mass flow rate (from 1.5 to 2.2% according to ISO 5167 (2003)) and the uncertainty on the air pressure drop sensor (1 to 2.5 Pa depending on the sensor used), the experimental measurements are on sufficiently good agreement with the model.

5.2   Thermal performance in dry conditions and calibration of the correlations

5.2.1   Comparison with non calibrated model

Figure II-28 offers a comparison between the thermal performance prediction and the thermal performance measurement. As it can be observed, the non-calibrated model overestimates the measured thermal performance. The maximal deviation between the prediction by the model and the measurements for the thermal performance is 8.5% and the mean deviation is equal to 5.2%.
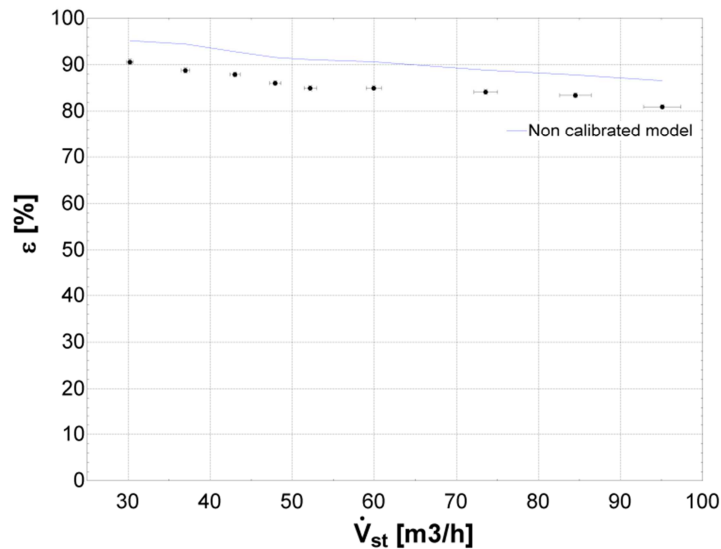
Figure II-28: Comparison between the developed model before the calibration and the experimental measurements

Even if both curves have similar shapes, such differences are unacceptable and require a tuning of some parameters of the model. To do so, a sensitivity analysis was performed and is detailed here after.

5.2.2   Sensitivity analysis

The influence of **three parameters** on the heat transfer rate has been investigated. These three parameters are given hereafter:

-        the **convective heat transfer coefficient in part B**. Given the high value of $prop_B$ compared to $prop_A$ and $prop_C$ and the counter flow configuration in part B instead of cross flow configuration in part A and C, the main part of the heat transfer rate appears in the central part of the heat exchanger. A discretized model indicates that in the dry regime, about 90.5% of the heat transfer rate occurs in the central part of the heat exchanger. As a result, the present sensitivity analysis does not focus on the variation of the convective heat transfer coefficients in part A and C,

-        the **geometry** dimensions of the heat exchanger,

-        the **mal-distribution** of one or both fluids through the heat exchanger.

Carrying out a sensitivity analysis involving flow rate distribution in a heat exchanger is not so obvious. To do so, the heat exchanger has been fictitiously divided into two identical semi heat exchangers in parallel configurations, as shown in Figure II-29. The total mass flow rate on both indoor and fresh air sides are considered equal:

$$\dot{M}_{ind;total} = \dot{M}_{fresh;total}$$
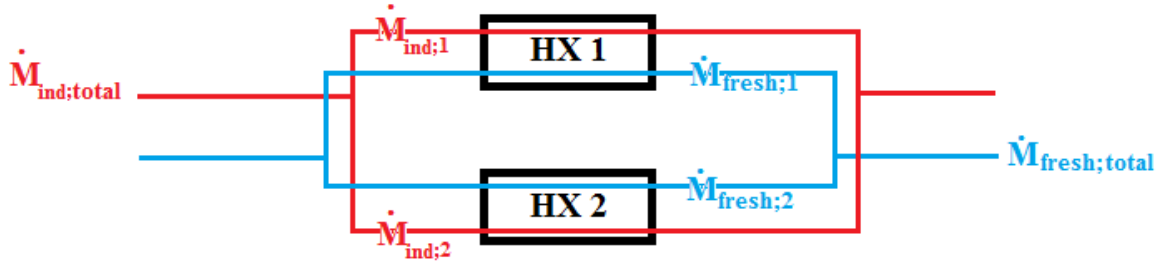<div align="right">II-41</div>

Figure II-29 : Sensitivity analysis - Flow rate maldistribution (fictitious division of heat exchanger)

The maldistribution of each flow rate is characterized by the **term X** in Table II-6. Obviously, the sum of each flow rate entering in each fictitious heat exchanger is equal to 1. To investigate the influence of maldistribution on the heat transfer rate, it has been decided to vary X from 0.9 to 1.1. This range of variation close to unity is justified by the presence of damper which is supposed well distribute the flows. The other parameters taken into account in our sensitivity analysis (convective heat transfer coefficient in part B and each measured geometry dimensions of the heat exchanger) have been modified in a similar manner.

Three different cases of maldistribution have been investigated.

<u>**In Case 1**</u>, flow rates through $\underline{HX_1}$ and $\underline{HX_2}$ are well balanced even if there is an overall misdistribution for both flow rates.

HX₁:	$\dot{M}_{fresh;1} = \dot{M}_{ind;1} = 0.5 * \dot{M}_{ind;total} * X$	II-42
HX₂:	$\dot{M}_{fresh;2} = \dot{M}_{ind;2} = 0.5 * \dot{M}_{ind;total} * (2 - X)$	II-43

<u>**In Case 2,**</u> flow rates of indoor air side remains constant and well-balanced between $\underline{HX_1}$ and $\underline{HX_2}$ ($0.5 * \dot{M}_{ind;total}$). From this fact, contrary to case 1, flow rates are no longer well-balanced for $\underline{HX_1}$ and $\underline{HX_2}$.

HX₁:	$\dot{M}_{fresh;1} = 0.5 * \dot{M}_{fresh;total} * X$ **vs** $\dot{M}_{ind;1} = 0.5 * \dot{M}_{ind;total}$	II-44
HX₂:	$\dot{M}_{fresh;2} = 0.5 * \dot{M}_{ind;total} * (2 - X)$ **vs** $\dot{M}_{ind;2} = 0.5 * \dot{M}_{ind;total}$	II-45

<u>**Case 3**</u> is the one leading to the worst heat transfer rate degradation since it is the one generating the worst maldistribution inside the heat exchanger.

|		
HX₁: $\dot{M}_{fresh;1} = 0.5 * \dot{M}_{fresh;total} * (2 - X)$ <u>**vs**</u> $\dot{M}_{ind;1} = 0.5 * \dot{M}_{ind;total} * X$		II-46
HX₂: $\dot{M}_{fresh;2} = 0.5 * \dot{M}_{fresh;total} * X$ <u>**vs**</u> $\dot{M}_{ind;2} = 0.5 * \dot{M}_{ind;total} * (2 - X)$		II-47

Table II-6 summarizes the investigated cases in terms of flow rates. Nomenclature used is the same as the one presented in Figure II-29.

Table II-6 : Flow rate maldistribution for each investigated cases

	$\dot{M}_{ind;1}$	$\dot{M}_{ind;2}$	$\dot{M}_{fresh;1}$	$\dot{M}_{fresh;1}$
Case 1	$0.5 * \dot{M}_{ind;total} * X$	$0.5 * \dot{M}_{ind;total} * (2-X)$	$0.5 * \dot{M}_{fresh;total} * X$	$0.5 * \dot{M}_{fresh;total} * (2-X)$
Case 2	$0.5 * \dot{M}_{ind;total}$	$0.5 * \dot{M}_{ind;total}$	$0.5 * \dot{M}_{fresh;total} * X$	$0.5 * \dot{M}_{fresh;total} * (2-X)$
Case 3	$0.5 * \dot{M}_{ind;total} * X$	$0.5 * \dot{M}_{ind;total} * (2-X)$	$0.5 * \dot{M}_{fresh;total} * (2-X)$	$0.5 * \dot{M}_{fresh;total} * X$

The sensitivity analysis has been carried out for an indoor volumetric flow rate of 60 m³/h. The inlet indoor air temperature is equal to 20°C and the inlet fresh air temperature is equal to 10°C. Results of the carried out sensitivity analysis are graphically given in Figure II-30.
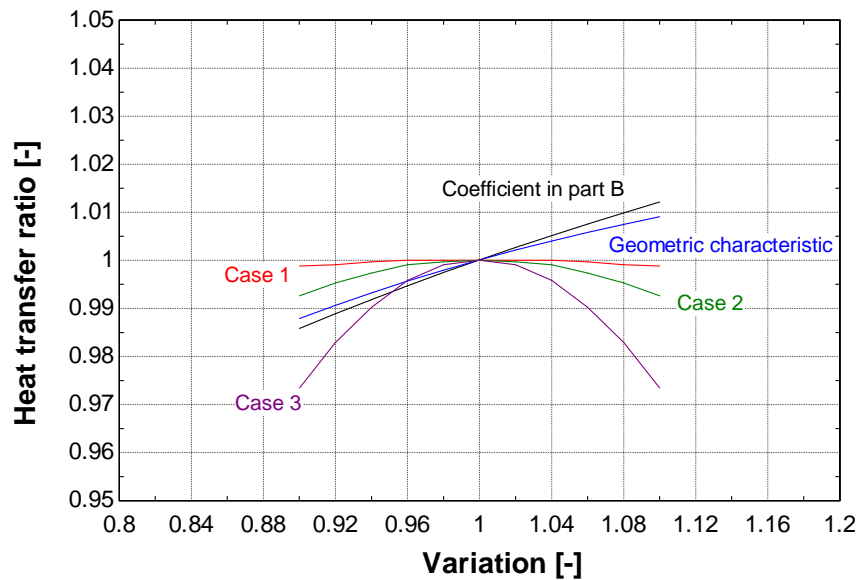
*Figure II-30 : Results of the sensitivity analysis*

As shown in Figure II-30, except for the Case 3 of misdistribution flow rate, the convective coefficient in part B appears to be the most influential parameter; even if each measured geometric characteristic varied by 10%. This seems unrealistic since the geometry characteristics are known with a high level of accuracy (high precision of used calipers). Case 2 and 1 of maldistributions appears to be the less influential parameters.

It is important to precise that special attention has been paid to ensure a homogeneous repartition of flow rate (placement of dampers in the box upstream of the heat exchanger as seen in Figure II-19). Moreover, even without dampers, due to the test bench configuration, its symmetry and the air inlet configuration in the box containing the heat exchanger, a potential maldistribution of flow rates through the heat exchanger would be close to Case 1.

Considering these results and also the fact that the original correlation was developed for slightly different heat exchanger (regenerator matrix), degradation of the heat transfer coefficient in part B seems to be most relevant one.

5.2.3   Calibration of the model

From results of the sensitivity analysis, it was decided to alter the correlation for the determination of the value of the convective heat transfer coefficient in part B of the heat exchanger. The tuning was achieved by multiplying the correlation presented in section 2.3 by a factor of 0.59.
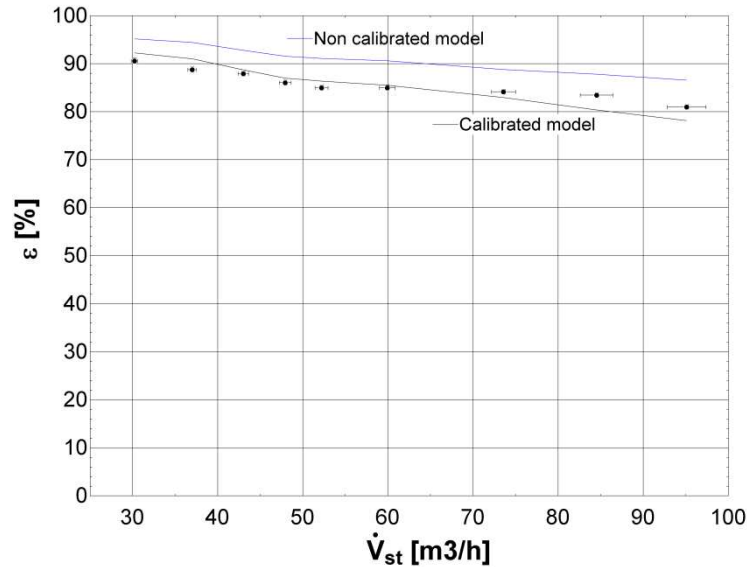
Figure II-31: Comparison between the developed model before/after the calibration and the experimental mesurements

As it can be observed in Figure II-31, the model with new correlations predicts the thermal efficiency with a mean relative error of 1.6% which is of the same order as the experimental uncertainty (from 1.5 to 2.2% according to ISO 5167 (2003)).

5.3   Thermal performance in partially wet conditions and validation of the new moving boundary model

The aim of this section is to compare simulation results of the calibrated model with experimental results in partially wet conditions and thus to evaluate the variable boundary model. In the rest of the paper (and in particular for the comparison between model and experimental results in partially wet conditions), the convective heat transfer coefficient is determined by the calibrated correlations, established in the previous section 5.2.

The quality of the model is evaluated by comparing simulation and experimental results in terms of:

- Total heat transfer rate;

- Sensible heat transfer rate;

- Latent heat transfer rate or condensate flow rate.

The total heat transfer rate was measured on the fresh air side, where only sensible heat transfer occurs. This is justified by the fact that sensible heat transfer measurements present less error than the latent heat transfer measurements (RH sensors present an important uncertainty measurement compared to the type T thermocouples). Thus, the considered measurements taken into account for the validation are:
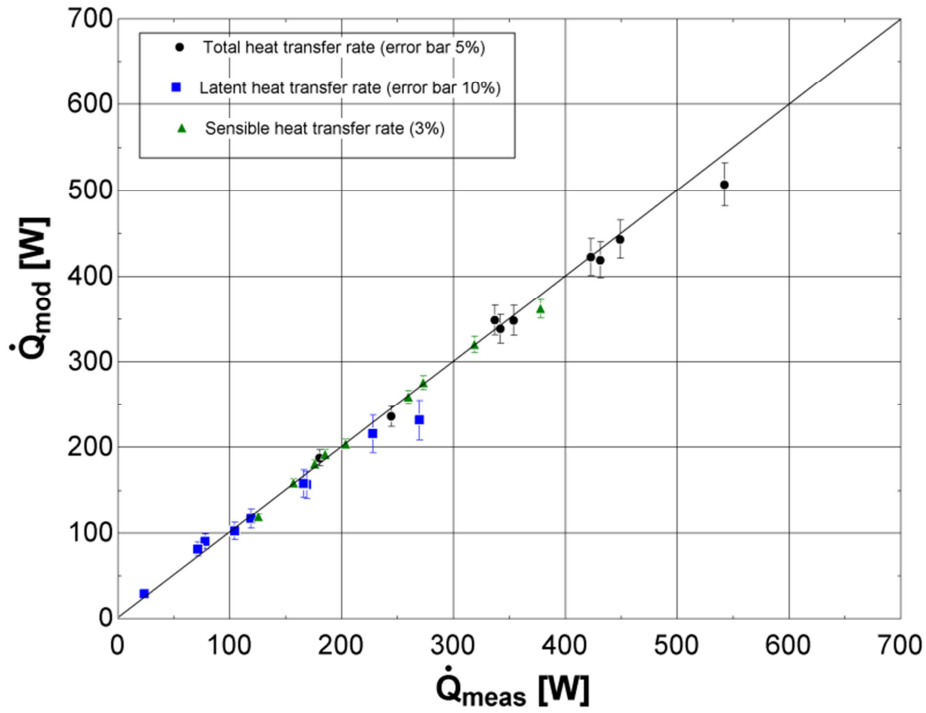
$$\dot{Q}_{meas,tot} = \dot{Q}_{meas,fresh} \qquad \text{II-48}$$

$$\dot{Q}_{meas,tot} = \dot{M}_{meas,fresh} \cdot cp_{fresh} \cdot \Delta t_{meas,fresh} \qquad \text{II-49}$$

$$\dot{Q}_{meas,sen} = \dot{M}_{meas,ind} \cdot cp_{ind} \cdot \Delta t_{meas,ind} \qquad \text{II-50}$$

$$\dot{Q}_{meas,lat} = \dot{Q}_{meas,tot} - \dot{Q}_{meas,sen} \qquad \text{II-51}$$

Figure II-32 presents the comparison between model and experimental results in terms of total, sensible and latent heat transfer rate.

Figure II-32: Comparison between model and experimental results in terms of total, sensible and latent heat transfer rates

The model is able to predict the total, sensible and latent heat transfer rate within 5%, 3% and 10% respectively.

6   PARAMETRIC STUDIES

The model presented in the previous section has been used to investigate the influence of operating conditions on condensation and freezing issues. The current section gives some conclusions that can be drawn from these uses of the model.

6.1   Influence of the operating conditions on the evolution of the latent and sensible heat transfer rate

As mentioned before, it is relevant to quantify accurately both the sensible and the latent heat transfer rates extracted from the indoor air. Based on the simulation model presented and validated in the previous sections, the evolution of these heat transfer rates was computed as a function of the air indoor relative humidity for several outdoor temperatures. Values presented in Figure II-33 correspond to an indoor temperature of 20°C, an indoor air volumetric flow rate of 60 m³/h, outdoor temperatures of 0 and 10°C and well-balanced air mass flow rates.
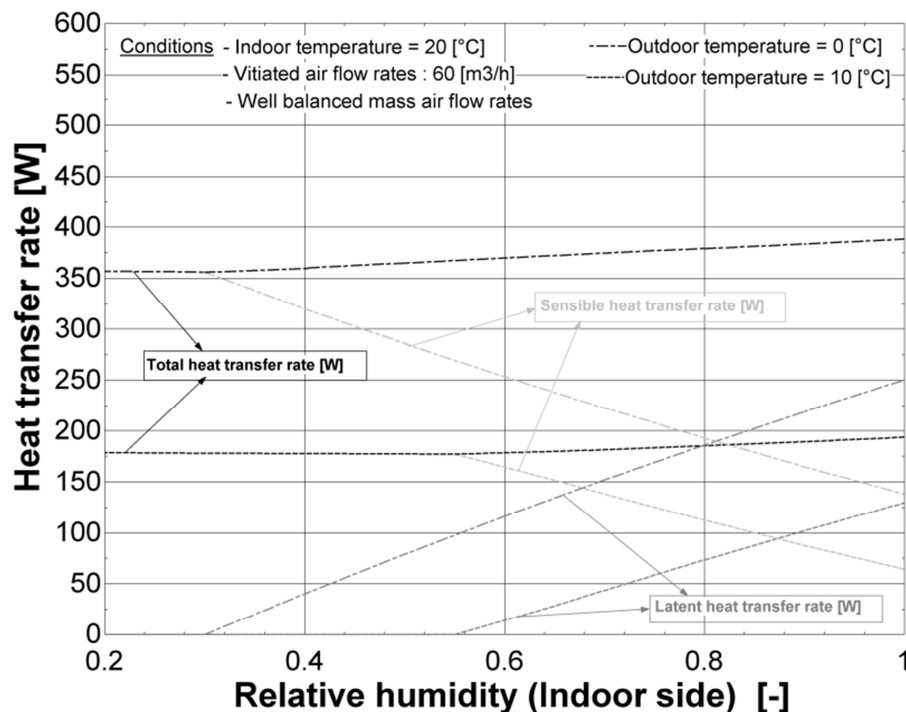
Figure II-33: Evolution of total, latent and sensible heat transfer rates as a function of the air indoor relative humidity for two outdoor temperatures

As observed in Figure II-33, the maximal increase of the total heat transfer rate, due to condensation, for the presented conditions is equal to 8.3 % and 8.1% for fresh air supply temperatures of respectively 0 and 10°C.

Figure 16 also permits to stress the fact that the part of latent heat becomes larger than the sensible one only for rather high relative humidity (82% for an outdoor temperature of 0°C and 88% for an outdoor temperature of 10°C).

To highlight this fact in a real case, the model can be used to determine the yearly amount of condensate and the annual energy transferred by the device by integrating the model into an hourly-based simulation model of a domestic building, since the computational time (less than one second in Matlab environment) of the presented model is quite low.

A coupling between building indoor hygro-thermal climate model and the presented variable boundary model was realized by Masy et al. (2011). The aim of this investigation was to assess the efficiency of decentralized air handling terminals in a semi-detached house located in Belgium. Annual simulations were performed with EES solver on an hourly basis with typical Belgium weather data. Simulations over a whole year showed that energy savings provided by latent heat recovery, due to condensation of the indoor exhaust air humidity, is equal to 1.6% of the whole energy saving provided by the heat recovery. Even if the energy saving provided by latent heat recovery seems negligible compared to the sensible one, it represents a yearly total amount of condensate of 67 liters.

6.2 Partial investigations under frosting conditions

Looking at the exhaust surface temperature allows for the prediction of when the freezing occurs in the heat exchanger for specific volumetric flow rates.

Figure II-34 permits to visualize the supply fresh air temperature under which freezing appears for three different indoor volumetric flow rates:
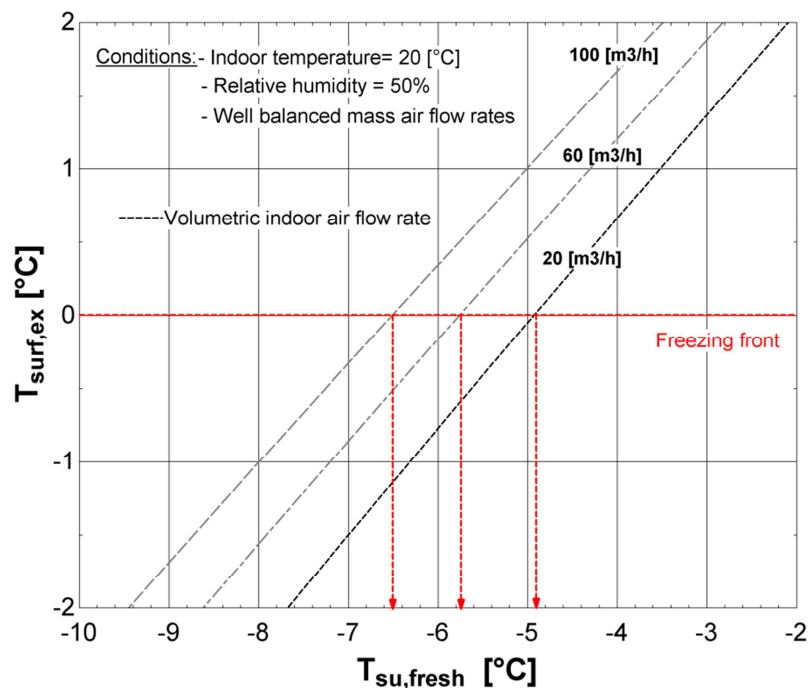

Figure II-34: Determination of a freezing front

As observed in Figure II-34, freezing occurs for an indoor volumetric flow rate of 60 m³/h, equal mass flow rates, an indoor air temperature of 20°C and an indoor air relative humidity of 50% at an outdoor temperature of -5.7°C.

The model also allow for the investigation of some strategies to prevent frosting in the heat exchanger. One of them consists in keeping the indoor air flow rate constant and reducing the fresh air flow rate. As an example, in order to avoid any freezing, the percentage of reduction of the fresh air mass flow rate is equal to 47% compared to an initial well-balanced mass flow rate situation, for an outdoor temperature of -15°C, an indoor volumetric flow rate of 60 m³/h, an indoor air temperature of 20°C and an indoor air relative humidity of 50%.

7   COMPARISON WITH DISCRETIZED MODELS

The first part of this discussion section concerns the comparison with a discretized heat exchanger model proposed by Rose et al. (2008). Steps of the development of the Rose model are the same as the model presented in this thesis (starting from the geometry characteristics of the heat exchanger to deduce the convective heat transfer coefficient by correlations). However, their model is based on a discretization of the heat exchanger. The latter is split into a finite number of segments, wherein the heat exchange is considered to occur as 1D steady state. Conservation of mass and energy is expressed for each of the defined control volumes. Based on this discretization, Rose et al. (2008) offer a representation of temperature evolution inside the heat exchanger.

The model proposed in this chapter allows for an easier implementation because of the absence of discretization. The use of the moving boundary model permits to determine where condensation occurs in the heat exchanger. From this point of view, application of the moving boundary concept presents the same advantages as the discretization of the heat exchanger. However, unlike the present model, the precision in partially wet conditions of a discretized model such as Rose's model (2008) is highly dependent on the number of segments considered and so on, on the calculation time. Moreover, the model of Rose et al. (2008) has only been partially validated through one single experimental point.

Even if the present model is able to predict if freezing occurs or not (c.f. section 6.2), the model could be improved by adding a description of the frost formation in order to simulate the heat exchanger under frosting conditions. Description of three zones heat exchanger model (dry, wet and freezing part) under frosting condition will be detailed in Chapter 3.

It is important to stress the fact that the exposed method (pre-model, calibration in dry condition and validation in partially wet conditions) can be extended to all types of air-to-air heat exchangers.

8   CONCLUSIONS

The aim of this chapter was to investigate an **off-the-shelf air-to-air** heat recovery exchanger device through modeling and experimental approaches with a **reverse engineering objective**.

First, a **semi-empirical model** using correlations already existing in the literature in order to determine the hydraulic and the thermal performance of the heat recovery device **in dry conditions** was presented. Then, an improved model based on **several existing cooling coil models** was applied to describe the heat exchanger behavior in partially wet conditions. A **solving procedure** to identify the regime was also proposed. The moving boundary model as well as the solving procedure for predicting performance under partially wet conditions can be applied for all types of air-to-air heat exchangers.

Secondly, the developed **experimental apparatus**, the testing conditions and the measured performance were described in the second part of the chapter.

Thirdly, a comparison between prediction by the model and measurements was conducted. **Hydraulic performance** was predicted by the developed model with a **satisfying accuracy** (mean deviation between the prediction and the measurement of 4.6%). Although results were of the same order of magnitude in terms of thermal performance (absolute mean deviation of 5.2% in terms of effectiveness), an **adjusted correlation for the convective heat transfer coefficient** was proposed to increase the accuracy of the model (absolute mean deviation of 1.6% in terms of effectiveness). The choice of only altering the convective heat transfer coefficient was justified by a **sensitivity analysis**. This latter takes into account influence of the geometric characteristic, flow rate misdistribution and heat transfer coefficient in part B.

Then, thermal performance tests in **partially wet conditions** were presented. The developed variable boundary model predicts with a **good accuracy** the total heat transfer rate (within 5% of error) as well as latent (within 10% of error) and sensible (within 3% of error) ones.

Finally, **parametric study** was carried out to investigate the **influence of operating conditions** on condensation (evolution of sensible and latent heat transfer rates as a function of indoor inlet relative humidity). The model has also been coupled to a building simulation model to quantify the influence of condensation on the annual thermal gain under a Belgian climate. Results of this simulation show that condensation has a really limited impact on annual heat recovered energy. From this fact, in the rest of the thesis, **influence of condensation on thermal annual performance will be neglected**.

By determining the **exhaust surface temperature**, the model is also able to determine the air flow control strategy to apply to **avoid freezing in the heat exchanger**. That could be particularly interesting in the design step of heat recovery ventilation, for the implementation of the fans control under freezing conditions. This strategy will be compared to other strategies conditions in Chapter IV.

9   REFERENCES

Adamski, M., 2008. *Heat transfer correlations and NTU number for the longitudinal flow spiral recuperators.* Applied Thermal Engineering 29, (2009), 591-596

Adamski, M., 2009. *Longitudinal flow spiral recuperators in building ventilation systems.* Energy and Buildings 40, (2008), 1883–1888

Adamski, M., 2010. *Ventilation system with spiral recuperator.* Energy and buildings 42, (2010), 674-677

Brandemuehl, M.J., S. Gabel, and I. Andersen. 1993. *A toolkit for secondary HVAC System Energy Calculations.* Published for ASHRAE by Joint Center for Energy Management, University of Colorado at Boulder.

Braun, J.E. 1988. *Methodologies for the design and control of central cooling plants.* Ph.D. dissertation. University of Wisconsin, Madison.

Curr, R. M., D. Sharma, and D.G. Tatchell, 1972. *Numerical predictions of some three-dimensional boundary layers in ducts.* Comput. Methods Appl. Mech. Eng. 1, (1972), 143-158

EES, 2013. Engineering Equation Solver, F-Chart Software

Fernandez-Seara , J., Diz, R., Uhia, F., Dopazo, A., Ferro, M., 2010. *Experimental analysis of an air-to-air recovery unit for balanced ventilation systems in residential building.* Energy conversion and management (2010)

Hesselgreaves, J.E. 2001. *Heat exchangers: Selection, Design and Operation.* Pergamon, An Imprint of Elsevier Science. (2001)

Incropera F. P., De Witt, D. P., 2002. *Fundamentals of heat and mass transfer (fifth edition).* John Wiley and Sons. (2002)

ISO 5167. *Measurement of fluid flow by means of pressure differential devices inserted in circular cross-section conduits running full.* ISO Standard. First edition (2003)

Jin, G.-Y., W.-J. Cai, W. Wang, and Y. Yao. 2006. *A simple dynamic model of cooling coil unit.* Energy Conservation and Management 47:2659-2672.

Lebrun, J., X. Ding, J.-P. Eppe, and M.Wasac. 1990. *Cooling Coil Models to be used in Transient and/or Wet Regimes. Theoretical Analysis and Experimental Validation.* Proceedings of SSB (1990), Liège, 405-411

Lemort, V., Rodríguez, A. and Lebrun, J. 2008. Simulationcof HVAC Components with the Help of an Equation Solver, Final Report of the IEA Task34/Annex43 Subtask D, University of Liège, Belgium.

Kakaç, S., R. K. Shah, and W. Aung. 1987. *Handbook of single phase convective heat transfer*, Wisley-Interscience, 1987

Kays, W.M., & London, A.L., *Compact heat exchangers*, 3rd ed., McGraw Hill, New York, (1984)

Kragh, J., Rose, J., Nielsen, T.R., Svendsen, S. 2008. *New counter flow heat exchanger designed for ventilation systems in cold climate.* Energy and buildings 39, (2008), 1151-8

Masy, G., Lebrun, J., Gendebien, S., Hansen, N., Lengele, M., Prieels, L. 2011. *Performances of DAHT connected to building airtightness and indoor hygrothermal climate.* Proceedings of the 32nd AIVC Conference. Bruxelles. 2011.

Morisot, O. 2000. *Modèle de batterie froide à eau glacée adapté à la maîtrise des consommations d'énergie en conception des bâtiments climatisés et en conduite d'installation.* Ph D. dissertation. Ecole des mines, Paris.

Morisot, O., Marchio, D. 2002. *Simplified Model for the Operation of Chilled Water Cooling Coils Under Nonnominal Conditions.* HVAC&R Research 8(2), (2002), 135-158.

Nasif, M. S., Morrison, G. L., Behnia, M. 2005. *Heat and Mass Transfer in Air to Air Enthalpy Heat Exchangers.* Proceedings of the 6th World Conference on Experimental Heat Transfer, Fluid Mechanics, and Thermodynamics April 17-21 (2005) Matsushima, Miyagi, Japan

Nellis, G., Klein, S. 2009. *Heat transfer.* Cambridge University Press

Nielsen, T. R., Rose, J., Kragh, J. 2009. *Dynamic model of a counter flow air to air heat exchanger for comfort ventilation with condensation and frost formation.* Applied Thermal Engineering 29, (2009), 462-468

NIST Technical Note 1297. Taylor B.N. and Kuyatt, C.E., *Guidelines for Evaluating and Expressing the Uncertainty of NIST Measurement Results*, National Institute of Standards and Technology Technical Note 1297, 1994.

Rose, J., Nielsen, T. R., Kragh, J., Svendsen, S. 2008. *Quasi-steady-state model of a counter-flow air-to-air heat-exchanger with phase change.* Applied energy 85, (2008), 312-325

Shah, R. K. and A. L. London, *Laminar flow forced convection in ducts*, Academic Press, New York, (1978)

Söylemez, M.S. 2000. *On the optimum heat exchanger sizing for heat recovery.* Energy Conversion and Management 41, (2000), 1419-1427

Wang, J., and E. Hihara. 2003. *Prediction of air coil performance under partially wet and totally wet cooling conditions using equivalent dry-bulb temperature method.* International Journal of Refrigeration 26:293-301.

Wang, Y.-W., W.-J. Cai, Y.-C Soh, S.-J. Li, L. Lu, and L. Xie. 2004. *A simplified modeling of cooling coils for control and optimization of HVAC systems.* Energy Conservation and Management 45:2915-2930.

Wang, G., M. Liu, and D. Claridge. 2007. *Decoupled Modeling of Chilled-Water Cooling Coils* , ASHRAE Transaction 113(1).

Wibulswas, P. 1966. *Laminar Flow heat Transfer in Non circular Ducts*, Ph.D. Thesis, London University, London, (1966).

CHAPTER III:

DEVELOPMENT STEPS OF HEAT RECOVERY EXCHANGER DEDICATED TO SINGLE ROOM VENTILATION

CHAPTER III: DEVELOPMENT STEPS OF A HEAT EXCHANGER DEDICATED TO SINGLE ROOM VENTILATION

1   INTRODUCTION

The present chapter focuses on the **development step** of the heat exchanger by proposing **numerica**l and **experimental procedures**.

First, a methodology in order to determine the best trade-off between hydraulic and thermal performance for a specific geometry of heat exchanger dedicated to single room ventilation with heat recovery is proposed. This consists in an optimization of the **Coefficient of Performance** (ratio between the heat recovered and the supplied electrical power), called COP of the device. However, the COP is not the only parameter to take into account: it also depends on technical, economic and acoustic considerations. A **numerical optimization** method is proposed in the frame of this chapter. Optimization is first performed by using a semi empirical model based on a division of the heat exchanger in three parts and using correlations derived from Chapter 2. The semi-empirical model allows for a parametric study in order to identify what the most effective geometry is (COP optimization). Then, the second step was to compare the numerical results determined by the **semi empirical** model with the results coming from **CFD simulations**.

Concerning SRVHR, great attention has to be paid to the **hydraulic performance** since it is directly related to the fan noise level. Thus, in order to be sure of the hydraulic performance predicted by models (semi empirical and CFD) related to the selected geometry and before launching the expensive manufacturing process of the thermoforming mold, it has been decided to experimentally check the hydraulic performance of the geometry by means of a **rapid prototyping process**. It consists in measuring the pressure drop related to the air flow passage through two corrugated plates. Several geometries have also been investigated. Details about the experimental investigations are given in Section 5.

Finally, experimental investigations on the final heat exchanger have been carried out by means of the test bench described in Chapter 2. Only the box containing the heat exchanger has been modified. Some details about this modification will be given. Experimental results in terms of **hydraulic and thermal** performance are presented. From the fact that differences between theoretical and experimental results have been observed, the heat exchanger has been cut apart and its internal structure investigated. Some **manufacturing defaults** have been identified thanks to this investigation.

These defaults imply an overall misbalancing of the flow rate inside the heat exchanger, which leads to a decrease of performances (thermal and hydraulic as well) compared to the predicted one, especially for low flow rates. A **new heat exchanger** model taking into account manufacturing default has been built up. After a calibration procedure, the newly developed model is in accordance with experimental results.

## 2 MAIN CHARACTERISTICS OF THE DEVELOPED HEAT EXCHANGER

The aim of this section is to present the main features of the developed heat exchanger. Definition of the specific geometry will be realized by the optimization process (see Section 3). However, some intrinsic characteristics (as well as the manufacturing process) have been defined/fixed at the early beginning of the project in collaboration with the industrial partner.

2.1 Flow configuration

In order to maximize the heat exchanger efficiency, the initial idea was to develop a U-flow configuration heat exchanger, as shown in Figure III-1. Nasif et al. (2008) has already investigated an enthalpy heat exchanger which presents a quite similar flow configuration (Z-flow configuration).

Such exchangers (also called quasi-counter flow heat exchanger) present a counter flow configuration over the major part of their heat transfer area. This latter is often called the central part of the heat exchanger.

A schematic representation of such heat exchanger is given in Figure III-1:
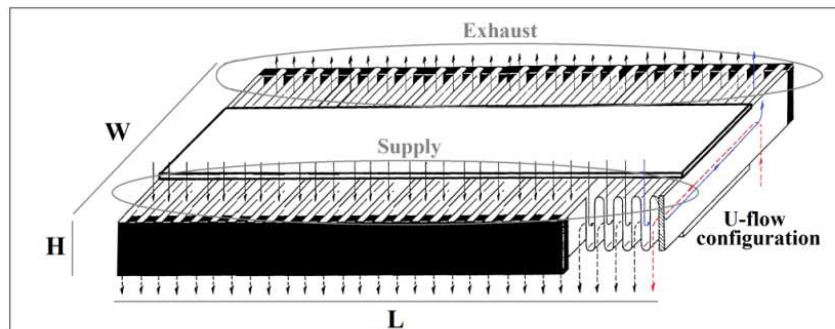
Figure III-1: U-flow configuration heat exchanger

In the rest of the chapter (as well as in the rest of the thesis), the overall dimension of the heat exchanger is assumed to be:

- W=0.22 [m];
- H=0.06 [m] ;
- L=0.45 [m].

Those overall dimensions correspond to those of a heat exchanger supposed to be installed in a single room ventilation standard unit (initial choice of the manufacturer).

2.2 Materials and structures

It has been decided to develop a heat recovery exchanger made in **synthetic material**, and more particularly polystyrene.

The main drawback of polystyrene heat exchangers concerns their low thermal conductivity compared to aluminum, as an example. However, this drawback can be counter-balanced by the high enlargement factor (ratio of the developed length to the protracted length) that can be reached with polystyrene heat exchangers (theoretically 400%) compared to traditional plate heat exchangers made of metal (rarely superior to 150% Ayub et al. (2008)).

Moreover, as shown in Chapter 2, the decrease in terms of efficiency for envisioned wall thickness (0.3 mm) is lower than 0.6% compared with a heat exchanger made with a wall resistance equal to zero.

Economic criteria have also been taken into account in the material choice.

2.3 Manufacturing process

The first step of the manufacturing process is to thermoform plate coming from a plastic roll. According to NCPS Board of Consultants and Engineers (2014), the general definition is:

"Thermoforming is a manufacturing process where a plastic sheet is heated to a pliable forming temperature, formed to a specific shape in a mold, and trimmed to create a usable product. The sheet, or "film" when referring to thinner gauges and certain material types, is heated in an oven to a high-enough temperature that it can be stretched into or onto a mold and cooled to a finished shape."

Once the thermoforming process is finished, the idea is to fold up the several corrugated plates like an accordion. This idea was first submitted by Kleeman (1978). A schematic representation of the several steps is given in Figure III-2:
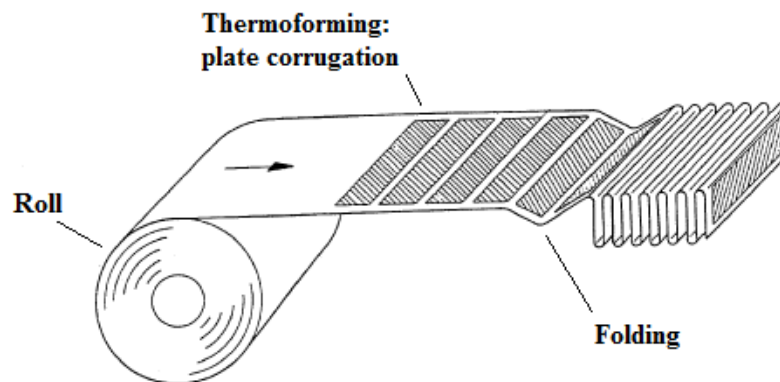
Figure III-2: Heat exchanger manufacturing process

The main advantages about this manufacturing process are:

- Easiness for assembling the heat exchanger;
- Possibility of adjustment of the heat exchanger length.

3   OPTIMIZATION OF THE HEAT EXCHANGER GEOMETRY

The optimization of the heat exchanger geometry is first based on the variation of the COP as a function of two defined geometric parameters (creation of a COP map). Then, some technical, economic and acoustic considerations will be taken in consideration to determine which the most effective final geometry is.

A discussion on some influencing parameters on the COP will also be proposed.

3.1   Coefficient of performance of SRVHR: Definition

The overall performance of centralized heat recovery ventilation is highly dependent on the hydraulic circuit (length and bending of the pulsing and extracting ducts) and therefore on the house and ducts configuration. In contrary, the overall performance of single room heat recovery ventilation is not influenced by the rest of the installation. As a result, performance of single room ventilation with heat recovery does not depend on the house characteristics but only on the characteristics of the device itself.

The overall performance of each unit can be defined by the ratio of the recovered heat transfer rate to the electrical power of the fans and is given by Equation III-1:

$$COP_{SRVHR} = \frac{Recovered\ heat\ transfer\ rate}{Electrical\ supplied\ power} = \frac{\dot{Q}_{recovered}}{\dot{W}_{fans}} \qquad \text{III-1}$$

By only taking into account the sensible part of the study (the total amount of latent heat rate compared to sensible recovered heat can neglected in moderate climate as Belgium: see Chapter 2), the recovered heat transfer rate is given by Equation III-2 and depends on the heat exchanger effectiveness (varying with the mass flow rate), the delivered mass flow rate and on the indoor/outdoor temperature difference:

$$\dot{Q}_{recovered} = \dot{M}_{fresh} \cdot c_p \cdot \varepsilon \cdot (T_{ind} - T_{out}) \qquad \text{III-2}$$

With

- $\dot{M}_{fresh}$ the fresh air mass flow rate in [kg/s];
- c_p the air capacity in [J/kg-K];
- ε the heat exchanger effectiveness [-];
- T_{ind} the indoor temperature;
- T_{out} the outdoor temperature.

As represented in Figure III-3, the parameters influencing the COP of the unit are:

- **Fan** performance;
- **Hydraulic performance of the unit**. This can be divided in two parts: one related to the passage of the air flow in the **heat exchanger itself** and another one related to the flows through **the rest of the unit** (filter, supply and exhaust of the unit);
- **Effectiveness** of the heat exchanger;

- **Climate**: indoor/outdoor temperature difference. From a yearly performance point of view, the interest of use of heat recovery ventilation is highly dependent on the climate (recovered heat over one year v s electrical consumption due to fans).
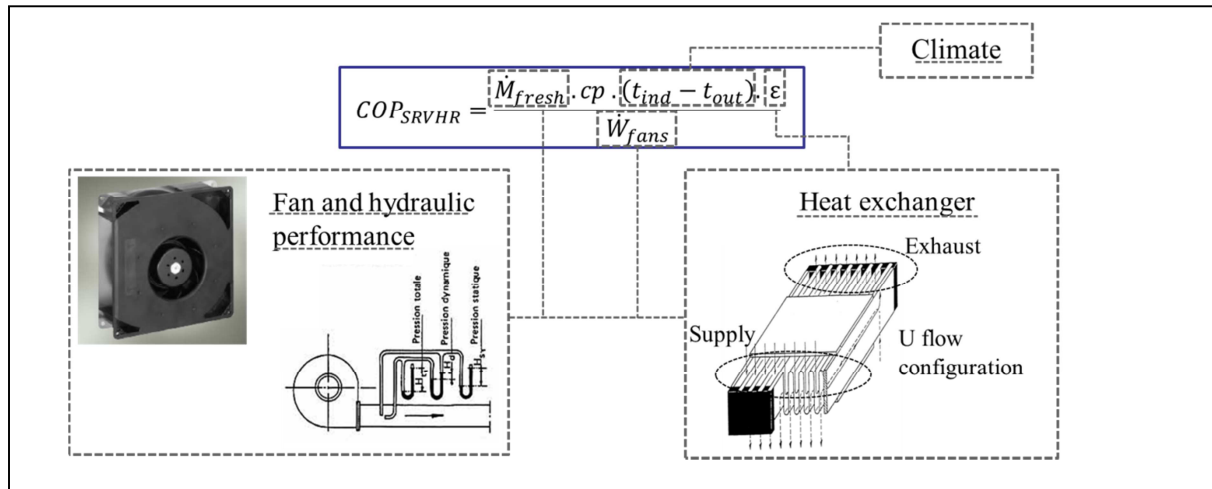

$$COP_{SRVHR} = \frac{\dot{M}_{fresh} \cdot cp \cdot (t_{ind} - t_{out}) \cdot \varepsilon}{\dot{W}_{fans}}$$

Figure III-3: Parameters influencing the COP$_{SRVHR}$

It is interesting to notice that most of heat exchanger manufacturers only indicate their heat exchanger effectiveness but not its hydraulic performance. It raises also question that only heat exchanger effectiveness (and not the Specific Fan Power SFP, and therefore the overall performance of heat recovery ventilation) is taken into account by government to deliver incentives.

3.2 Optimization procedure

The aim of the present section is to describe the procedure followed to determine the best dimension dedicated to a specific heat exchanger geometry. The several steps are summarized hereafter and schematically represented in Figure III-4:

- The first step is to determine/define heat exchanger characteristics depending on geometric factors. In the investigated case, the geometric characteristics are a_1 and b_1 and are defined in Section 3.5.

- The second step is to develop a heat exchanger model able to determine the thermal and hydraulic performance of the heat exchanger itself (efficiency and pressure drop due to air flow passage in the heat exchanger) as a function of these two defined geometric characteristics.

- By setting a volumetric flow rate and knowing both pressure drops related to the heat exchanger and the rest of installation, it is possible to determine the electrical consumption dedicated to fan (identification of the electrical consumption on the performance fan curve: ΔP vs $\dot{V}$).

- Knowing the heat exchanger effectiveness and the fans power consumption (and by setting the indoor/outdoor temperature difference), it is possible to determine the COP of the device. By varying independently the geometric dimensions of the heat exchanger (a_1 and b_1), it is possible to create a COP map depending on these geometric dimensions.

- The last step consists in taking into account the technical, economic and acoustical constraints to identify the values for a_1 and b_1 that optimizes the COP.
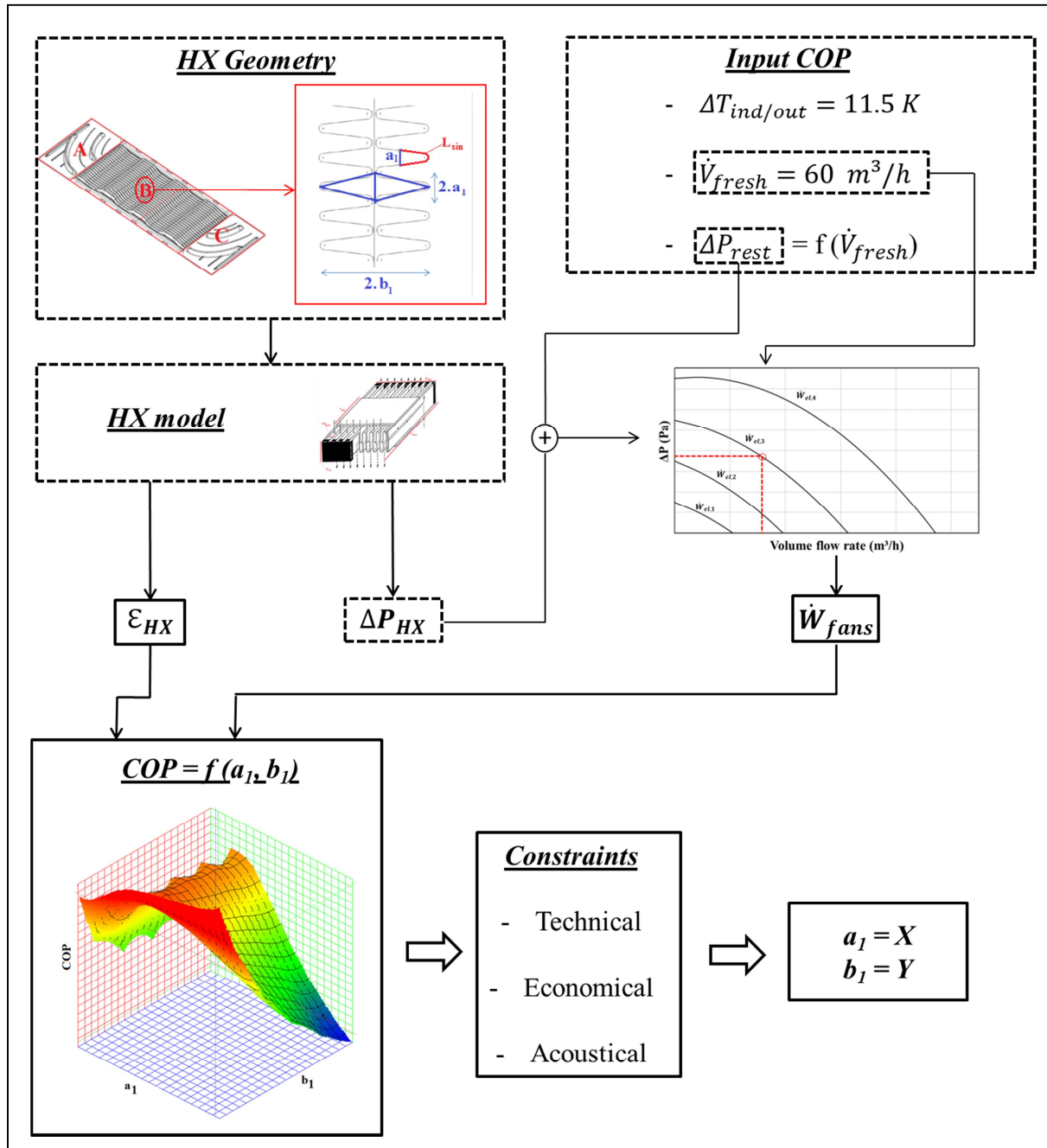
Figure III-4: COP optimization procedure

3.3 Optimization : parameters settings

The present section also consists in setting some values of the previously defined parameters influencing the COP determination:

-   In the rest of the optimization process, the indoor and outdoor temperature are respectively set to 20°C and 8.5°C, which corresponds to the mean indoor and outdoor Belgian temperature.

-   Flows are considered perfectly well-balanced in mass.

-   Electrical consumption is determined using fan characteristic curves by means of an interpolation drawn from experimental points, depending on the volumetric flow rate and

pressure drop of the whole unit (HX and rest of the unit). Used fan curves have been first experimentally determined.

- Pressure drop related to the rest of the installation have been first experimentally determined before the COP optimization phase.

COP optimization is first conducted by setting a fresh air flow rate of 60 m³/h (considered first at the nominal flow rate) but results related to some other flow rates will also be presented. Some parametric studies on the hydraulic performance of the rest of installation have also been performed.

3.4 Optimization Constraints

The aim of this section is to list the several constraints to take into account in the optimization process of the geometry of the heat exchanger. These constraints are divided into three categories:

- **technical** (manufacturing constraints);
- **acoustic** (pressure drop limit);
- **economic** (manufacturing costs).

All of these three constraints are detailed hereafter.

3.4.1 Technical constraints

Due to technical manufacturing constraints, the minimal values for a_1 and b_1 are respectively:

- **$a_1 = 1$ mm**
- **$b_1 = 2.5$ mm.**

According to the definition proposed by Ayub (2008), the **enlargement factor Φ** is the ratio of the developed length to the protracted length. As already mentioned, the enlargement factor that could be reached with polystyrene heat exchanger is much higher than with aluminum heat exchangers. However, the enlargement factor for polystyrene heat exchanger has also a limit. Using the current manufacturing technology, the maximum enlargement factor that could be reached is **400%**. To the author's knowledge, a heat exchanger presenting such value (as realized in the frame of this thesis) is a world first.

3.4.2 Acoustic constraints

As already shown in Chapter 1, great attention is paid to noise level of the device since the units are placed in living rooms. In order to obtain the best acoustic performance of the device, several guidelines can be followed:

- Choice of the most silent fan (step realized at the early beginning of the project);
- Placement of sound absorber. In SRVHR, impact of their use is really limited (comparison with acoustical performance with and without silencers as shown in Chapter 5). This is mainly due to the lack of space dedicated to SRVHR;
- Maximizing the **hydraulic performance** of the device (reduction of the pressure drop of the unit).

A first parameter to take into account in the COP optimization is the hydraulic performance of the heat exchanger. From this fact, a map of **ΔP as a function of a_1 and b_1** will also be drawn in order to check the hydraulic performance of the determined optimized COP.

3.4.3 Economic constraints

From an economic point of view, manufacturing process cost is highly dependent on the **number of plates** composing the heat exchanger. Therefore, for a same overall performance, a geometry presenting a **higher factor b_1** will always be preferred.

3.5 Geometry of the heat exchanger

The central part of the heat exchanger is corrugated in a sinusoidal form. The sinus form can be defined by only considering two parameters: a_1 and b_1.

Nomenclature used for the geometry definition is indicated in Figure III-5. The crucial question is: *"what are the best values for a_1 and b_1 in order to optimize the COP (trade-off between the hydraulic and thermal performance)?"*
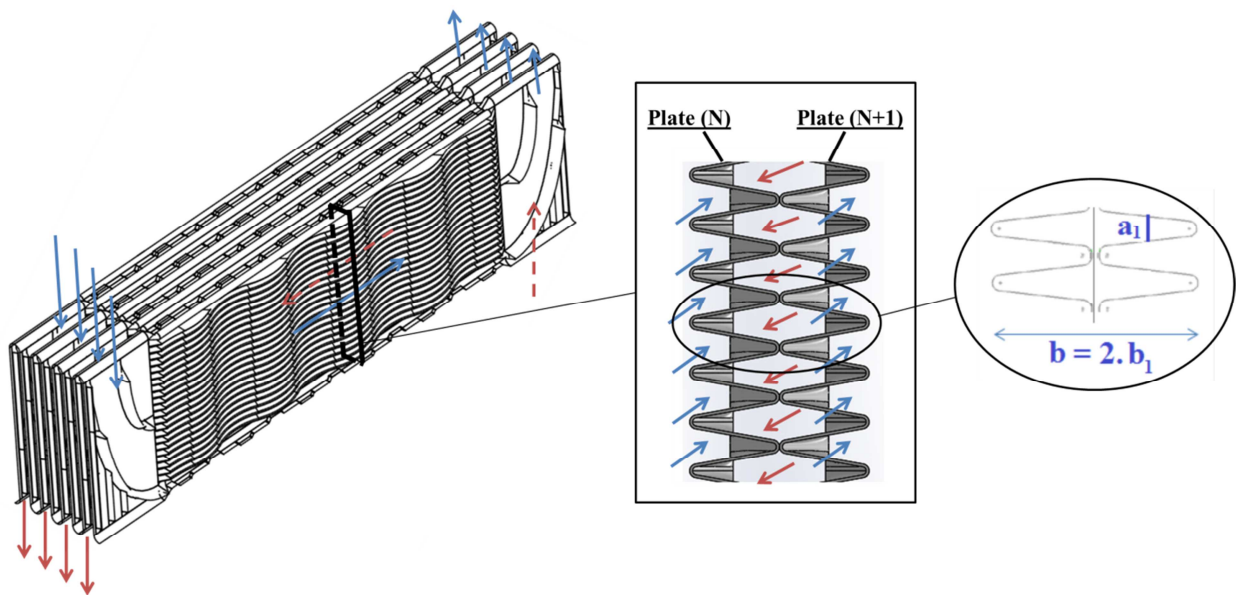
Figure III-5: Geometry of the central part of the heat exchanger (nomenclature)

A plastic sheet used to stiffen the heat exchanger is inserted between two corrugated sheets, as shown in Figure III-6.
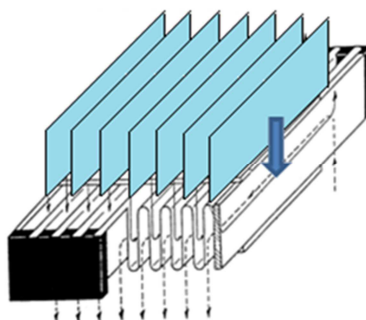
*Figure III-6: Insertion of plastic sheet in order to stiffen the heat exchanger*

3.6 Semi-empirical heat exchanger model

In order to carry out the optimization procedure, a semi-empirical model (SEM) was built in the EES environment. The aim of this section is to give features of the model (assumptions used, heat transfer area determination, pressure drop correlation,…).

3.6.1 Discretized heat exchanger model

The model is based on a discretization of the heat exchanger in three zones (two supply/exhaust zones: A and C; one central part: B), as represented in Figure III-7.

This division is employed because of the difference in terms of geometry of the several zones. Moreover, configuration is in counter flow arrangement in central part and in cross flow arrangement in supply and exhaust parts.
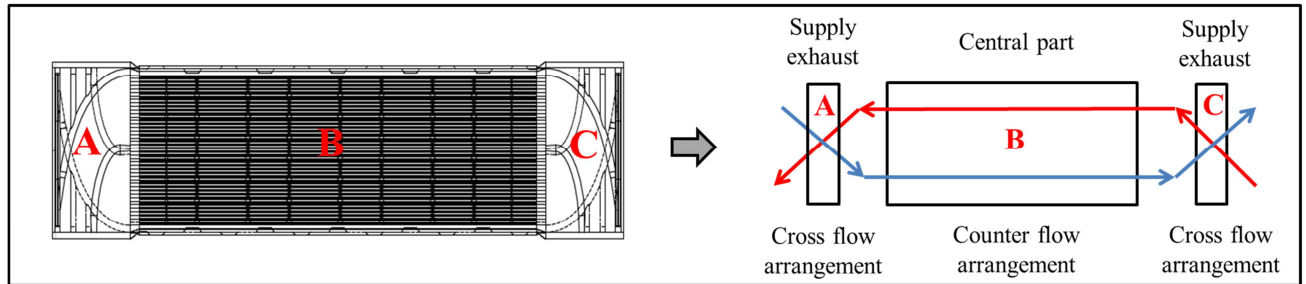
*Figure III-7: Discretized heat exchanger model*

Concerning the hydraulic performance of the heat exchanger, the same method exposed in Chapter 2 has been applied. It consists in the identification of the friction factor and the convective heat transfer coefficient for each zone.

The heat transfer is determined for each zone by the ε-NTU method. Then, the overall effectiveness of the heat exchanger is defined by Equation III-*3*:

$$\varepsilon = \frac{\dot{Q}_A + \dot{Q}_B + \dot{Q}_C}{\dot{C}_{min} \cdot (t_{su,ind} - t_{su,out})} \qquad \text{III-3}$$

3.6.2 Enlargement factor determination

As mentioned in section 3.5, the central part of the heat exchanger is assumed to be corrugated following a *"sinus"* form. Nomenclature concerning the two geometric parameters (a_1 and b_1) used in the frame of the COP optimization process is given in Figure III-8:
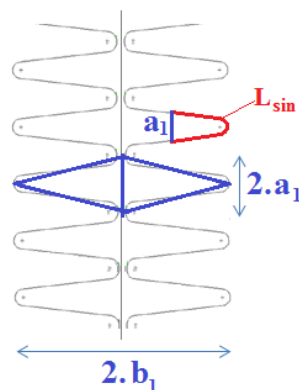
Figure III-8: Central part of the matrix, nomenclature used in the COP optimization process

The enlargement factor (and therefore the heat exchanger area) for the central part of the matrix is calculated, as a function of a_1 and b_1, by using Equation III-4. This corresponds to the ratio between the length of the sinus semi wavelength (L_{sin}) and a_1 :

$$\Phi = \frac{L_{sin}}{a_1} \qquad \text{III-4}$$

L_{sin} is determined by Equation III-5 (application of the Pythagorean theorem). This elliptic integral cannot be analytically solved. The resolution of the equation is numerically obtained by the EES software:

$$L_{sin} = \int_0^{a_1} \sqrt{1 + f(x)'^2}\,dx = \int_0^{a_1} \sqrt{1 + \left(\frac{b_1.\pi}{2.b_1}.\cos\frac{x.\pi}{a_1}\right)^2}\,dx \qquad \text{III-5}$$

3.6.3   Employed correlations for friction factor and convective heat transfer coefficient

Correlations dedicated to sinus form are given in literature (Hesselgraves (2001)) but only for ratio between a_1 and b_1 less than two. From this fact, as schematically represented in Figure III-8, sinusoidal channels have been approximated by assuming triangular channels.

Investigations carried out in the frame of the Chapter 2 provide calibrated correlations for friction factor as well as for convective heat transfer coefficient for triangular channels with a similar shape. It has been decided to use them for correlations dedicated to the central part of the heat exchanger.

Concerning parts A and C, correlations dedicated to rectangular cross section area have been used (see Chapter 2).

3.7   Optimization results

### 3.7.1   COP optimization: a_1 and b_1 determination

The aim of the present section is to show the results of the optimization process. This could be graphically determined by representing the COP evolution as a function of a_1 and b_1.

COP optimization is given in Figure III-9. Presentation of the results is made by varying a_1 and b_1 from 0.5 mm to 5 mm. Then, COP optimization is made by taking into account the constraints.

Dashed lines correspond to the technical constraints ($a_1 > 1$mm, $b_1 > 2$mm, $\Phi < 400\%$).

The dashed arrow corresponds to the economic constraint. It aims to reduce the number of plates and therefore to choose the highest value of b_1 for a same value of COP.

The purple cross corresponds to the optimized set of values for a_1 and b_1.
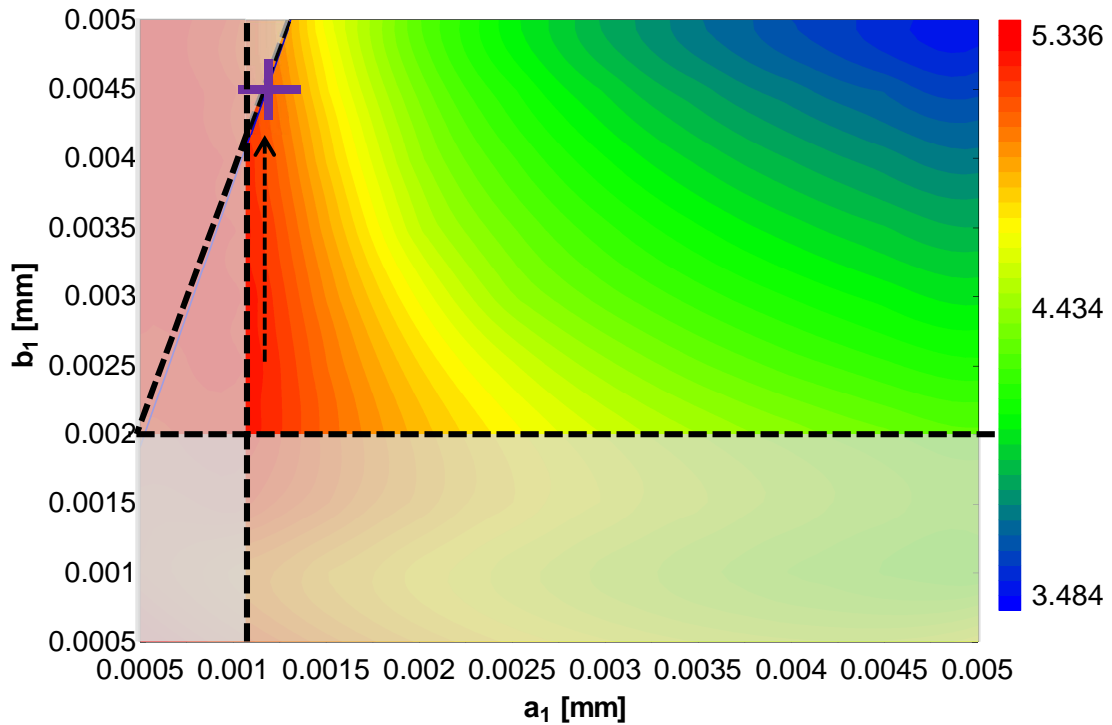
Figure III-9: COP optimization

As observed in Figure III-9, the most effective set of values for a_1 and b_1 seems to be:

- **a_1 = 1.22 mm;**
- **b_1 = 4.50 mm.**

The predicted COP is equal to 4.93. In the rest of the section, some features of the heat exchanger such as effectiveness, pressure drop and heat transfer area are presented.

3.7.2 Effectiveness

Figure III-10 shows the evolution of the effectiveness as a function of a_1 and b_1. For optimized a_1 and b_1, the calculated effectiveness is equal to 70% for a well-balanced flow rate of 60m³/h. Given the geometric constraints, it seems difficult to obtain better effectiveness.
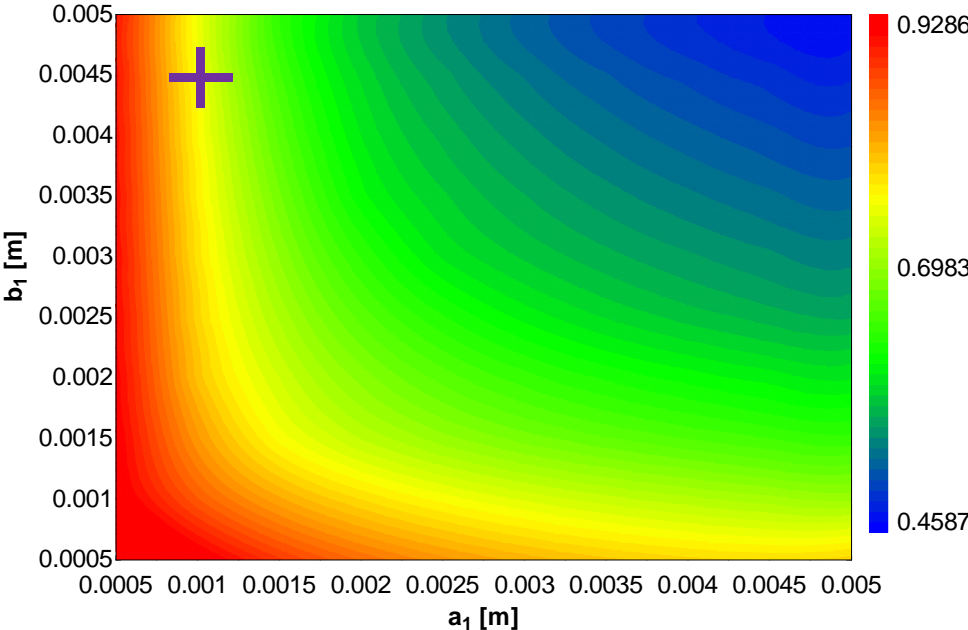
Figure III-10: Effectiveness as a function of a_1 and b_1

3.7.3 Pressure drop

Figure III-11 shows the evolution of the pressure drop as a function of a_1 and b_1. Contrary to effectiveness evolution, it is possible to obtain better hydraulic performance if setting a higher value for a_1. However, the determined value for 60m³/h (34 Pa) remains reasonable compared to maximal value that could be reached for the allowed values of a_1 and b_1 (260 Pa).
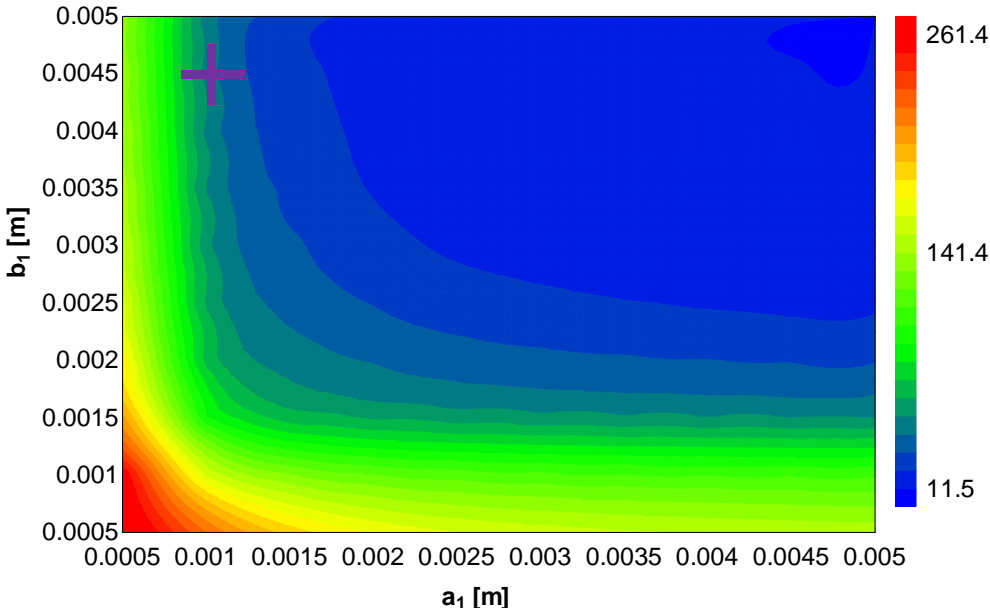

Figure III-11: Pressure drop as a function of a_1 and b_1

3.7.4 Heat transfer area

Figure III-12 presents the heat transfer area evolution as a function of a_1 and b_1. By comparing Figure III-10 and Figure III-12, it can be observed a similarity between the heat transfer area and the effectiveness of the heat exchanger.
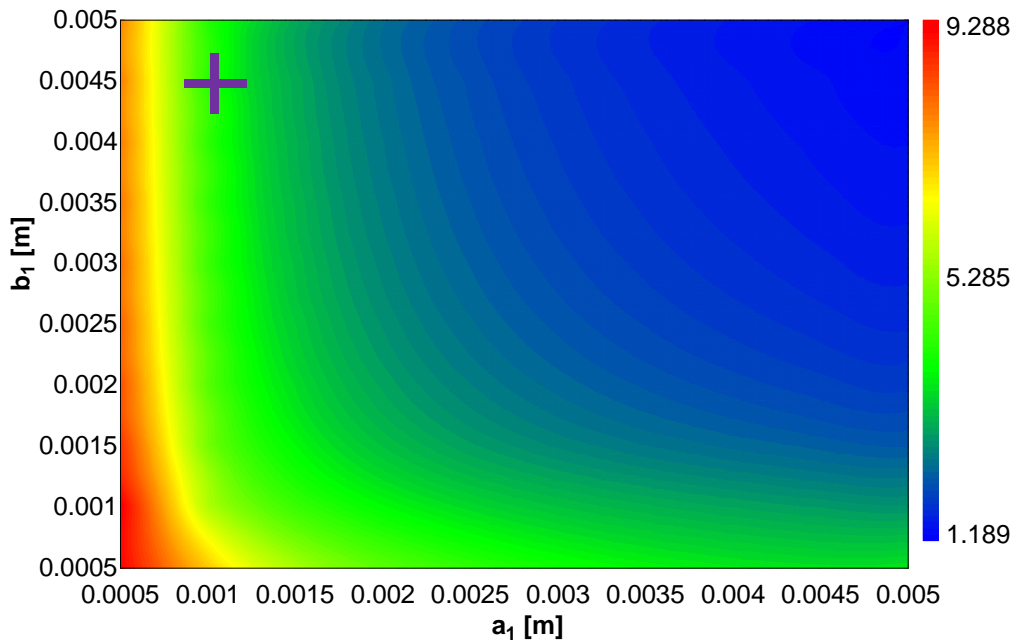
Figure III-12: Heat transfer area as a function of a_1 and b_1

3.8 Discussion

The aim of this discussion section is to investigate the influence of some parameters/inputs on the values of the optimal COP. It is realized by varying the flow rates, the hydraulic performance of the rest of the installation and the overall dimensions (H or L) of the heat exchanger (cfr Figure III-1).

3.8.1 Flow rates

COP optimization procedure for well-balanced flow rate of 30m³/h has been performed. It gives the same values for a_1 and b_1 as when COP optimization is realized with a flow rate of 60m³/h.

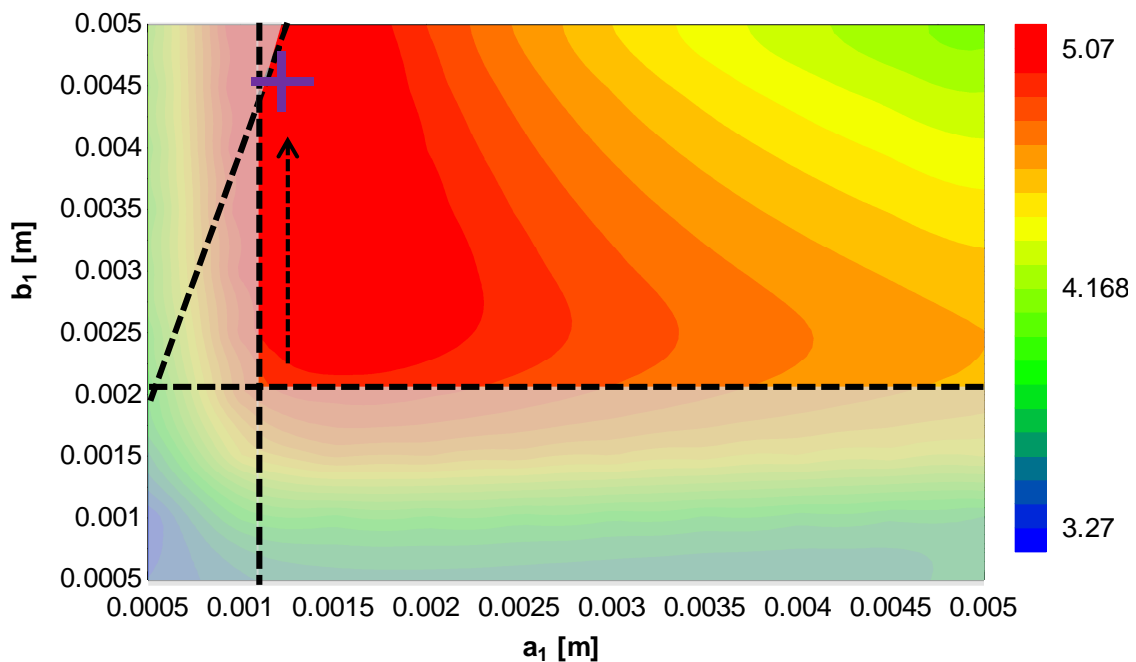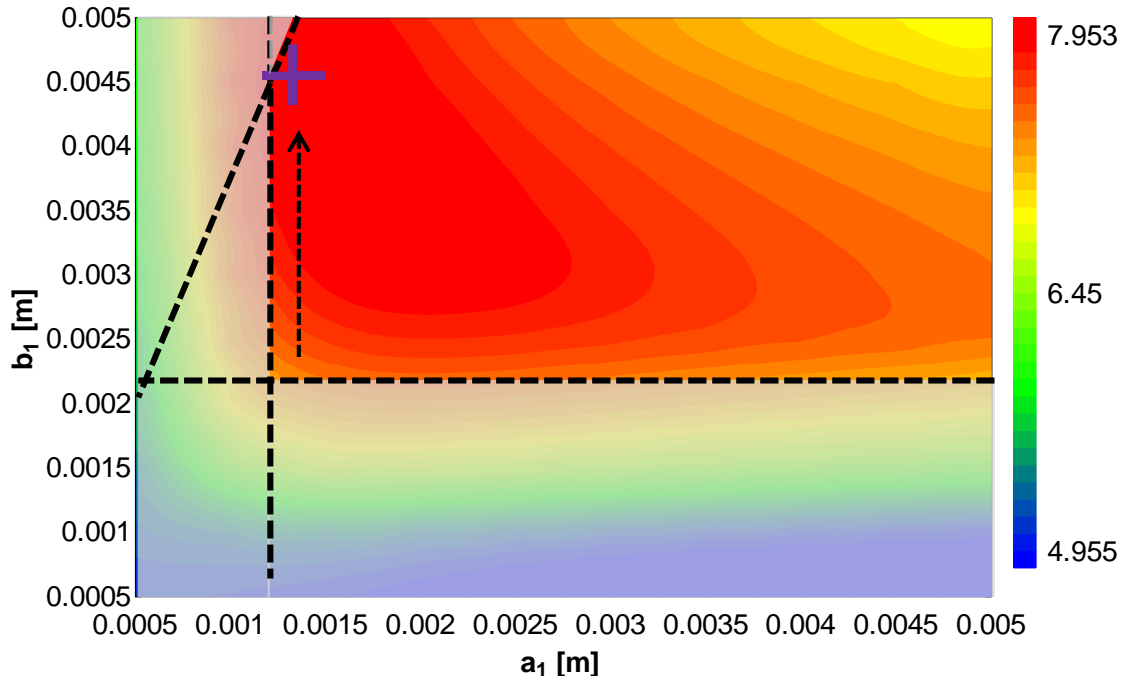*Figure III-13: COP optimization procedure for well-balanced flow rates of 30 m³/h*

3.8.2   Rest of the installation: hydraulic performance

If setting the pressure drop related to the rest of the installation equal to 0 (thus by reducing the unit to only a fan and a heat exchanger), the COP optimization is obtained and presented in Figure III-14. Obviously, the present investigated parametric study is an ideal case but it allows investigating the sensitivity of the COP with the hydraulic performance of the rest of the installation.

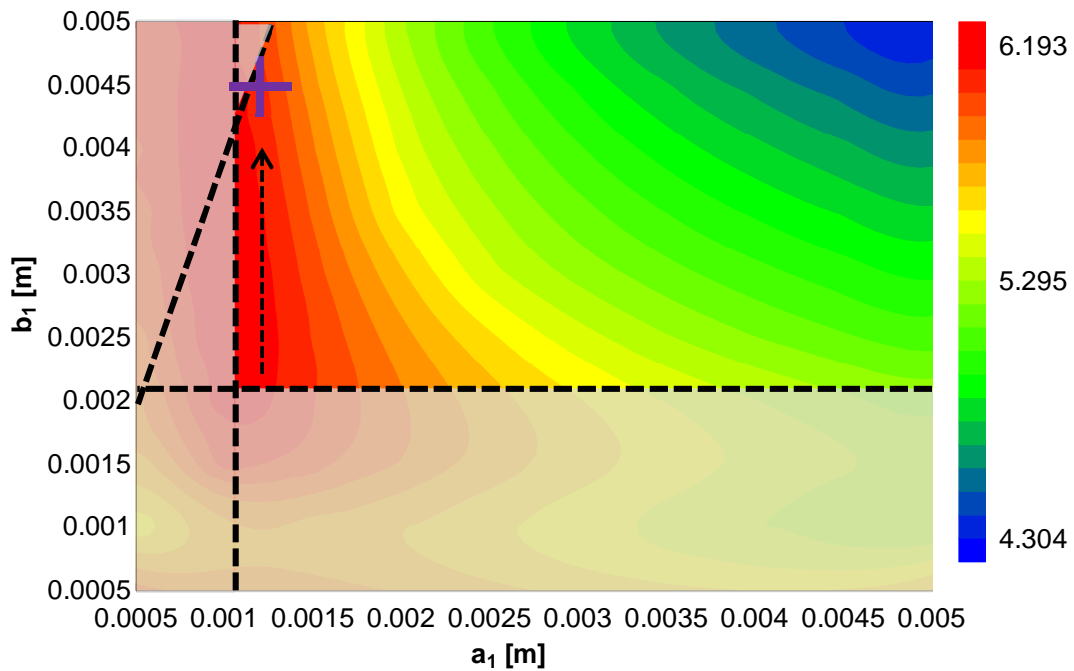*Figure III-14: COP optimization for well-balanced flow rates of 60 m³/h (with ΔP$_{rest}$=0)*

The same results are obtained concerning the values of a_1 and b_1. However, it can be observed a difference concerning the range where the COP is optimized. This latter is larger and other set of values of a_1 and b_1 could be picked up. This observation is particularly interesting when regarding the hydraulic (and thus acoustic) performance of the unit. Another set of a_1 and b_1 reducing the pressure drop could be chosen (Figure III-11). That shows the importance of the hydraulic performance of the rest of the installation when optimizing the COP.

Also, it can be observed a high difference in terms of COP map (and thus on the maximum value of COP) if taking or not taking into account the pressure drop related to the rest of installation (COP is almost doubled). It highlights the fact that hydraulic performance of the unit has a crucial role on the performance of such unit (and not only the effectiveness of the heat exchanger).

3.8.3   Overall dimensions of the heat exchanger (W, H and L)

Changing the height H or changing the length of the heat exchanger L (see Figure 1 for nomenclature) is the same in terms of changes of the performance (COP) of the unit. Both of the changes consist in adding a heat exchanger in parallel.

Figure III-15 gives the result of the optimization process if H or L is doubled (that consists in using two exchanger of dimensions given in Figure III-1 in parrallel).

Figure III-15: COP optimization procedure for well-balanced flow rates of 60m³/h (by assuming a height H of the heat exchanger equal to 12 cm or a length L equal to 90 cm)

As shown in Figure III-15, it is really interesting to notice that even by doubling the volume of the heat exchanger (by doubling either W or H), the maximal value reached by the COP (6.2) is lower than by reducing to zero the pressure drop of the rest of the installation (COP=8, as shown in Figure III-14). Once again, this highlights the importance of the hydraulic performance and its impact on the COP.
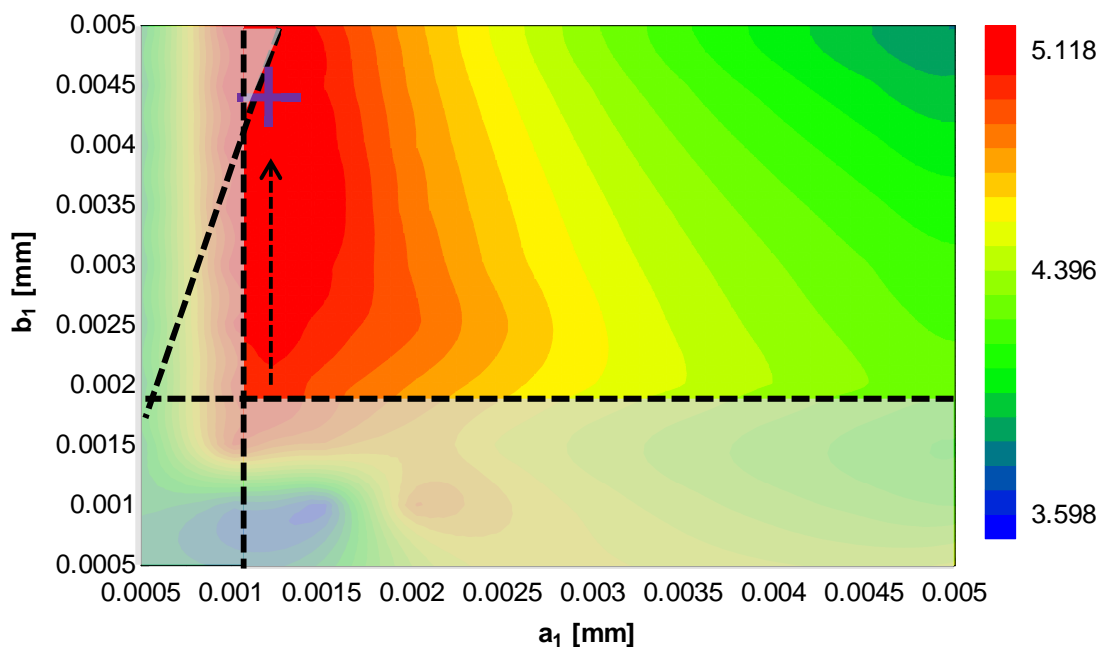

Figure III-16: COP optimization procedure for well-balanced flow rates of 60m³/h (by doubling the length of the central part)

Contrary to modifying dimensions L and H, modifying W (by doubling the length of the central part of the heat exchanger) is not equivalent to add a heat exchanger in parallel but to add an exchanger in

series. This leads to a complete change in the maximal value reached by the COP (5.11, as shown in Figure III-16). This could be easily explained by the fact that adding a heat exchanger in series raises the effectiveness of the heat exchanger but also double the pressure drop (and thus raise the electrical power supplied to the fans). This is not the case by adding a heat exchanger in parallel where both thermal and hydraulic performances of the unit are improved.

This fact can be highlighted by realizing a parametric study by varying the length of the central part of the heat exchanger. Results of this study are given in Figure III-17. This study has been realized with optimized a_1 and b_1 values and same inputs chosen for the COP optimization process (well-balanced flow rates of 60 m³/h, indoor/outdoor temperature difference of 11.5 K, same pressure drops related to the rest of installation,…) .
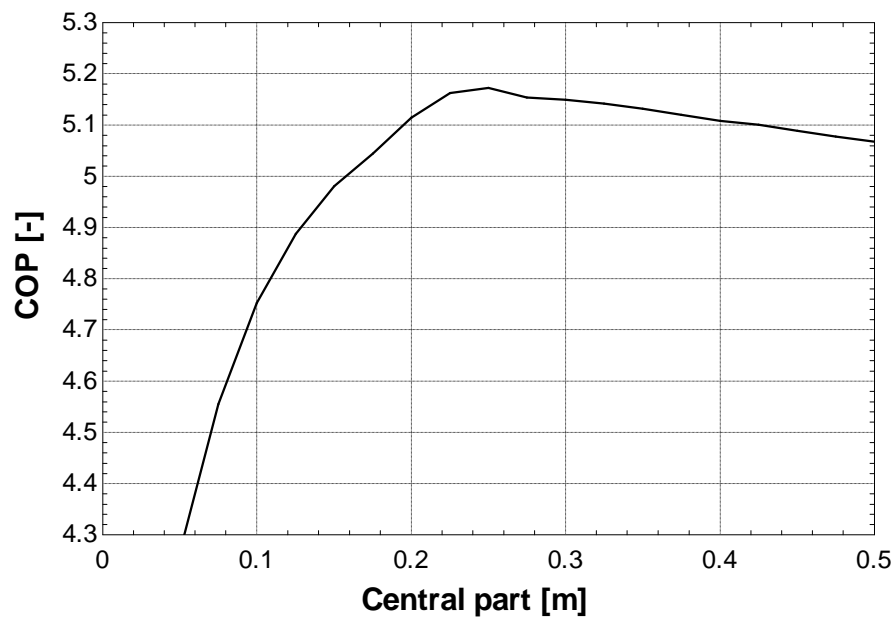
Figure III-17: COP as a function of the central part length of the unit

It can be observed that there exists a value (0.24) for the central part of the matrix that corresponds to an optimum for the COP. For higher values, rise of effectiveness is counterbalanced by the pressure drop which leads to an overall degradation of the COP.

3.8.4 Conclusions

Several conclusions can be drawn:

- Same results for a_1 and b_1 are obtained when varying the parameters/inputs used for optimization procedure;
- Hydraulic performance of the unit (and thus of the rest of installation) has a crucial importance and highly impacts on the COP;
- Increasing L or H is always a plus for the overall performance of the unit. It positively impacts on the hydraulic as well as the thermal performance of the unit;
- This is not the case when increasing W. This can be explained by the fact that increasing W degrades the hydraulic performance of the heat exchanger. As a result, there is a value for W that optimizes the COP. In the present case, it is impossible to reach this value given the geometric constraints fixed by the manufacturer at the beginning of the project.

4   CFD ANALYSIS

The aim of the CFD analysis was to validate/confirm geometry resulting from the optimization procedure by comparing CFD results and semi empirical results. The CFD study has been performed by Greencom s.c.r.l. company (heat exchanger manufacturer).

In terms of calculation time, semi empirical model permits to quickly determine what the most effective geometry is: it takes less than 15 seconds to perform a parametric study of 100 cases.

Calculation time for CFD ranges between 36 and 48 hours, depending on the flow rates set as inputs. Moreover, drawing the geometry could also be time consuming (approximately two days for a confirmed technical drawer). However, CFD simulations allow the possibility to obtain results coming from a specific geometry (without geometric assumptions) and also to highlight some misdistributions effects.

Some recent papers deal with the CFD in the frame of heat and energy exchanger, such as the ones of Yaici et al. (2013) and Al-Waked et al. (2013).

4.1 CFD Simulations

The following results have been obtained by using the CFD commercial package *"Solidworks flow simulation 2012"*.

The heat exchanger has been considered perfectly symmetric and in order to reduce the calculation time, only one plate of the heat exchanger has been modeled, as shown in Figure III-18. The rate of each flow at the entrance corresponds to the total flow rate divided by the number of plates.

The investigated domain corresponds to the space between two plastic sheets (see Figure III-6). The CFD model consists of one flow passage for the return stream and one flow passage for the fresh stream.

It has been assumed a steady state (no time evolution) model of the heat exchanger.

4.1.1 Governing equations

The conservation laws for mass, angular momentum, and energy in the Cartesian coordinate system are used in the conservation form, according to "Solidworks 2012" for the CFD simulations.

4.1.2 Boundary conditions

One "pressure" type boundary condition and one "flow" type boundary conditions have been set for both fluids (internal flow boundary conditions).

At the entrance, temperature and dynamic flow properties (i.e. the flow direction, and volume flow rate) have been imposed. At the exhaust, the atmospheric pressure has been set. The hydraulic performance (ΔP) is determined by the difference of the supply pressure drop and the atmospheric pressure.

Concerning the wall boundary conditions, the velocity boundary condition at solid wall corresponds to the well known *"no slip"* conditions: the velocity at the wall is equal to zero (the fluid at the wall is not moving).

No penetration and no cross flow is imposed on the solid wall boundary (the wall is considered impermeable). That implies that the velocity normal to the wall is equal to zero.

A zero heat flux conditions is imposed at the symmetry plan (at the plastic sheet), assuming that the profile temperature is the same on the other side of the plastic sheet (same flow rate and heat exchanger considered symmetric).

The heat conductivity in solid media is described by the Fourier's law:

$$q_h = -\mathrm{k}\,\frac{\partial T}{\partial x_i} \qquad\qquad \text{III-6}$$

The wall properties (conductivity, density and heat capacity) are defined directly by the solver when setting the type of used materials.

4.1.3 Mesh generation

Mesh generation is automatically performed using "Solidworks flow simulation 2012". It has been decided to use a fine grid. The total number of cells to perform the study has been set up equal to 2536000 cells.

4.1.4 Example of results

Figure III-18 provides the velocity and temperature profiles for flow rates of 60 m³/h for the total heat exchanger (and thus a flow rate of 0.625 m³/h per plate for both flows).
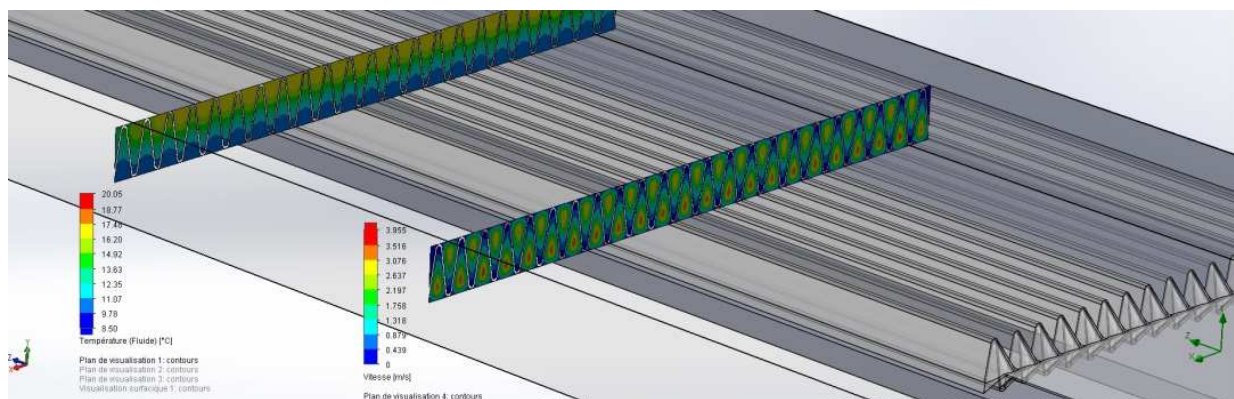
Figure III-18: Temperature and velocities inside the heat exchanger according to CFD simulations

Figure III-19 shows a zoom on the velocity profile for both parts of the plate. As it can be observed, the below part of the channel is well supplied contrary to the upper part of the channel. This is due to the sinusoidal form of the channel.
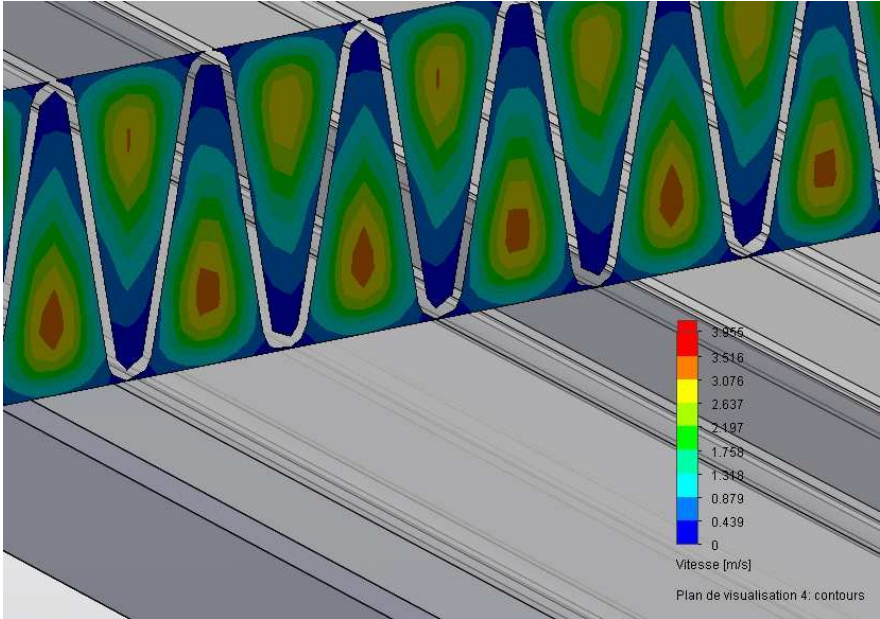
Figure III-19: Velocities profiles inside the heat exchanger according to CFD simulations

4.2 CFD vs Semi-Empirical Model (SEM)

The aim of the section is to compare results predicted by the semi empirical model and CFD in terms of effectiveness and pressure drop. Three CFD simulations have been performed for three different flow rates (5, 60 and 100 m³/h). Results coming from these three simulations are represented by blue squares in Figure III-20 and Figure III-21.
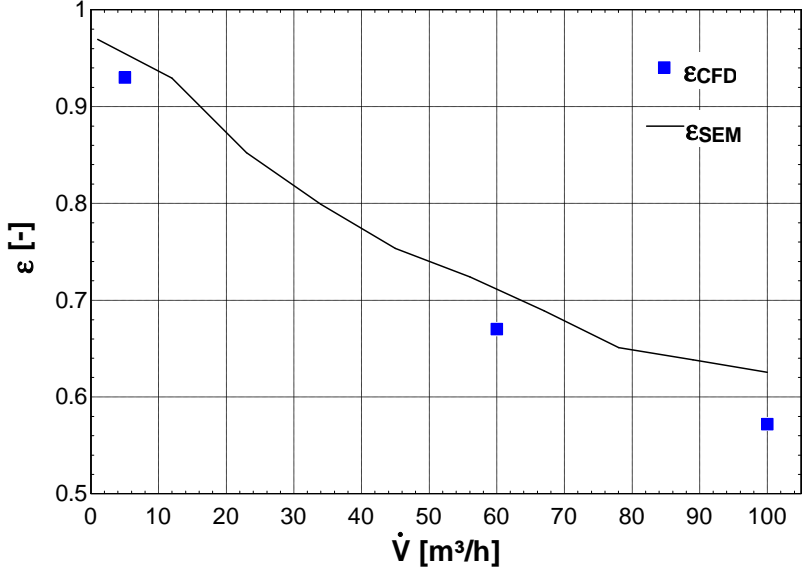
4.2.1 Effectiveness comparison

Figure III-20: Effectiveness vs flow rates (comparison between SEM and CFD results)

Effectiveness determined by CFD and by SEM follows the same evolution as it can be observed in Figure III-20, even if the SEM always presents values superior to results given by CFD. However, the maximal deviation between the two models is inferior to 5 points of efficiency.

4.2.2   Hydraulic performance comparison

Pressure drop follow the same evolution for both models, as shown in Figure III-21. It can be observed that the CFD overestimates the pressure drop compared to SEM but results stays relatively close (maximal absolute difference is less than 15 Pa for the highest flow rate).
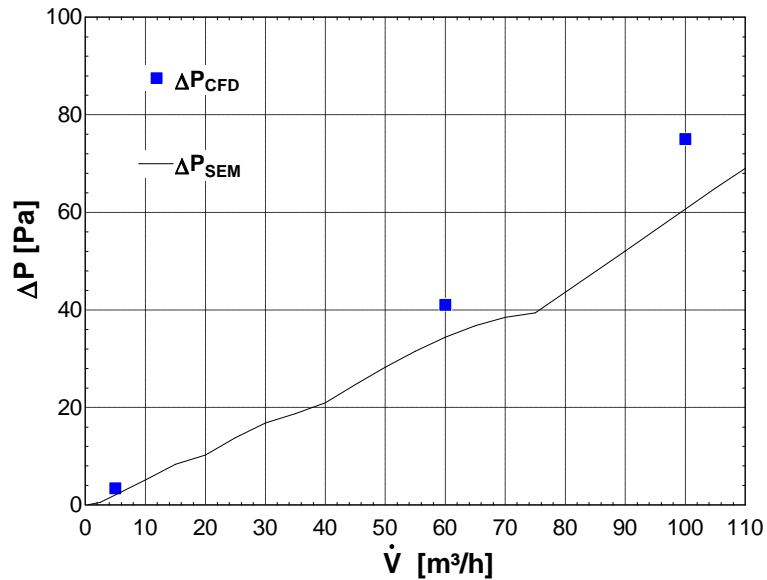

Figure III-21: CFD vs SEM (hydraulic performance)

4.2.3   COP comparison

For well-balanced flow rates of 60m³/h, COP varies from 4.93 for SEM to 4.7 for CFD. Values are considered close and both of them are considered as acceptable for the developed product. From this fact, it has been decided to keep the values determined for a_1 and b_1.

5 "RAPID PROTOTYPING" TESTING METHOD

As already mentioned, the manufacturing process of thermoforming mold is quite expensive ($\pm$ 75 000 €). Before launching it and in order to confirm the numerical results and more particularly the one related to the hydraulic performance, a unique method in the field of heat exchanger analysis has been applied. This method consists in measuring the pressure drop due to the passage of air between two rapid prototyped plates.

According to Behrendt and Shellabear (1995), *"Rapid prototyping (RP) is a concept concerned with producing a physical part as quickly as possible from a design idea, as part of the product development process"*.

To the best author's knowledge, only the paper of Alm et al. (2005) deals with the use of rapid prototyping method in the field of manufacturing process of heat exchangers. However, the type of heat exchanger (ceramic micro heat exchanger) as well as the application field is completely different as the one presented in the frame of this thesis.

Producing two rapid prototyped plates does not allow for determining the efficiency of the final heat exchanger presenting the specific chosen geometry. However, it has been considered that the knowledge of the hydraulic performance was an essential piece of information because of its influence on the overall performance of the unit (COP) but also on the acoustic performance of the unit. Moreover, tests on rapid prototyped plates allow for determining precisely the hydraulic performance of the heat exchanger and therefore to verify/check values predicted by CFD and SEM.

5.1 Manufacturing process of rapid prototyped plates

One of the main advantages of rapid prototyping method is that it allows creating a piece in a small amount of time (around one day for the corrugated plates presented in the frame of this chapter). It makes this process particularly suitable in the design step of heat exchanger, especially when testing several geometries. Moreover, the rapid prototyping process costs around 250 € per two rapid prototyped plates, which is considered as negligible especially compared to the price of thermoforming mold.

There are many different rapid prototyping technologies available. According to Pham and Gault (1998), *"rapid prototyping method may be divided by those involving the addition of materials and those involving its removal"*. The material addition technologies can also be divided into process involving a liquid, process involving discrete particles and process involving solid sheets. Each of them can also be divided in several parts.

Rapid prototyped plates have been realized by the Sirris Company by means of Selective Laser Sintering method that can be classified as a discrete particles addition process. According to Kruth et al. (1998), *"Selective Laser Sintering produces parts by fusing or sintering together successively layers of powder material"*. SLS process uses a laser to melt powder of plastic (or other material such as metal ceramic or glass) to create a mass that has the desired 3D shape, as schematically represented in Figure III-22.
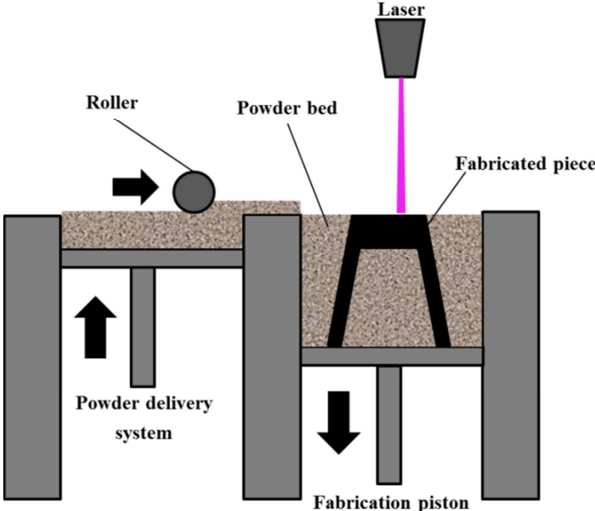
Figure III-22: Schematic representation of Selective Laser Sintering (SLS) process

5.2 Rapid prototyped geometry

Figure III-23 shows the precise geometry of the rapid prototyped plates, resulting from the COP optimization process.
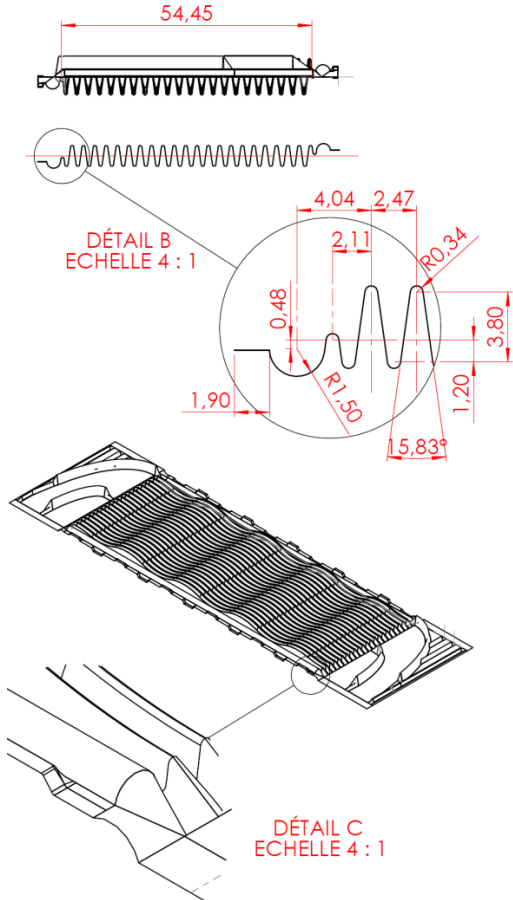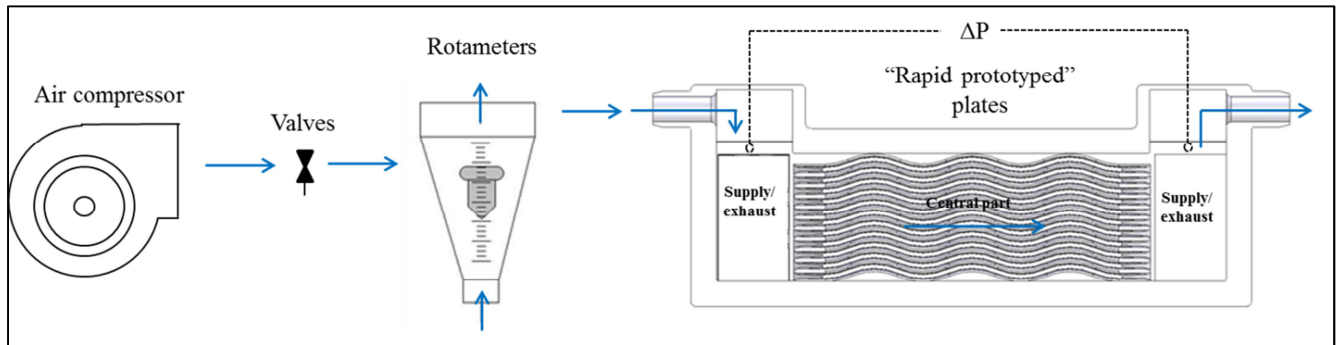

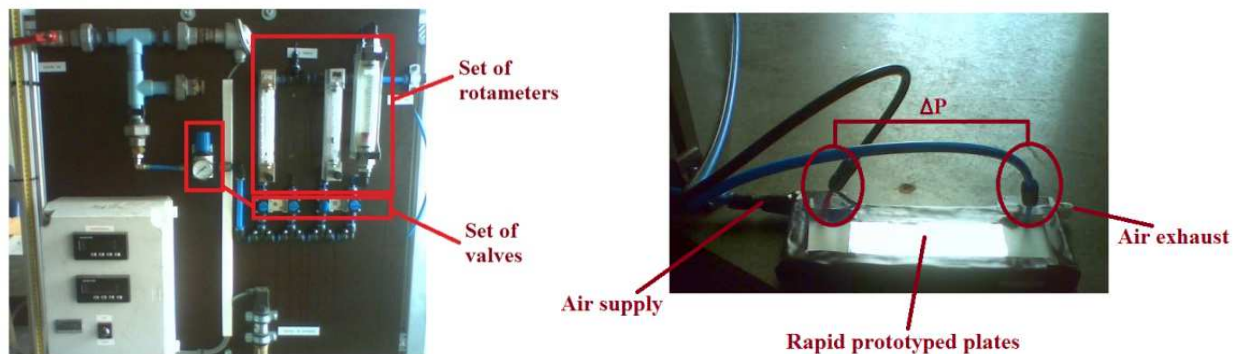*Figure III-23: Rapid prototyping geometry*

5.3 Experimental apparatus

Experimental apparatus, schematically represented in Figure III-24, is composed of:

- an air compressor to supply the flow;
- a set of valves to adjust the flow rate;
- a set of rotameters to measure the flow rate (with different full scale values: 40, 300, 1500 and 108000 l/h);
- a set of differential pressure drop sensors (with different full scale values);
- a temperature measurement at the air inlet of the sample;
- the rapid prototyped heat exchanger plates.

Figure III-24: Schematic representation of the experimental apparatus

Some pictures of the practical achievements are shown in Figure III-25:

Figure III-25: Practical achievements of the rapid prototyping campaign testing process

A differential pressure drop sensor of 125 Pa of full scale (sensirion SDP 1000-L05) has been used for all the measurements. The accuracy of the used sensor corresponds to the maximum between 0.2% FS and 1.5% m.v. Accuracy of the used rotameters corresponds to 1.25% FS.

One of the aims of the rapid prototyping test campaign was also to check if the flow rate was well distributed along the heat exchanger. That is the reason why it has been decided to bore nine holes along the heat exchanger. This allows to take several differential pressure drop measurements and therefore to quantify the flow rate repartition along the heat exchanger.

The nine holes have been symmetrically bored in the central part of the rapid prototyped plates, as schematically shown in Figure III-26:
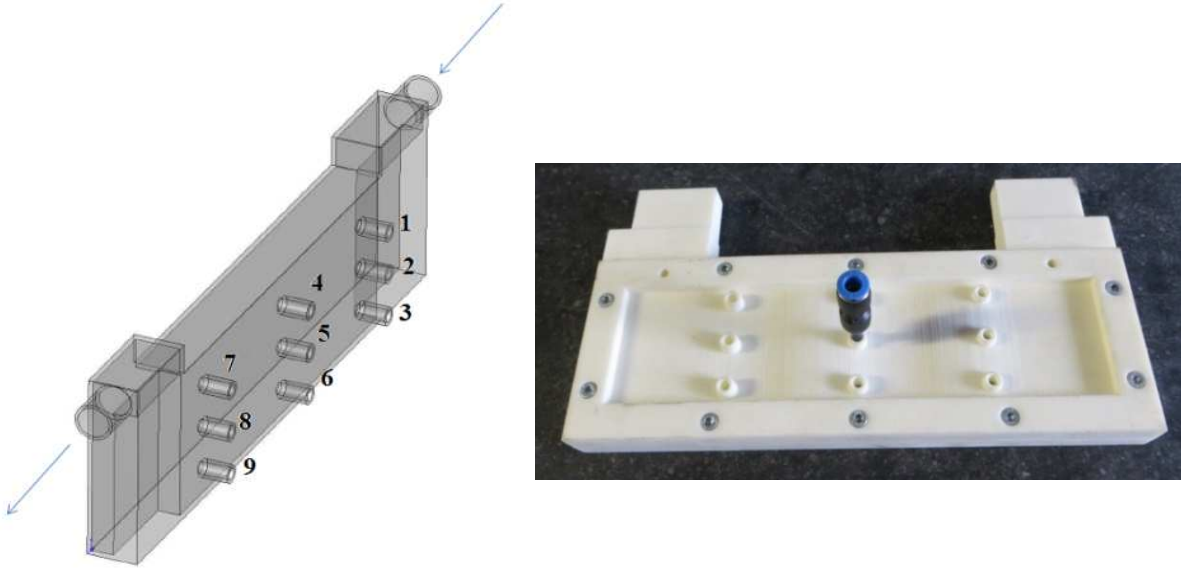
Figure III-26: Nomenclature of the nine drilled holes and practical achievements of the differential pressure drop measurements along the heat exchanger

5.4   Experimental results

The present section focuses on the rapid prototyped experimental results.

5.4.1   Overall pressure drop on the entire sample

First, it is important to mention that the sample is considered symmetric given the negligible observed difference in terms of pressure drop if flows are diverted. Figure III-27 shows the comparison between the predictions by SEM and CFD models and the measurements in terms of hydraulic performance.
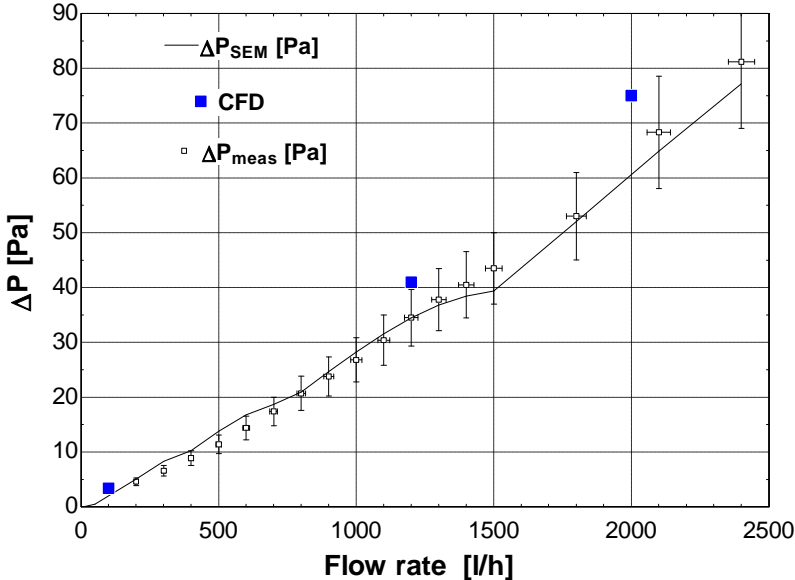

Figure III-27: Comparison of hydraulic performance between experimental, SEM and CFD results

The black full line represents the simulation results from the SEM. The mean deviation between the prediction by the model and the measurement is 7.5% and the maximal absolute difference is less than 4 Pa.

Blue full squares represent simulation results from CFD. CFD simulation seems to overestimates a bit the pressure drop but follow the same trend as the experimental results.

5.4.2   Pressure drop repartition on the tested sample

As already mentioned before, one of the concerns about the accordion heat exchanger was about the flow repartition along the height of the heat exchanger. This misdistribution could lead to performance degradation of the heat exchanger.

In order to check that specific potential issue, pressure drop has been taken along the heat exchanger by means of the nine drilled holes.

The pressure drop map is presented for three different flow rates: 600 l/h, 1000 l/h and 1400 l/h. Nomenclature (1 to 9) of the nine drilled holes is the same as the one proposed in Figure III-26.
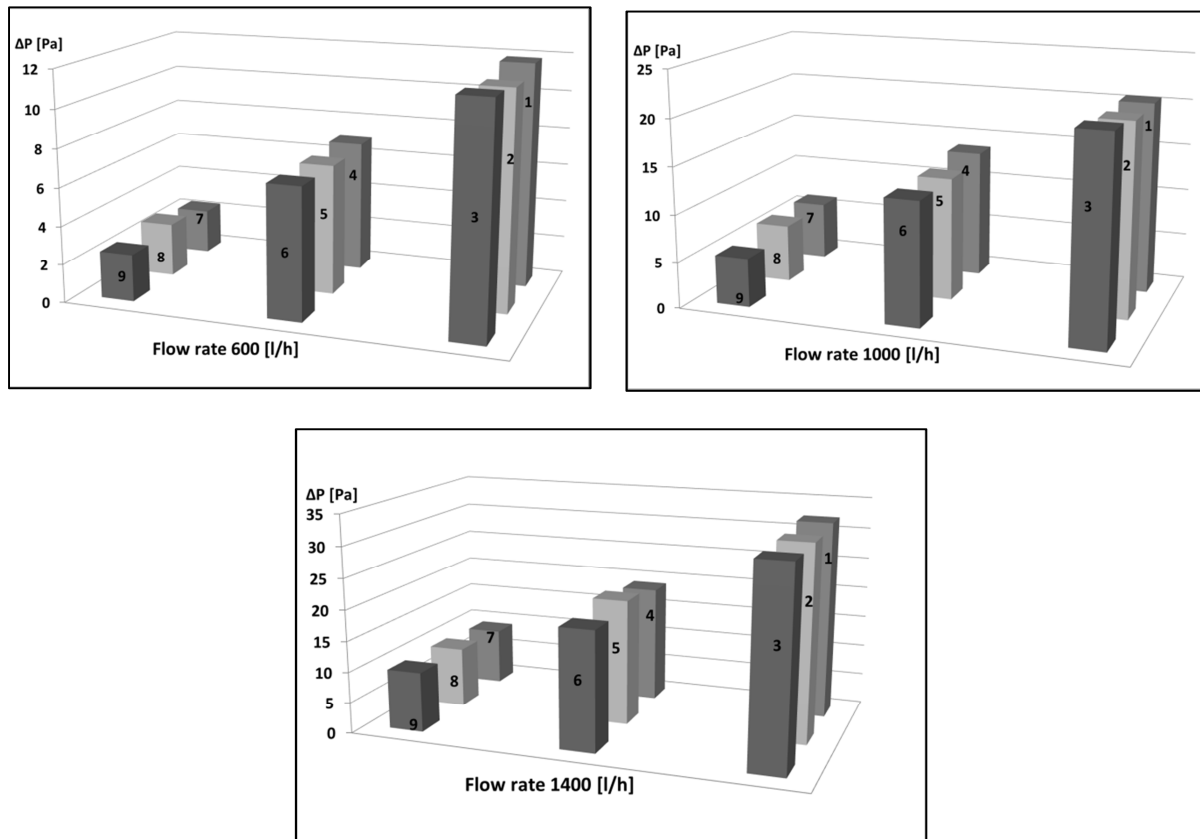
Figure III-28: Pressure drop map for 600 l/h, 1000l/h and 1400l/h

As shown in Figure III-28, the flow rate seems to be well distributed along the heat exchanger, since the negligible difference in terms of ΔP for the three investigated flow rates.

5.5   Conclusions about rapid prototyping tests

Tests on rapid prototyped plates allow confirming the hydraulic performance predicted by the SEM and confirm the trends given by the CFD simulation results.

Pressure drop measurements by means of the nine drilled holes show the good distribution in the direction perpendicular to the flow.

6   CHARACTERIZATION OF THE FINAL HEAT EXCHANGER

The aim of the present section is first to describe the experimental results concerning the final prototype of the heat exchanger. Then a comparison between numerical and experimental results is proposed.

Regarding the difference between experimental and numerical results, it was decided to cut off the heat exchanger in order to deeply study the corrugation form by scanning the central part of the matrix. This investigation permits to highlight a manufacturer default inducing an overall misbalancing impacting on the heat exchanger performance. The numerical model is modified and calibrated to quantify this overall misbalancing.

6.1   Manufacturing process of the heat exchanger

As already mentioned in Section 2, the final heat exchanger was realized by first corrugating a roll of plastic sheet through a thermoforming process. Figure III-29 shows the thermoforming mold used:

(a)   *(b)*

*Figure III-29: Thermoforming mold (a) and zoom on the central part
of the thermoforming mold (b)*

Once the thermoforming process is over, a corrugated plastic sheet is obtained, as represented in Figure III-30:
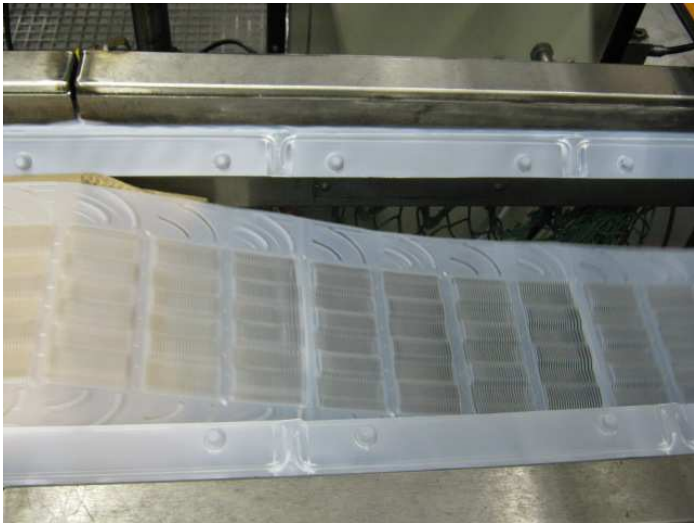
Figure III-30: Corrugated plastic sheet

The plate is folded manually and then inserted in a guide, as shown in Figure III-31:

Figure III-31: Heat exchanger assembly

Once the plastic plates are inserted in the guide, plates of the future heat exchanger are pressed according to the Figure III-32:


Figure III-32: Press of the heat exchanger

The last step of the heat exchanger manufacturing process is to place an angle iron full of glue to fix all the folded sheets together, as shown in Figure III-33:


Figure III-33: Placement of the angle iron

6.2   Test bench modification

The same experimental apparatus as the one presented in the second Chapter of this thesis was used to test the final heat exchanger prototype. The experimental apparatus was designed in such a way that several heat exchangers could be tested. Compared to the test bench presented in the second chapter, the only modification concerns the box containing the heat exchanger in order to fit the dimensions of the tested exchanger, as shown in Figure III-34:
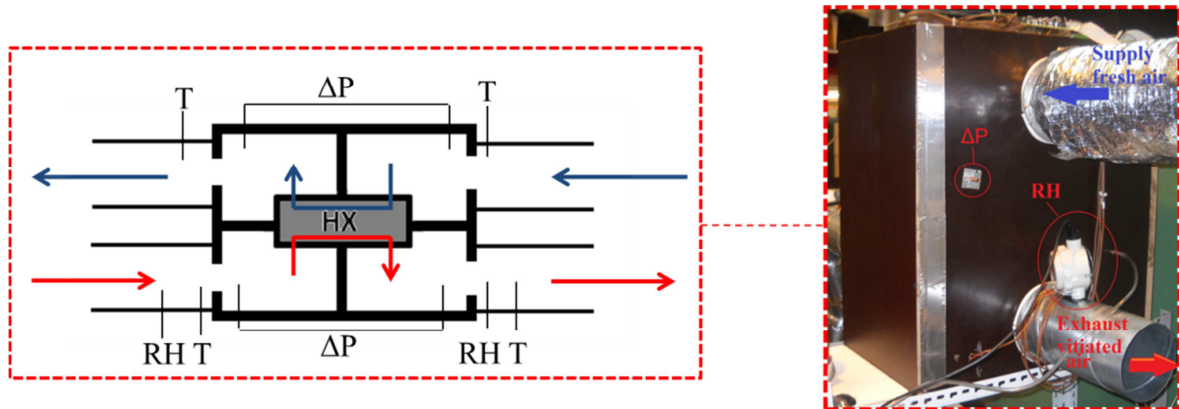
Figure III-34: Adaptation of the test bench

Concerning the supply and exhaust air temperature measurements, guidelines indicated by European Standard EN 308 have been applied: 5 type T thermocouples have been placed as schematically and practically represented in Figure III-35.
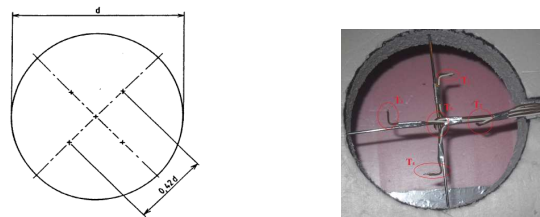
Figure III-35: Supply and exhaust air temperature measurements (EN 308)

A damper has been placed upstream the heat exchanger to ensure a well-balanced flow rate along the heat exchanger. The box is insulated by means of polystyrene plate of 3 cm thickness in order to reduce ambient heat loss. A special attention has been paid to air tightness between the tested heat exchanger and the different parts of the box, as shown in Figure III-36:

Figure III-36: Box containing the heat exchanger

6.3 Comparison between experimental and numerical results

6.3.1 Hydraulic performance

The comparison between the prediction by the CFD and SEM and the experimental measurements in terms of hydraulic performance is given in Figure III-37.
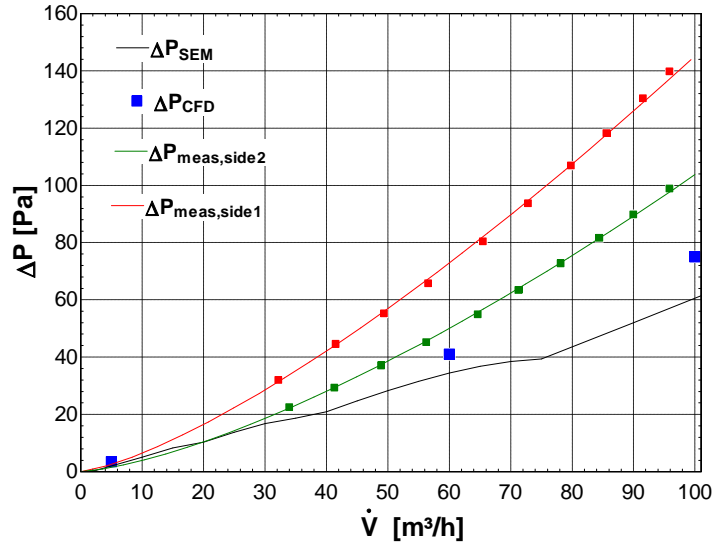

Figure III-37: Experimental side 1, side 2, SEM and CFD

Several remarks can be enounced regarding those results:

- The first one concerns the difference between hydraulic performance measured on side 1 and side 2 even though the heat exchanger is theoretically symmetric.

- The hydraulic performances is underestimated by both CFD and SEM. Nevertheless, SEM predictions have been previously validated by means of tests on the rapid prototyped plates (cfr. Figure III-27). That obviously implies a difference between the geometry of the rapid prototyped plates and the final heat exchanger.

6.3.2 Thermal performance

Comparison between models and experimental results in terms of efficiency is presented in Figure III-38:
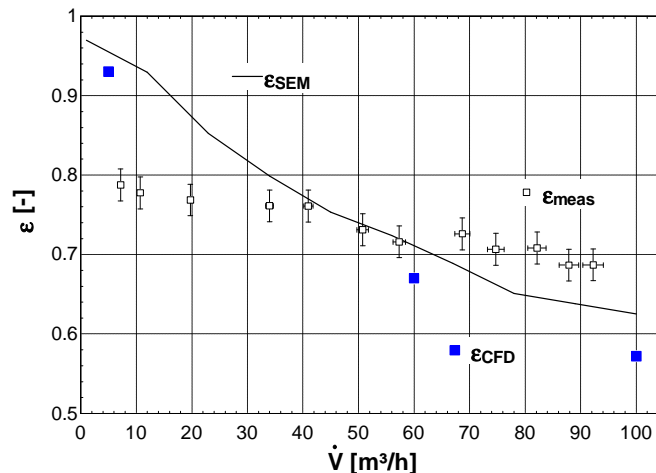

Figure III-38: Experimental results vs SEM vs CFD

As shown in Figure III-38, effectiveness seems to be poorly predicted by both of CFD and SEM. Some physical phenomena are clearly not taken into account by the models. This confirms the observation done regarding the hydraulic results.

Even the evolution trend (especially for low flow rate) is not well predicted by models. That means that only a modification of the convective heat transfer coefficient is not applicable in this case and that an overall misbalancing of flow rates is to be taken into account.

In order to better understand the difference between models and reality, a deep investigation on the heat exchanger is carried out in the next section. Starting from the observation done in Section 6.4, a new model (called post-model) will be built in (Section 6.5).

6.4 Heat exchanger diagnosis

In order to understand the difference observed between experimental and numerical results in Section 6.3, it has been decided to deeply investigate the central part of the heat exchanger. To do so, the heat exchanger has been cut off and scanned, as schematically represented in Figure III-39.

The scanning permits to zoom and therefore to identify the some manufacturer defaults, impossible to visualize at naked eye.
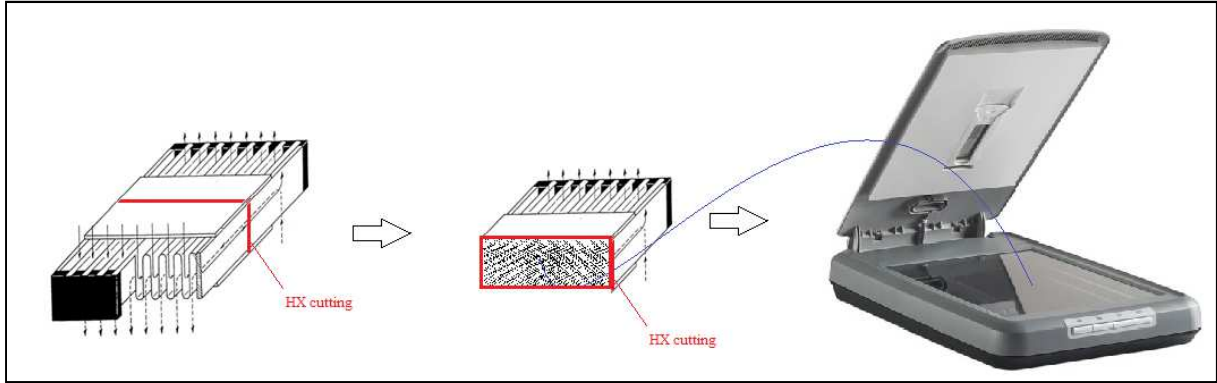

Figure III-39 : Investigation of the central part of the heat exchanger

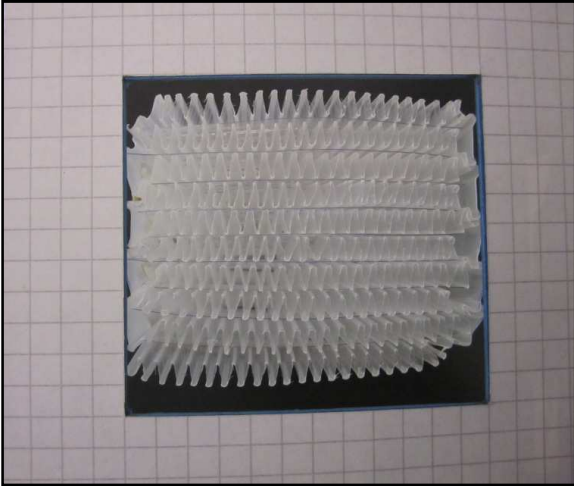Result of the scanning procedure is given in Figure III-40:

Figure III-40: Scanning of the central part of the heat exchanger

Thanks to this scanning procedure, two types of defaults have been detected/defined:

- Random defaults;
- Systematic defaults.

These defaults are investigated in the next sections.

6.4.1 Random defaults

So-called "random" defaults means that these defects appear in a non recurrently way. Their repetition is non-systematic but indicative of problems inherent during the manufacture phase of the exchanger.

Even if they are non-systematic, their occurrence is quantitatively quite high which bring us to the conclusion that the geometry is "uncontrolled" in the central part. This can be explained due to a crush of the corrugation during the *"accordion"* assembly (observed difference between corrugated plates before and after the assembly).

An example of manufacturing defects called "random" is given in Figure III-41:
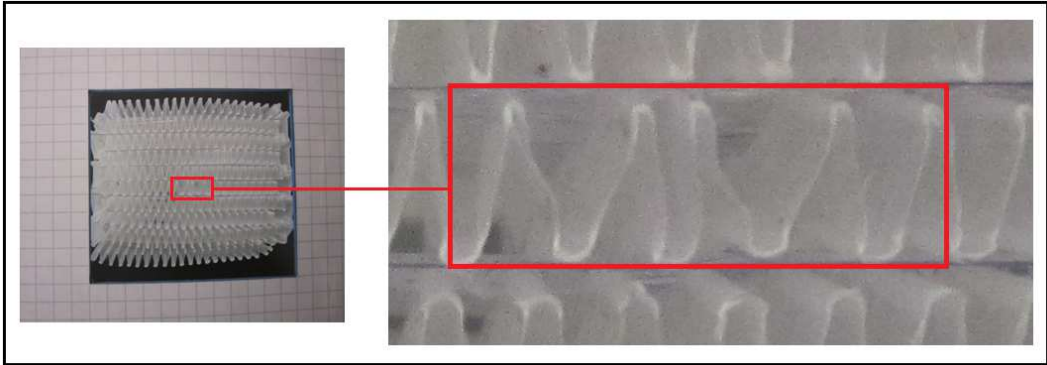
Figure III-41 : Random defects

By their definition, the so-called random defects are impossible to model for a full exchange but the knowledge of their presence is paramount in our investigations. They allow highlighting the fact that the general elongation factor of our matrices results in a low rigidity of the plates and therefore a little controlled geometry, mainly in the central part. These defects inevitably lead to non-uniformity of flow over the height of the heat exchanger, which impacts directly on the thermal and hydraulic performance of the exchanger.

6.4.2 Systematic defaults

Scanning the central part has allowed to highlight major difference between the theoretical geometry and the actual geometry of the exchanger.

Figure III-42 : Identification of the differences between theoretical and real geometry

As it can be seen in Figure III-42, the differences between the theoretical and actual specification is striking. Channels that were designed to be symmetric are actually unbalanced (blue comparison).

Thus, a deeper observation of Figure III-42 allows better understanding the profile of the experimental results:

- The asymmetry and the difference in terms of cross section area allows explaining the existence of a difference between pressure drops measured on side 1 and pressure drops measured on side 2.

- The observation of the channel geometry also allows for an explanation of the low effectiveness of the heat exchanger for low flows. Indeed, narrowing seen in Figure III-42 involves an important non-uniformity of flow within a same channel of the central part of the heat exchanger. In other terms, upper portion of each channel is less air supplied than the lower portion. Furthermore, this small flow of air is in contact with the portion of the channel better supplied over the opposite side. From this fact, a flow imbalance along the height of a channel is to be deplored.

The concern now is to numerically quantify this cross section area asymmetry. To do this, an industrial design software ("Solidworks") has been used to determine the length of the sides and the area of the portion of a channel.

The results given in Figure III-43 concerns what seems to be a "typical" channel:
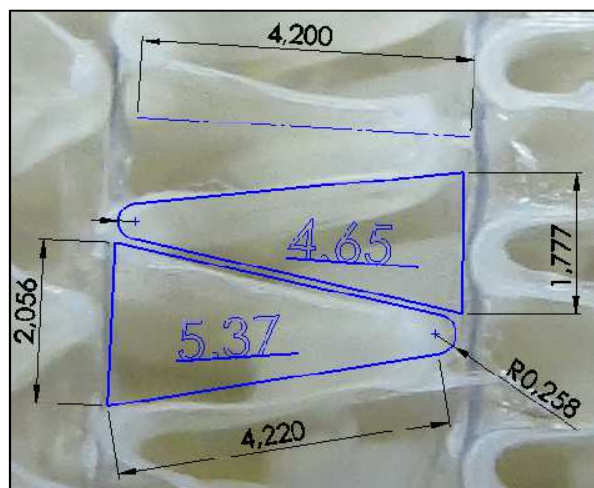
Figure III-43 : Quantification of the channels asymetry

First of all, it is important to notice that the measured height of a channel is 4.2 mm. Theoretically, the height of a channel is supposed to be equal to 4.5 mm. This involves a diminution of the cross section area for both channels compared to the theoretical channels. This leads to an enlargement factor equal to 371%.

The total cross sectional areas of a "typical" half-channel from side 1 and side 2 are respecively 4.65 mm^2 and 5.37 mm². The side 2 has a passage surface greater than 15% compared to side 1.

6.5 Post-modeling

In order to better understand phenomenon's appearing in the heat exchanger, it has been decided to develop a new model, called post-model, based on the observation realized in the previous section.

Chapter III: Development steps of a heat exchanger dedicated to single room ventilation

First of all, it is important to mention that it is not possible to take into account all the singularities of the geometry (presence of random defects). The first assumption is to neglect all the defaults in the post model.

The second assumption is to extend the dimension of a "typical" channel (see Figure III-43) to all the channels, even if in practice the geometry is globally uncontrolled.

6.5.1 Discretization of the heat exchanger

The same discretization as the one defined in Section 3 is proposed, except that the central part of the heat exchanger is also discretized in two parts. This is done in order to take into account the misbalancing observed in the previous sections, as schematically represented in Figure III-44:
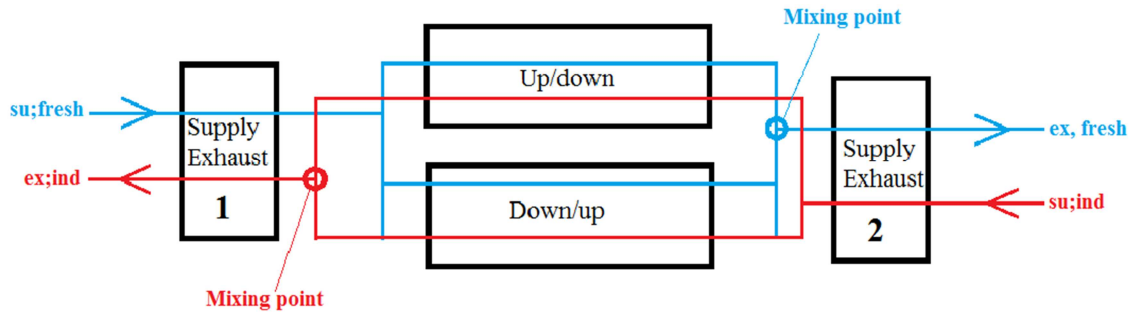

Figure III-44: Discretization of the heat exchanger

For the mixing point, energy conservation equations for both fluids are:

$$\dot{M}_{ind} \cdot cp_{ind} \cdot T_{su;ind;SE1} = \dot{M}_{UD;ind} \cdot cp_{ind} \cdot T_{ex;ind;UD} + \dot{M}_{DU;ind} \cdot cp_{ind} \cdot T_{ex;ind;DU} \qquad \text{III-7}$$

$$\dot{M}_{fresh} \cdot cp_{fresh} \cdot T_{su;fresh;SE2} = \dot{M}_{UD} \cdot cp_{fresh} \cdot T_{ex;fresh;UD} + \dot{M}_{DU} \cdot cp_{fresh} \cdot T_{ex;fresh;DU} \qquad \text{III-8}$$

with:

- SE1 : Supply/exhaust 1
- SE2 : Supply/exhaust 2
- UD : Up/Down
- DU : Down/UP

Determination of the flow rates related to the upper and lower parts of the channel (for both sides) is realized by an iterating process. The stopping criterion for the algorithm is to obtain the same pressure drop for both parts of the channel:

$$\Delta P_{UD;ind} = \Delta P_{DU;ind} \qquad \text{III-9}$$

$$\Delta P_{UD;fresh} = \Delta P_{DU;fresh} \qquad \text{III-10}$$

Determination of the pressure drop as well as the convective heat transfer coefficient have been realized by using correlations dedicated to rectangular channels for upper and lower parts of the channel (see sections 2.3 and 2.6 of Chapter 2).

6.5.2 Calibration process

The calibration process has been realized by adjusting three parameters. The first one corresponds to the factor a that fictively divides the channels in two parts (Up/Down and Down/up). The two others

parameters concern the determination of the pressure drop (adjustment of the factor 4 of the Equation 34 of the Chapter 2), for both sides of the heat exchanger.
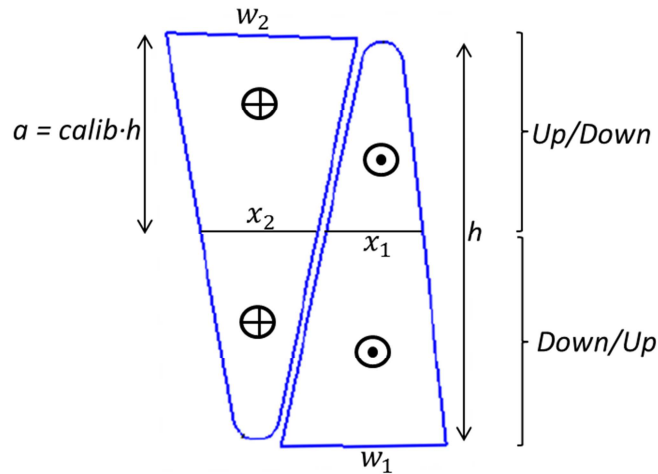

Figure III-45: Discretization of the channels

6.5.3 Calibration results

The calibration parameters have the following numerical values:

- The calibration factor which fictively divides the heat exchanger (parameters *"calib"* to determine *"a"*) is equal to 0.475;
- The factor 4 in the Equation 34 of Chapter 2 has been increased by the factor 1.2 and 1.3 respectively for side 1 and side 2. This increase of the friction factor coefficient can be physically justified by singularities observed in the previous section (Sections 6.4.1and 6.4.2).

Results of the calibration process concerning the effectiveness of the heat exchanger are given in Figure III-46. Blue point corresponds to the measured effectiveness and the black full line corresponds to the effectiveness determined by the post-model. As it can be observed in Figure III-46, the model with new correlations predicts the thermal efficiency with a maximal absolute error of 3.2% and a mean relative error of 1.7%, which is of the same order as the experimental uncertainty (from 1.5 to 2.2% according to ISO 5167 (2003)).
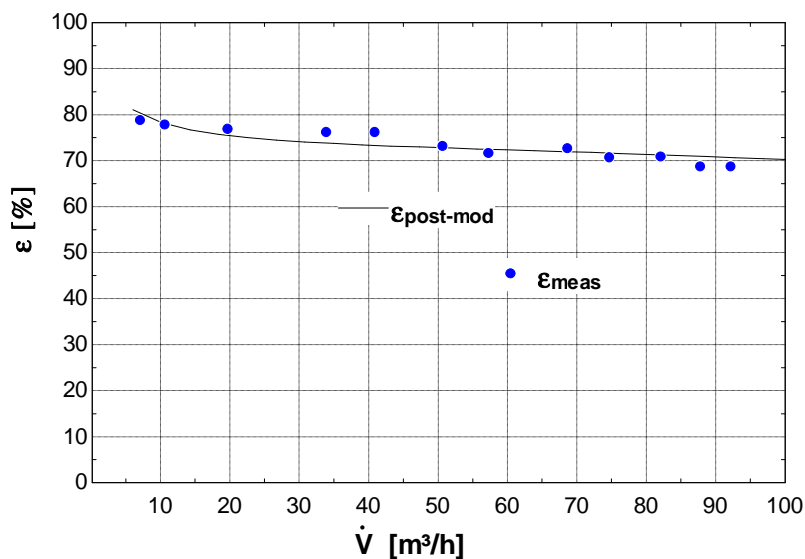

Figure III-46: Results of the calibration process in terms of effectiveness

Calibration concerning the hydraulic performance for both sides is represented in Figure III-47:
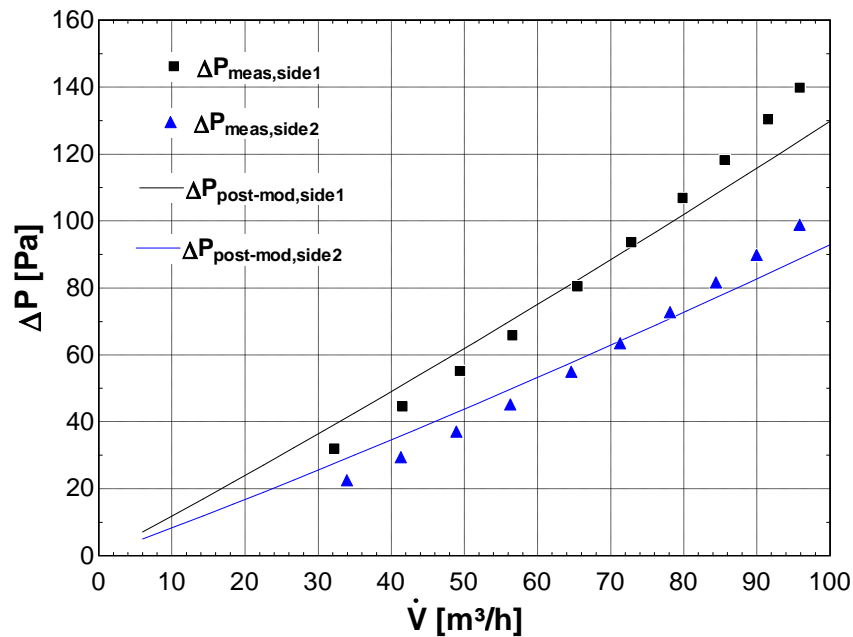

Figure III-47: Results of the calibration process in terms of hydraulic performance

A mean relative error of 8.7% and 9.7% for respectively side 1 and side 2 are obtained. The calibration has been judged satisfying given the large amount of singularities not taken into account by the post-model.

6.5.4   Results analysis

The post-model allows quantifying the flow rate misbalancing appearing in each channel. This is schematically represented in Figure III-48 for well-balanced flow rates of 60 m³/h.

Performance degradation, especially for low flow rates, can be easily explained regarding the overall misbalancing for flow rates in the channel.
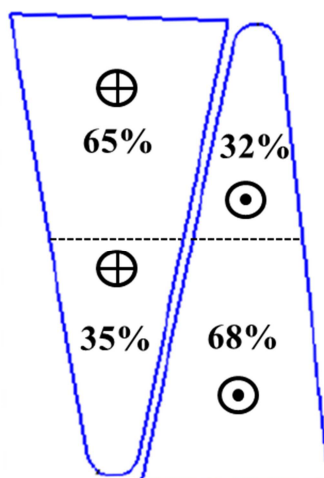

Figure III-48: Misbalancing determination

6.6 Conclusions about investigations on the final heat exchanger

The aim of this section is to summarize the main conclusions about the heat exchanger investigations. First, the main observed differences between the "theoretical" (i.e. as it was designed) heat exchanger and the actual one are listed.

Then, it is proposed to investigate a rectangular geometry in order to estimate the maximal performance that could be reached given the volume for a so called ideal heat exchanger. This perfect heat exchanger is impossible to manufacture with the technology described here above. This is mainly due to the fact that it is impossible to reach the enlargement factor of 400% with perfect rectangular channels (impossible to thermoform a sharp-edged 90° bend). However, this investigation allows for setting a maximal value for the effectiveness/pressure drop of such a heat exchanger.

### 6.6.1 Theoretical geometry versus experimental investigations

One can list the differences between theoretical and manufactured geometry:

- Height of the channel is lower for the manufactured geometry than for the theoretical geometry. That leads to a decrease of the enlargement factor (400% to 371%);

- Many singularities defects have been identified. In overall, a non-controlled geometry has to be deplored. This is mainly due to a strength weakness of the matrix;

- A dissymmetry (cross section area 15% higher in one channel compared to the other) between channels has been observed.

6.6.2 Ideal rectangular geometry

Given results obtained by the post modeling, it is stated that performance degradation is mostly due to an uncontrolled geometry yielding a channel form that induces an overall misdistribution. This channel form results from technical constraint due to thermoforming mold, as previously explained.

However, let's imagine that a perfect rectangular form in the central part could be obtained, as schematically represented in Figure III-49. Let's also imagine a perfect heat exchanger (with absolutely no singular and random defects). The idea of modeling such heat exchanger is to determine a maximal limit of performance of unit given the dedicated volume and the proposed geometry.
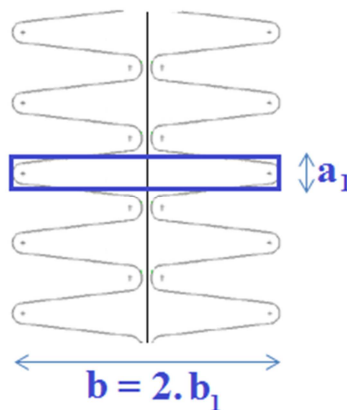
Figure III-49: Definition of an ideal rectangular geometry

Just like the previous model, the model is based on a discretization. The only difference with the previous model is that the previous one considers convective heat transfer correlation dedicated to rectangular channels for the central part.

First of all, the same procedure for COP optimization has been applied. It gives the same value for a_1 and b_1 as the one determined by using the calibrated correlation from Chapter 2.

Difference in terms of hydraulic performance is negligible compared to the one calculated with calibrated triangular correlations determined from Chapter 2 and the one measured on the rapid prototyped plates.
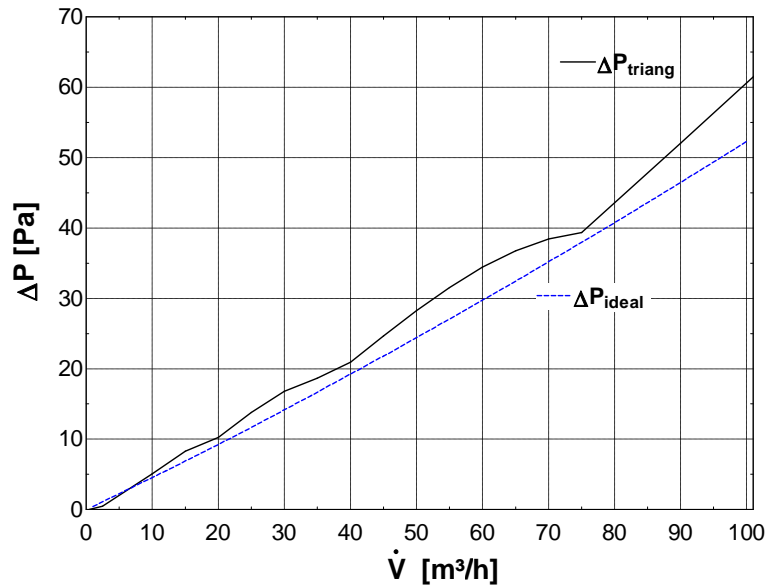

Figure III-50 : Comparison in terms of pressure drops between triangular and rectangular channels

In contrary to hydraulic performance, effectiveness determined by the model considering the rectangular channels highly differs from experimental results and theoretical results determined with calibrated correlation from Chapter 2, as shown in Figure III-51.
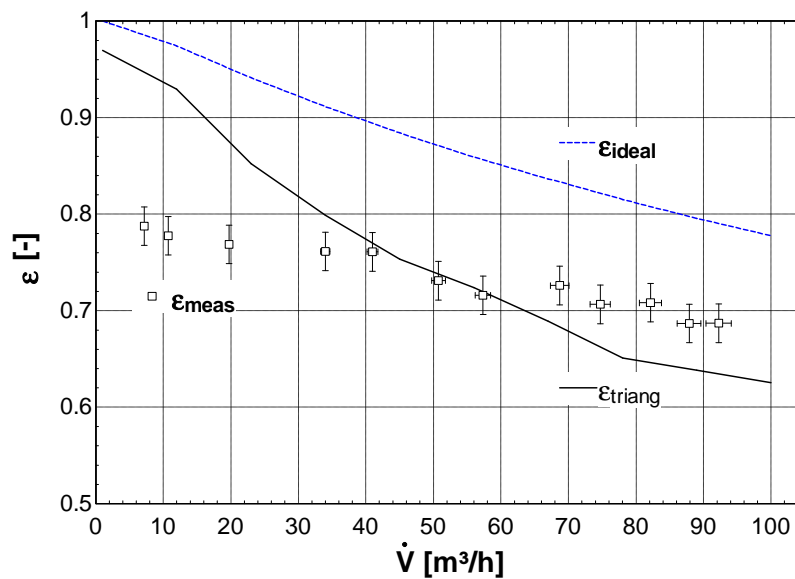

Figure III-51: Comparison in terms of effectiveness between experimental data and theoretical results realized with triangular and rectangular correlations

Mean average difference between ideal theoretical model and experimental data is equal to 16% in terms of effectiveness and maximal difference is 20% (for the lowest flow rate), considering a range in terms of flow rate from 0 to 75 m³/h. COP varies proportionally with the effectiveness. As a result and by assuming a same electrical consumption regarding the hydraulic performance comparison, the same trend will be observed in the COP evolution.

7   CONCLUSIONS

The present chapter first proposes a method to determine the best parameters for a specific geometry dedicated to Single Room Ventilation with Heat Recovery exchanger, by means of a COP optimization procedure. Most of heat exchanger manufacturers only present efficiency of their products without including the pressure drop which has a strong impact on the overall performance of the installation.

The COP optimization is realized by means of the development of a discretized heat exchanger model, using correlation for the determination of the friction factor and the convective heat transfer coefficient. The hydraulic performance of the rest of the installation as well as the fan curve must be previously known or approximated to carry out this optimization.

Then, two steps to check the so called "optimized" geometry are proposed:

- Use of CFD analysis to confirm numerical results coming from the optimization process (semi empirical model);
- Measurement of hydraulic performance of the specified geometry by means of two rapid prototyped plates. This method seems to be particularly suitable in the design step of heat exchanger, and more particularly for SRVHR where hydraulic performance is important since its impact on the acoustic performance of the unit.

Once the geometry has been judged "validated" by means of the previous steps, some explanations about the manufacturing process are presented.

Then, the last part of the chapter focuses on the final heat exchanger. To the author's knowledge, a heat exchanger presenting such a high enlargement factor (400%) is a world first. A difference between theoretical and experimental results that could be explained by identified manufacturing defects (random and systematic defaults) has been observed.

Those defaults involve an overall misbalancing of the flow rates through the heat exchanger. A numerical model is then presented and calibrated in order to fit the experimental results.

Finally, modeling of a heat exchanger with perfect rectangular channels is proposed in order to determine the maximal performance that could be reached given the specific volume and an enlargement factor of 400%.

It is important to notice that the exposed method can also be applied when designing centralized heat recovery ventilation if knowing or approximating or mean averaging the hydraulic performance of the rest of the installation. The knowledge of the fan performance curve is also primordial.

In the case of centralized heat recovery ventilation, parameters constraints can also be modified: especially constraints concerning the sound level (and thus the pressure drop).

The proposed methodology could also be applied to other several geometries. Then, a comparison between all the optimized geometries could be done.

8   REFERENCES

Alm, B., Knitter, B., Hausselt, J. 2005. *Development of a ceramic micro heat exchanger: design, construction and testing.* Chem. Eng. Technol. 2005, 28, No. 12

Al-waked, R., Nasif, M, Morrison, G. 2013. *CFD simulation of air-to-air enthalpy exchanger.* Energy and conversion management 74 (2013) 377-385

Ayub, Z. H. 2003. *Plate heat exchanger survey and new heat transfer and pressure drop correlations for refreigerant evaporators.* Heat Transfer Engineering. 24(5):3-16, 2003

Behrendt, U., Shellabcar, M., 1995. *The EOS rapid prototyping concept.* Computers in Industry 28 (1995) 57-61

Da Siva, D. L., Hermes, C., Melo, C. 2011. *First-principles modeling of frost accumulation on fan supplied tube fin evaporators.* Applied Thermal Engineering 31 (2011) 2616-2621

Hesselgreaves, J.E. 2001. *Heat exchangers: Selection, Design and Operation.* Pergamon, An Imprint of Elsevier Science. (2001)

ISO 5167. *Measurement of fluid flow by means of pressure differential devices inserted in circular cross-section conduits running full.* ISO Standard. Fourth edition (2003)

Kleeman, M., (1978). *Exposé d'un nouveau récupérateur compact.* Thèse défendue oralement le 6 juillet 1978.

Kruth, J-P., Leu, M.C., Nakagawa, T., 1998. *Progress in Additive Manufacturing and Rapid Prototyping.* Keynote paper. CIRP Annals-Manufacturing technology. Volume 47, Issue 2, 1998, Pages 525-540

Nasif, M. S., Morrison, G. L., Behnia, M. 2005. *Heat and Mass Transfer in Air to Air Enthalpy Heat Exchangers.* Proceedings of the 6th World Conference on Experimental Heat Transfer, Fluid Mechanics, and Thermodynamics April 17-21 (2005) Matsushima, Miyagi, Japan

NBN EN 308. Norme nationale belge. *Echangeurs thermiques – Procédures d'essai pour la détermination de la performance des récupérateurs de chaleur air/air et air/gaz.* Mars 1997

NPCS Board of Consultants and Engineers. 2014. *Disposable Products Manufacturing Handbook.* NIIR Project consultancy service. 2014.

Pham D.T., Gault, R.S., 1998. *A comparison of rapid prototyping technologies.* International Journal of Machine Tools and Manufacture (1998) 1257-1287

Solidworks. 2012. *Solidworks Flow Simulation 2012.* Technical Reference.

Wanniarachchi, A. S., Ratnam, U., Tilton, B. E., Dutta-Roy, K. 1995. Approximate Correlations for Chevron-Type Plate Heat Exchangers, *30th National Heat Transfer Conference*, vol. 12, HTD vol. 314, ASME, New York, pp. 145–151, 1995

Yaici, W., Ghorab, M., Entchev, E., 2013. *Numerical analysis of heat and energy recovery ventilators performance based on CFD for detailed design.* Applied thermal Engineering 51 (2013) 770-780

CHAPTER IV:

INVESTIGATIONS OF STRATEGIES UNDER FROSTING CONDITIONS

CHAPTER IV: INVESTIGATIONS OF STRATEGIES UNDER FROSTING CONDITIONS

1   INTRODUCTION

Frost formation can be a major problem encountered in heat exchangers. Under certain conditions so called frosting conditions, a frost layer can form on the heat exchanger surfaces. This frost layer leads to a **reduction of the cross section area**. Obviously, this reduction generates an **increase of the pressure drop** through the heat exchanger and thus an **increase of the electrical power** delivered to the fans (Fisk et al. (1984)). If electrical power delivered to the fans remains constant, the **air flow rate flowing through the heat exchanger decreases** (Da Silva et al. (2004), Chen et al. (2003)) which can leads to unbalanced flow rates. In extreme cases, the frost layer can create a **full blockage of air flow passages** (Xia et al. (2006)). Frost layer also corresponds to a **new thermal resistance** which affects the exchanged heat transfer rates between the two air streams (Fisk (1985)). As a consequence, **overall energy performances** will be affected by the presence of frost inside the heat exchanger. The aim of this chapter is to quantify the impact of the frost layer on air-to-air heat exchanger dedicated to SRVHR performances.

Fisk et al. (1984) **experimentally investigated** air-to-air heat exchangers under frosting conditions. They **did not develop** a numerical model but they quantified the amount of time required to defrost the heat exchanger's core as well as the decrease in terms of efficiency due to the frost layer. Bantle et al. (1987 a), b) and c)) investigated experimentally a counter flow heat exchanger under frosting conditions. They divided their heat exchanger model in two zones (dry and condensing parts) and they presented the **first mathematical model for frost** in counter-flow plate heat exchanger by using empirical correlations. The **same trends were observed** in terms of thermal performances but a **lack of good agreement has been found between simulation and experimental results** and a much more complex model is required. Philips et al. (1989) also developed a discretized simulation model in order to investigate the heat transfer rates under freezing conditions. However, they did not investigate the impact of the frost layer on the hydraulic performance and their model has **not been experimentally validated**. More recently, Nielsen et al. (2008) developed a **discretized model** in order to **only predict the heat transfer rate under frosting conditions**. However, they did not take into account both the thermal resistance due to frost layer in their model as well as the impacts of the frost layer on the hydraulic performances. Even if their model shows good agreement with the measured values, they concluded their studies by stating that **more precise measurements are needed** for the model validation. Moreover, they also stated that it is necessary **to improve the calculation model, especially for defrosting phase**. Rafati Nasr et al. (2014) reported that important topics such as **effect of frost accumulation on airflow rate** have been barely covered in the literature and that the problem of **frosting in air-to-air heat exchanger is still unresolved**.

In the current Chapter, a **dynamic "three zones" heat exchanger model** (taking into account a dry, wet and frost zones) is developed in order to investigate frosting/defrosting strategies. The model is based on the same structure as the "two zones" model previously validated in the frame of the Chapter II. This model is completed **by adding a frost part**. The three zones are determined by using the moving **boundary method**.

Many publications concerning the frost growth can be found in scientific literature (especially for uniform plate temperature). A **frost growth model** (based on several publications) is first presented and **validated** by comparing results with experimental results found in literature (Hermes et al. (2009)). A **defrost model** will also be developed in order to investigate strategies allowing frost presence in the heat exchanger (so called defrost methods).

The second part of the chapter concerns experimental investigations. The same experimental apparatus developed in the Thermodynamics Laboratory of the University of Liège and presented in the frame of the Chapter II is used to investigate the behavior of a **quasi-perfect counter-flow heat exchanger**. Before investigating the behavior of the heat exchanger under frosting conditions, the two zones model is first checked on this specific heat exchanger presenting a different geometry to the one investigated in the frame of the Chapter II (corrugation angle of 30°). Under frosting conditions, **pressure drop evolution** as well as **heat transfer rate** will be experimentally determined for several supply parameters under frosting conditions. The model seems able to predict the time evolution of the heat transfer rates as well as the pressure drops (except when the wet part is significant).

Finally, some **strategies under frosting conditions** are presented and classified depending on whether the frost is allowed in the heat exchanger or not. **Advantages and drawbacks** in terms of implementation of each method are presented, especially in the case of single room ventilation with heat recovery. Each of these strategies will be compared by means of a newly defined criterion of overall energy performance (ratio between energy recovered by the unit and energy supplied to the fans). To the best of the author's knowledge, only the proposed method permits to determine the **overall performance of a specific method**. Calculation will be realized by **using the three zones model** (determination of the heat transfer rates and the pressure drop for each calculation steps). This implies the knowledge of **fan curve** performance considering that energy supplied to the fans depends on the flow rate and the pressure drop (and thus on the frost layer which is calculated at each second).

2   HEAT EXCHANGER MODEL UNDER FROSTING CONDITIONS

This section describes the characteristics of the developed model under frosting conditions (so called three zones model). The first step consists in developing and validating a model able to predict the frost growth on a plate surface temperature. Validation of the frost growth model is realized by means of experimental data collected in the literature. Then, the validated frost growth model is added to the two zones model already validated in the frame of the Chapter II.
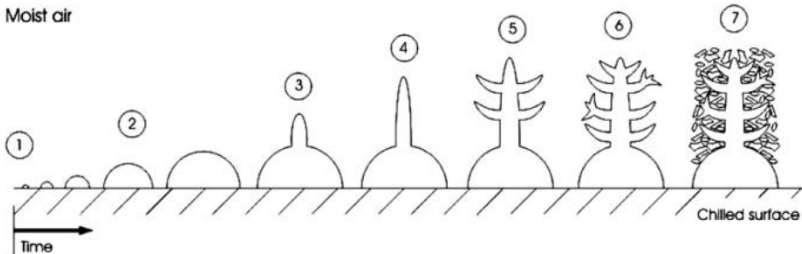
2.1   Frost formation

Many authors give the same definition for the supply conditions required for the frost formation (Hermes et al., (2008); Le Gall et al., (1996) and Kandula (2011)):

"Indeed, if the surface temperature is above the dew-point, only sensible heat transfer occurs. Moreover, if this surface temperature is below the dew-point, but above 0°C, then vapour condensation occurs. Otherwise, if the surface temperature is below 0°C, the condensed vapour freezes. Finally, a vapour desublimation occurs when both surface and dew-point temperatures are simultaneously below 0°C. The water vapour may change directly into solid."

Hayashi et al. (1977) considered three processes that lead to the formation of a frost layer. This description of the frost growth is widely accepted in the scientific community (Pröls and Schmitz (2006), Lee et al. (1998)).

Tao et al. (1993) and Hermes et al. (2009) proposed to divide the frost and growth nucleation process into several stages, schematically represented in Figure IV-1:

Figure IV-1: Schematic representation of the frost nucleation and growth processes (Hermes et al. (2009))

More recently, Cheikh and Jacobi (2014) observed the same steps during frost formation on a chilled flat surface: condensation, freezing of the droplets and then frost crystal growing. Observed phenomena are given in Figure IV-2:
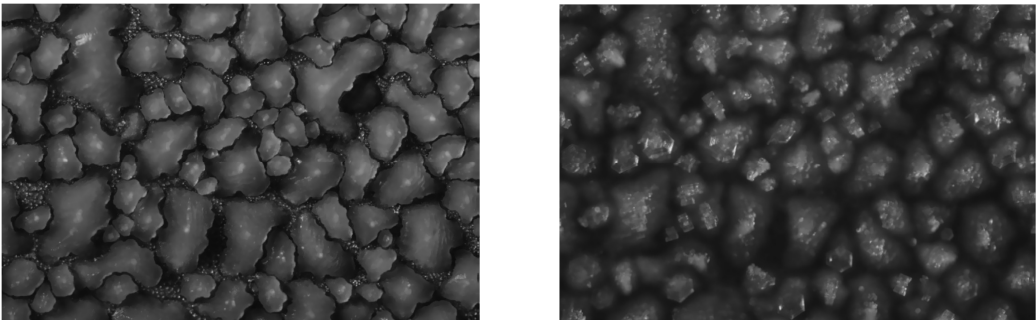
Figure IV-2: Frozen droplets on a cold surface (right) and frost crystals growing on top of the frozen droplets (left)(Cheikh and Jacobi (2014))

2.2 Frost growth model

Developed frost formation model is mainly based on the publications of Hayashi (1977), Lee et al. (1997), Cheng and Cheng (2001), Na and Webb (2003), Hermes et al. (2009) and da Silva et al. (2011).

Experimental data presented in the paper of Hermes et al. (2009) are used to validate the frost formation model developed in the frame of this Chapter.

2.2.1 Assumptions

Most of the models released in the literature are based on a series of assumptions:

- All processes (mass and heat transfer) are treated as a quasi-steady state and one dimensional phenomenon;
- The frost density is a layer-averaged value at any moment;
- The air pressure is uniform in the air stream and within the frost layer;
- The thermal conductivity of frost is a function of density;
- The frost thickness was assumed uniform along the wall ;
- The Lewis analogy (analogy between heat and mass transfer) is applicable.

Most of the models consist of dividing the overall mass mass flux m into two parts, called the growth $\dot{m}_g$ and the densification $\dot{m}_d$ mass fluxes. The nomenclature used for the frost growth model is given in Figure IV-3:
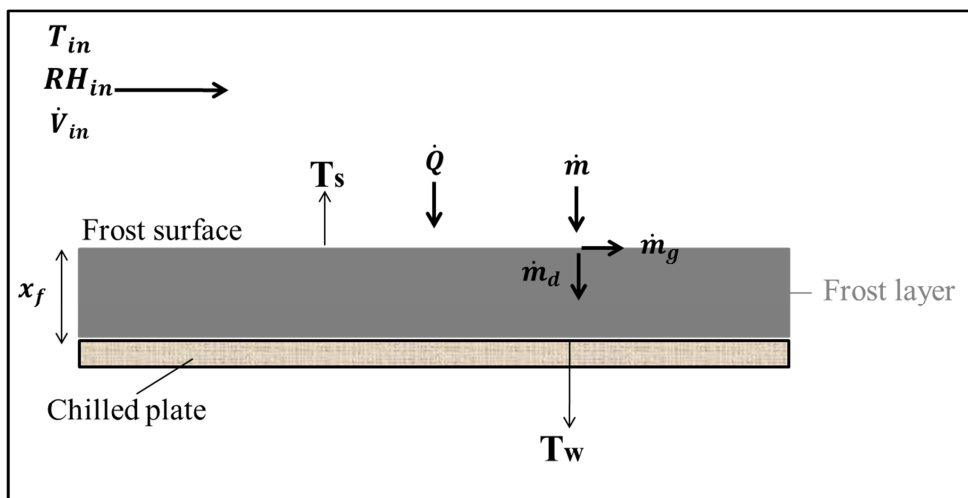
Figure IV-3: Air/frost surface interface (nomenclature used for the frost growth model)

2.2.2 Empirical relations

The model depends on empirical information for several parameters:

- the vapor diffusivity in air D [m²/s];
- the frost layer density [kg/m³];
- the frost thermal conductivity k_f [W/m-K];
- the convective heat transfer coefficient h_h [W/m²-K];
- the mass transfer coefficient h_m [kg/m²-s];
- the tortuosity of the frost layer τ [-];
- the porosity of the frost layer ε [-].

Vapor diffusivity in air

The vapour diffusivity in the air is interpolated as a function of the air temperature from the data of Lee et al. (1997), presented in Table IV-1:

Table IV-1 - Diffusion coefficient for water-air

T [°C]	D [cm²/s]
-45,6	0,163
-40,0	0,169
-34,4	0,176
-28,9	0,183
-23,3	0,190
-17,8	0,198
-12,2	0,205
-6,7	0,213
-1,1	0,220
4,4	0,228
10,0	0,236
15,6	0,243

Frost layer density

Hayashi et al. (1977) proposed a correlation for the frost density depending on the surface temperature:

$$\rho_f = 650 \ exp(0.277 \ T_s) \tag{IV-1}$$

Hermes et al. (2009) recently proposed a correlation depending on the wall surface temperature T_W and the frost layer temperature T_s for the frost layer density. It has been shown that this correlation produced better prediction than the one of Hayashi et al. (1977):

$$\rho_f = a \ exp(b \ T_s + c \ T_w) \tag{IV-2}$$

with the following values for the coefficients *a*, *b* and *c*:
- a = 207.3;
- b = 0.266;
- c = -0.0615

Finally, Da Silva et al. (2011) used a correlation depending on the frost surface and the supply air dewpoint temperature:

$$\rho_f = a \ exp(b \ T_s + c \ T_{dp,in}) \tag{IV-3}$$

Based on their experimental data, the coefficients a, b and c were adjusted to minimize the root mean square difference between calculated and measured air-side pressure drops:
- a = 494;
- b = 0.11;
- c = -0.06

Frost thermal conductivity

Several empirical correlations have been released in the literature for the frost thermal conductivity as a function of the frost layer density. Yonko et al. (1967) proposed:

$$k_f = 0.02442 + 7.214 \ x10^{-4} \ \rho_f + 1.18 \ x10^{-7} \ \rho_f^{\ 2} \tag{IV-4}$$

IV-7

While O'neal (1992) suggested:

$$k_f = 1.202 \ x \ 10^{-3} \ \rho_f^{0.963}$$

IV-5

More recently, Lee et al. (1997) proposed:

$$k_f = 0.132 + 3.13x10^{-4} \ \rho_f + 1.6 \ x10^{-7}. \ \rho_f^2 \text{ (for } \rho_f \text{ comprised between } 50 \text{ and } 400 \text{ kg/m}^3)$$

IV-6

Convective heat transfer coefficient
The convective heat transfer coefficient was deduced from the Nusselt number proposed in the paper of Yamakawa et al. (1972), as suggested by Hermes et al. (2009) for the frost growth model validation. Other correlations will be used in the investigation on the heat exchanger realized in Section 3.

Mass heat transfer coefficient
The mass heat transfer coefficient is determined by applying the Lewis boundary layer analogy:

$$h_m = \frac{h_h}{cp_{in}. \ Le^{2/3}}$$

IV-7

where $Le = \frac{\alpha. \ \tau}{\varepsilon. \ D}$ is the Lewis number. α is the thermal diffusivity in m²/s. τ and ε are respectively the tortuosity and the porosity of the frost layer.

Tortuosity of the frost layer
The tortuosity factor is a representation of the water vapor molecular diffusion in the frost layer. The tortuosity of the frost layer is deduced from the model of Na (2004):

$$\tau = \frac{\varepsilon}{1 - \sqrt{1 - \varepsilon}}$$

IV-8

Porosity of the frost layer
The porosity of the frost layer is calculated from:

$$\varepsilon = \frac{\rho_f - \rho_{ice}}{\rho_{vap} - \rho_{ice}}$$

IV-9

with ρ_{ice} the density of ice (917 kg/m³).

2.2.3 Air and frost interface

Sensible and latent heat transfer occurs simultaneously, due to the difference temperature and humidity between air and the surface of the frost layer. The total heat flux per square meter is given by the following equation:

$$\dot{Q}_{tot} = \dot{Q}_{sens} + \dot{Q}_{lat}$$

IV-10

with the sensible heat transfer:

$$\dot{Q}_{sens} = h_h . (T_{in} - T_s)$$

IV-11

and the latent heat transfer:

IV-8

$$\dot{Q}_{lat} = h_m . (\omega_{in} - \omega_s) . L_s \qquad \text{IV-12}$$

L_s is the latent heat of sublimation:

$$L_s = 2830 \text{ kJ/kg} \qquad \text{IV-13}$$

2.2.4 Mass transfer in the frost layer

According to Lee et al. (1997), it is assumed that the amount of water vapour absorbed in the control volume is proportional to the density of water vapour in a control volume. Consequently, the equation for the diffusion of water vapour in the frost layer is given by:

$$D_{eff} \frac{d^2 \rho_w}{dx^2} = \alpha_f \rho_w \qquad \text{IV-14}$$

where α_f represents a coefficient to be determined.

The boundary conditions are given by:

-   At $x = 0$:

$$\begin{cases} \rho_w = \rho_{w,sat} (T_w) \\ \dfrac{d\rho_w}{dx} = 0 \end{cases} \qquad \text{IV-15}$$

-   At $x = x_f$:

$$\rho_w = \rho_{w,sat} (T_s) \qquad \text{IV-16}$$

The general expression of $\rho_w(x)$ can be expressed by:

$$\boldsymbol{\rho_w(x) = \rho_{w,sat} (T_p) cosh(\gamma x)} \qquad \text{IV-17}$$

Finally, the absorption coefficient in the frost layer is given by:

$$\boldsymbol{\alpha_f = D * \left[\frac{1}{x_f} cosh^{-1} \left(\frac{\rho_{w,sat} (T_s)}{\rho_{w,sat} (T_p)} \right) \right]^2} \qquad \text{IV-18}$$

where:

$$\boldsymbol{\gamma = \sqrt{\frac{x_f}{D}}} \qquad \text{IV-19}$$

2.2.5 Frost surface temperature

The temperature distribution in the frost layer is determined using the energy balance in the control volume. It is obtained by using the analysis of Lee's (Lee and al. 1977):

$$T_s = T_w + \frac{(\dot{Q}_{sens} + \dot{Q}_{lat})}{k_f} . x_f - \frac{\alpha_f . \rho_{w,sat,s} . L_s}{k_f . \gamma^2} . (cosh(\gamma . x_f) - 1) \qquad \text{IV-20}$$

2.2.6 Frost mass and frost growth

The model consist of dividing the overall mass flux $\dot{m}$ into two distinct parts, namely the growth $\dot{m}_g$ and densification $\dot{m}_d$, as represented in Figure IV-3:

$$\dot{m} = \dot{m}_g + \dot{m}_d \;=\; \rho_f \cdot \frac{dx_f}{dt} + x_f \cdot \frac{d\rho_f}{dt} \qquad\qquad \text{IV-21}$$

As demonstrated by Hermes et al. (2009), the mass flux of frost growth can be determined by:

$$\left(\frac{L_s \cdot b \cdot x_f}{k_f}\right) \dot{m}_g{}^2 + \left(1 + \frac{b \cdot x_f \cdot \dot{Q}_{sens}}{k_f}\right) \dot{m}_g - \frac{\dot{Q}_{lat}}{L_s} = 0 \qquad\qquad \text{IV-22}$$

Therefore, the evolution of the mass of frost growth is given by:

$$mass(t) = \int \dot{m} * d\tau \qquad\qquad \text{IV-23}$$

2.3 Frost model validation (on chilled surface plate)

As already stated, the developed model has been validated by means of the experimental data presented in the frame of the paper of Hermes et al. (2009). They observed and quantified the frost formation under several air supplied conditions on a controlled temperature chilled plate of 100 cm².

2.3.1 Frost layer evolution

Figure IV-4 shows the comparison between the model and the experimental data in terms of frost layer evolution for four different wall temperatures:
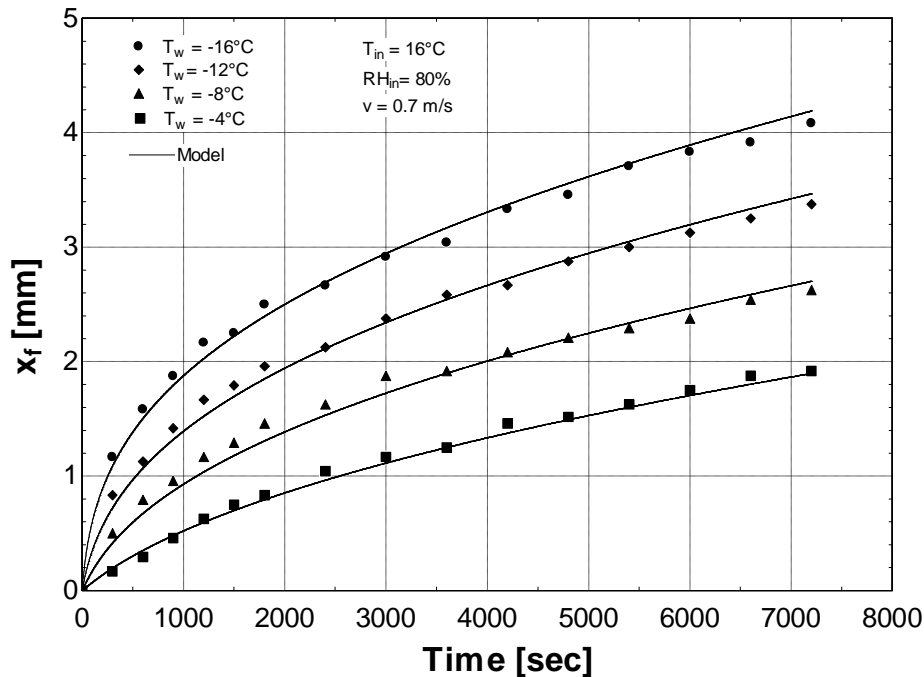

Figure IV-4: Frost layer evolution

Results in terms of frost layer thickness evolution are satisfying regarding results presented in Figure IV-4.

2.3.2 Validation under several air inlet conditions and wall temperatures

Hermes et al. (2009) carried out 12 experiments by varying the air relative humidity from 50% to 80%; the air inlet temperature from 16 to 22°C and the plate surface from -5 to -15°C.

They presented the results in terms of surface temperature T_s (°C), mass of frost $Mass_{frost}$ (g), thickness of the frost layer x_f (mm), and density of the frost ρ_f (mm). Those parameters are given for test duration of one and two hours. Figure IV-5 shows the dynamic validation of the developed frost growth model for the different operating conditions:
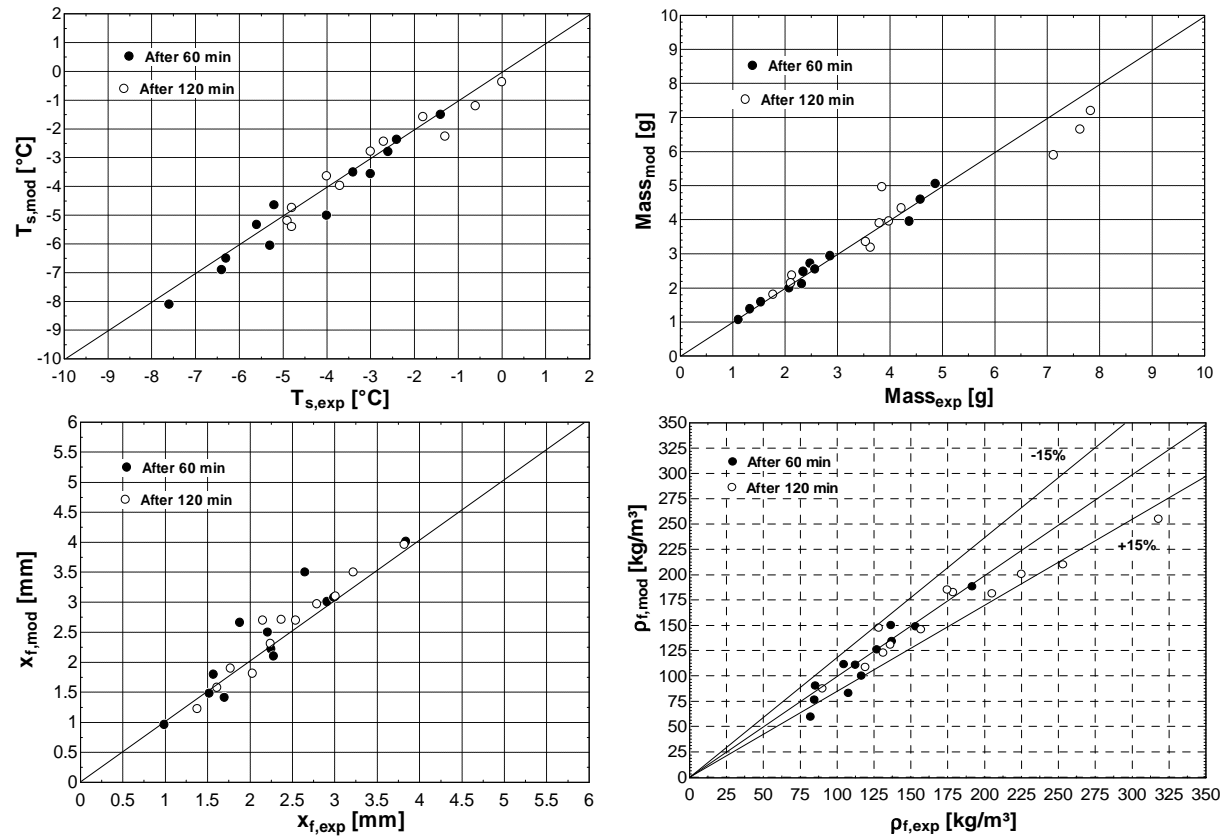

Figure IV-5: Frost model validation

Regarding the results, model prediction is judged satisfactory.

2.4 "Three zones" heat exchanger

As already stated, the idea was to divide the heat exchanger in three parts (dry, wet and frost). To do so, the two zones model presented and validated in the frame of the Chapter II is improved by adding a frost part. A schematic representation of a counter-flow heat exchanger under the three regimes is given in Figure IV-6. It can be noticed that the situation is different in cross flow heat exchanger where appearance of condensation and frost is a two dimensional problem, as reported by Mercadier et al. (1993).
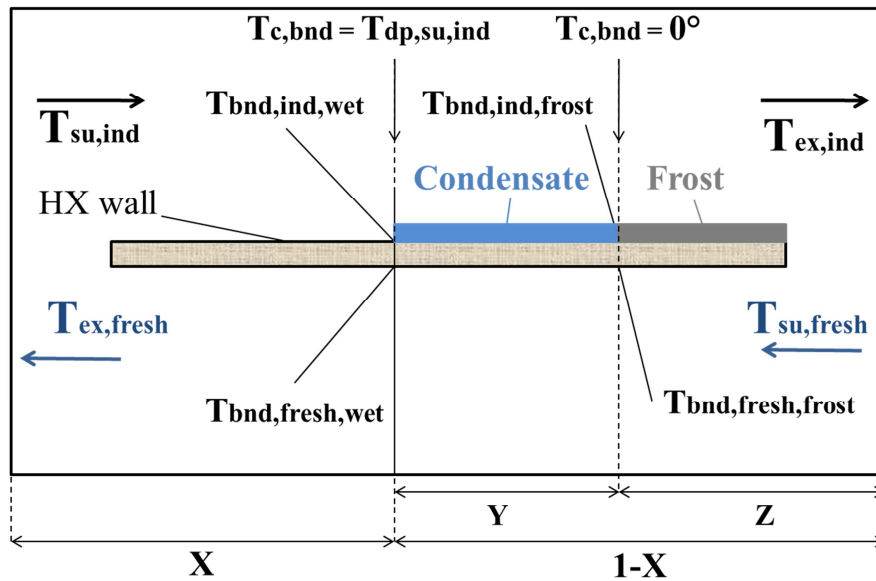
***Figure IV-6: Schematic representation of a counter flow heat exchanger presenting three zones
(Dry, wet and frost parts)***

The boundary condition to determine the frost part corresponds to a wall temperature of 0°C and the boundary conditions to determine the wet part corresponds to a wall temperature equal to the supply air dewpoint temperature. Psychometric processes for both air sides are schematically given in Figure IV-7.
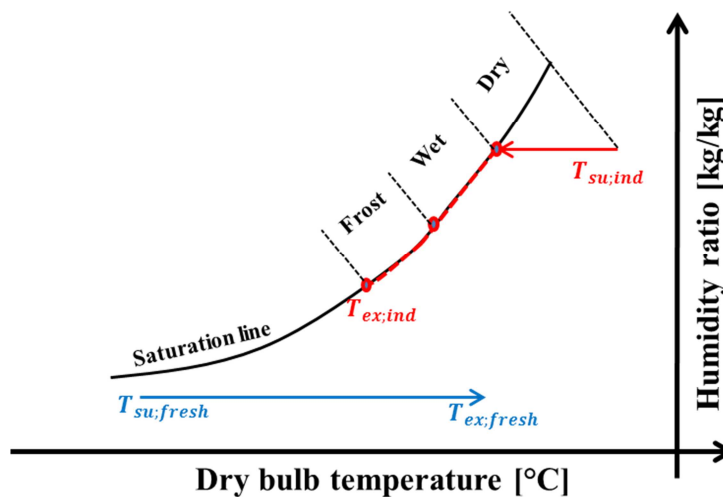

Figure IV-7: Psychometric process for both fresh and indoor air side (under three regimes)

In order to decrease the number of iterations, final values of time "t-1" are used as initial conditions for time "t".

2.5 « Three zones conditions » validation

In order to experimentally validate the definition of the boundary conditions of the three zones model, an experiment was carried out on a sample supposed to represent two channels of a perfect counter flow heat exchanger (and thus presenting a continuous temperature evolution). Given the impact of the thermal inertia on the experimental results because of the low flow rate passing in the channels, this experiment did not permit to validate the three zones heat exchanger model. However, the main goals of the experiment were qualitative:

- to visually observe the three zones of the heat exchanger;
- to check if the three zones are well delimited by the dewpoint temperature of the supply indoor air and 0°C;
- to observe the frost formation on a vertical wall (most of the experiments described in the literature have been carried out on horizontal plate).;
- to check if the frost layer can be assumed uniform all along the frosting part.

A schematic representation of the test bench is presented in Figure IV-8:
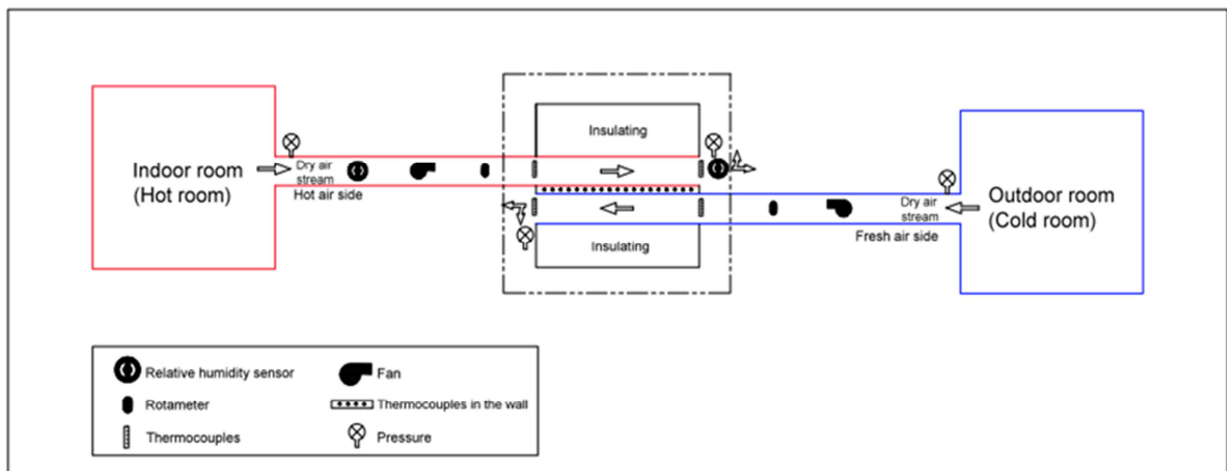
Figure IV-8: Visualization of the three zones (as viewed from above)

Temperature wall evolution has been realized by equipping the plate separating the two channels with 30 thermocouples. The dry-bulb temperature measurements are made at the supply and exhaust of the fresh and indoor air side. Relative humidity measurement is performed for the supply and exhaust indoor air side. Rotameters are used for the flow rate measurement and two fans are used for pulsing up the flows in the channels.

In order to have a precise temperature measurement along the heat exchanger wall, the plate separating the two channels has been milled by a 3D CNC milling machine. Thermocouples have been inserted in the milled channels, as represented in Figure IV-9:

Figure IV-9: Temperature measurement along the plate

In order to ensure an optimal thermal contact between the thermocouples and the plate, thermal paste has been inserted in the thinnest part of the milled channels.

In order to reduce the impact of the ambient heat losses, a system involving Plexiglas plate was imagined. The idea was to maintain the vacuum between two Plexiglas plates by means of a vacuum pump running all along the tests. The system is presented in Figure IV-10:
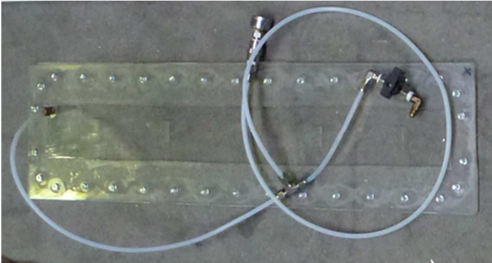

Figure IV-10: Vacuum between Plexiglas plates

Practical realization of the test bench is given in Figure IV-11:

Figure IV-11: Practical realization of the test bench

As expected, the boundary conditions delimiting each zone are well respected (appearance of condensation at the dewpoint temperature and the frosting at 0°C) and each zone is well delimited by those conditions. An example of wall temperature after 2 hours of tests is given in Figure IV-12. Visual observation confirms the presence of frost starting from the thermocouple 19:
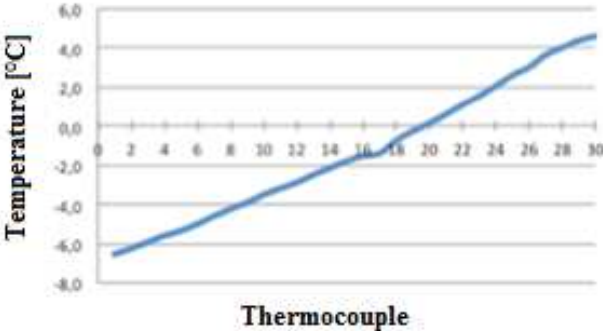

Figure IV-12: Wall temperature evolution

In the frost part, frost formation follows the same steps as the one presented in Figure IV-2, despite the verticality of the plate. Frost layer has been measured by means of caliper at different places: the frost layer can be considered uniform along the plate in the frost part.

All these observations confirm the basis/assumptions used for the three zones model and the frost formation description model.

2.6 Pressure drop evolution under frosting conditions

The pressure drop was calculated for each calculation time step (one second), by taking into account the impact of the calculated frost layer thickness, as schematically shown in Figure IV-13. At each second, the hydraulic diameter is determined. This has a high impact on the regime (Reynolds number) and thus the Nusselt number and the friction factor. The knowledge of pressure drop is important to determine the electrical power to be delivered to the fans (use of fan curve). Da Silva et al. (2011) applied the same procedure in order to determine the decrease of flow rate during the frost formation on an evaporator.
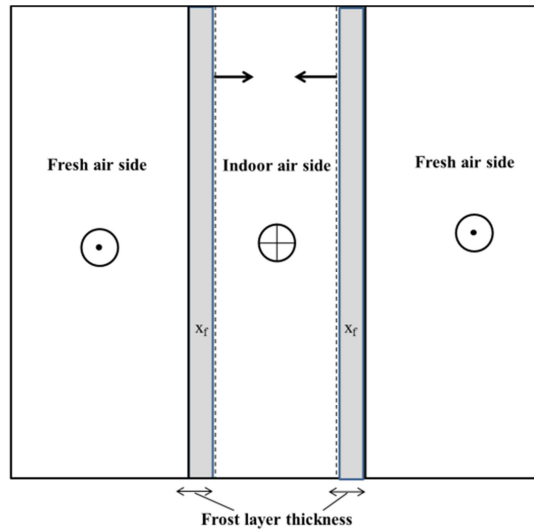

Figure IV-13: Hydraulic diameter calculation

2.7 Model for defrosting cycle

Defrosting is performed in two distinct stages.

In the first stage, the available heat from the indoor flow is used to increase the temperature of the frost layer so that it reaches the melting temperature, i.e. $T_{melting} = 0°C$. During the first stage, the frost mass is assumed to be constant and is equal to the mass of frost at the end of the frosting phase.

In the second stage, the heat provided allows the phase change. Consequently, the frost begins to melt. During the phase change, the frost temperature is assumed to be constant and equal to 0 ° C.

The rate at which the mass of the frost varies is given by Nielsen et al. (2008):

$$\frac{dM_{frost}}{dt} = \frac{\Delta Q}{\Delta h_{ls}} \qquad \text{IV-24}$$

The latent heat of fusion for frost Δh_{ls} is assumed to be constant during the whole process and equal to 333000 J/kg.

First stage: sensible heat trasnfer

The calculation of the sensible power requires the determination of heat transfer rate exchanged on the side of the indoor and fresh air. During the defrosting phase, no fresh air is supposed to flow in the heat exchanger. The convective heat transfer coefficient has been chosen equal to 7 [W/m²-K]. Heat transfer rates for both sides are respectively given by:

$$\begin{cases} \dot{Q}_{ind} = \varepsilon_{ind}. \ \dot{C}_{ind} \ . \left(T_{su,ind} - T_{frost}\right) \\ \dot{Q}_{fresh} = h_{h,fresh} \ . A \ . \left(T_{frost} - T_{fresh}\right) \end{cases}$$

IV-25

T_{frost} is approximated by the mean average temperature of the wall temperature T_w and the frost surface temperature T_s. Effectiveness of the heat exchanger has been determined by using correlation dedicated to a semi-isothermal wall.

The heat transfer delivered to the mass of frost can be approximated by:

$$\dot{Q}_{transfered \ to \ frost} = \ \dot{Q}_{ind} - \ \dot{Q}_{fresh}$$

IV-26

The difference in temperature of the frost layer can be determined by the following equation:

$$\dot{Q}_{transfered \ to \ frost} = \ M_{frost} * cp_{frost} * \Delta T$$

IV-27

The thermal capacity of the frost is assumed to be constant and equal to 2060 J/kg.

This expression is used to determine the temperature difference ΔT for each second, which is used to determine the new temperature of the frost layer T_{frost}.

During this stage, the mass of frost is assumed constant in the heat exchanger core. The only parameter varying is the temperature of the frost layer.

Second stage: latent heat transfer

Similar to the first stage, heat transfer rates are determined on the side of the indoor and fresh air. In this case, the temperature of the frost layer is assumed to be constant and equal to 0°C.

The heat flow rate exchanged by each fluid is given by:

$$\begin{cases} \dot{Q}_{ind} = \varepsilon_{ind}. \ \dot{C}_{ind} \ . \left(T_{su,ind} - 0\right) \\ \dot{Q}_{fresh} = h_{h,fresh}. A \ . \left(0 - T_{mean,fresh}\right) \end{cases}$$

IV-28

Those values are used to determine the ΔQ required for the change phase (Equation IV-26). The evolution of the mass over time is obtained by using Equation IV-24.

Knowing the mass of frost and thus the thickness of the frost layer at time t, it is possible to determine the convective heat transfer coefficient on the side of the indoor air at time t, $h_{h,in}(t)$. If no fresh air flow rate is flowing in the heat exchanger, a convective heat transfer coefficient of 7 [W/m² K] is assumed (natural convection).

The thickness of the frost layer is calculated by Equation IV-29:

$$x_f(t) = \frac{M_{frost}(t)}{\rho_f}$$
<div style="text-align:right">IV-29</div>

Where ρ_f is assumed to be constant and equal to the last value calculated during the frosting phase.

During the defrosting phase, liquid water resulting from frost melting is supposed to be directly ejected from the heat exchanger. The hydraulic diameter is calculated by taking into account the mass of frost remaining in the heat exchanger.

3 EXPERIMENTAL INVESTIGATIONS

The aim of the experimental investigations was first to confirm the validity of the *"two zones"* heat exchanger model developed in frame of Chapter II but with a different corrugation geometry. The idea was first to apply exactly the same methodology as the one described in the frame of Chapter II: calibration of the correlations under dry conditions followed by the application of the variable boundary method under partially wet conditions. Then, investigations under frosting operating conditions were carried out. The goal was to validate the *"three zones"* heat exchanger model and also to experimentally investigate the different strategies under frosting conditions. The studied exchanger presents the same overall geometry but presents different corrugation forms in the central part than the one presented in Chapter III. In reality, this heat exchanger presents an enlargement factor of only 140% which makes the investigated geometry better controlled during the manufacturing process. This well characterized geometry allows for easier study of the freezing phenomena. One of the advantages of this heat exchanger is that it allows for an easy observation of the frost in the central part of the heat exchanger.

3.1 Experimental apparatus

The same experimental apparatus as the one presented in the frame of Chapter II was used (wood box with insulation).

For tests under frosting conditions, the box containing the heat exchanger is in Plexiglas in order to better observe the frost formation (especially at the indoor air exhaust of the heat exchanger), as shown in Figure IV-14.
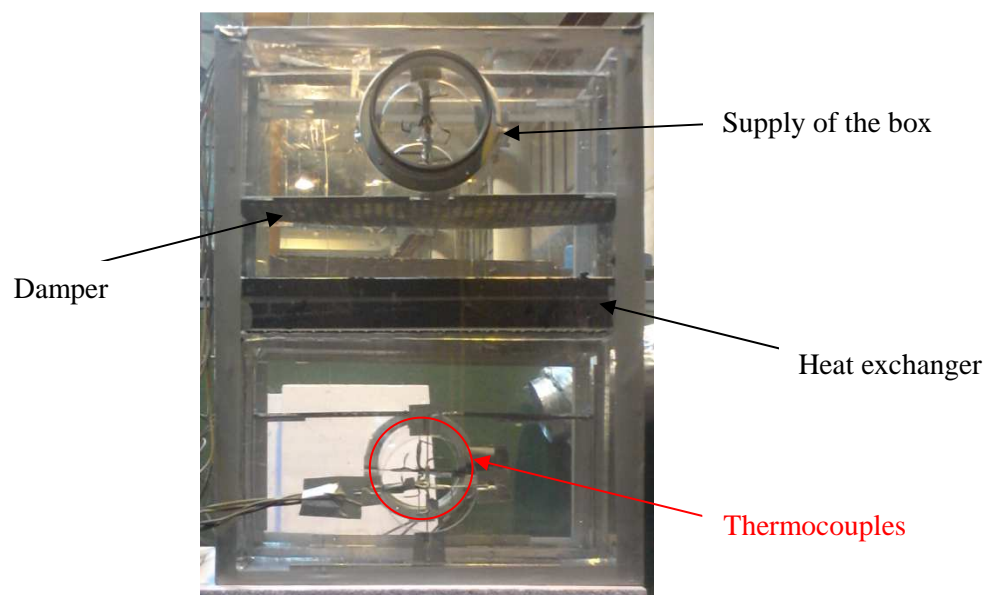

Figure IV-14: Plexiglas box

The Plexiglas box has been recovered by flexible insulation in order to reduce the heat ambiance losses.

3.2 Presentation of the heat exchanger geometry

The present section aims at presenting the geometric characteristics of the investigated heat exchanger. The manufacturing process is exactly the same as the one exposed in Chapter III. And just like the so-called final heat exchanger, the investigated heat exchanger presents a U flow configuration and is assembled in accordion, as schematically represented in Figure IV-15.
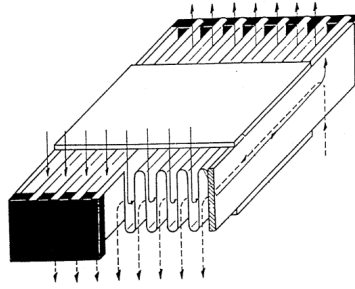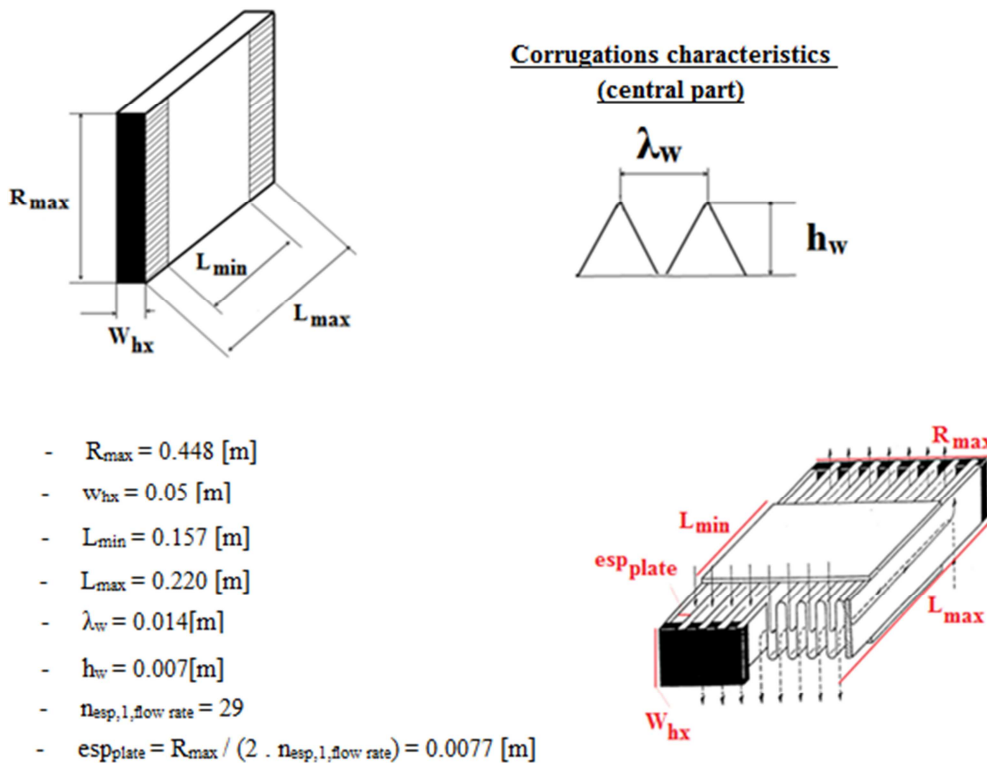
Figure IV-15 : U-flow configuration

Pictures of the tested heat exchanger are given in Figure IV-16:
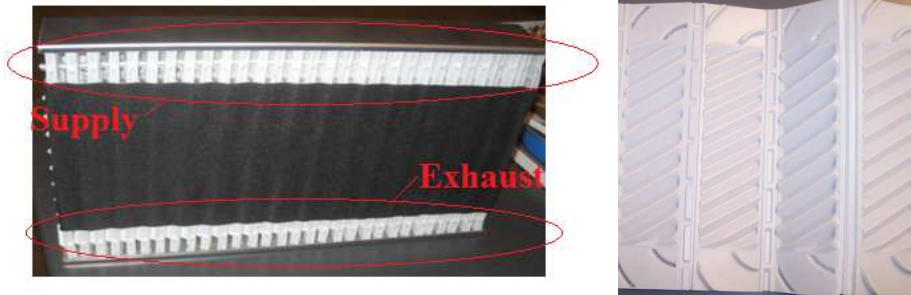
Figure IV-16: Tested heat exchanger

The central part of the heat exchanger presents corrugations. Geometric characteristics of the tested heat exchanger are given in Figure IV-17:

- $R_{max} = 0.448$ [m]
- $w_{hx} = 0.05$ [m]
- $L_{min} = 0.157$ [m]
- $L_{max} = 0.220$ [m]
- $\lambda_w = 0.014$ [m]
- $h_w = 0.007$ [m]
- $n_{esp,1,flow\ rate} = 29$
- $esp_{plate} = R_{max} / (2 \cdot n_{esp,1,flow\ rate}) = 0.0077$ [m]

Figure IV-17 : Overall geometric characteristics of the heat exchanger and corrugations of the central part

Corrugation angle definition corresponds to the same one provided by Ayub et al. (2003). Corrugation angle β of the central part is equal to 30°:
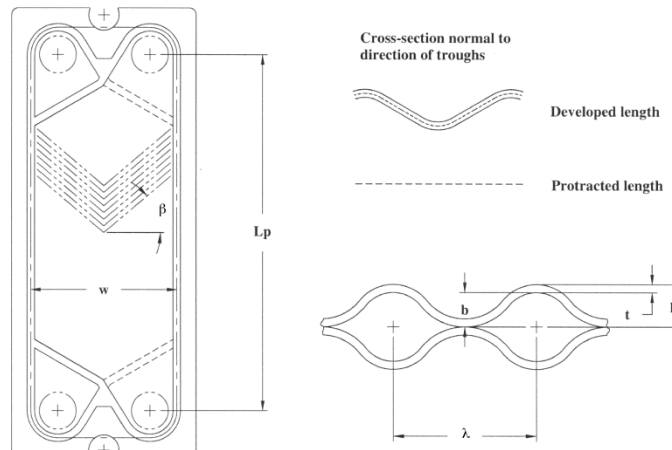

Figure IV-18 : Corrugation angle definition according to Ayub et al. (2003)

The Reynolds number is defined by:

$$Re = \frac{v \cdot D_h}{\nu}$$

IV-30

And the hydraulic diameter is determined by:

$$D_h = \frac{4\,A}{P} = \frac{4\,A}{2\,(b + \Phi\,w)} \simeq \frac{2\,b}{\Phi}$$

IV-31

With Φ, the enlargement factor.

3.3 Used correlations for Nusselt and friction factor number

Concerning the Nusselt number determination, correlation provided by Wanniarchchi et al. (1995) has first been used before the calibration. This correlation can be applied to heat exchanger presenting a corrugation angle comprised between 20 and 62°. Area of validity concerning the Reynolds number is comprised between 1 and 10^4. The correlation is given under the form of the following relationship:

$$Nusselt = [(3.65 \cdot \beta^{-0.455} \cdot \phi^{0.661} \cdot Re^{0.339})^3 + \left(12.6 \cdot \beta^{-1.142} \cdot \phi^{[1-m]} \cdot Re^m\right)^3]^{1/3} \cdot Pr^{1/3}$$

IV-32

with :

$$m = 0.646 + 0.0011.\beta$$

IV-33

Correlation for the friction factor determination is also provided by Wanniarchchi et al. (1995):

$$Nusselt = 4 \cdot [(1174 \cdot \beta^{-1.026} \cdot \phi^2 \cdot Re^{-1})^3 + \left(46.6 \cdot \beta^{-1.08} \cdot \phi^{[1+p]} \cdot Re^{-p}\right)^3]^{1/3}$$

IV-34

with:

$$p = 0.00423 \cdot \beta + 0.0000223 \cdot \beta^2 \qquad\qquad \text{IV-35}$$

Given experimental results in dry regime (application of the method exposed in Chapter II), the Nusselt number and the friction factor have been respectively tuned of by a factor of 1.1 and 0.9. The calibration factors are closer to unity than the ones determined in the frame of Chapter II. This can be explained by the fact that the geometry is better controlled and also simpler (corrugations such as the one investigated have been many times studied in the scientific literature).

Next section compares experimental results with results coming from the calibrated model.

3.4 Hydraulic performance in dry regime

Hydraulic performance has been experimentally measured on both parts of the heat exchanger. As can be observed in Figure IV-19, the differences in terms of pressure drop evolution as a function of the flow rate is considered negligible and the heat exchanger is considered symmetric.
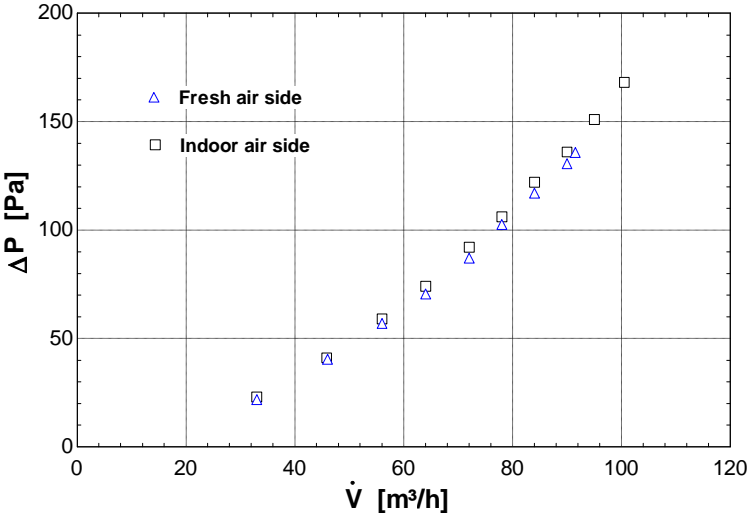

Figure IV-19: Pressure drop as a function of volumetric flow rate for fresh and indoor air side

Hydraulic performance is well predicted by the calibrated model, as can be observed in Figure IV-20:
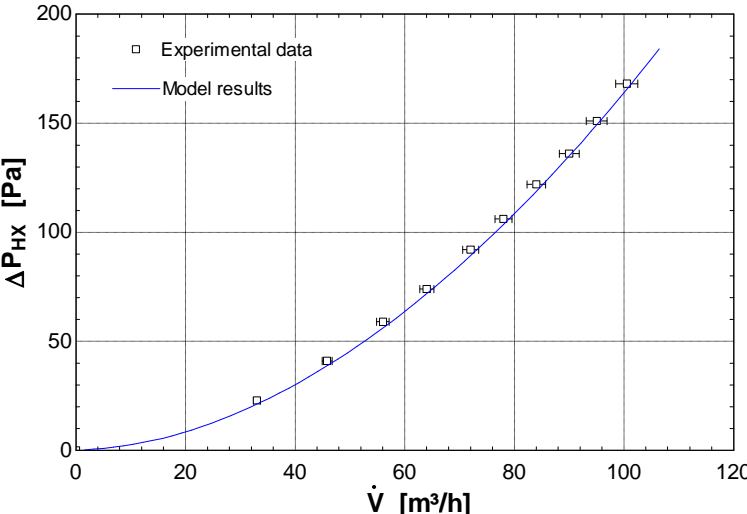

Figure IV-20: Hydraulic performance (measured data vs model results)

3.5 Thermal performance in dry regime

A comparison for well-balanced flow rates in terms of effectiveness is given in Figure IV-21:
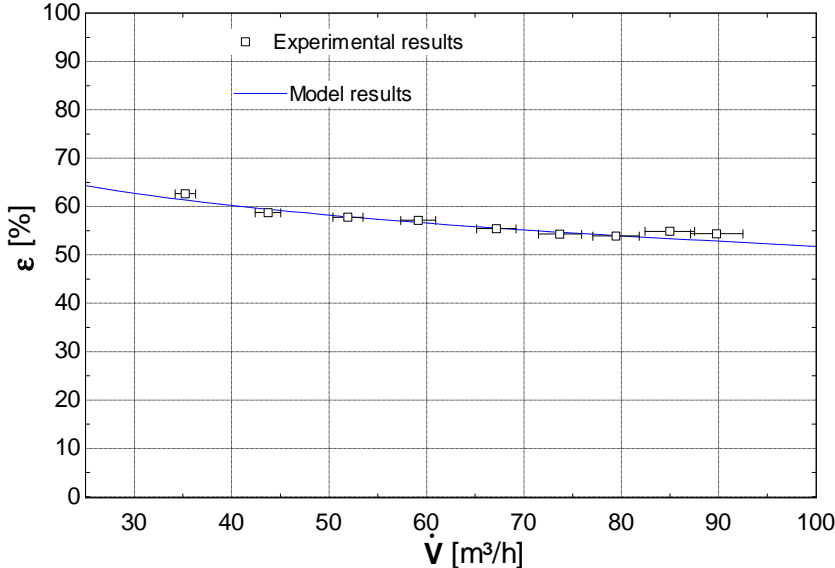

Figure IV-21: Comparison between experimental and model results in terms of effectiveness

Comparison in terms of AU (by assuming the heat exchanger in perfect counter-flow) is given in Figure IV-22:
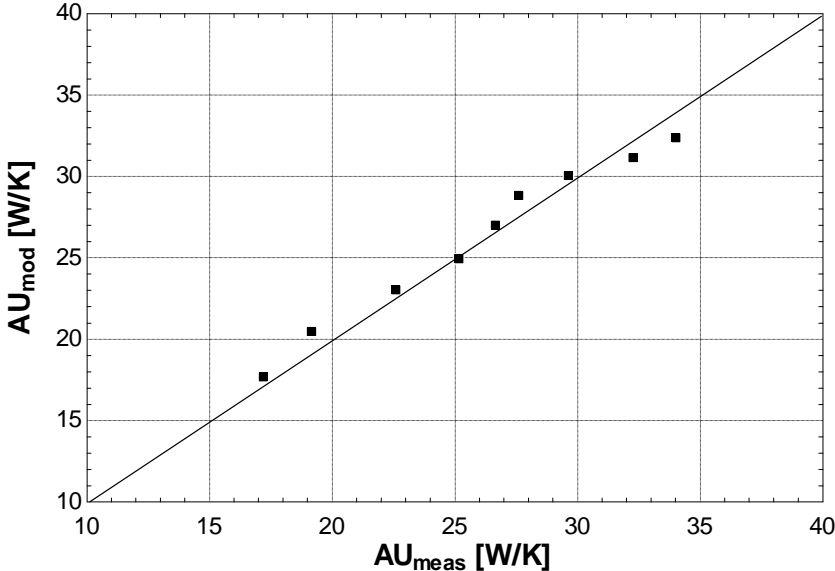

Figure IV-22: AU_{meas} vs AU_{mod}

3.6 Performance in wet and partially wet regimes

The same procedure as the one exposed in the frame of the Chapter II has been applied for experimentally determining the sensible and latent load. As shown in Figure IV-23, results are considered satisfactory as well for the tested heat exchanger in terms of heat transfer rates:
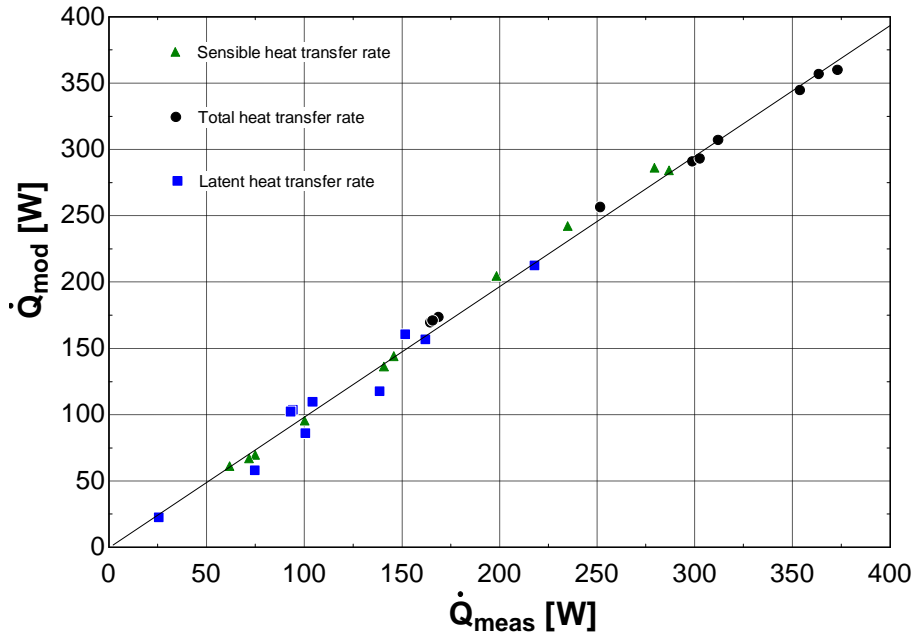
Figure IV-23: Validation in wet and partially wet regimes

Concerning the hydraulic performance under wet and partially wet regimes, same conclusions as the ones given in Chapter II can be drawn. It can be first observed a rising of the pressure drop followed by a stationary period where the pressure drop remains constant.

3.7 Performances under frosting conditions

3.7.1 Test supply conditions

Performance under frosting conditions has been realized for different supply conditions given in Table IV-2:

Table IV-2: Supply conditions (experimental conditions)

Test	Fresh air			Indoor air		
	T_{su} [°C]	RH_{su} [%]	$\dot{M}$[kg/s]	T_{su} [°C]	RH_{su} [%]	$\dot{M}$[kg/s]
1	-18.4	n.m.*	0.029	19.1	40	0.029
2	-14.5	n.m.	0.019	19.0	35	0.019
3	-17.5	n.m.	0.029	19.0	64	0.029
4	-14.0	n.m.	0.029	20.0	44	0.019
5	-14.2	n.m.	0.029	20.0	37	0.029

*: not measured

Supply conditions have been chosen to validate the model in different operating conditions under frosting conditions. All of the tests have been realized with balanced flow rates, except Test 4 which presents a ratio between fresh and indoor air flow rate different from one ($\frac{\dot{M}_{fresh}}{\dot{M}_{ind}} = \frac{0.029}{0.019}$).

Presence of frost for each of these tests has been visually checked. This observation was made possible thanks to the transparent Plexiglas box. The frost layer at the exhaust of the heat exchanger can be shown in Figure IV-24.
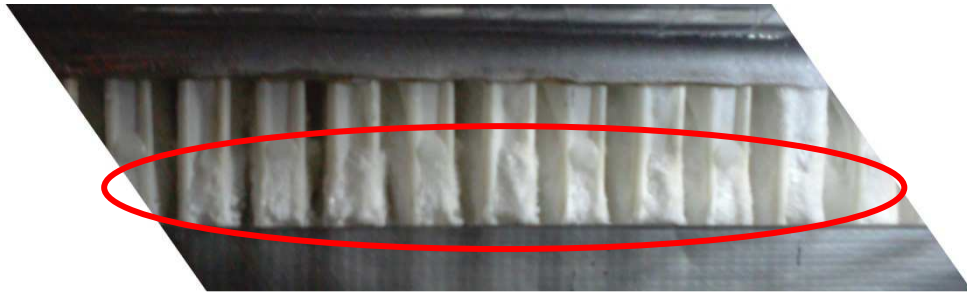
Figure IV-24: Check of the presence of frost at the exhaust of the heat exchanger

3.7.2   Tests description

Each performed test presents two phases: the frosting and the defrosting phases. For each of these phases, the measured time evolution of heat transfer rates and pressure drop will be compared with the numerical model.

During the defrosting phase, the fresh air flow rate is stopped while the indoor air flow rate remains constant. As an example, the pressure drop evolution for Test 4 is given in Figure IV-25.
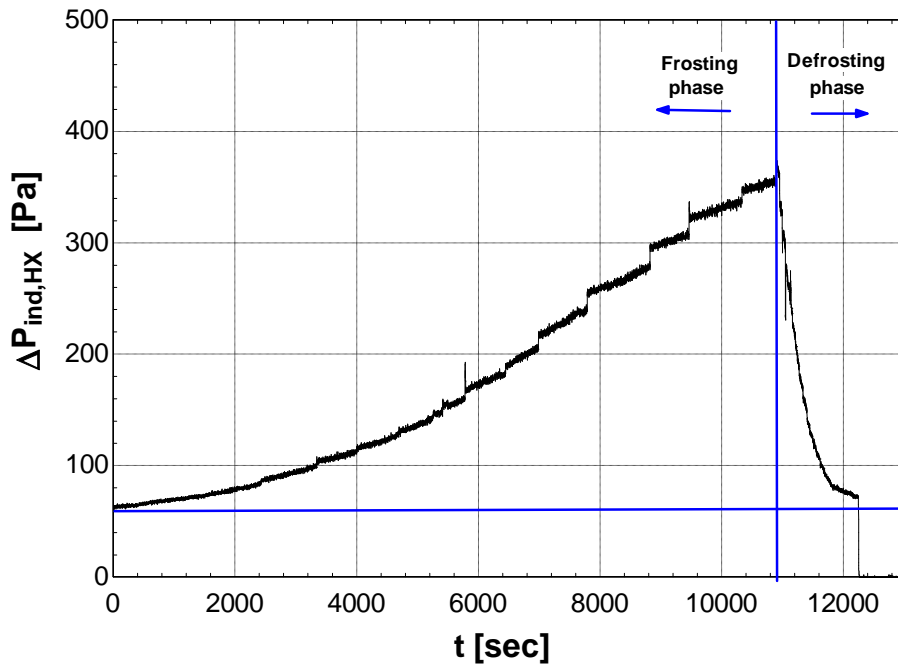
Figure IV-25: Frosting and defrosting phase during experimental test

As expected, the frosting phase lasts longer than the defrosting phase. The supply/exhaust temperature evolution for Test 4 is given in Figure IV-26:
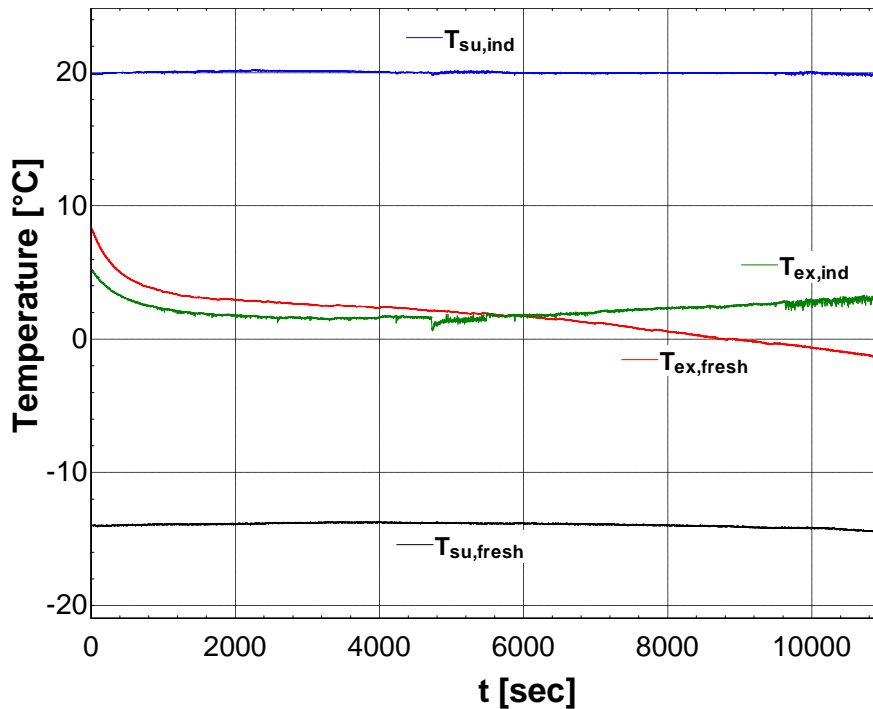
Figure IV-26: Supply and exhaust temperature evolution for Test 4

The indoor and fresh air mass flow rates evolutions are represented in Figure IV-27 during the frosting phase of Test 4. In order to counter balance the increase of pressure drops due to the presence of the frost layer, the indoor mass flow rate is manually adjusted by means of valves during the whole frosting and defrosting phase in order to keep the flow rate constant. Those adjustments correspond to flow rate steps, as shown in Figure IV-27. This is also the reason why the pressure drop evolution is not continuous in Figure IV-25. Concerning the fresh air side, the mass flow rate does not need an adjustment to remain constant all along the process.

Figure IV-27: Indoor and fresh air mass flow rates for Test 4

3.7.3   Comparison of Tests 1, 3 and 5 in terms of pressure drop evolution

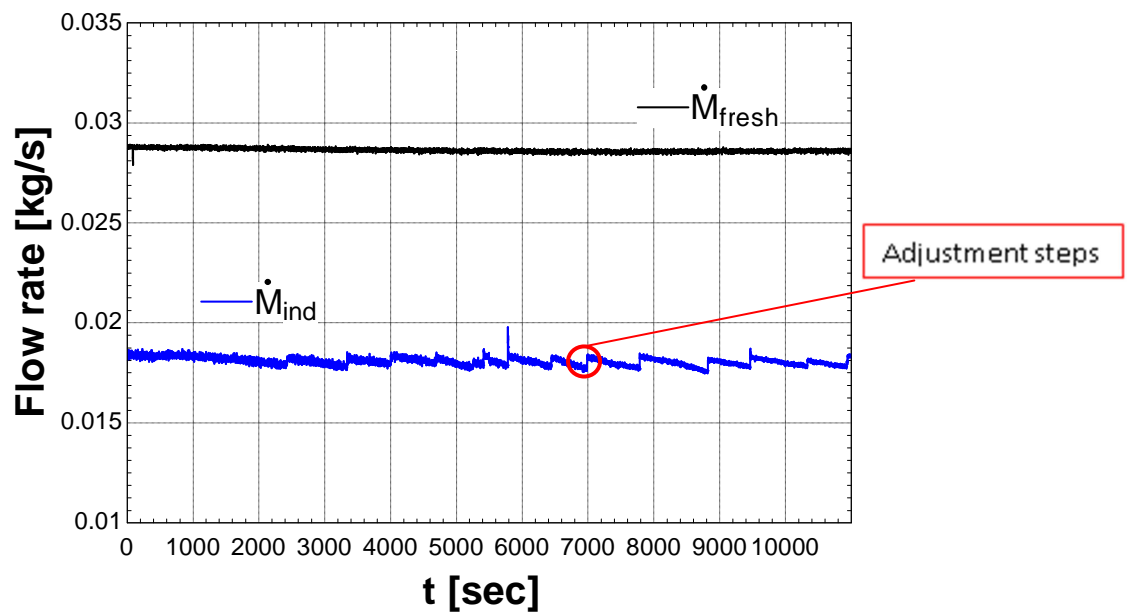Figure IV-28 shows the comparison between the pressure drop evolution for tests 1, 3 and 5.

Differences between Test 1 and Test 5 seem intuitive and logical: for the same air supply conditions, the rate of increase of the pressure drop is lower for Test 5 compared to Test 1. This is due to the fact that the supply fresh air side is cooler (-18.5 vs -14.5°C) which obviously implies a cooler plate temperature and then a quicker frost layer formation.

On the contrary, comparison analysis between Test 1 and Test 3 is not intuitive. In reality, the test with the air supply conditions presenting the highest values in terms of relative humidity (Test 5) is the one presenting the smoothest pressure drop evolution. That observation is in contradiction with the observation carried out on chilled flat surface (Cheng and Cheng (2001)). In those situations, the supply air presenting the highest relative humidity is the one presenting the thickest frost layer after a certain amount of time.

In reality, situation in heat exchanger is very different compared to chilled plates because of the interaction of the different zones: those differences can be explained by the fact that the condensate flows out of the heat exchanger when the wet part of the heat exchanger is important. This condensation flows perturbs the theoretical frost formation. Figure IV-28 brings the most relevant findings of this chapter. This phenomenon is observed by means of the Plexiglas box: condensate flushes out of the heat exchanger and condensation interacts with the frost part.
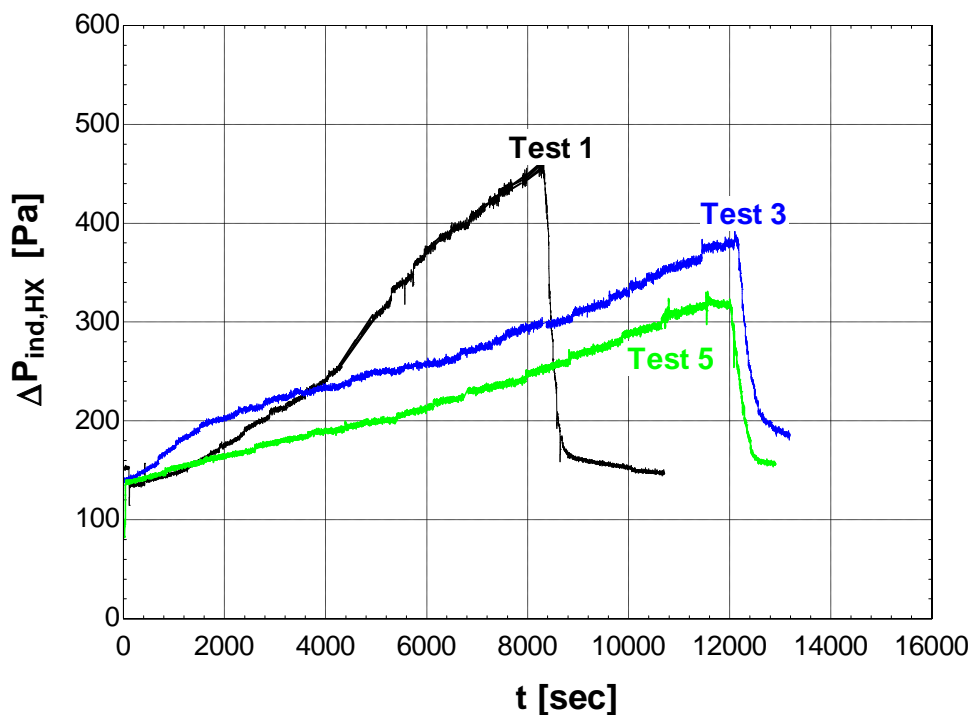
Figure IV-28: Pressure drop evolution for Test 1, 3 and 5

3.8   Three zones model versus experimental results: dynamic comparison

Dynamic comparison between numerical and experimental results has been realized for hydraulic and thermal performances. The only parameter that has been adjusted is the factor "a" in Equation IV-2 concerning the frost density determination. The parameter "a" has been chosen equal to 270 instead of 207.

Thermal performances are well predicted by the model as shown in Figure IV-29, for Test 3 and Test 4:
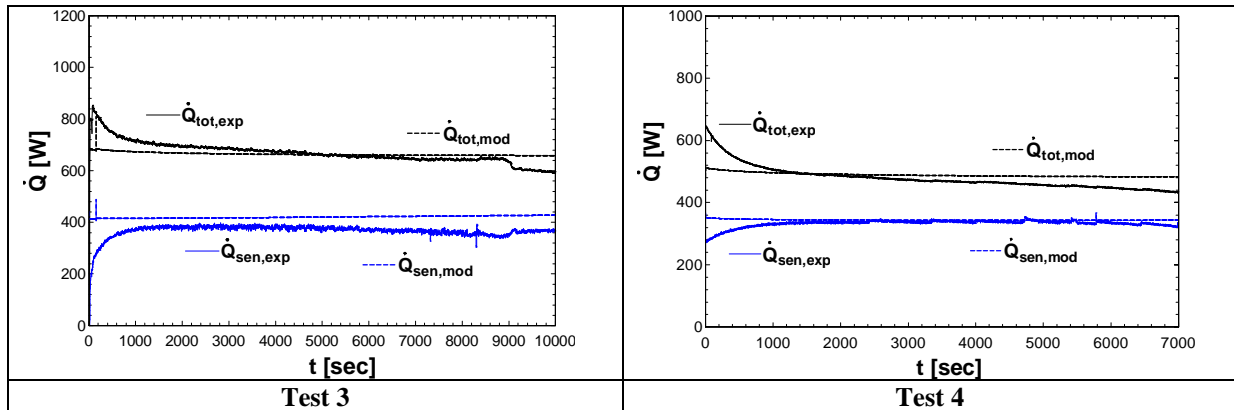
Figure IV-29: Thermal performance comparison for Test 3(left) and Test 4 (right)

Discrepancies in terms of thermal performance at the beginning of the test can easily be explained by the thermal inertia of the heat exchanger and the experimental apparatus. This has been neglected by the model. On the other hand, this has never been highlighted for dry and partially wet tests which have been realized under stabilized conditions. Except for this identified problem, predictions fit well with the experiment.

Test 5
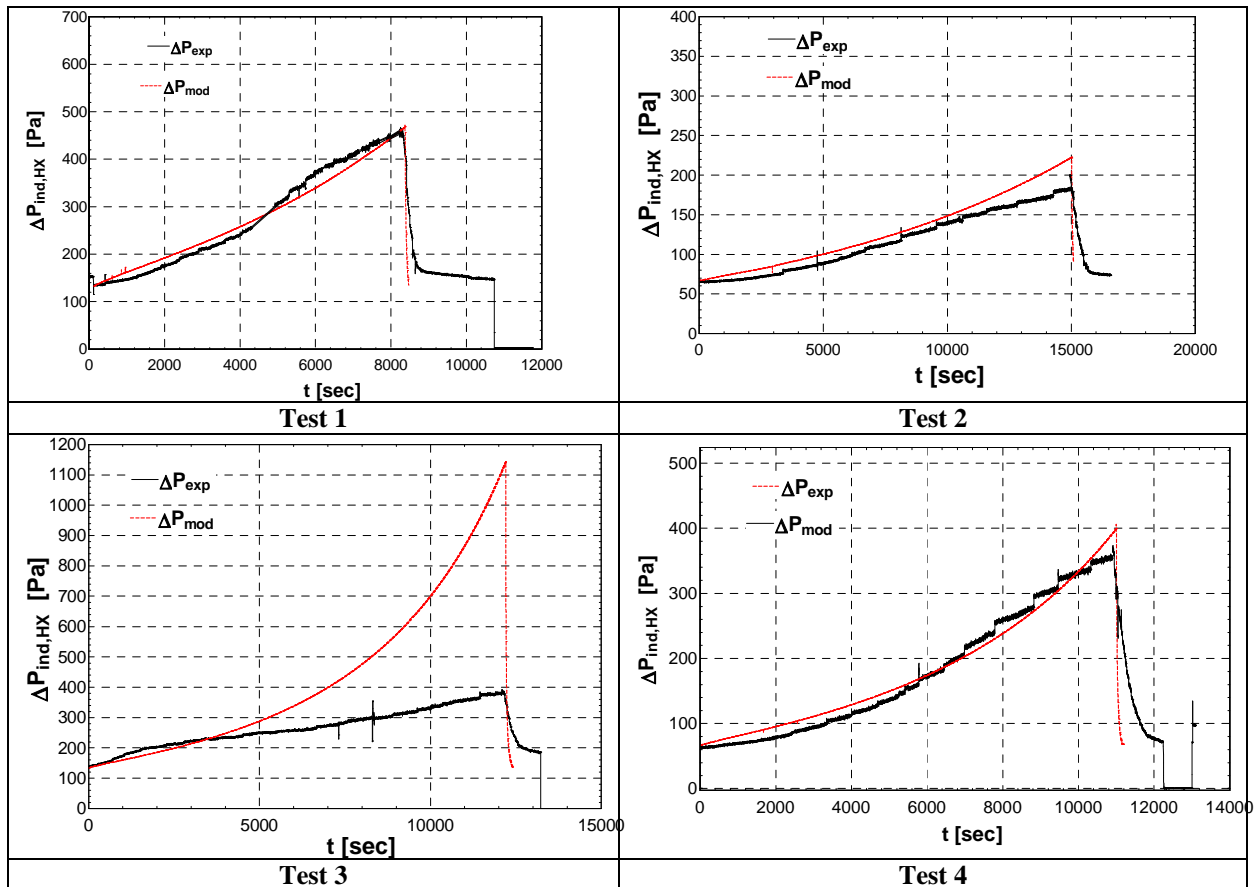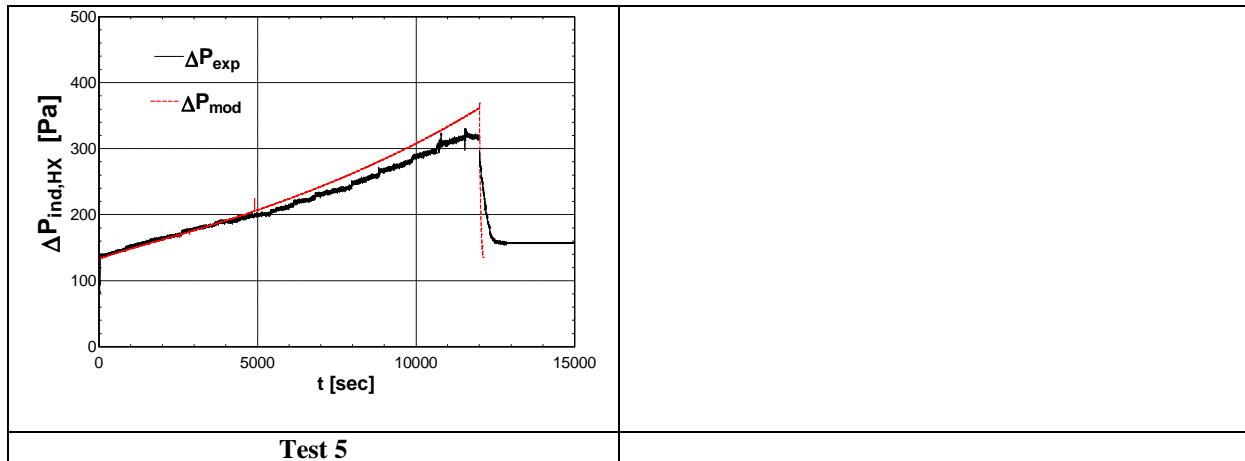
Figure 30: Pressure drop evolution (comparison between model and experimental results)

Concerning the hydraulic performance <u>during the frosting phase</u>, the model seems able to well predict the behavior of the heat exchanger under frosting conditions, except for the Test 3. This can be explained by the interaction of the wet parts on the frost part which has already been mentioned earlier. The developed model does not consider the perturbation due to the condensate flushing out of the heat exchanger. As shown in Table IV-3, if regarding the numerical results in terms of surface proportion, difference between Test 1 and Test 3 are quite important. Wet part is three times larger in Test 3 than in Test 1. This can explain the difference between model and experimental results for test 3.

Table IV-3: Surface proportion (determined by the model)

Test 1	Test 3
- $Prop_{dry} = 35\%$ - $Prop_{wet} = 25\%$ - $Prop_{frost} = 40\%$	- $Prop_{dry} = 7\%$ - $Prop_{wet} = 73\%$ - $Prop_{frost} = 20\%$

Concerning the hydraulic performance <u>during the defrosting phase</u>, it seems that the model predicts a quicker decrease of the pressure drop in comparison with the experimental results. This can be explained by the assumption concerning the direct evacuation of each mass of melt frost. In reality, each melt frost is not directly removed from the heat exchanger, as it has been observed by visual observation through the Plexiglas box.

4   STRATEGIES UNDER FROSTING CONDITIONS

As already stated, the major problem encountered in heat exchangers is the frost, e.g. during the winter time. The formation of a frost layer on the surface generates a fouling inside ducts. Consequently, it reduces the flow section and the air flow rate (Xia & al., 2006). The frost quantity may increase until it blocks the passage ways for exhaust air and stops completely the airflow.

Several methods are mentioned in the scientific literature (Shurcliff (1988), Philips et al. (1989), Nielsen et al. (2008) and Rose et al. (2008)). However, there is little literature available on the evaluation performance related to these methods. A method in order to take into account the unbalanced flow rate is proposed. In the following section, presentation and classification of each technique is proposed and a method of evaluation based on the determination of an "energy" factor is proposed to determine the best method to apply. This is realized by using the three zones dynamic model presented above. Advantages and drawbacks of each method in terms of implementation are also discussed.

As described by Philipps et al. (1989), the ideal strategy under frosting conditions is a strategy where the frost is continuously removed without putting any energy into the removal process. Consequently, there wouldn't be heat exchanger fouling. However, in this way, the latent and sensible energy from cooling and freezing water vapor to frost are still recovered completely.

Strategies involving an intrinsic modification of the device in terms of materials and/or configuration will not be investigated in the frame of this thesis:

-   Use of phase change materials (Qarnia et al. (2001));
-   Use of two heat exchangers working alternatively (Krag (2007));
-   Changing surface properties (Liu (2010)).

4.1   Strategies Classification

In order to control the impacts of frost, several methods of frost control and defrost strategies are applied on the heat exchangers. These strategies help to **avoid** or to **remove** the frost layer on the exchange surface of the heat exchangers.

There are three categories of methods under frosting conditions:

•   **Defrost method** (Philips et al., (1989));

•   **Frost control method** (Nielsen et al. (2008), Shurcliff (1989) and Rose et al. (2008));

•   **Hybrid method.**

The difference between the two first methods arises from the presence or absence of a frost layer:

-   In the **defrost method**, a frost layer on the exchange surface of the heat exchanger is accepted. That implies cycles of frost followed by cycles of defrost. Indeed, this method attempts to remove the frost from the heat exchange surface before reaching a "defined" degradation of heat exchanger performances (raise of pressure drop).

-   In the **frost control method**, no amount of frost on the exchange surface is accepted. The main idea is to prevent any frost formation in the heat exchanger. Several frost control methods exist. For instance, an electrical air heater can be used to rise the fresh air

temperature at the inlet of the exchanger. It allows to maintain the supply fresh air temperature above the frost threshold temperature. Generally, the frost control method starts when a criterion defined by the manufacturer is reached. In most of the cases, if the outdoor temperature equals to a threshold temperature then the frost control method starts.

- One can also imagine **hybrid methods**. This would results in a combination of "defrost" and "frost control" methods. Indeed, the presence of a frost layer is accepted but the frost formation is reduced.

Defrost methods are summarized in Figure IV-31:
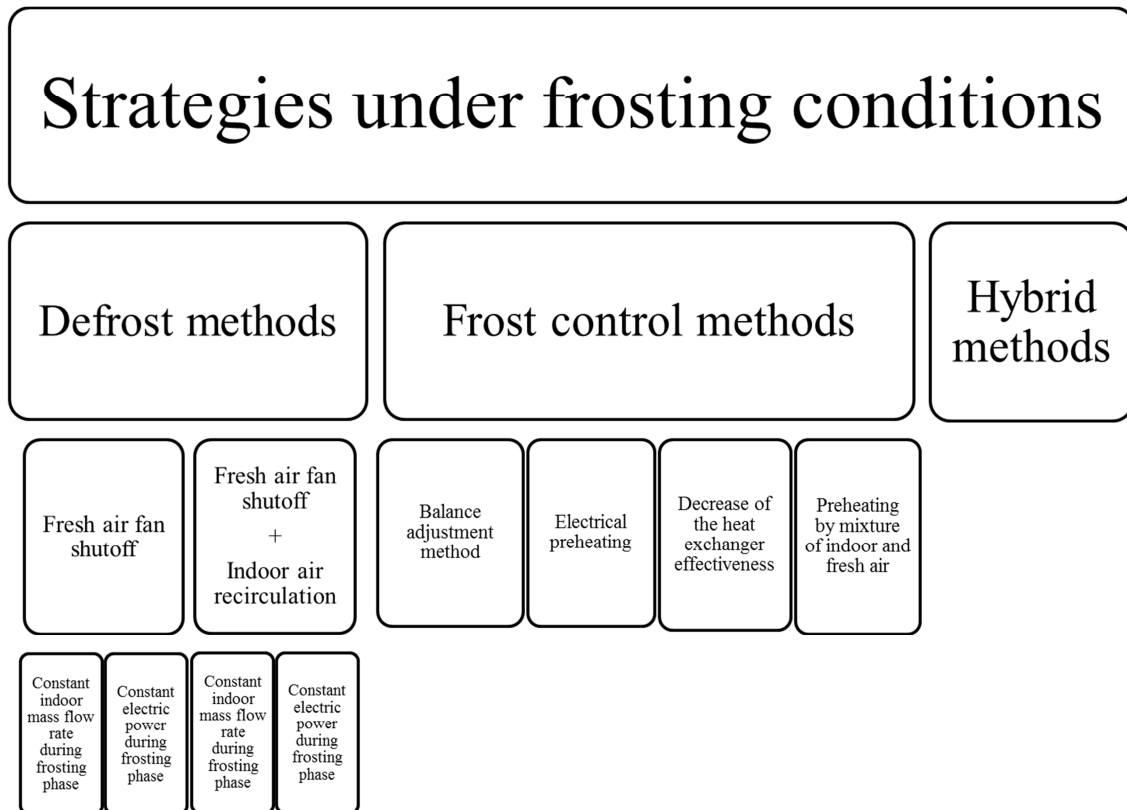
Figure IV-31: Strategies under frosting conditions

4.2 Defrost methods

Defrost methods generally consists in a cycle involving two phases:

- A frosting phase,
- A defrosting phase.

The frosting phase corresponds to the formation of a frost layer on the heat exchanger surface.

The defrosting phase corresponds to the decrease/melting of the frost mass. This phase starts when the degradation of heat exchanger performances is considered too high. As an example, a criterion on the pressure drop or on the volume flow rate can be imposed. When this criterion is reached, the defrosting phase begins.

The so called frosting/defrosting cycle ends when the frost has disappeared (melt) from the exchange surface.

Several defrost methods can be applied depending on the strategy applied during the frosting phase (constant supplied electrical power or constant mass flow rate) and the defrosting phase (fresh air fan shutoff or fresh air fan shutoff with recirculation). Each strategy for both frosting and defrosting phases are detailed here.

4.2.1 Frosting phase

During the frosting phase, the system can be controlled in two ways, depending on the operating variable which is maintained constant:
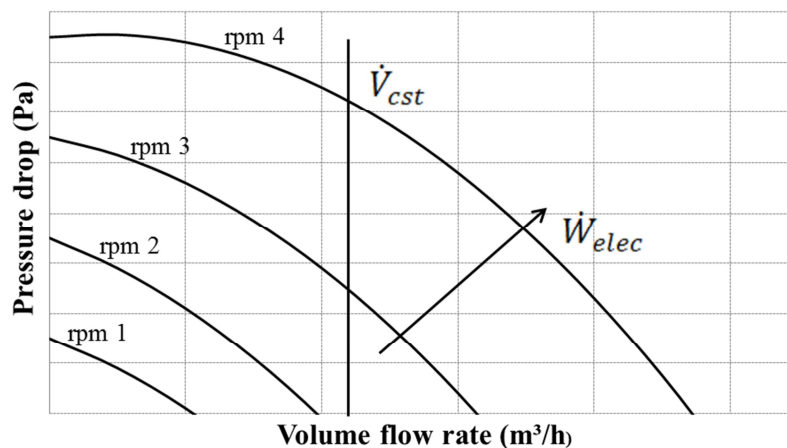
- The indoor air mass flow rate is kept constant during the cycle,
- The electric power supplied to the fans is kept constant during the cycle.

a)   Constant indoor flow rate

In this case, the indoor air volume flow rate is kept constant during the frosting phase. During the formation of the frost layer on the exchange surface, the pressure drop will increase which involves an increase of the electrical power delivered to the indoor fan in order to keep a constant volume flow rate. The opposite phenomenon appears during defrosting phase: the pressure drop decreases involving a reduction of the electrical power delivered to the indoor fans. The model calculates the electrical power delivered to the fans at each time step (one second).

The defrost starts when a criterion on the pressure drops is reached. This criterion is the maximum pressure drop accepted inside the heat exchanger for a specific flow rate. A parametric study on this criterion will be carried out.

This strategy is schematically represented in Figure IV-32:

Figure IV-32: Schematic representation of the constant mass flow rate strategy (frosting phase)

Evolution of the electrical power supplied to the fans is deduced from the knowledge of the fan curve experimentally determined.
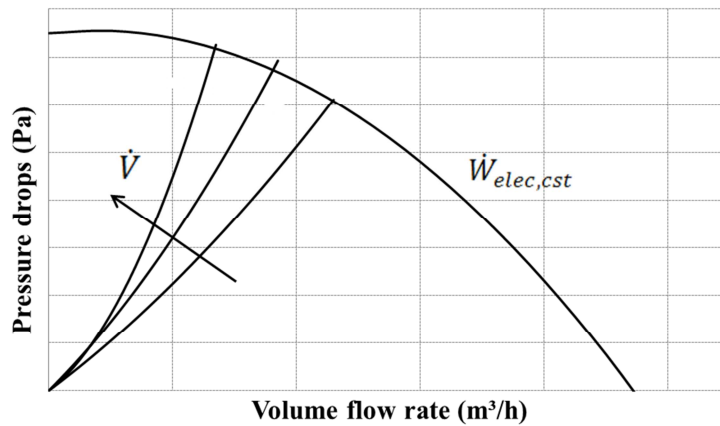
b) Constant electric fan power

In this case, the electric power delivered to the indoor fan is kept constant during the frosting cycle. During the formation of the frost layer, the pressure drop will increase which leads to a decrease in the volume flow rate of indoor air for a given electrical power. During the defrosting phase, the pressure drop decreases increasing the volume flow rate of indoor air.

The consumed electrical power is constant during the frost/defrost cycle. However, the exchanged heat transfer rate decreases in proportion with the volume flow rate of indoor air. Thus, the recovered thermal energy is lower over an entire cycle.

The defrost phase starts when the defined criterion on volume flow rate is reached. This criterion represents the minimum volume flow rate accepted for a specific electrical power delivered to the indoor fan.

This strategy is schematically represented in Figure IV-33.

Figure IV-33 : Schematic representation of the constant electrical fan power strategy (frosting phase)

In the simulations, a function expressing the flow rate depending on the pressure drops and the electric power fan is used in order to determine the variation of volume flow rate in this strategy. This function is given by:

$$\dot{V} = f(\Delta P, \dot{W}_{elec})$$

Where ΔP represents the total pressure drop (Pa).

The pressure drops are determined by using the *"Three zones exchanger"* model described in the previous section. The electric power fan is imposed as a supply condition. Once again, the fan curves are experimentally determined. Finally, the flow rate can be deduced from the knowledge of the pressure drops and the electric power fan.

4.2.2 Defrosting phase

The defrosting phase can be performed in two ways:

- Fresh air fan shutoff;
- Fresh air fan shutoff and indoor air recirculation.

a) *Supply outdoor air fan shutoff*

This strategy (Philips et al. (1989)) is the simplest and most commonly used method to reduce the frost layer. This method implies shutting off the fresh air fan while leaving on the indoor air fan, as schematically represented in Figure IV-34. By this way, the indoor air is no longer cooled down and

the frost layer on the exchange surface begins to melt. Generally, the frosting/defrosting phases correspond to a determined set time period (i.e. 40 minutes of frost period and 5 minutes of defrost phase) that can be a function of the outdoor temperature.
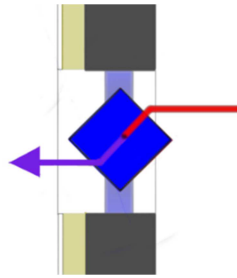
Figure IV-34: Schematic representation of supply outdoor air fan shut off (during defrosting time)

The considered parameter could also correspond to the pressure drops on the indoor air side. When a criteria on the pressure drop is reached (i.e. when the pressure drop is more than X Pa for a specific flow rate), the defrosting phase starts. The strategy can be optimized to recover as much energy as possible. This optimization involves minimizing the fraction of time spent in the defrosting phase. Optimization of the method can be obtained by investigating the impact of a reduction in the defrost phase time or a decrease of the frequency of defrosts period. It is quantified in the frame of this chapter.

The advantage of the method is that it can be easily implemented while the drawbacks are:

- Frequency of frost/defrost cycle can acoustically perturb inhabitants for single room ventilation;
- During the defrost mode, the house is placed under a negative pressure because the outdoor air fan is shut off while the indoor air fan continues to operate.

b) *Indoor air recirculation*
This method (Philips, 1989) proposes to block the entrance of the duct of the fresh air to prevent it to flow within the exchanger. The exhaust duct of the indoor air is connected with the supply of the duct of the outdoor air so that the indoor air flows through both ducts. In other words, a recirculation of indoor air is introduced; as a consequence, only the indoor air circulates within the heat exchanger.
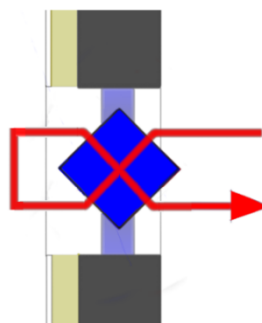
Figure IV-35: Schematic representation of an indoor air recirculation method (during defrosting phase)

The advantage of the method is that it reduces the defrosting time compared to fresh air fan shut off.

The drawbacks are:

- Difficulty of practical implementation, especially for single room ventilation;
- Frequency of frost/defrost cycle can acoustically perturb inhabitants for single room ventilation;

- Ventilation is interrupted.

Compared to the other defrosting method, the main advantage is that the house is not subjected to negative or positive pressure imbalances. However the main disadvantage is the interruption of the ventilation.

In order to compensate for the interruption of the ventilation rate when the heat exchanger is in the defrosting phase, the indoor air flow rate must be higher during frosting time. This increase helps to maintain the average desired ventilation rate throughout the hour or day.

4.3 Frost control methods

Four frost control methods can be distinguished:

- The balance adjustment method (Nielsen et al. 2008);
- The electric preheating (Philips et al. 1989);
- The decrease in the effectiveness of the heat exchanger (Philips et al. 1989);
- The preheating by mixture of indoor air and outdoor air (Rose et al. 2008).

As already stated, the aim of all these strategies is to avoid the formation of frost in the heat exchanger. The considered parameters to determine the presence of frost or not is the contact temperature at the outlet of the heat exchanger $T_{c,ex}$: frost will not form on the heat exchange surface if this temperature is above 0°C.

4.3.1   Balance adjustment method

This method implies to adjust the volume flow rate of each side to prevent the formation of a frost layer, as represented in Figure IV-36. Unlike the method of defrost cycle, this method does not require the complete stop of the fresh air fan. However, it requires the determination of the contact temperature. This temperature can be known directly or deduced from the outside temperature by means of a model predictive control (use of the "two zones" variable boundary model).
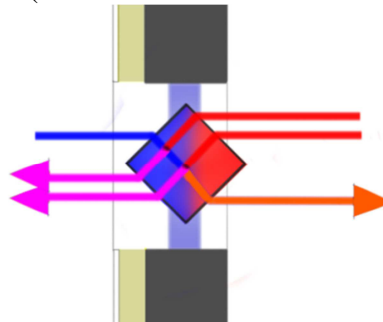
Figure IV-36: Schematic representation of the balance adjustment method

This method can be implemented in different ways. It may be decided to vary only one of the two flow rates. In other words, just an air flow can be increased or decreased, i.e. indoor or outdoor air. In another way, both rates can vary simultaneously. For instance, the outdoor air flow can be decreased and indoor air flow rate can be increased at the same time (the most important is to ensure an unbalancing of the two flow rates).

The advantages are:

- Ease of implementation (fans can be controlled independently);
- Ventilation is not interrupted;
- Safer for the systems than defrost strategies;

- Several strategies can be applied (rise of indoor air side flow rate, decrease of fresh air side flow rate or variation of both flow rates).

The drawbacks are:

- Mechanical unbalanced flow rates (depressurization of the building);
- If the fresh air flow rate is set to the minimum, the indoor air flow rate has to be increased. This can lead to fan noise problem, especially in the case of units placed in bedrooms.

4.3.2 Electrical pre-heating

This method implies to preheat the fresh air before it enters inside the heat exchanger. It can be realized by using an electric heater positioned upstream of the heat exchanger, as schematically represented in Figure IV-37. This preheating can be done in several stages (use of several resistances). In fact, the preheating can be split into two or three stages. The method is initialized when a threshold outdoor temperature is reached within the heat exchanger.
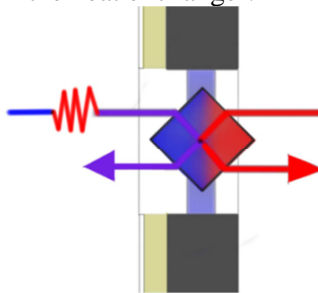
Figure IV-37: Schematic representation of the electrical pre-heating method

The advantages are:

- Diversity of possible strategies (one or more stages) ;
- Can be easily implemented (variation of the electrical power delivered to the resistances as a function of the outdoor temperature);
- Air flow rates remains balanced;
- Ventilation is not interrupted.

The drawbacks are:

- Additional electrical consumption;
- Limited to the available space.

4.3.3 Decrease of the heat exchanger effectiveness

This method involves a reduction of the heat exchanger effectiveness. In order to implement it, some passes of the heat exchanger that allow the passage of the volume flow rate can be blocked. Consequently, the effectiveness decreases and the contact temperature of the exchange surface is kept above 0°C. The main advantage of this method is to maintain the ventilation on. Unfortunately, the practical implementation of this method seems quite complicated, especially for devices such as single room ventilation with heat recovery.

The advantage is that the ventilation is not interrupted.

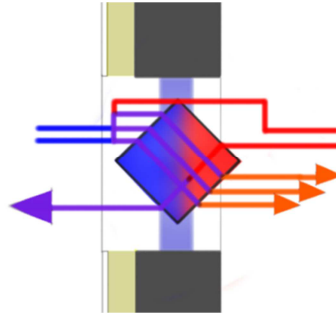The drawbacks of the method are:

- Difficulty of practical implementation in single room ventilation;
- Low heat recovered energy;

- Important fan consumption if blocking a large part of the supplies of the heat exchanger (increase of the pressure drop).

4.3.4   Preheating by mixture of indoor and outdoor air

This method consists in a preheating of the fresh air going to the heat exchanger by means of a mixing with indoor air. The principle is to derive a part of the indoor air flow rate to the fresh air side heat exchanger supply. It can be realized by adding a duct/section in direct contact with outdoor air. When the threshold temperature is reached, a valve can be proportionally opened and the mixture can take place. In other operating conditions, the valve remains closed. The situation under frosting conditions is schematically represented in Figure IV-38.

Figure IV-38: Schematic representation of the "preheating by mixture" strategy

The advantages of the method are:

- Ventilation is not interrupted;
- Precise valve control offering several strategies.

The drawbacks of the method are:

- Difficulty of practical implementation;
- Increase of the electrical power delivered to the fan to ensure the derivation of the indoor air for the mixing (passage through the valve and duct). In the simulation, an increase of fan consumption of 10% has been assumed due to this flow rate deviation;
- Increase of the electrical power delivered to the fan due to the passage of a higher flow rate in the heat exchanger in fresh air side.

Due to the difficulty of implementation of the "decrease effectiveness" method in single room ventilation unit, only three methods have been implemented:

- The balance adjustment method ;
- The electrical preheating ;
- Preheating by mixture of indoor and outdoor air.

4.4   Criteria of energy performance: definition

In order to compare the strategies, a criterion of energy performance is required. The criterion is defined as the ratio between the energy recovered and the energy delivered to the fans:

$$\Omega = \frac{E_{recovered}}{E_{elec}} \ [-]$$ IV-36

With

- $E_{recovered}$: the thermal energy recovered in [J];

- E_{elec} : the electrical energy supplied to the fans in [J].

Some authors such as Rose et al. (2007) preferred to compare some strategies by considering the yearly energy consumed and recovered. They carried out investigations for two different climates (Denmark and Nuuk). They introduced a factor of 2.5 on the electrical energy in order to take into account the CO_2 emissions associated with the electrical production. In reality, Rose et al. (2007) investigated a method involving two heat exchangers in parallel. They performed a combination between the balance adjustment method and the defrosting/frosting cycle. This strategy is impossible to apply to single room ventilation given the restriction on the available volume.

In the frame of this chapter, strategies will only be compared by means of Equation IV-37. The integration is realized on a cycle involving a frosting time of 7200 sec:

$$\Omega_{device} = \frac{\int \dot{Q}_{recovered} \, d\tau}{\int \dot{W}_{elec} \, d\tau}$$

IV-37

with $\dot{Q}_{recovered}$, the power recovered at each time step in [W]. If flow rates are unbalanced, it is assumed that the flow rate difference comes from infiltration as schematically represented in Figure IV-39 for a case where the indoor flow rate is higher than the fresh air flow rate:
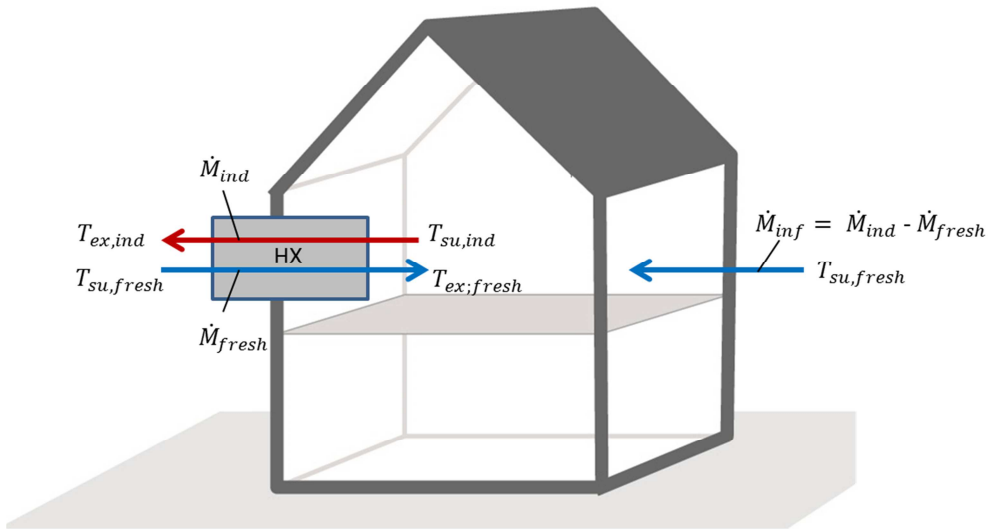

Figure IV-39: Infiltration resulting from unbalanced flow rates ($\dot{M}_{ind} > \dot{M}_{fresh}$)

In this case, the recovered heat rate at each time step is determined by:

$$\dot{Q}_{recovered} = (\dot{M}_{fresh} + \dot{M}_{inf}) \cdot c_p \cdot (T_{mix} - T_{su,fresh})$$

IV-38

with T_{mix}, the temperature resulting from the fictitious mixing of the infiltration and the flow rate flowing through the heat exchanger:

$$T_{mix} = \frac{\dot{M}_{inf} \cdot c_p \cdot T_{su,fresh} + \dot{M}_{fresh} \cdot c_p \cdot T_{ex,fresh}}{\dot{M}_{ind} \cdot c_p}$$

IV-39

The experimentally determined fan curves have been used and coupled to perform the investigations of the strategies.

4.5 Comparison of strategies

4.5.1 Energy performance criteria

The above presented strategies have been compared by considering the supply conditions given in

Table IV-4:

Table IV-4: Supply conditions for investigations on frost/defrost strategies

$\dot{V}_{fresh}\,[m^3/h]$	$\dot{V}_{ind}\,[m^3/h]$	$T_{su,ind}\,[°C]$	$T_{su,fresh}\,[°C]$	$RH_{su,ind}\,[-]$
50	50	18	-15	0.5

Note that the supply conditions are kept constant during the whole simulation time.

Comparison of the different strategies in terms of energy performance is given in Table IV-5. A frosting time of 7200 sec has been assumed for each of investigated frost/defrost cycles. Thanks to the developed model, it is also possible to quantify the ratio between flow rate mechanically supplied and removed from the building over a period. This factor is a representation of the (de)pressurization and/or on the indoor air quality.

Table IV-5: Methods of defrost

Methods under frosting conditions						
Strategy		**Frosting time [s]**	**Defrosting time [s]**	**Cycle time [s]**	Ω_{device} [-]	$\dfrac{M_{ind}}{M_{fresh}}$ [-]
$\dot{V}$ constant	Supply air outdoor fan shutoff	7200	238	7438	10.3	1.03
	Indoor air recirculation	7200	153	7353	10.4	1.02
$\dot{W}_{fan}$ constant	Supply air outdoor fan shutoff	7200	118	7318	10.8	0.91
	Indoor air recirculation	7200	102	7302	10.8	0.91
Balance adjustment method		0	0	0	11.5	2.40
Electrical preheating		0	0	0	1.2	1.00
Pre-heating by mixture of indoor and outdoor air		0	0	0	8.0	1.00

As an example, it is possible to determine the flow rate evolution if the power delivered to the indoor air side fan is kept constant, as shown in Figure IV-40. Same figure could be realized for the electrical power delivered to fans if the flow rate is kept constant.
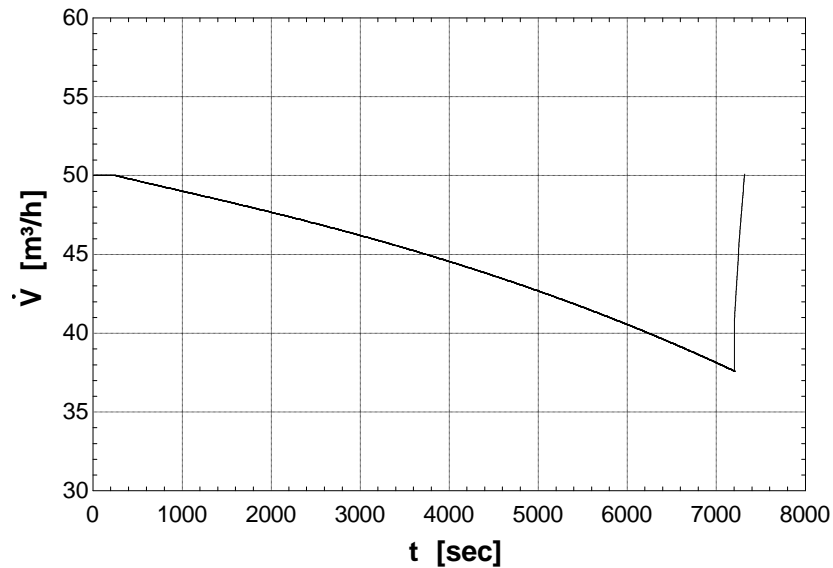
Figure IV-40: Flow rate evolution in the case ($\dot{W}_{fans} = constant$)

4.5.2 Strategy classification in terms of energy performance and implementation

It is now possible to determine a classification of the method in terms of energy performance, implementation and mechanical unbalancing (ratio between flow rates mechanically supplied and removed from the building over a period), especially for single room ventilation unit with heat recovery. Table IV-6 summarizes the advantages and the drawbacks of each strategy in terms of these parameters:

Table IV-6: Strategy in terms of energy performance and implementation

Advantages and drawbacks				
Strategy		**Energy performance**	**Implementation**	**Mechanical unbalancing**
$\dot{V}$ constant	Supply air outdoor fan shutoff	+	-	++
	Indoor air recirculation	+	--	++
$\dot{W}_{elec}$ constant	Supply air outdoor fan shutoff	+	+	+
	Indoor air recirculation	+	--	+
Misbalancing		++	++	--
Electrical preheating		--	-	++
Pre-heating by mixture of indoor and outdoor air		-	+ -	++

4.5.3 Influence of the cycle time on the energy criteria

As already specified, in the simulations performed for frosting/defrosting cycle, a frosting time of 7200 sec has been imposed. That corresponds to a certain amount of pressure drop (if $\dot{V}$ has been set constant, as an example).

The present section studies the impact of this criterion (or frosting/defrosting time cycle) on the energy performance criteria. The investigation is carried out for frost/defrosting cycle with fresh air fan shut

off without recirculation and during the frosting time, the volumetric flow rate is kept constant. The supply conditions are the same as the one presented in Table IV-4 and results are given in Table IV-7:

Table IV-7: Variation of the criterion on the pressure drops

Variation of the criterion on the pressure drops					
Frosting time [s]	**Defrosting time [s]**	**Cycle time [s]**	**Pressure drop at the end of the frosting cycle[Pa]**	Ω_{device} **[-]**	$\dfrac{M_{ind}}{M_{fresh}}$ **[-]**
3000	108	3108	64	10.70	1.036
6000	203	6203	74	10.45	1.033
9000	291	9290	80.5	10.15	1.032

As it can be observed, if the frosting time is reduced, the energy performance criterion seems better and the mechanical flow rate unbalanced stays almost the same. A strategy with a higher frequency of frost/defrost cycle will be preferred.

5   CONCLUSIONS

The aim of this chapter was to investigate the impact of the frost layer on the performance of an air-to-air heat recovery. The first step was to adapt the "two zones" model presented in the frame of Chapter II by adding a third zone (so called frost zone). To do so, a frost growth model was first developed. This latter is based on several publications and validated by means of experimental data from the scientific literature. The model has been validated by comparing the frost layer thickness evolution under several operating conditions.

Considering the behavior of a heat exchanger under frosting conditions, experimental investigations have been carried out on a U-flow heat exchanger with corrugations of 30° in the central part. The first part of the experimental investigations was to confirm the validity of the "two zones" heat exchanger model but on a heat exchanger presenting a geometry different from the one presented in the frame of the Chapter II. The same methodology was applied (calibration of the heat transfer coefficient for friction factor and Nusselt number). Then, investigations under frosting conditions have been performed and analysis of the experimental data has been realized. The first conclusions to be drawn concern the influence of the humidity: tests performed under air supply conditions with a high relative humidity show an evolution different from the one predicted by the model. This is due to the influence of the condensates flowing out of the heat exchanger and perturbing the theoretical formation of frost. This influence is reduced when the wet part is smaller.

Once the model has been judged validated, several methods under frosting conditions have been presented. Discussion in terms of ease of application has been realized for each of them, especially in the case of the development of a single room ventilation with heat recovery. Then, all the methods have been compared by means of two coefficients: an energy performance coefficient and a ratio of mass mechanically supplied and removed from the building.

6   REFERENCES

Ayub, Z. H., (2003). *Plate heat exchanger literature survey and new heat transfer and pressure drop correlations for refrigerant evaporators.* Heat transfer engineering, 24(5): 3-16

Bantle, R., Barber, E.M., Moysey, E.B., Moysey, Sokhansanj, S., 1987. *Maximizing heat recovery in air-to-air heat exchanger operating under frosting conditions.* Presentation to the Canadian Society of Agricultural Engineering. Montreal. May 18-22, 1987

Bantle, R. 1987. *Prediction and control of frost formation in air-to-air heat exchanger.* Master thesis. University of Sakatchewan. 1987

Bantle, R., Barber, E.M., and Besant, R.W., 1987. *A mathematical model of a plate type air –to-air heat exchanger operating under frost forming conditions.* University of Saskatchewan, 1987

Cheng , C.-H., and Cheng, Y-C. 2001. *Predictions of frost growth on a cold plate in atmospheric air.* Int. Comm. Heat Mass Transfer, Vol. 28, N°7, pp 953-962, 2001.

Chen, H., Thomas, L., and Besant, R. 2003. *Fan supplied heat exchanger performance under frosting conditions.* International Journal of Refrigeration. Volume 26, Issue 1, January 2003, Pages 140-149

Da Silva, Hermes and Melo. 2010. *Experimental Study of Frost Accumulation on Fan-Supplied Tube-Fin Evaporators.* International Refrigeration and Air Conditioning Conference, 2110(1013), 1-7

Fisk WJ, Archer, KM, Chant, RE, Offerman, F.J., Pedersen, B.S., 1983. *Freezing in residential air-to-air heat exchangers: an experimental study.* Lawrence Berkeley Laboratory.

Fisk WJ, Chant, RE, Archer KM, Hekmat D. 1984. *Onset of freezing in residential air-to-air heat exchangers.* ASHRAE Trans 1984; 91: 145-158

Fisk WJ, Chant, RE, Archer KM, Hekmat D., Offerman, FJ, Pedersen, BS. 1985. *Performance of residential air-to-air heat exchangers during freezing and periodic defrosts.* ASHRAE Trans 1985; 91: 159-172

Hayashi, Y., Aoki, A., Adachi, S., and Hori, K. 1977. *Study of frost properties correlating with frost formation types.* Journal of Heat transfer, 1977, 99, 239-245

Kragh, J., Rose, J., Nielsen, TR., Svendsen, S. *New counterflow heat exchanger designed for ventilation systems in cold climate.* Energy and Buildings. 2007; 39:1151-8

Lee, Kim and Lee (1997). *A one-dimensional model for frost formation on a cold flat surface.* International Journal of Heat and Mass Transfer, 40(18), 4359-4365.

Le Gall and Grillot. 1996. *Modelling of frost growth and densification.* International Journal of Heat and Mass Transfer, 40(13), 3177-3187.

Liu Z., Huang, L., Gou., Liu, Y., Experimental investigation of frost release by hydrophilic surface. Front energy Power Eng China 2010; 4:475-87

Mercadier, Y., Duong, T., Lagace, F., 1993. *Dynamic performance of a cross flow heat recovery ventilator operating under frost conditions.* In: proceedings of the fourth international symposium on the thermal proengineering and science for cold regions, Hanover, NH; 1993. Pp.113-21

Nielsen, T.K., Kragh, J., Svendsen, S. 2008. *Evaluation of a dynamic model for a cold climate counter flow air-to-air heat exchanger.* Proceedings of the 8th Symposium on Building Physics in the Nordic Countries. Copenhagen, June 16-18, 2008

O'neal, D.L. and Tree D.R. 1992. *A review of frost formation in simple geometries.* ASHRAE Transactions, 1992, 98(Part 2), 65-78

Philips, E.G., Chant, R.E., Bradley, B.C. and Fisher D.R. 1989. *An investigation of freezing control strategies for residential air-to-air heat exchangers.* ASHRAE. Technical Committee 5.5. Air-to-air Energy Recovery. Atlanta, Georgia, 1989.

Prölss, K. and Scmitz, G. 2006. *Modeling of frost growth on heat exchanger surfaces.* Presentation at the Modelica association, September 4th and 5th 2006

QarniaHE, Lacroix, M., Mercadier, Y. 2001. *Use of phase change materials to prevent frosting in a compact crossflow heat exchanger.* Energy Conversion Management 2001; 42; 1277-96

Rafati Nasr, M., Fauchoux, M., Besant, R.W. and Simonson, C.J. 2014. *A review of frosting in air-to-air heat exchangers.* Renewable and Sustainable Energy Reviews 30 (2014) 538-554

Shurcliff, W., 1988. *Air-to-air heat exchangers for houses.* An. Rev. Energy. 1988. 13:1-22

Wanniarachchi, A. S., Ratnam, U., Tilton, B. E., Dutta-Roy, K. 1995. *Approximate Correlations for Chevron-Type Plate Heat Exchangers,* 30th National Heat Transfer Conference, vol. 12, HTD vol. 314, ASME, New York, pp. 145–151, 1995.

Xia, Zhong, Hrnjak and Jacobi. 2006. *Frost, defrost, refrost, and its impact on the air-side thermal-hydraulic performance of louvered-fin, flat-tube heat exchangers.* International Journal of Refrigeration, 29(2006), 1066-1079

Yonko, J. D. and Sepsy, C. F. 1967. *An investigation of the thermal conductivity of frost while forming on a flat horizontal plate.* ASHRAE Transactions,1967, 73, 1.1-1.11.

CHAPTER V:

EXPERIMENTAL CHARACTERIZATION OF SINGLE ROOM VENTILATION WITH HEAT RECOVERY

CHAPTER V: EXPERIMENTAL CHARACTERIZATION OF SINGLE ROOM VENTILATION WITH HEAT RECOVERY

1   INTRODUCTION

In spite of the growing interest for room based mechanical ventilation with heat recovery these last few years, only a few experimental works are presented in technical and scientific literature. To the best knowledge of the authors, only the papers of Manz et al. (2000) and Schwenzfeier et al. (2009) makes mention of experimental characterization of single room ventilation with heat recovery. However, they barely detailed their experimental lay out for the determination of the thermal and hydraulic performance of the units.

The first part of the current chapter consists of a description of the characteristics and properties of the final developed device (features, components, flow configuration,…).

In the second part of the chapter, an approach is presented to experimentally characterize the unit. As already stated, the criteria of performance are based on:

- Thermal effectiveness (effectiveness of the recovery heat exchanger),

- Hydraulic aspects (flow rates delivered by the unit versus electrical power supplied to the unit),

- Acoustic aspects.

Figure V-1: Final unit

This chapter mostly focuses on the experimental determination of the hydraulic performance of the unit. One can distinguish two types of investigations, depending on the phase of development of the unit:

- Experimental studies realized **during the development steps** of the unit. These investigations realized in the development steps aim to characterize each component separately. In this context, the idea was to develop **one single** experimental apparatus that could be easily adaptable to determine performance of each component as well as the overall unit;

- Experimental investigations to **characterize the final device**. This was realized in the climatic chamber of the Thermodynamics Laboratory of the University of Liege.

The overall performance (COP) of the unit can be established based on the experimental results. A map of the COP (ratio between the recovered heat transfer rate and the supplied electrical power) can

be constructed, depending on the flow rates delivered by the unit and the indoor/outdoor temperature difference. In order to have all the performance characteristics of the device in one single figure, the sound level is also specified for each delivered flow rate (as well as the acoustic performance of the unit).

In the last part of the chapter, the seasonal performance of the developed device is determined by using the Heating Degree Day (HDD) method. This method allows to quickly compare the performance of the system to natural, simple exhaust and traditional centralized ventilation systems in terms of primary energy, consumer price and carbon dioxide emissions for a given climate. The method seems particularly suitable to easily assess the potential of use of heat recovery device at a regional/national level.

2 PRESENTATION OF THE FINAL DEVICE

Before describing the experimental investigations carried out on the unit, the aim of the current section is to present in detail the characteristics/features of the developed unit.

2.1 Characteristics of the device

Contrary to single room ventilation with heat recovery units installed on a wall (so called wall mounted) with air inlet and air outlet through the building façade, the specificity of the unit is the easiness of integration in the windows ledge, which makes them especially convenient in the frame of a house retrofitting implying windows replacement. Overall dimensions (except the casing length which is adaptable, according to the window's ledge) of the unit are given in Figure V-2:
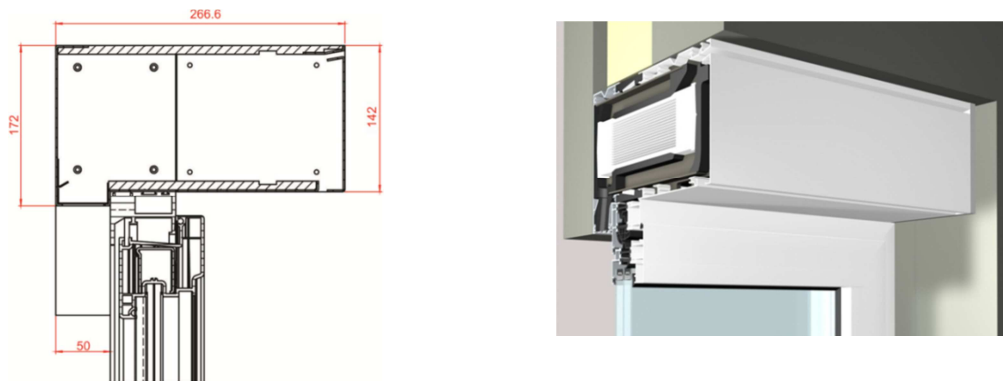
Figure V-2: Window mounted device

2.2 Parts of the unit

One can consider two parts of the unit: the "active" and the "passive" parts:

- The so-called "active" part of the unit consists of a parallelepiped box (made in polystyrene) containing two fans and two filters (for both fresh and indoor air sides), an electronic control board, an AC/DC inverter, a set of sensors (depending on the model) and obviously, the heat recovery exchanger. The standard length of the active part is equal to one meter. However, some studies on active parts on longer and shorter length have been carried out. Results are presented in the present chapter. The weight of the active part is equal to 5.5 kg (for 1m).
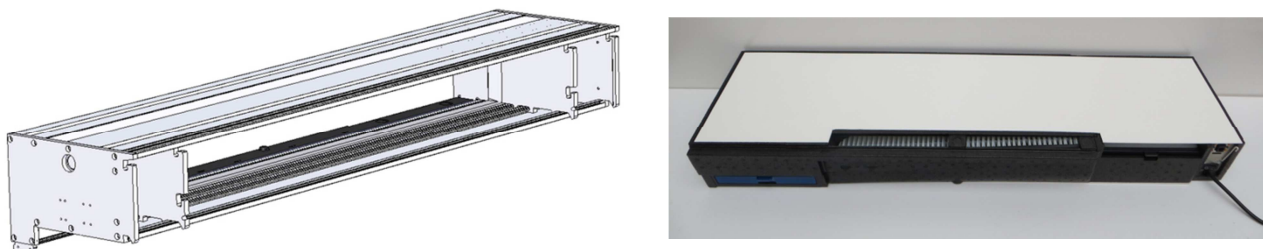
Figure V-3: Passive (left) and active (right) parts of the unit

- The so-called "passive" part of the unit consists in an aluminum casing that can be directly mounted upon the window ledge. This part is custom made and adjustable to the window ledge. If the length of the "active" part is smaller than the length of the "passive" part, the casing incorporates a thermal break (insulation material) to prevent thermal bridges. Those thermal breaks are situated on each side of the active parts. Obviously, it is also possible to

insert several "active" parts in one single passive part, depending on the available space. The unit also comprises an anti-insect grille on the outer side. The casing also includes a rigid shells; the aim of this rigid shell is to stiffen the casing. Two side profiles collect condensate. For a length of 1200 mm, the weight of the case (1200 mm) is 8.8 kg.

This "active" unit is inserted in the "passive" casing, as schematically represented in Figure V-4:
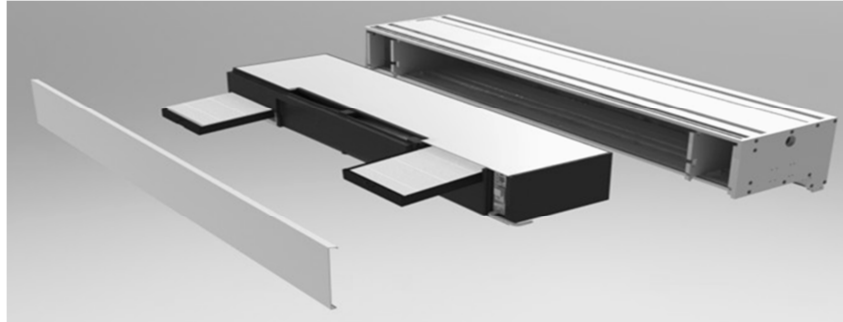
Figure V-4: Insertion of the active part of the unit in passive parts of the unit

The separation of the active and passive parts is realized in order to optimize:

- The industrialization process: each part is manufactured separately. As already mentioned above, the passive parts dimensions are adjusted to the windows ledge (adaptation on demand of the unit). This adjustment is realized by the window ledge manufacturer;

- The installation: the "passive" part is directly mounted on the windows ledge. Once the windows is placed, one can manually insert the active part in the aluminum box, as shown in Figure V-5;

- The maintenance: filter replacement (as well as the replacement of the whole active parts) is really to perform.

Figure V-5: Insertion of the active parts in the passive parts (practical achievements)

2.3 Flow configuration inside the unit

Flow configurations inside the unit are represented in Figure V-6:
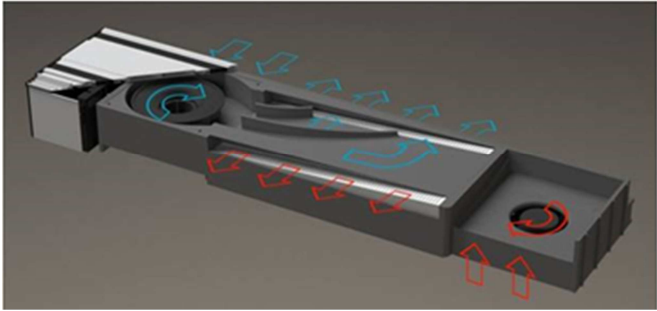
Figure V-6: Flow configurations inside the unit

2.4 Filters

Filters dedicated to the indoor and fresh air flow rates are placed upstream of the fans and thus upstream of the heat exchanger in order to protect the unit and its components against dust accumulation. As a result, filters have two roles: air filtration and protection of the system. Moreover, the system is designed in such a way that both filters are accessible from the inside of the building, as shown in Figure V-4 and Figure V-7. Types of available filters for the unit are G4, M5 or F7 (as defined in the EN 779 Standard).
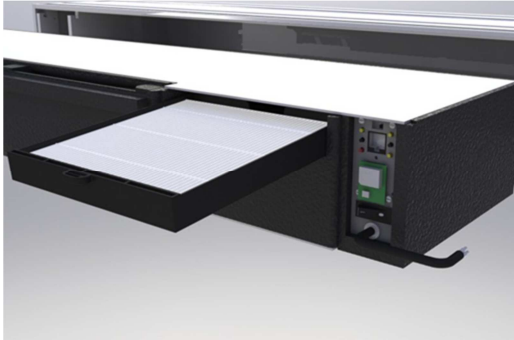
Figure V-7: Filters insertion

Note: Unless otherwise specified, experimental results given in the frame of this thesis concerns units equipped with G4 filters.

2.5 Fans and electrical current converter

The device is supplied by electrical network AC current 230V, 50Hz. As the unit was supposed to be symmetric, the same DC centrifugal fans (EBM Papst RG 160) are used for both streams (fresh and indoor sides). The rotational speeds of each fan can be controlled independently.
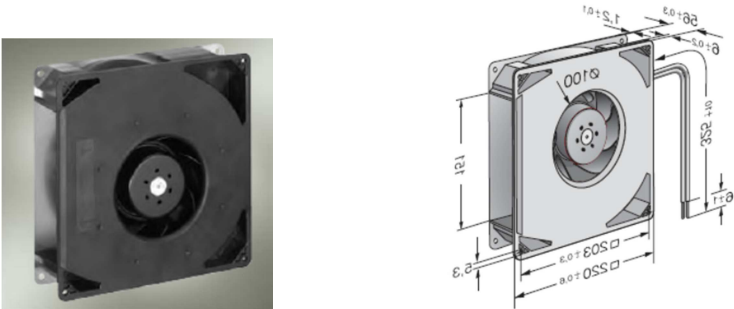
Figure V-8: EBM Papst RG 160 fans

Fan performance characterization ($\dot{V}$ versus ΔP) is realized for different rotational speeds in section 3.

2.6 Conduction heat losses of the unit

The heat losses due to conduction through the system (when the fans are off) are represented by an overall heat transfer coefficient U_{loss}.

U_{loss} values for several length of the unit (depending on the number of active units placed in the passive parts) are given in Figure V-9. U value is a decreasing function of the length of the unit: the higher the length of the unit, the higher the section of the thermal break.
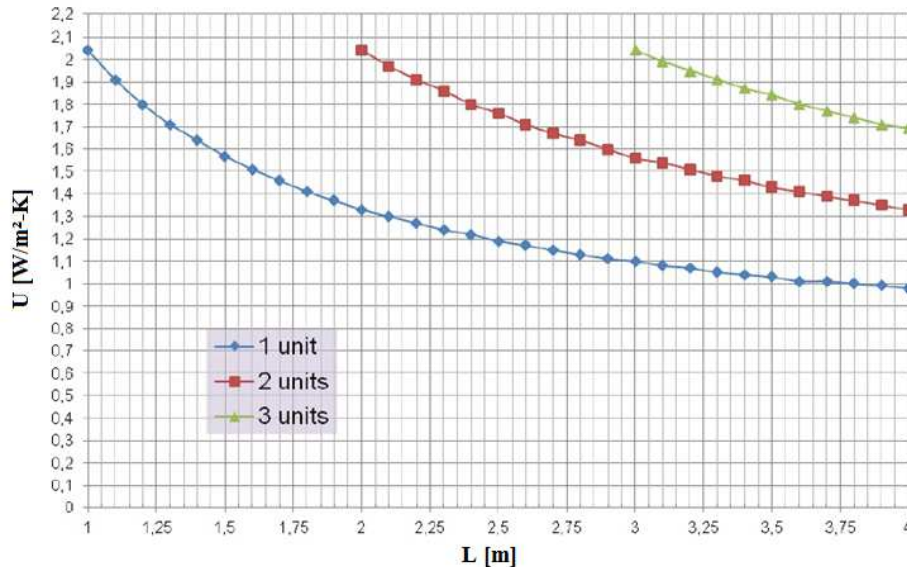
Figure V-9: U value for several length of the unit
(as a function of the number of inserted "active" parts)

2.7 Mode

The device can be controlled by the user via a wireless remote control. The remote control includes:

- 5 different levels of balanced delivered flow rates (15, 25, 36, 50 and 75 m³/h);
- A sleep mode (stop for 2 hours);
- A boost mode (maximal speed during 15 minutes);
- A simple exhaust or a simple supply mode.

The unit can also be equipped with air quality sensors (humidity or CO_2) which allow regulation of the flow rate depending on those parameters.

2.8 Condensation evacuation

Condensate is removed by means of a drain channel situated at the exhaust of the indoor air side, as represented in Figure V-10.
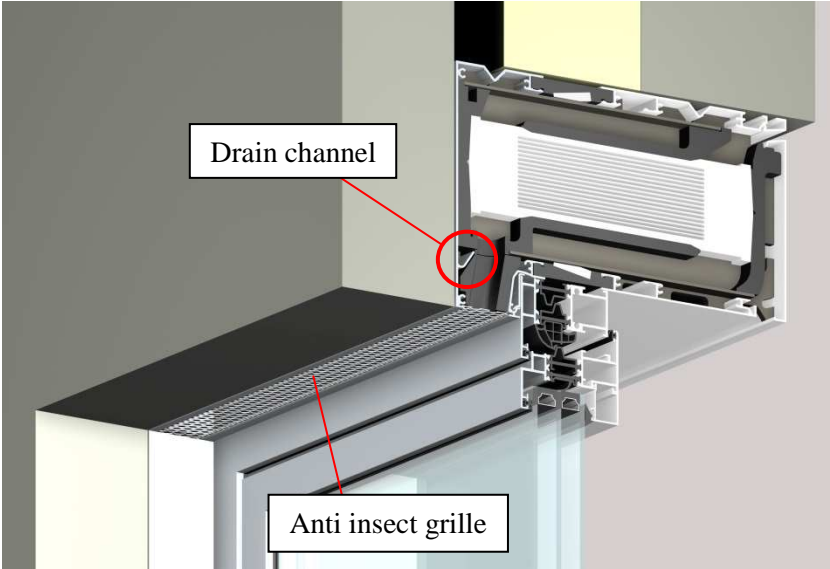
Figure V-10: Condensation evacuation

2.9 Examples of integration of the unit

Final products have been integrated in real buildings. Practical achievements (outdoor and indoor views) are given in Figure V-11 and Figure V-12. Units are installed in office buildings in Olen, Belgium.

Figure V-11: Installed unit (indoor view)

Figure V-12: Installed unit (outdoor view)

It is important to mention that as shown in Figure V-12, unit can be visible from outside but it is also possible to make them completely invisible by inserting the unit behind the wall facing or the brick veneer, as shown in Figure V-13.
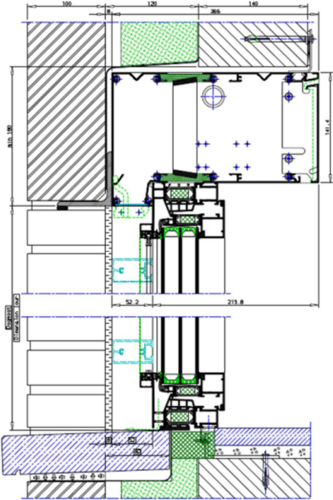
Figure V-13: Installed units (invisible from the outdoor side)

Comparing to the off -the-shelf devices presented in the frame of Chapter 1, the developed device can be distinguished by the configuration flow as well as a different type of heat exchanger (U flow heat exchanger: cfr Chapter 3).

3 HYDRAULIC PERFORMANCE ESTABLISHMENT DURING DESIGN STEP

The present section describes the experimental apparatus developed to characterize the hydraulic performance of a single room ventilation unit with heat recovery during the development steps. Experimental investigations have been carried out on the entire unit in order to determine the flow rate it delivers but also on some single component (such as the fan or filters) of the device.

The initial idea was to develop one single test bench that could be easily adaptable in order to measure several types of components, several dimensions, types and configurations of units.

3.1 Experimental procedure

3.1.1 Delivered flow rate by the device

It is rather difficult to determine the delivered flow rates by means of velocity sensors since the cross sectional velocity profile at the exhaust of the device is not known (the flow is pulsed through a slit or a mesh screen). Measurements given by the sensors vary, depending where the velocity sensor is placed. Moreover, use of intrusive sensors can modify the delivered flow rate.

As a result, a method initially dedicated to fan-coil units and described by Hannay and Lebrun (1972) was applied. A schematic representation of the experimental apparatus is given in Figure V-14:
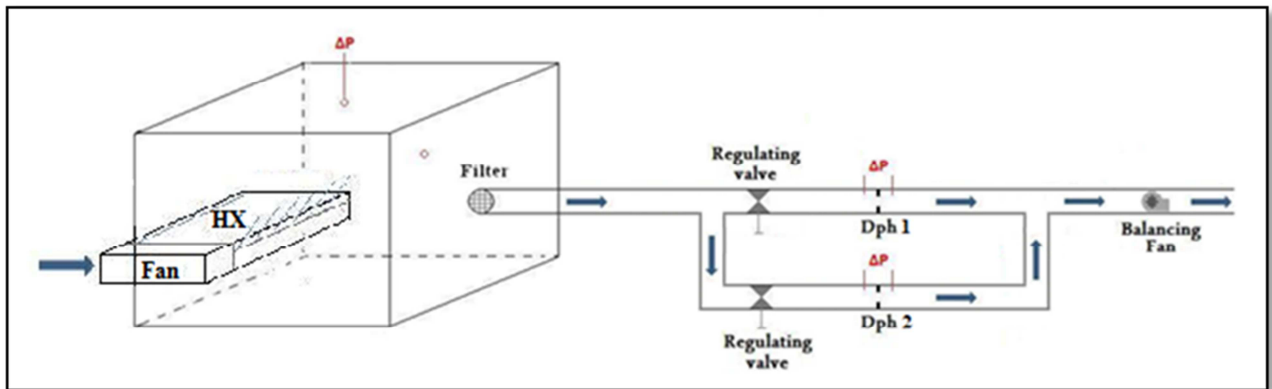
Figure V-14 : Schematic representation of the experimental apparatus to determine the delivered flow rate delivered by the device

This method consists in connecting the exhaust slit of the device into a pressure-compensated box, as shown in Figure V-15. As it can be observed, the only removal (and thus adjustable) part of the test bench is the fixation board where the unit is inserted. Air tightness of the pressure compensated box is ensured by means of silicone. Air tightness between the unit and the pressure compensated box is ensured by means of tapes.

Figure V-15: Insertion of the unit in the pressure compensated box

At the exhaust of the compensating box, a set of orifice plates is used to determine the flow rate, as shown in Figure V-14 and Figure V-17. In order to eliminate the decrease of the delivered flow rate due to the passage through the orifice plates (which induces an additional pressure loss), a balancing (also called compensating) fan is used. Several regulating valves are used to adjust manually the flow rate. Used compensating fan and regulating valves are shown in Figure V-16. A differential pressure sensor is placed between the atmosphere and the inside of the compensated box. The compensating fan rotational speed can be modified by means of the Software "Labview" in order to automatically reach a given differential pressure drop between the inner side of the box and the atmosphere.
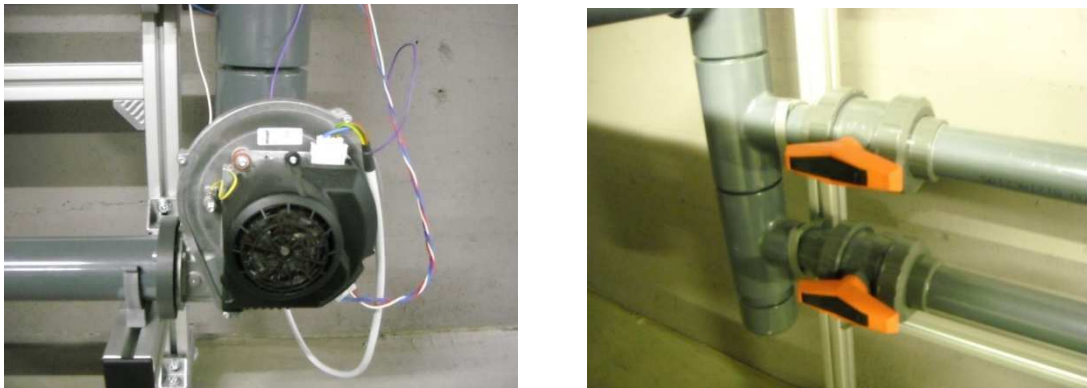
Figure V-16: Compensating fan and regulating valves

Once the measured differential pressure between the atmosphere and the inner side of the box is equal to zero, the device is supposed to operate in nominal conditions and the volumetric flow rate measured by means of the orifice plate (according to ISO 5167) is the one really delivered by the unit.

A set of two orifice plates placed in parallel has been used in order to measure a large range of delivered flow rate (use of one orifice plate or use of both orifice plates). A practical achievement of the test bench is given in Figure V-17.
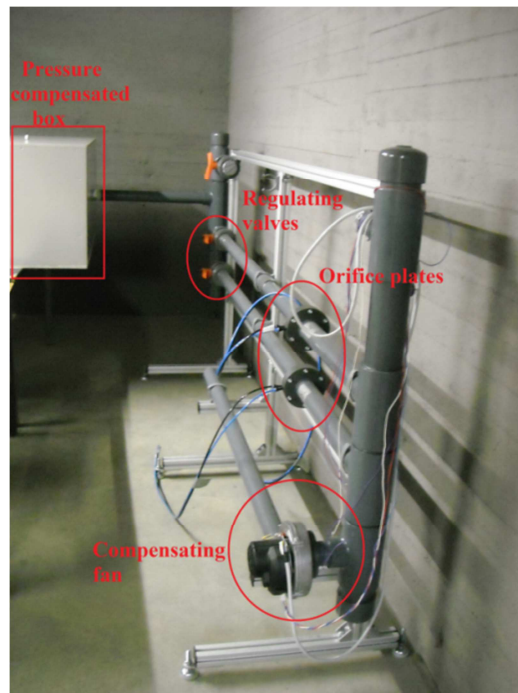
Figure V-17: Flow rate measurement at the exhaust of the pressure compensated box

A T type thermocouple has been placed at the exhaust of the pressure compensated box in order to determine the flow rate with precision. Accuracy of the thermocouple is ± 0.5K. Depending on the delivered flow rate, several "Sensirion" differential pressure sensors (with several full scale values: ±62.5 Pa, 125 Pa and 500 Pa) have been used.
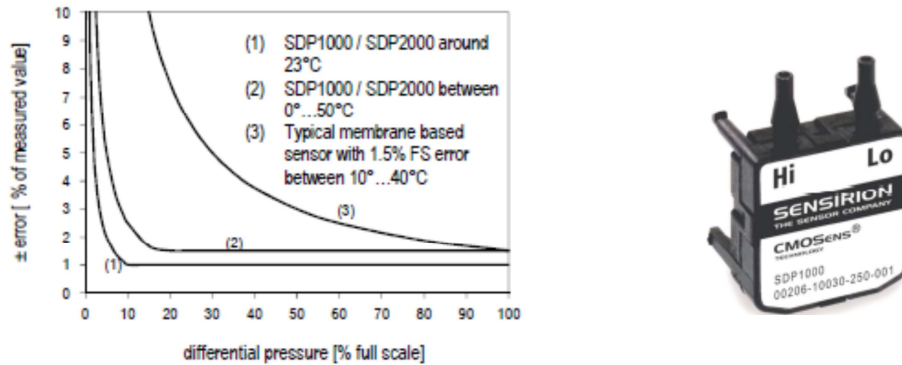
Figure 18: Accuracy (includes errors caused by offset, linearity, hysteresis and repeatability) of the "Sensirion" sensors

The delivered flow rate was measured for each side of the unit (with and without filter) and for several rotational speeds of the fan (see Section 3.2.).

3.1.2   Determination of hydraulic curve of the unit

The same experimental apparatus as the one described in the previous section is used to determine the total pressure drop associated with a specific volumetric flow rate passing through the unit. The unit fans are switched off while only the balancing fan is operating. The balancing fan is able to ensure the flow rate delivered by the unit fans at a given rotational speed.

By measuring the pressure drop between the atmosphere and the pressure compensated box, it is possible to determine the total pressure drop associated with a given rotational speed of the unit fan by delivering the same flow rate, as previously established in section 3.1.1. This was realized for flow rates associated to five rotational speeds for the fresh and indoor sides of the unit.

3.1.3   Determination of fan curve

Once again, the same experimental apparatus as the one used to determine the delivered flow rate has been used to determine fan curves (total pressure versus volume flow rate). Fan rotational speed can be modified by means of an electronic control integrated in the device. Since the fan manufacturer only indicates the fan curve for the nominal rotational speed, it has been decided to determine the curves for several other rotational speeds. The developed experimental apparatus is shown in Figure V-19. For a given rotational speed, it is possible to modify the total differential pressure drop between the inlet and the outlet of the fan by means of the set of regulating valves and/or the rotational speed of the balancing fan. The same experimental apparatus as the one described in the previous section is used.
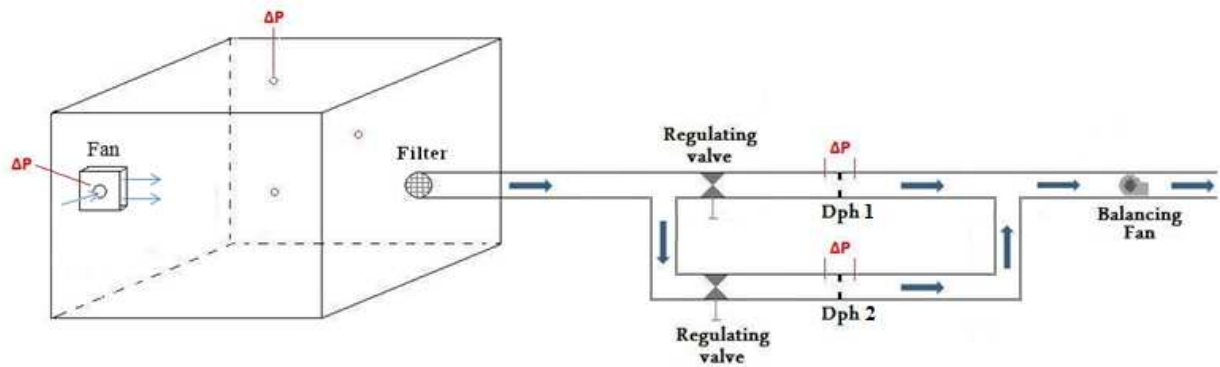
Figure V-19 : Determination of fan curve for several rotational speeds

The total pressure drop between the inlet and the outlet of the fan is given by the following equation:

$$\Delta P_{tot} = \Delta P_{stat} + \Delta P_{dyn} \ [Pa] \qquad \text{V-1}$$

The differential static pressure drop is measured by means of differential pressure drop sensor and the dynamical pressure drop is deduced, knowing the measured volumetric flow rate (orifice plates) and the cross sectional areas of the fan supply and exhaust ports.

3.1.4   Determination of filter curve

Determination of filter curve is realized by following the same experimental procedure as described in Section 3.1.2. Several filters have been tested: M5, F7 and G4. Filters are inserted in a plastic frame (dimension 0.195*0.175) as represented in Figure V-20:

Figure V-20: G4 filters

3.2   Experimental results

The aim of the current section is to present the performance of each single component of the unit.

3.2.1   Fan curves

Two fan curves have been established: one related to the indoor side and one related to the fresh side. In reality, the flow configuration at the exhaust of the fan volute for fresh and indoor air side induces differences in conversion efficiency.

| Indoor air side | Fresh air side |
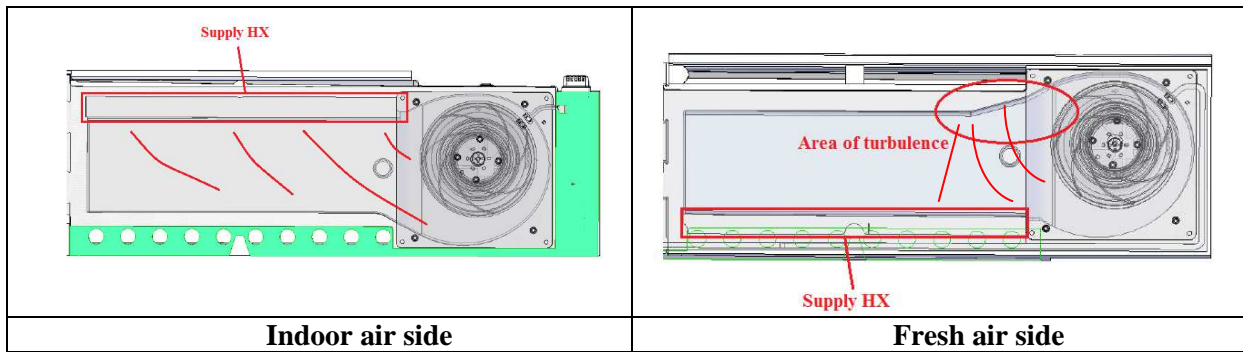
Figure V-21: Flow configuration at the exhaust of the fan for both sides

For the fresh air side, as observed in Figure V-21, the air flow at the outlet of the fan will first hit the side opposite to the inlet of the exchanger. This change of direction induces turbulence, recirculation and therefore a loss of conversion efficiency.

Concerning the exhaust air side, the conversion seems to be more efficient (flow is smoothly guided to the supply of the heat exchanger).

In order to experimentally observe the phenomena related to the change of direction of fresh air side at the exhaust of the volute, a plexiglas plate was placed upon the heat exchanger supply area. Moreover, in order to get a qualitative map of the air speeds and possible turbulence at the inlet of the heat exchanger, strings of Teflon were placed in the flow. Turbulence can be observed in the area of change of flow direction (the exhaust of the fresh air fan).

Figure V-22: Area of turbulence at the fresh air fan exhaust

As a result and in order to take into account this effect, two fan curves have been experimentally determined by inserting the fan in the "upper" and the "lower" parts of the unit (cfr. Figure V-21). The so called "upper" and "lower" parts of the unit are the parts of the unit between the fan exhaust and the heat exchanger supply respectively corresponding to the indoor and fresh air side. In this case, those parts are considered as an extension of the volute, inducing a difference in terms of energy conversion.

Figure V-23 gives the comparison between fan curves related to indoor and fresh air side for different rotational speeds:
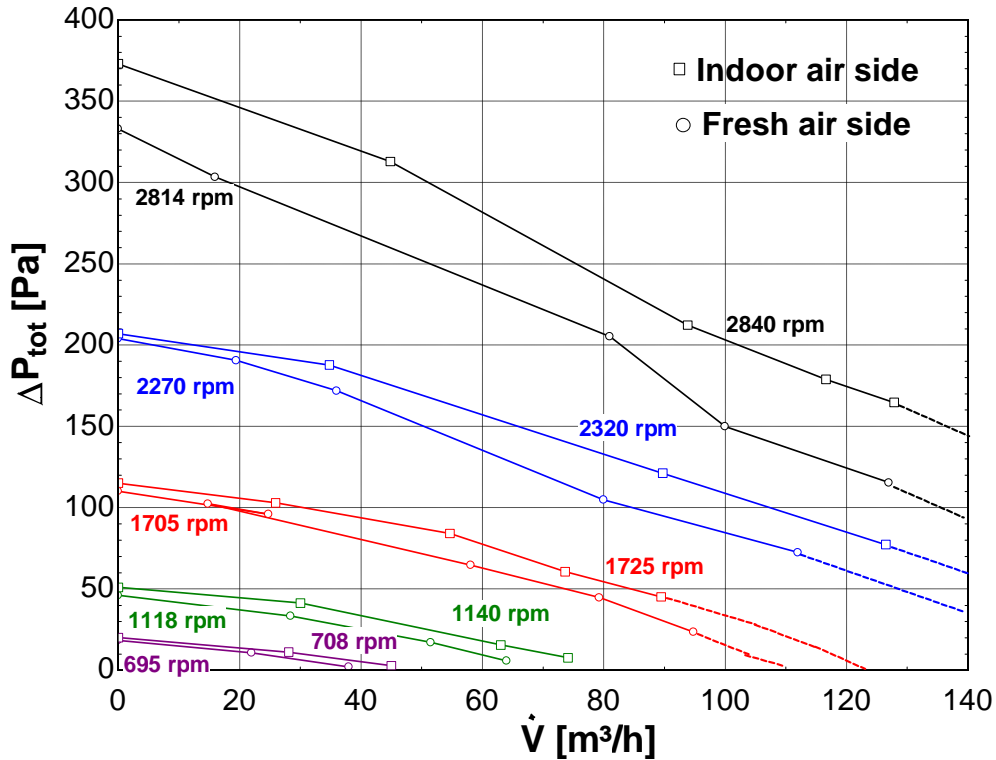
Figure V-23: Fan curves dedicated to indoor and fresh air sides

Experimental investigations have also been carried out in order to determine the variation of supplied electrical power delivered to the fans (without taking into account the current converter losses). Results are presented in Figure V-24 for the indoor air side fan. As can be observed, the supplied power remains almost constant for a given rotational speeds whatever the delivered flow rates.
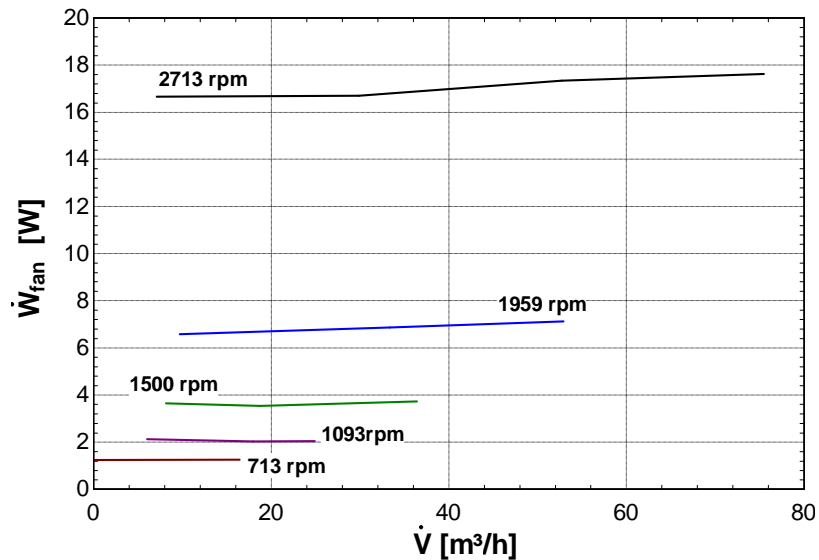
Figure V-24: Electrical consumption as a function of the delivered flow rates and the rotational speeds of the fan

3.2.2 Unit curves

The standard length of an active part corresponds to 1 m (which corresponds to a unit containing a heat exchanger with length of 0.45 m). However, during the development steps, units with several active parts lengths have been tested. Results are given for both sides in Figure V-25:
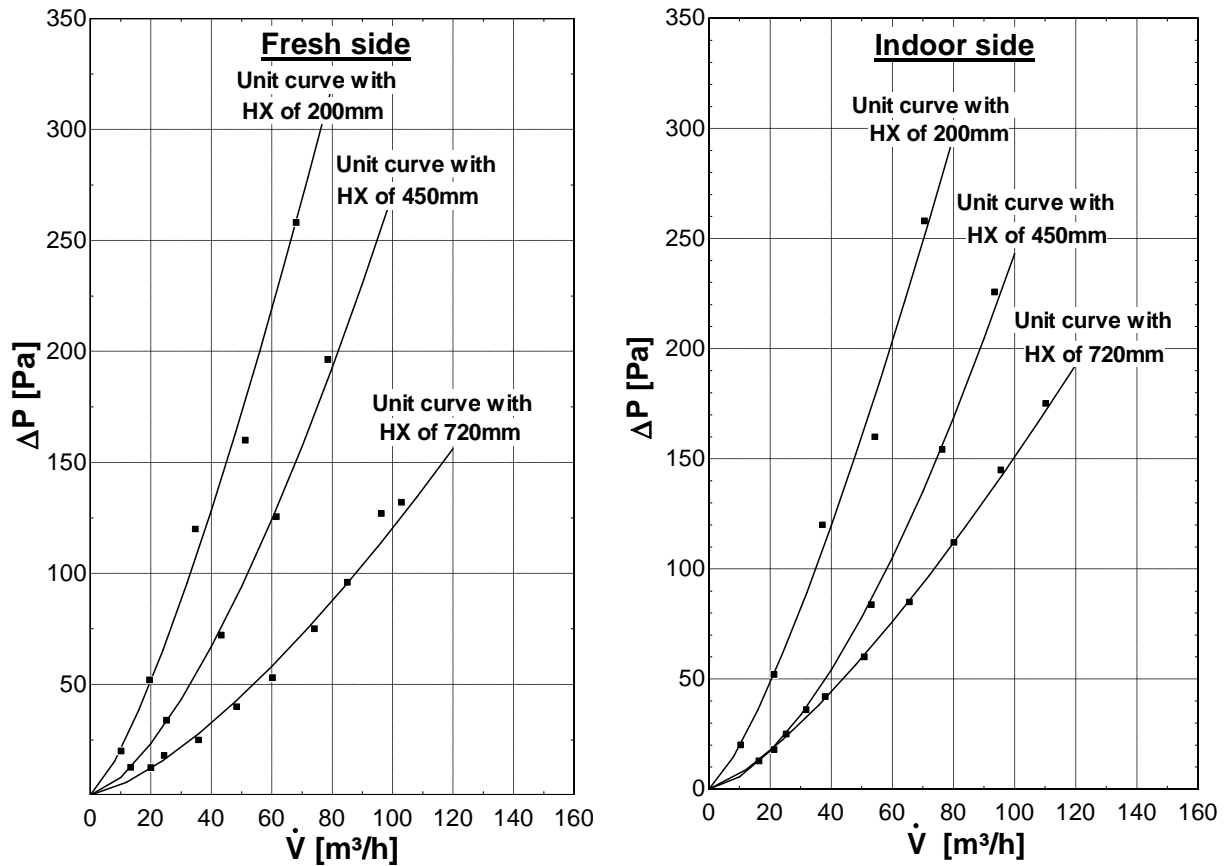
Figure V-25: Hydraulic curve of units presenting several dimensions of the heat exchanger (for both indoor and fresh air sides)

It is therefore experimentally confirmed that increasing the length of the heat exchanger will also increase the thermal and the hydraulic performance of the unit.

In the rest of the chapter, the presented experimental results only concern unit presenting active part of one meter long. That corresponds to the only available size on the market today. But the presented methodology can also be applied to other sizes of active parts of the unit.

3.2.3 Filters

As already specified, the unit can be equipped with several types of filters, depending on the use of the device. Each of them has been experimentally characterized. Hydraulic performance curves (as well as proposed correlations) are given Figure V-26:
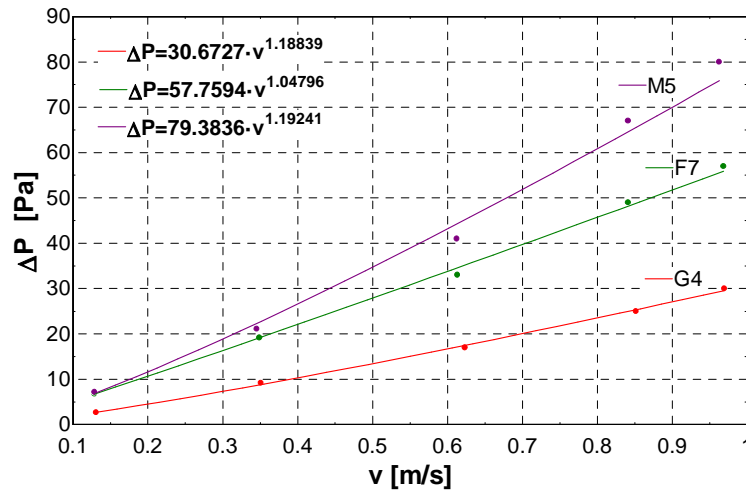
Figure V-26: Filters hydraulic curves

3.2.4 Unit and fan curves : experimental reconciliation

Knowing the hydraulic curve as well as the fan performance for both sides of the unit, it is now possible to experimentally reconcile the curves of the unit. Results are given for both sides of the unit in Figure V-27. As it can be observed, five couples of delivered flow rate and pressure drop related to specific rotational speeds have been experimentally determined for each side of the unit (white circles or squares in Figure V-27). The imposed rotational speeds correspond to the rotational speeds of the five fan curves.

Experimental reconciliation has been judged satisfactory given the assumptions made on the dynamic pressure drop at the exhaust of the fan (determination of a mean average velocity determined by knowing the delivered flow rate and the exhaust surface area).
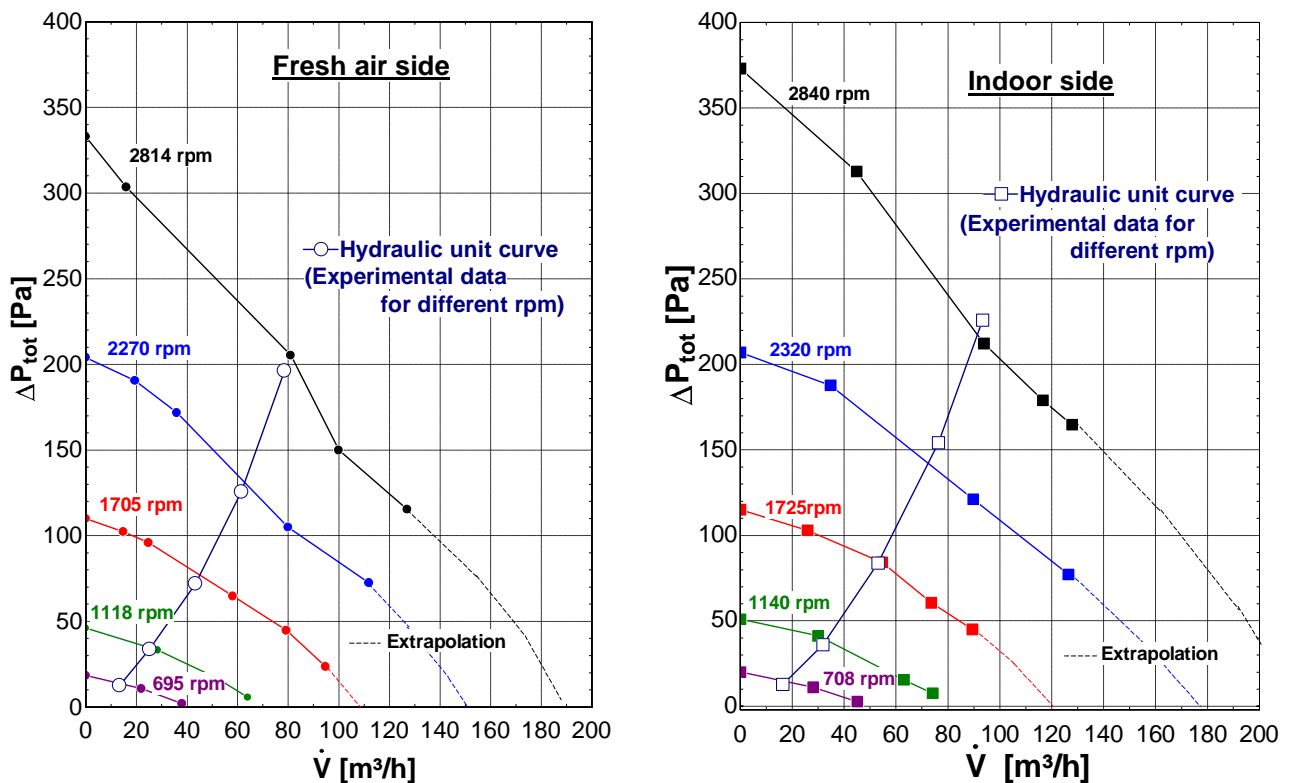
Figure V-27: Fan curves and hydraulic curve of the unit for both sides (experimental reconciliation)

3.2.5 Experimental analysis

It is also possible to represent the contributions of each single component as well as the total pressure drop curve of the unit. This is represented in Figure V-28 for both sides of the unit.
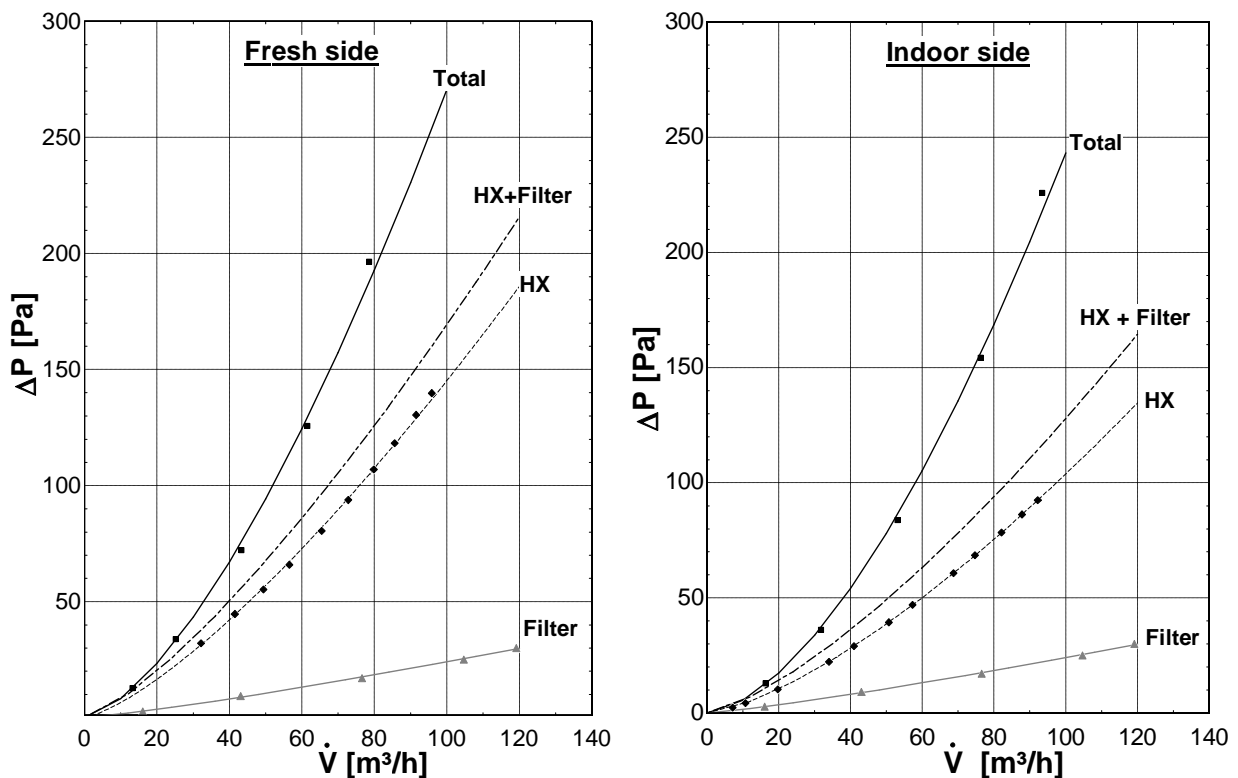
Figure V-28: Filters hydraulic curves for fresh and indoor side of the unit

As it can be observed, the unit is not symmetric concerning the hydraulic performance. The hydraulic curve of the indoor air side seems to present less pressure drop for a given volumetric flow rate (and thus to present a better efficiency). In addition with the fact that the fresh air fan curve is less efficient, one can notice a high difference in terms of maximum delivered flow rate for the fresh air side compared with the indoor side. It can be deduced different delivered flow rates related to several fan rotational speeds (see squares in Figure V-28). As an example, the maximal delivered flow rates for the indoor and fresh air side are respectively 78 m³/h and 93 m³/h (cfr. Figure V-28).

One can also notice that the contributions of the supply/exhaust passages is not negligible compared to the contribution of the heat exchanger and the filter. As an example, for the indoor air side, it accounts for approximately half of the pressure drop for a given flow rate. This is mainly due to the flow configuration inside the unit and the design of the active part of the unit. It seems difficult to reduce this contribution given the placement and the space dedicated to the unit. However, it could certainly be reduced if considering a wall mounted device.

As already proposed in Chapter 3, one can divide the pressure drop related to heat exchanger and the pressure drop related to the rest of the installation. This latter represents the contribution to filter, supply and exhaust parts of the unit (also called "out of heat exchanger" contribution).

The contribution of the rest of installation (Su/Ex + Filter) can be easily deduced knowing the total pressure drop and the pressure drop related to the heat exchanger. The contribution of the rest of installation (equipped with G4 filter) is shown in Figure V-29:
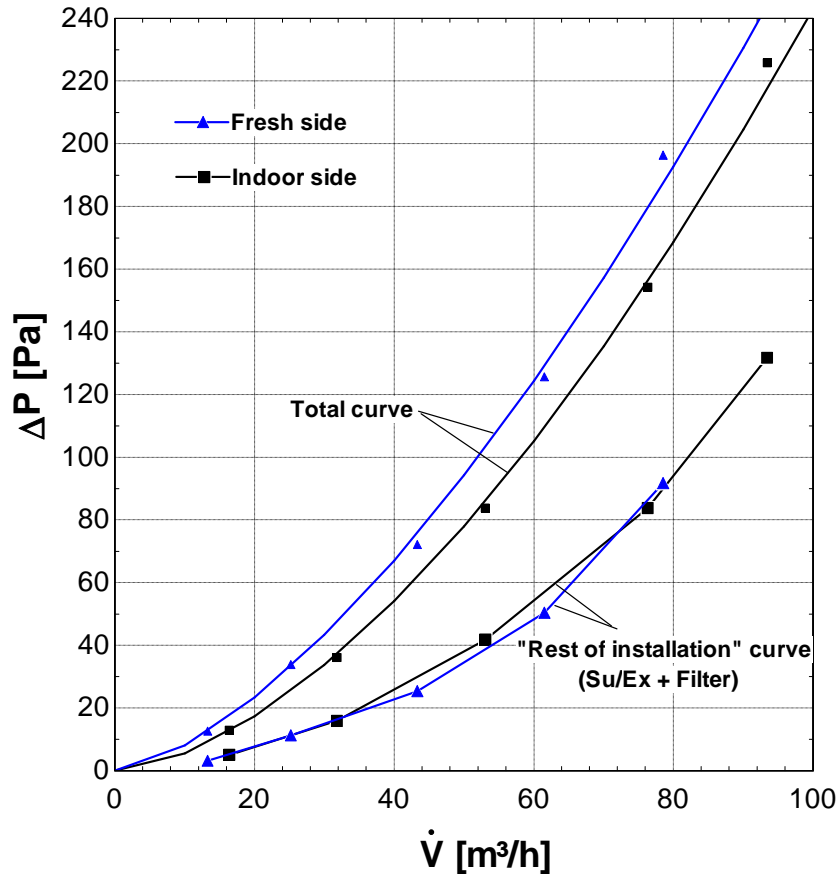
Figure V-29: Total hydraulic curve for both sides of the unit as well as the rest of installation curve (pressure drop not including the heat exchanger)

As shown in Figure V-29, the "rest of installation" curve seems to be similar for both sides of the unit. Since the filters are the same for both sides of the units, it can also be deduced that the supply/exhaust contributions are the same. The only difference in terms of total hydraulic curve for both sides of the unit comes from the dissymmetry of the heat exchanger (see experimental investigations carried out in the frame of the Chapter 3).

Note: The rest of installation curve presented in Figure V-29 have been used for the COP optimization process in Chapter 3.

Applied improvements

As previously observed, two things can explain the dissymmetry in terms of delivered flow rates for a given rpm between both parts of the unit:

- Fresh air fan efficiency is lower than indoor fan efficiency due to its position;
- The pressure drop related to a specific flow rate is higher (total hydraulic fan curve presents poorer performance).

As a result, the fresh air side is two times penalized. In order to better balance the hydraulic performance of the unit as well as to reduce the power delivered to the unit, a small modification of the active part of the unit allowed to inverse the heat exchanger. Therefore, this change implies the modification represented in Figure V-30:
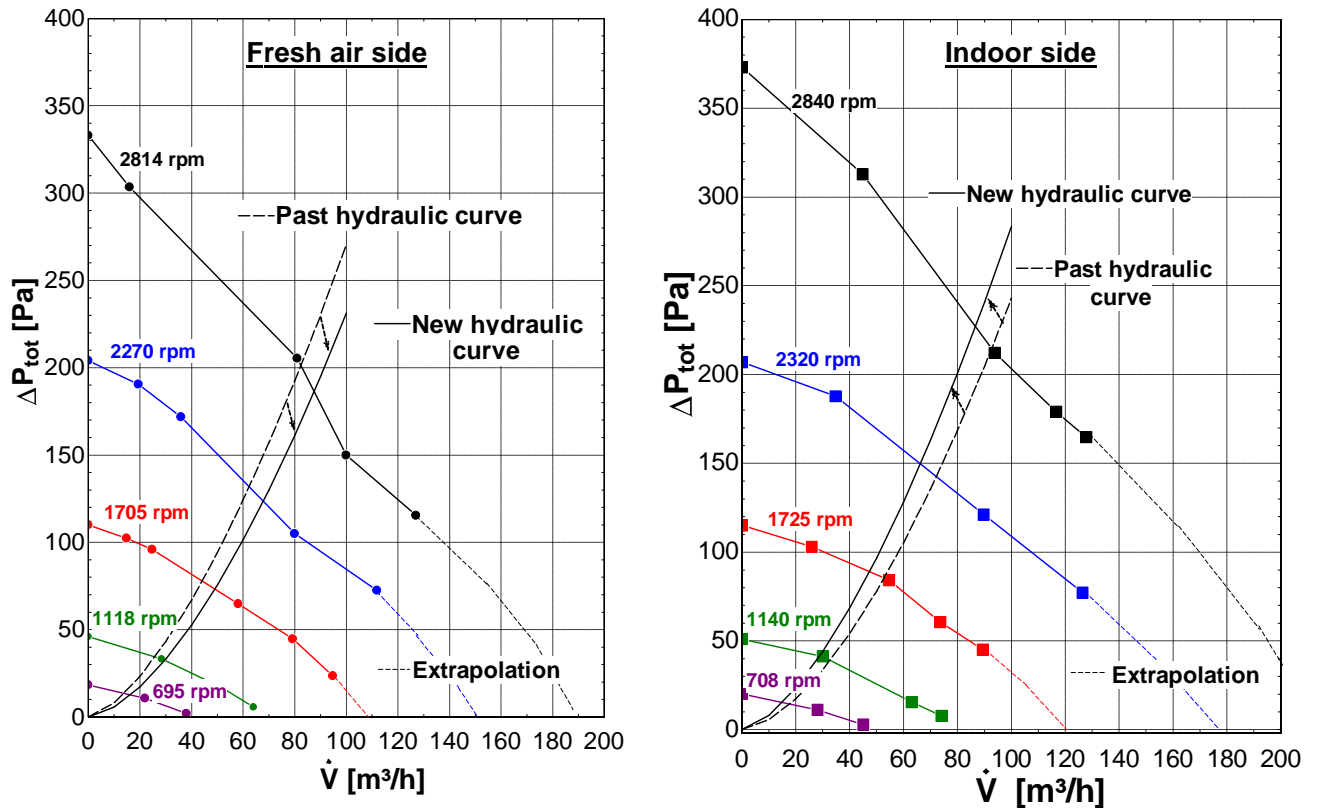
Figure V-30: Fan curves and hydraulic curve of the unit for both sides (experimental reconciliation)

Now, the best hydraulic curve is coupled with the worst fan curve. Experimental investigations have been carried out on the unit with this new configuration. Experimental results perfectly fit the envisioned predictions.

Please note that the experimental results presented in the rest of the chapter are related to this configuration.

Suggested improvements

It is clear that the fresh air fan position induces a loss of conversion efficiency due to a rough direction change at the exhaust of the fresh fan. This induces non-symmetry in fan performance between indoor and fresh air side. This could be corrected by developing a new mold of the active parts of the unit in order to avoid this phenomenon. This would permit the possibility to raise the hydraulic performance of the unit and thus at the same time, the acoustic performance of the unit. This amelioration will likely be applied for the second generation of the device.

3.3   Calibration to well-balance the delivered flow rates

As already specified in the frame of Chapter 1, one of the main advantages of this type of unit is the opportunity to well balance the fresh and indoor flow rates during the development phase (and not on site, as required for centralized systems). An electronic control board (ECB) is used for this purpose. The electrical diagram of the unit is given in Figure V-31:
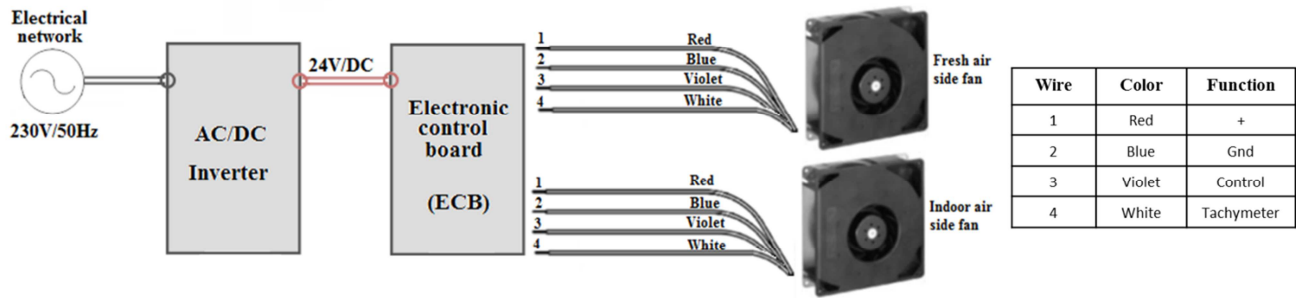
Figure V-31: Electrical schema of the unit

The ECB allows the user/designer to set a specific flow rate via the rotational speed of the ventilator. A function of the type " $\dot{V} = a*rpm^2 + b*rpm + c$ " needs to be implemented into the ECB. Thus, thanks to this function, the ECB impose the ventilator velocity in order to reach the requested flow rate. The imposed velocity depends on the voltage delivered by the ECB to the fans by means of the control wire (see Figure V-31). The parameters a, b and c were determined based on the experimental characterization. The interpolation curve for the indoor air side is given in Figure V-32:
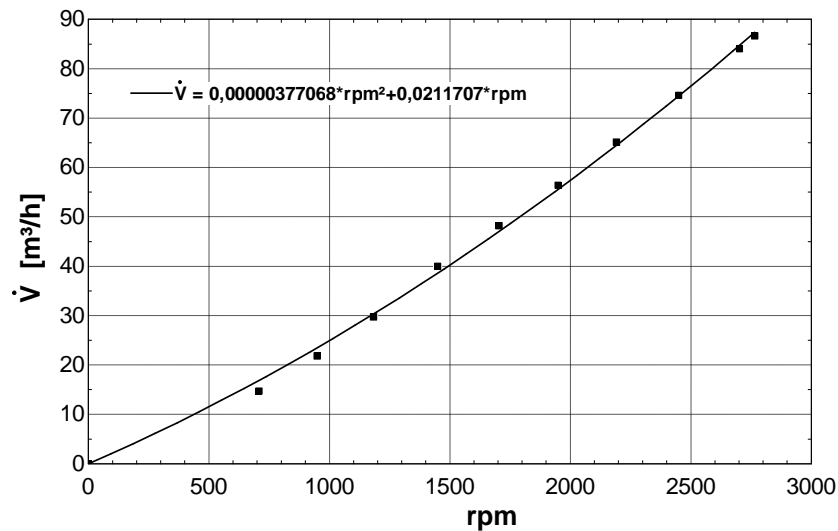
Figure V-32: Interpolation curve (flow rate as a function of rpm) for indoor side

Once the parameters are implemented, the ECB can deliver 5 different flow rates that need to be specified. That corresponds to the five levels of delivered flow rates by the unit (see section 2.7). Thanks to the tachometer (the white wire), the ECB adapts constantly the fan rotational speed. Thus, each 10 second, it slightly increases or decreases the delivered voltage on the (violet) instruction wire in order to reach the appropriate speed. Once the ECB has been programed, tests have been carried out in order to check out the reliability of the ECB.

4   ACOUSTIC PERFORMANCE OF THE FINAL UNIT

Acoustic performance determination was realized by the CEDIA Laboratory of the University of Liège. Only the main outlines of acoustic investigations are given in this section.

The acoustic performance of the unit can be divided in two parts:

- The acoustic insulation of the device;
- The sound level produced by the unit. Measurements have been realized for each flow rates delivered by the unit.

4.1 Acoustic insulation

The sound insulation of the prototype was tested. For that purpose, the prototype has been placed in a double wall composed of MDF and chipboard between two reverberation chambers of the laboratory. Picture of the practical achievements are given in Figure V-33:

Figure V-33: Acoustic insulation measurement

After measurement in the different frequency bands of 1/3 octave, sound attenuation is expressed as the D_{ne} index applicable to the measurement of sound insulation of small elements according to ISO 717. Values C and C_{tr} are the adaptation terms respectively for pink noise and road noise.

The D_{ne} index is the equivalent of a perfectly insulated wall of 10 m² including a small component. In this case the perfect double partition wall (which is more insulated than the prototype) and the construction element is the prototype itself.

The measured value is **D_{ne} (C, C_{tr}) = 42 (-1, -3)**.

4.2 Generated Sound level

Once again, the system has been inserted in a double wall composed of MDF and chipboard, as represented in Figure V-34:

Figure V-34: Generated sound level measurement

Measurements were carried out for each of the delivered flow rates by the unit (15, 25, 36, 50 and 75 m³/h). An "acoustic" version of the device has also been developed. This modification consists of making the passive part deeper (310 mm instead of 266mm) and to fill up the additional space with acoustically insulating material (INM1 absorbent). This latter does not show significant improvement of the overall acoustic performance of the unit. This is mainly explained by the low space dedicated to acoustic insulation. That means that the only way to make the unit quieter is to improve the hydraulic performance and/or to improve acoustic fan performance. Results are given in Table V-1, for each of the delivered flow rates.

Table V-1: Generated sound level

Flow rate	15 m³/h	25 m³/h	36 m³/h	50 m³/h	75 m³/h
Standard system	28.3 dB	33.4 dB	40.1 dB	47.3 dB	54.3 dB
Acoustic system	26.8 dB	33.2 dB	40.0 dB	46.9 dB	53.0 dB

As expected, it can be seen that the generated sound level is the main weakness of the unit. Except for the low flow rates (15 and 25 m³/h), the device does not meet the requirements in terms of generated sound level, according to NBN S01-400-1 and the WHO (see values given in Table I-3).

5   PERFORMANCE MAP OF THE FINAL UNIT

In order to take into account the conduction effects in the unit and an eventual degradation of thermal performance due to a misdistribution of the flow rate through the heat exchanger, the best way to determine the overall performance of the final device is to test it into a climatic chamber, as schematically shown in Figure V-35. This procedure is supposed to represent the nominal operating conditions of the unit.

5.1   Experimental apparatus

The idea is to place the unit in a wall separating an outdoor and an indoor room of a climatic chamber. Flow rate delivered by each side of the unit are measured by the pressure compensated box method (Lebrun and Hannay, 1972). The mean outlet temperature of each side of the device is determined by means of five thermocouples T (placed as mentioned by NBN 308) situated at the exhaust of the pressure-compensated box. Concerning the mean inlet temperature measurement, five thermocouples have been placed on both filters.
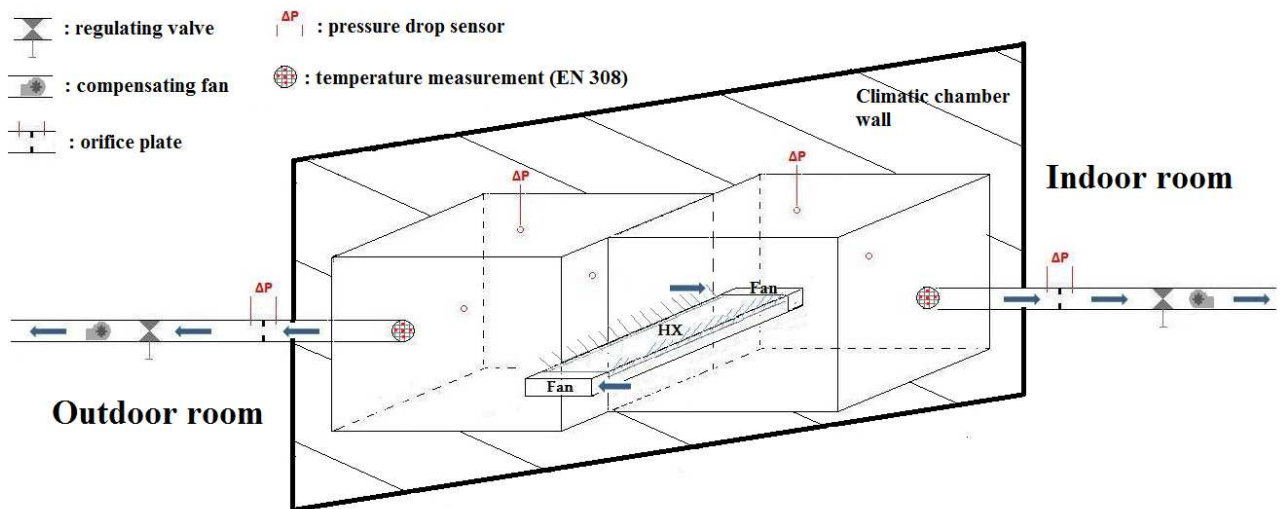
Figure V-35: Schematic representation of the experimental apparatus dedicated to the thermal performance of the entire unit

Since the supply and the exhaust ports of the unit consists of slits, it is important to mention that ensuring the air tightness between the unit and the experimental apparatus takes a large amount of time. That is the reason why this experimental apparatus is not suitable for the design step of the device but only for the overall performance of the final version of the device (once the device is considered as "optimized" by the manufacturer).

Test bench developed in the climatic chamber of the Thermodynamics Laboratory of the University of Liège is given in Figure V-36:
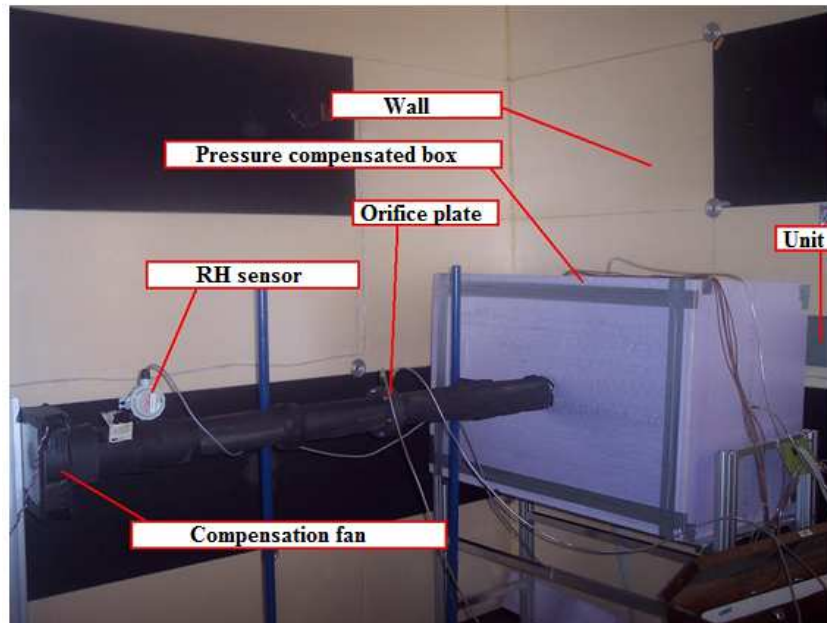
Figure V-36: Climatic chamber test (Outdoor side)

5.2 Supplied electrical power

The COP of the system is directly deduced by measuring the supply electrical power delivered to the unit. As shown in Figure V-37, three types of electrical measurements have been realized:

- Power supplied to the unit (P_1);
- Power supplied to the electronic control board (P_2);
- Power supplied to the fans (P_3).
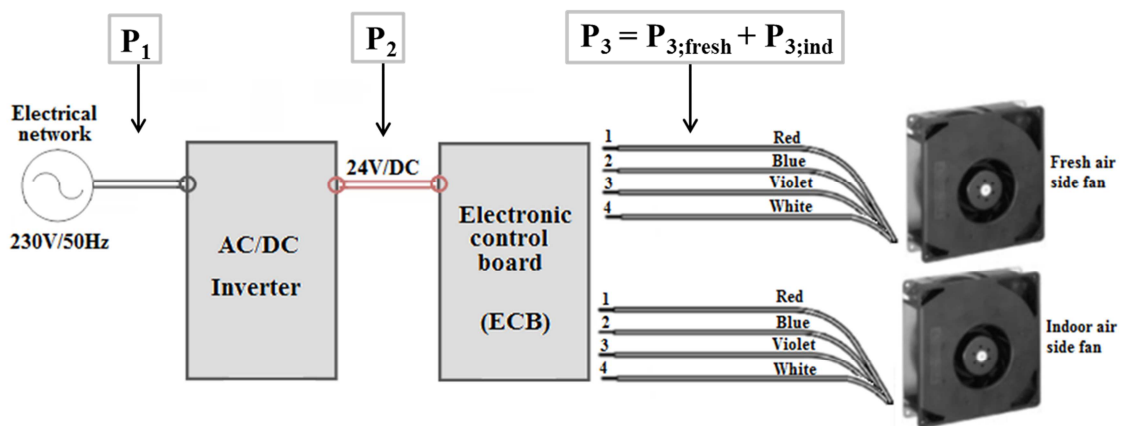
Figure V-37: Electrical power measurement

The AC electrical power supplied to the unit has been measured by an alternative current analyzer (Voltech analyzer 1000 PM), as the one given in Figure V-38. Concerning the power supplied (DC current) to the ECB and the fans, two voltmeters have been used: one dedicated to the current measurement and one dedicated to the voltage measurement.
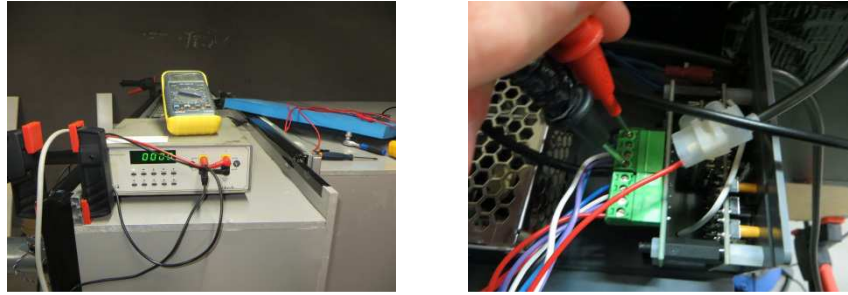
Figure V-38: Electrical power measurement: AC (left) and DC (right)

A summary of the supplied electrical power measurement is given in Table V-2:

Table V-2: Supplied power to the unit for different delivered flow rates levels

Level	Flow rate (m³/h)	P_1 (W)	P_2 (W)	$P_{3;ind}$ (W)	$P_{3;fresh}$ (W)	$P_{3;total}$ (W)	Losses 1 to 2 (W)	Losses 2 to 3 (W)	Losses 1 to 3 (W)
5	75	38.4	32.89	17.52	14.67	32.19	5.51	0.7	6.21
4	50	17.77	15.08	7.92	6.33	14.25	2.69	0.83	3.52
3	36	10.05	8.43	4.13	3.32	7.45	1.62	0.98	2.6
2	25	6.54	5.13	2.26	1.85	4.11	1.41	1.02	2.43
1	15	4.84	3.66	1.36	1.33	2.69	1.18	0.97	2.15

Specific Fan Power can be deduced from Table V-2 for each measurement points specified in Figure V-37. They are summarized in Table V-3:

Table V-3: Specific Fan Power

Level	Flow rate (m³/h)	$P_{1;norm}$ (W/m³-h)	$P_{2;norm}$ (W/m³-h)	$P_{3;ind;norm}$ (W/m³-h)	$P_{3;fresh;norm}$ (W/m³-h)	$P_{3;tot;norm}$ (W/m³-h)
5	75	0.256	0.219	0.234	0.196	0.215
4	50	0.177	0.151	0.158	0.127	0.1425
3	36	0.139	0.117	0.115	0.092	0.103
2	25	0.131	0.102	0.09	0.074	0.082
1	15	0.161	0.122	0.091	0.089	0.09

The European standard EN 13779 specifies SFP 3–4, 0.21–0.55 W/m³-h per fan, as default values for heat recovery systems and SFP 2, 0.14–0.21 W/m³-h, for simple exhaust systems. The Belgian organization for building technics CSTC (2013) recommends to reduce the fan consumption to SFP2 (0.21 W/m³-h) for system D. In Germany, the Passive Haus Institut (2009) fixed the upper limit of the operational range to 0.45 W/m³-h for transported air flow as a requirement for passive house ventilation.

Fan performance seems to fulfill the requirements given here-below (even by taking into account the current converter losses) and shows excellent performance (SFP 1) for levels 2 and 3.

5.3 Thermal performance

The mean average effectiveness (determined of each side) has been determined for the 5 different flow rates on the whole device in climatic chamber. The balance of measured heat transfer rate is within 5% for each test point.

The thermal performance measured in the climatic chamber does not show significant differences compared with thermal performance determined on the heat exchanger alone (see Chapter III). Differences in terms of effectiveness are less than 1.8% for each of the measured performance point. That means that the flow rate is well distributed along the heat exchanger.

5.4 Performance map determination

As defined in Chapter 3, the overall performance of the unit can be defined by the ratio of the recovered heat transfer rate to the electrical power of the fans. A performance map can be drawn, depending on the delivered flow rate by the unit and the indoor/outdoor temperature difference, as shown in Figure V-39. This performance map could be coupled to a building model in order to determine the seasonal performance of the unit.

As seen in Section 4, sound pressure levels have been determined on the inner side of the unit. In order to have a complete performance map of the device (thermal, hydraulic and acoustic), the level of generated noise related to a specific flow rate is also indicated, as well as the acoustic insulation level.
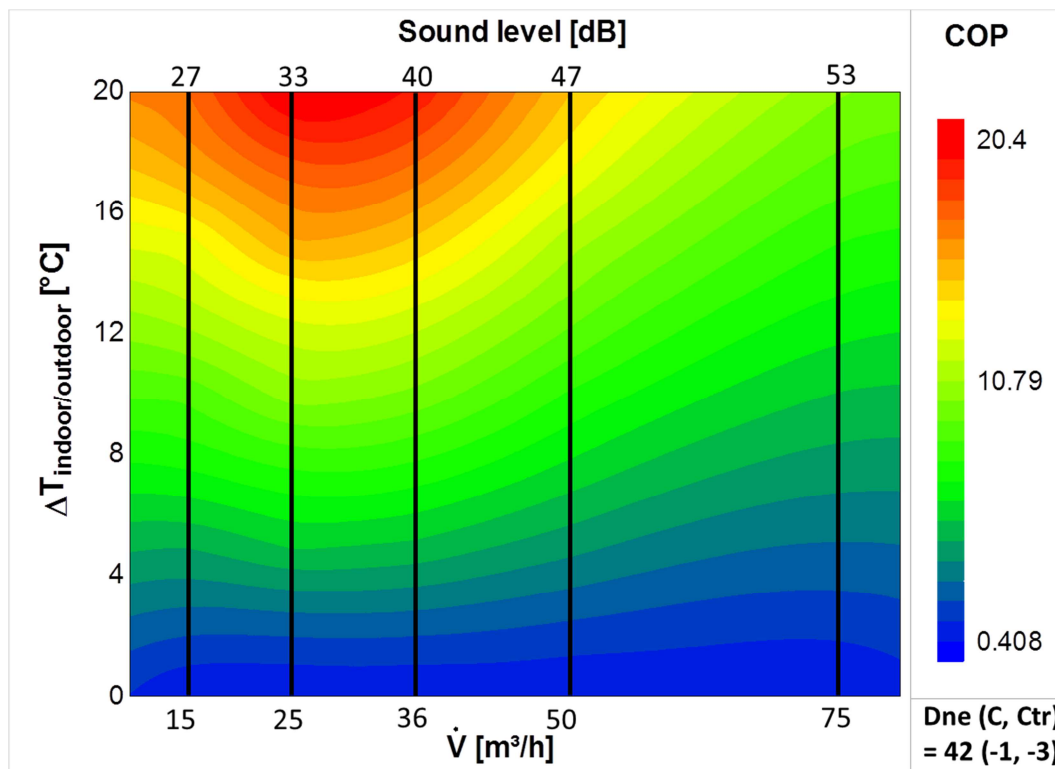
Figure V-39 : COP [-] vs flow rate in [m3/h] and difference indoor/outdoor temperature in [°C] (Performance Map of the unit by considering the AC/DC current converter losses)

In Figure V-40, the performance of the unit by taking the power delivered only to the supply and exhaust fans (in others terms by neglecting the AC/DC current converter losses) is presented. Once

again, sound level is also indicated on the performance map in order to represent the overall performance of the device:
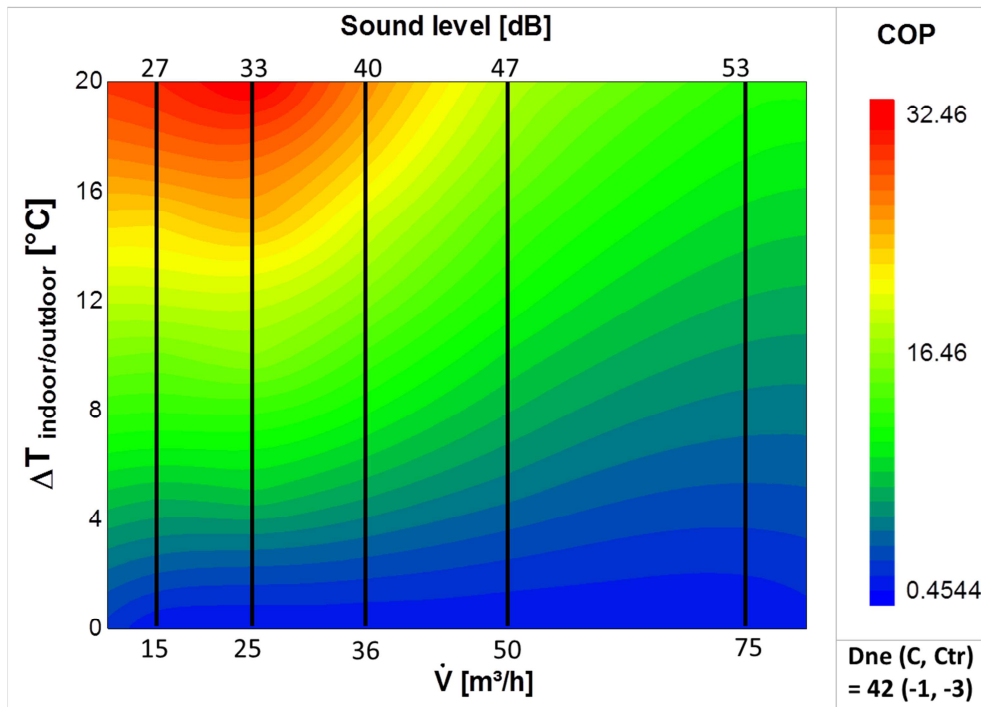
Figure V-40 : COP [-] vs flow rate in [m3/h] and difference indoor/outdoor temperature in [°C] (Performance Map of the unit by neglecting the AC/DC current converter losses)

In order to better observe the impact of the losses due to the AC/DC current converter, it has been decided to show the COP evolution as a function of the flow rates for an outdoor temperature of 8.5°C and an indoor temperature of 20°C, as represented in Figure V-41.
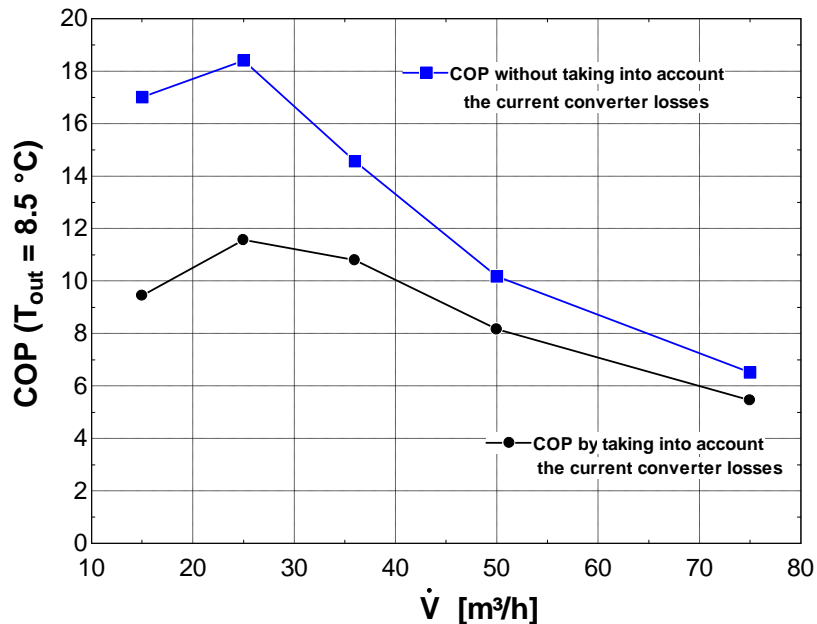
Figure V-41: Comparison of the COP of the device by taking into account or neglecting the AC/DC current converter losses

Figure V-41 highlights one of the most important findings of the current chapter. As seen in previous chapters (geometry optimization), many efforts have been realized during the development steps of the device to optimize the heat exchanger considered as the *"key"* component of Single Room Ventilation with Heat Recovery. However, it is clearly shown that, in the case of the presented developed device, the AC/DC inverter (and the electronic control for low flow rates) highly impacts the coefficient of performance, especially for low delivered flow rates (ECB losses are approximately constant and therefore impact more on small delivered electrical power).

The measured value of COP is higher than the value of COP obtained during the optimization process in Chapter 3. This is easily explained by the fact that the current converter losses have been taken into account for each fan during the optimization process (so the total current converter losses have been multiplied per two compared to the final device). Moreover, the worst fan curve has been used for the optimization process. Only the value of the maximal COP changes but not the results of the optimization process, as already demonstrated by the parametric studies.

6 HEATING DEGREE DAY METHOD

As shown in the previous section, the energy saved by the investigated device is highly dependent on the climate and more precisely on the indoor/outdoor temperature difference. The aim of the present section is to assess the overall performance of the unit given a specific climate.

Many authors use a heating degree days (HDD) method to determine the potential of use of heat recovery system in a given climate. For example, Adamski (2010) used it to estimate the financial effects of a ventilation system with a spiral recuperator in Poland. Kristler and Cussler (2002) combined the heating degree days and the absolute humidity days to define a cost effectiveness ratio (division of the actual energy cost savings of the investigated device by these energy costs) to optimize the performance of their membrane heat exchanger. More recently, Laverge and Janssens (2012) used the Heating Degree Day method to evaluate the advantage of natural, simple exhaust mechanical ventilation and heat recovery ventilation over each other for European countries. In the frame of this thesis, the method is applied for mean average values for Europe and Belgium which can be considered as a typical moderate European climate.

The total annual heat recovered in [J/year] by the investigated device can be determined by integrating Equation V-2 over one typical year:

$$Q_{recovered} = \int \dot{V}(t) . \rho(t) . cp(t) . \varepsilon\left(\dot{V}\right) . \Delta T\left(t\right)\, dt \qquad \text{V-2}$$

The total electrical energy delivered to the unit over one year in [J/year] can be determined by Equation V-3:

$$E_{el} = \int [\, \dot{W}_{fan,fresh}(\dot{V}) + \dot{W}_{fan,indoor}(\dot{V})\,]\, dt \qquad \text{V-3}$$

Equations V-2 and V-3 are quite difficult to evaluate since the flow rate delivered by the unit and hence the effectiveness and the electrical fan consumption vary with time and is dependent on many factors: type of ventilation control, type of room where is placed the unit, user's behavior,… In the frame of this study, it has been decided to make some assumptions to solve them.

Used assumptions are the same than the one used by Laverge and Janssens (2012):

- The ventilation system is considered to permanently run all along the year,

- The specific heat capacity c_p [J/kg-K] and the air density ρ [kg/m³] are considered constant all year long and their product is equal to 1224 [J/m³-K],

- Integration of the indoor/outdoor temperature difference over a year can be realized through the use of the number of heating degree days HDD [K day]. According to Eurostat (2013), the heating degree for a given day is equal to the difference between 18°C and the mean outdoor temperature but only if this average daily outdoor temperature is inferior to 15°C. On the contrary, it is assumed equal to zero. The mean outdoor temperature is defined as the mathematical average of the minimum to the maximum temperature of that given day.

- Values used in the frame of this study for Europe and Belgium come from Eurostat (2013) and corresponds to the mean heating degree days over the period 1980-2004. They are respectively for Europe and Belgium equals to 3253 and 2872 [K day], effectiveness of the system is considered constant all year long.

By using the enounced assumptions and by normalizing Equation V-2 and V-3, one can determine the total annual heat recovered per m³/h $q_{recovered}$ in [Jh/m³-year] and the annual electrical energy delivered to the unit per m³/h for both fans e_{el} in [Jh/m³-year]:

$$q_{recovered} = 24.1224 . HDD.\varepsilon \qquad \text{V-4}$$

$$e_{el} = 24.365 . SFP \qquad \text{V-5}$$

with SFP, the specific fans power in [J/m³] and ε, the effectiveness of the heat exchanger [-]. In order to take into account some potential variation of the ventilation flow rate, the value used for the SFP of the unit and the effectiveness of the unit in Equations V-4 and V-5 corresponds to the mean average value related to five rotational speeds covering the flow rate range of the unit. The average effectiveness is equal to 0.748 and the total SFP for both fans is equal to 1246 [J/m³].

The device can be evaluated by means of three performance parameters: CO_2 emissions, primary energy and energy costs of the device. Hence, the competitiveness of the heat recovery device is demonstrated if the dimensionless number Ω, defined in Equation V-6, is superior to one for each of the investigated performance parameters:

$$\Omega = \frac{q_{recovered} \cdot f_{fuel}}{e_{el} \cdot f_{el}} = \frac{q_{recovered}}{e_{el} \cdot f} > 1 \qquad \text{V-6}$$

with f_{fuel} and f_{el}, the traditional conversion factors for the space heating fuel and electricity. It is assumed that the equivalent of the recovered heat is generated with a 100% efficient natural gas combustion. f is the conversion factor for 1J of electricity to 1J of gas fired heating for CO_2 emissions, primary energy and energy costs. Values used for f in the frame of the study for Europe (UE) and Belgium (BE) are listed in Table V-4:

Table V-4 : Used value for conversion factor for Europe and Belgium

Conversion factors	Values		References	
	UE	BE	UE	BE
CO2	1.72	1.16	Laverge and Janssens (2012)	Stabat (2009)
Primary energy	2.74	2.5		Walloon EPB decree (2008)
Energy costs	2.8	2.9		Eurostat (2013)

Numerical values for Ω_{SRVHR}, determined from Equation V-6, for CO2, primary energy and household consumer prices are resumed in Table V-5. Ω_{SRVHR} is higher than one for the UE as well as for Belgium. As a result, the investigated device seems to be competitive from an environmental and economic point of view.

It is also possible to use the method to determine the minimal HDD from which the device is competitive given several values of conversion factor. For Belgium, the most restrictive conversion factor concerns the energy costs (with $\Omega_{SRVHR} = 2$). By taking this latter, the minimal HDD from which

the device is competitive is 1450 [K day]. That corresponds to HDD of a low energy building in Belgium.

Table V-5 : Ω_{SRVHR} values

	Ω_{SRVHR}	
	UE	*BE*
CO2	4.3	5
Primary energy	2.7	2.3
Energy costs	2.3	2

6.1 Comparison with other ventilation systems

In the present section, the device is compared with three other ventilation systems: natural, simple exhaust and "traditional" centralized heat recovery ventilation. Given results in Table V-5, it is clear that the system is more efficient than natural ventilation since Ω_{SRVHR} is higher than one for each investigated case as well for Belgium as for Europe. The investigated system is even more competitive compared to the simple exhaust ventilation since the latter involves a supplementary electrical consumption related to exhaust fans compared to natural ventilation.

The comparison with traditional centralized heat recovery ventilation appears to be more complicated since the SFP of traditional centralized system is highly dependent on the used fan and on the hydraulic characteristics of ducts. According to the European standard EN 13779 (2007), Laverge and Janssens (2012) propose to take the boundary between SFP 3 and SFP 4 (1250 [J/m^3] per fan), as reference for heat recovery system.

A centralized ventilation system with heat recovery is assumed to be as competitive as the investigated device if Ω_{CHRV} is at least equal to the determined Ω_{SRVHR}. In other terms, the minimum effectiveness for centralized systems required to be as competitive as the investigated device is given by Equation V-7:

$$\varepsilon_{min,CHRV} = \varepsilon_{SRVHR} \cdot \frac{SFP_{CHRV}}{SFP_{SRVHR}} \qquad \text{V-7}$$

So, if assuming a total SFP of 2500 [J/m^3] (1250 [J/m³] per fan) for a centralized heat recovery device, the required minimum effectiveness has to be equal to 1.5 [-], which is physically unrealistic.

It is very difficult to find information on the SFP of centralized heat recovery in scientific literature. Recently, Caillou (2012) presented in situ measurements of SFP for centralized heat recovery ventilation systems in residential buildings. To the best author's knowledge, this is the only study presenting such results. These latter are given in Figure V-42 for n=28 investigated houses:
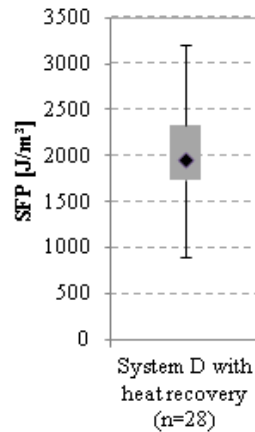
Figure V-42: Measurement of SFP in situ (Caillou (2012))

The required minimum effectiveness to be as competitive as the investigated single room ventilation is superior to unity (which is physically unrealistic) for 75% of the investigated systems (22 out of 28). By considering an average effectiveness equal to 0.9 for a centralized heat recovery exchanger, the investigated single room ventilation shows better performance for 82% of the investigated cases, as schematically represented in *Figure V-43*.

$$\Omega_{SRVHR} = \frac{24.\ 1224.HDD.\varepsilon_{SRVHR}}{24.\ 365.SFP_{SRVHR}} = \frac{24.\ 1224.HDD.\varepsilon_{CHRV}}{24.\ 365.SFP_{CHRV}} = \Omega_{CHRV}$$

75% 90 %

1246 [J/m³]   1495 [J/m³]

SRVHR > 82% of measured cases
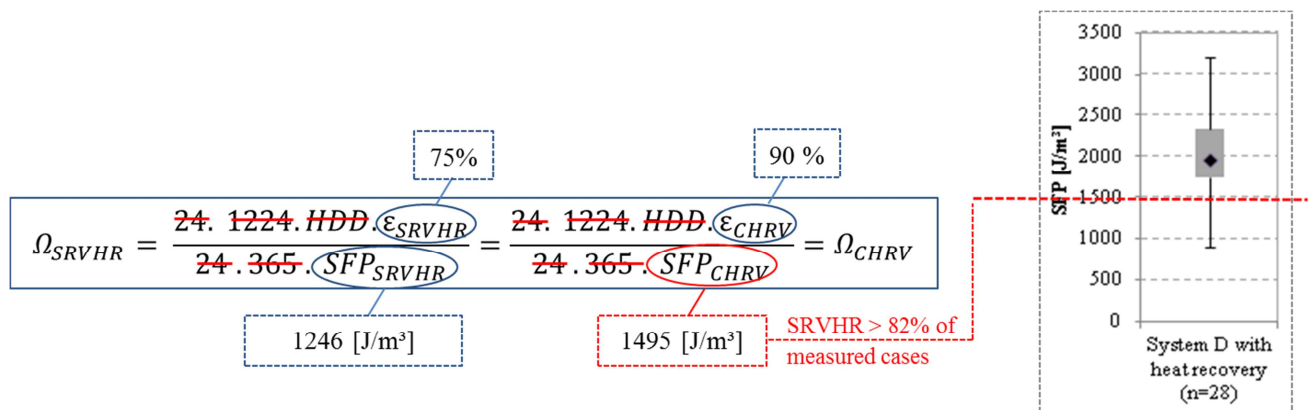
Figure V-43 : Performance comparison between CHRV and the final unit

To conclude, from an energetic point of view and compared to other systems tested on site, performance of the investigated device seems to be promising.

6.2 Discussion about the HDD method

The presented investigation was realized by using conservative conditions and by taking into account the electrical conversion losses: transformation from AC (230~) to DC (24V). These losses are not negligible compared to the electrical power delivered to the fans (especially for the low rotational speeds) and are entirely dependent on the current transformers used. In the determination of the SFP, these losses could be neglected if one assumes the presence of a DC domestic network, resulting from the use of photovoltaic panels for example.

By only taking a unique reference temperature, the method of the HDD is debatable since it doesn't take into account the thermal properties of the building, its air tightness characteristics, its occupancy, the solar and internal gains as well as the device operation/use. Moreover, definition itself of HDD (choice of the base temperature) leads to a lot of discussion.

However, despite its simplicity, the method allows pointing out some trends (at a national/regional level) and permits to compare different types of heat recovery balanced ventilation in a fair way (see Equation 6). This relationship could be particularly suitable for manufacturer to easily compare performances of two competitive products. Currently, the effectiveness of the heat exchanger seems to be the only parameters taken into account to compare systems between them.

Moreover, the method also allows determining a minimal HDD (defined as the relationship between climate and building characteristics) from which the device is competitive.

7 CONCLUSIONS

The current chapter presents the experimental investigations carried out in order to characterize the overall performance of the developed device.

During the development phase, hydraulic performance of each component (fan, filter, HX) has been determined separately. Results analysis allowed to better balance the hydraulic performance of each side of the unit by reversing the heat exchanger in the active part of the unit (see section 2).

Some suggested improvements can be presented in regards of the experimental results. The first one concerns the important impact of the AC/DC inverter losses (as well as the ECB for low flow rates) on the overall performance of the unit. In order to avoid them, a DC domestic network could be imagined. That could permit to reduce the AC/DC current converter losses because only one AC/DC current converter is required. Another solution could be to directly couple the unit to the domestic DC network or to photovoltaic panels.

Another improvement of the unit concerns the position of the fresh air fan. As seen in Section 3, its position is not optimized because of rough air change direction creating turbulence at the exhaust of the fan. A new mold of the active part could resolve this problem and improve the overall hydraulic performance of the unit.

The main drawback of the unit concerns its acoustic performance. Except for low flow rates (level 1 and 2), the unit does not meet the Belgian requirements. A deeper passive casing fill in with acoustic materials does not improve significantly the acoustic performance. Thus, the only ways to improve the acoustic performance of the unit is to choose a more silent fan or to increase (if it is possible) the length of the heat exchanger (and thus the length of the active part). This increase will greatly impact on the hydraulic performance as seen in Section 3.2.2.

However, despite these defaults, the specific fan power shows good performance especially for level 2 and 3 (SFP1). Moreover, the comparison between thermal performance measured on the whole unit and the heat exchanger alone allows for the confirmation that the flows are well distributed along the heat exchanger.

A method based on Heating Degree Day (HDD) has been used to determine the interest of use of the device given a specific climate. It has been shown that the device seems suitable for European and Belgian climate. Thanks to this method, it is also possible to compare the developed system with others ventilation systems. The system shows better performance than system A, B and C for European and Belgian climate. Performance of the system has also been compared to performance of systems D tested in situ. The system shows better performance than for 82% of the n=28 investigated houses.

8   REFERENCES

Adamski, M., 2010. *Ventilation system with spiral recuperator.* Energy and buildings 42, (2010), 674-677

Caillou, S., 2012. *Impact des systèmes de ventilation.* Séminaire bâtiment durable du 23 Novembre 2012. Améliorer et garantir la qualité de l'air intérieur. IBGE. Institut bruxellois pour la gestion de l'environnement. http://www.icedd.be/downloads/data/Semi_3_231112_livret_FR.pdf

CSTB. 2013. *Ventilation des bâtiments – La ventilation mécanique : les bouches, conduits, ventilateurs   et   groupes.* http://www.cstc.be/homepage/index.cfm?cat=publications&sub=infofiches&pag=42&art=8

EN 779. 2012. *New European Standard for General Ventilation Filters.* European standard.

EN 13779. 2007. *Ventilation des bâtiments non résidentiels – Exigences de performance pour les systèmes de ventilation et de conditionnement d'air.* European standard.

Eurostat, *Heating degree day by NUTS 2 regions- annual data. Mean heating degree-days over period 1980-2004.* http://epp.eurostat.ec.europa.eu/cache/ITY_OFFPUB/KS-SF-09-055/EN/KS-SF-09-055-EN.PDF

Hannay, J., Lebrun, J., 1972. *Méthode d'essais applicable aux ventilos convecteurs,* Thermique et aéraulique, Juin 1972.

ISO 5167. 1980. *Measurement of fluid flow by means of pressure differential devices inserted in circular cross-section conduits running full.* ISO Standard. First edition (1980)

ISO 717. 2013. *Acoustics - Ratings of sound insulation in buildings and of building elements.* ISO Standard. 2013.

Kistler K.R. and Cussler E.L., 2002. Membrane modules for building ventilation. Chem. Eng. Res. Des. 80, pp. 53–64.

Laverge and Janssens. 2012. *Heat recovery ventilation operation traded off against natural and simple exhaust ventilation in Europe by primary energy factor, carbon dioxide emission, household consumer price and exergy.* Energy and buildings. 50 (2012) 315-323

Manz. H., Huber, H., Schalin A., Weber, A., Ferrazzini M., Studer, M., 2000. *Performance characterization of single room ventilation unit with recuperative or regenerative heat recovery.* Energy and building 31 (2000) 37-47

NBN EN 308. 1997. Norme nationale belge. *Echangeurs thermiques – Procédures d'essai pour la détermination de la performance des récupérateurs de chaleur air/air et air/gaz.* Mars 1997

Passiv Haus Institut. 2009. Requirements and testing procedures for energetic and acoustical assessment of passive house ventilation systems for certification as "Passive house suitable component" www.passiv.de

Schwenzfeier, L., Akoua, J-J., Bianchina, M., Buseyne, S., Limoges, D., and Morel, R. 2009. *Use of compact balanced single room ventilation units with heat recovery in existing dwellings.* Proceedings of the 2009 AIVC Conference, Berlin.

Stabat, P. 2009. *Analysis of building heating and cooling demands in the purpose of assessing the reversibility and heat recovery potentials.* Annexes. IEA-ECBS Annex 48. Heat Pumping and Reversible Air conditioning.
http://www.ecbcs.org/docs/ECBCS_Annex_48_Final_Report_R1_Annexes.pdf

Walloon EPB decree. 2008. *Arrêté du gouvernement wallon déterminant la méthode de calcul et les exigences, les agréments et les sanctions applicables en matière de performance énergétique et de climat intérieur des bâtiments.*

http://www.cstc.be/homepage/download.cfm?dtype=na_energy&doc=EPB_RW_MB20080730.fr.pdf& lang=fr

CHAPTER VI:
CONCLUSIONS AND PERSPECTIVES

The aim of the thesis was to contribute to the scientific and technical knowledge about single room ventilation with heat recovery (SRVHR) units, and more specifically their model-based design and their experimental characterization.

Most part of the thesis focuses on the model development of air-to-air heat exchanger dedicated to SRVHR units. This involves a numerical and experimental analysis in order to assess its performance under various operating conditions. Three specific operating conditions have been particularly investigated: dry, partially wet and frosting conditions. Several heat exchangers have been experimentally tested in order to perform analyses in those different conditions.

The thesis also investigated a new SRVHR unit particularly suitable in the frame of a house retrofitting. The main characteristic of the investigated device is its possible integration into windows ledge. The studied device responds to an actual growing need, given the current energy context. Single room ventilation units with heat recovery present a large range of advantages compared to centralized heat recovery ventilation systems. However, development of such units implies a trade-off between hydraulic (and thus, noise generated by the fans of the unit) and thermal performances. An optimization procedure to determine the best combination of heat exchanger geometry parameters is proposed (design steps of the unit). The overall unit performance has also been determined by means of experimental investigations. The perfect knowledge of the map performance of the unit allows to assess the interest of use of this specific device given a specific climate by means of the heating degree day (HDD) method. An energy performance comparison with other ventilation systems has also been realized.

In the frame of this thesis, many technological aspects roughly related to SRVHR (which is a quite restricted scope) are described but all of the methods, models and approaches proposed in the frame of the thesis comes from (i.e. use of a method initially dedicated to cooling coil to predict sensible as well as latent heat recovery energy, experimental method to determine flow delivered by fan coil unit, etc.) or can be applied to other fields (i.e. application of variable boundary method, frost modeling, use of rapid prototyping method during the development phase of the device, etc.).

Experimental investigations

Test bench dedicated to air-to-air heat exchangers

An experimental apparatus has been developed in order to determine the thermal and hydraulic performance of air-to-air heat exchangers under several operating conditions. The initial idea was to construct a test bench able to test heat exchangers presenting different geometry characteristics and/or different overall volumes. The only modification involves a change of the insulated box containing the tested heat exchanger. The developed apparatus allows for testing the heat exchanger in various operating conditions and to evaluate the performance in several regimes. The test bench has been designed in order to perform long-term tests with stabilized supply conditions. The developed test bench can also be used in order to test other type of heat exchanger, e.g. air-PCM heat exchanger (Dechesne (2014)).

"Rapid prototyped" plates method

In the frame of the design of heat exchanger dedicated to SRVHR, it is important to experimentally check the hydraulic performance of the so-called optimized geometry. This check has to be realized before launching the expensive manufacturing process of the thermoforming mold. In reality, the hydraulic performance highly influences the overall performance as well as the acoustic performance

of the device. A method involving two rapid prototyped plates realized by means of the Selective Laser Sintering method has been imagined. A compressor was used to pulse the air through the rapid prototyped plates and a set of rotameters have been used to measure the flow rate. Thanks to this method, it was also possible to check some potential issues about flow maldistribution along the height of the heat exchanger (determination of a pressure drop map). This method can be used to test a large range of geometries in the frame of the development of a SRVHR heat exchanger. The method can also be applied to test a large range of heat exchanger applications and not only air-to-air heat exchangers (use of a pump instead of compressor for water application, as an example).

Hydraulic performance of constituting components

Single room ventilation with heat recovery is composed of components influencing the hydraulic performance of the device, such as fans, filters, heat exchanger, etc... In the frame of the development steps of such device, it is important to characterize separately each of these components (to choose the best combination of components for a specific unit). A test bench has been constructed to experimentally determine the hydraulic performance of a large range of components: fan, filter, overall unit, etc. It is based on a method initially dedicated to fan coil unit, so called "pressure compensated box". It has been shown that those investigations allow to optimize the position of each element.

Single room ventilation with heat recovery

As explained before, it is possible to determine separately the performance of each component of the unit. By combining all the information/data characterizing each component, it is possible to determine the overall performance of the whole device. However, the performance of each component is determined in specific conditions. As an example, thermal and hydraulic performances of the heat exchanger are determined with well distributed flow rates (use of a damper upstream the heat exchanger). The only way to determine the overall performance of the whole device is to test it in a climatic chamber. The device is inserted in a wall separating two chambers (supposed to respectively represent indoor and outdoor conditions). Pressure compensated box method has also been used in this specific case. The construction of this test bench is really time-consuming. Thus, this method is clearly not suitable in the frame of the design steps of the device but is essential to determine its overall performance, after the design process. However, no significant differences have to be deplored in terms of thermal performance, between single component performance combination and experimental results carried out on the unit in this specific case.

Numerical investigations

Dry conditions

Three heat exchangers presenting different geometries in the central part have been investigated in the frame of this thesis. Each of them has been experimentally tested in order to determine their hydraulic and thermal performances. Thanks to those experimental investigations, it has been possible to compare results predicted by the model developed with empirical correlation (available in the literature) with experimental results. A sensitivity analysis showed that the heat transfer coefficient is the most influential parameters compared to flow rate maldistribution and geometry dimensions (Chapter 2). New correlations have been developed/adapted for all the heat exchangers tested. For the newly designed heat exchanger based on the COP optimization, a new model based on a discretization of the central part has been developed in order to take into account the manufacturing defaults.

As already specified in the introduction section, only a few experimental results on polymer based ventilation heat exchangers have been reported in the scientific literature. In the frame of this thesis, several air-to-air heat exchangers in polystyrene have been tested. These investigations allow for a better understanding of the practical issues associated with such heat exchangers. The main disadvantage of polystyrene heat exchangers concerns their low thermal conductivity. However, this disadvantage is counter-balanced by the high enlargement factor that can be reached with polystyrene compared to traditional plate heat exchanger in metal. Other benefits include their lightness and the low cost related to raw materials.

Partially wet conditions

A two zones heat exchanger model has been developed in order to predict the total, sensible and latent load under condensing operations. This model is based on a variable boundary in order to determine each part (dry and wet) of the heat exchanger and results in a combination of several models initially dedicated to cooling coils.

The model has been first validated on an experimental data set of cooling coil. It has been shown that the developed model better predicts the total heat exchanger for sensible heat ratio (SHR) close to unity compared to others model based on the Braun's hypothesis, which considers simultaneously fully dry and fully wet regimes and considers that the regime to be selected (totally wet or totally dry) is the one leading to the maximal cooling capacity. In a second step, it was shown that the model can be used to predict the performance of the air-to-air heat exchangers. The model was successfully validated on two air-to-air heat exchangers presenting different geometries.

Frosting conditions

A model able to predict the dynamic behavior of air-to-air heat exchangers under frosting conditions has been developed. This latter consists in an improvement of the two zones heat exchanger model by adding a "frosting" zone. First, a frost growth model has been developed and validated by means of experimental data coming from literature. Each part (dry, wet and frosting part) of the heat exchanger is delimited by means of the variable boundary method. The model predicts pretty well the dynamic evolution of heat transfer rates (for both sensible and latent parts) as well as the pressure drop evolution. Some discrepancies between model and experimental results have to be deplored for supply conditions presenting high relative humidity for indoor air, especially in terms of pressure drop evolution. When the wet part is too important, condensation appearing in the wet part could perturb the theoretical frost formation. However, the developed model seems to yield conservative predictions whatever the conditions and allows to compare the different strategies under frosting conditions. All strategies have been compared by comparing two defined criteria:

- a so-called energy performance criterion (ratio between energy recovered by the unit and electrical power supplied to fans over a frosting-defrosting cycle). In order to assess the energy performance criteria, the three zones dynamic model is used to determine the heat transfer rate as well as the pressure drop evolution with a time step of one second,
- a mechanical flow rate unbalancing criteria. This is the ratio between flow rate mechanically supplied and removed from the building. This unbalancing can result from the presence of frost or can result from the application of a strategy (balance adjustment method),

Advantages and drawbacks of each method, especially in terms of implementation are also presented.

Heat exchanger design and COP optimization

An integrating methodology is proposed in order to optimize the geometry of a heat exchanger dedicated to single room ventilation with heat recovery. In this case, two parameters have been defined to characterize the geometry of the heat exchanger. The procedure is based on an optimization of the coefficient of performance (COP), which allows to find the best trade-off between hydraulic and thermal performance of the unit. In order to perform this heat exchanger optimization, fan curves of the unit have to be known as well as the "out of heat exchanger" (also called "rest of the installation") hydraulic characteristics. The optimization process also takes into account some technical, acoustic and economic constraints. Some parametric studies have demonstrated that the geometry parameters values deduced from the optimization procedure are independent on the chosen supply conditions in this specific case (such as flow rate, the hydraulic performance of the "rest of the installation", or the available volume dedicated to heat exchanger). The proposed methodology can obviously be applied to other types of ventilation system with heat recovery, such as centralized ventilation. It only involves modification of supply conditions and constraints.

A heat exchanger presenting an enlargement factor of 400% has been developed, resulting from the COP optimization. To the author's best knowledge, a heat exchanger presenting such a large enlargement factor has never been studied before. It has been demonstrated that the geometry was uncontrolled which leads to asymmetry in terms of cross section area as well as systematic and random defaults.

<u>Evaluation of the interest of use of the device and comparison with different ventilation systems</u>

The interest of use of single room ventilation with heat recovery is dependent on the climate, i.e., the outdoor/indoor temperature difference highly influences the COP of the device. The Heating Degree Day method is widely used in the literature to evaluate the interest of heat recovery ventilation systems. Based on the knowledge of the overall performance of the device (experimentally determined), it is possible to determine the interest of use of the device (ratio between the energy recovered and the energy delivered to the fans of the unit for a year) for a specific climate (only defined by the HDD). This method also allows to compare the developed device with other ventilation systems (A, C and D) by normalizing (per m³/h) the annual performance of the device. It is demonstrated that the developed device shows good energy performance in comparison with performances of systems D measured in situ.

Recommendations concerning the new investigated SRVHR system

<u>Conclusions about investigated features</u>

The aim of this section is to list the potential ameliorations that could be realized on the developed device, regarding experimental and numerical investigations.

Current transformer losses are not negligible compared to the electrical power delivered to the fans, (especially for the low rotational speeds). Those losses are entirely dependent on the used current transformers. Many efforts have been deployed to optimize the heat exchanger geometry but it has been demonstrated that the impact of the current converter has a huge impact on the overall energy performance of the unit (for some flow rate, the COP could be almost doubled if neglecting the current converter losses).

Experimental investigations carried out on the final heat exchanger, shows an uncontrolled geometry in the central part. This involves discrepancies between theoretical model and experimental results. Two kinds of defaults can be defined: random and systematic defaults. Systematic defaults involve a

different cross section area for indoor and fresh air side. Thus, hydraulic performances are not symmetric. However, it has been shown that an "ideal" rectangular controlled geometry could only raise the effectiveness of the heat exchanger (and thus the COP) of 20%. However, this potential improvement is less important compared to the impact of the current converter losses on the COP. Those losses could divide the COP by two depending on the delivered flow rates (i.e.15 m³/h).

It has been showed that the fresh air side fan is not well positioned. This induces a rough air change direction at the exhaust of the fan. It generates a less efficient energy conversion than for the indoor air side fan. A new mold for the active part of the unit could correct that dispositioning. The rest of the installation (supply/exhaust and filters hydraulic performance) account for a large part of the pressure drop (more than half of the total pressure drop) for most of the investigated flow rates (Chapter 5). The main weakness of the unit is the generated noise and more particularly for flow rate upon 25m³/h. For this reason, the first effort which has to be deployed concerns the improvement of the hydraulic performance of each component of the unit.

Conclusions about uninvestigated features

Some features of the device have not been investigated in the frame of the thesis but some effects could be particularly interesting to investigate.

In the specific case of this unit, indoor air exhausting from the unit is rejected along the windows. The air rejected from the unit is warmer than the outside air, since the effectiveness of the device is lower than unity. From this fact, the rejected air tends to increase the windows and frame surface temperature and hence, the thermal effectiveness of the windows. This effect has been qualitatively observed but not studied in details for now but some investigations on a typical frame window could quantify this effect. Condensation and frost formation on the window could also be interesting to investigate.

It could also be relevant to adjust the dimensions of the heat recovery exchanger and thus the active parts to the windows dimensions. Thermal, hydraulic, and hence acoustic performances of the device would vary with the volume dedicated to the unit.

The Belgian standard about the ventilation (NBN D 50-001) makes mention of the ideal ventilation flow rates for each room of the house by specifying that these flow rates can only be met by using inlet and exhaust mechanical ventilation for each room. The standard also indicates that the presence of an inlet and exhaust mechanical ventilation for each room is the most complete case and is rarely met in practice. Given the rarity and the low commonness of such system at the time when the standard was written, the standard proposes for the system D a supply or an exhaust flow rate for life room and bedroom at least equal as the "ideal" ventilation flow rate (exhaust and supply mechanical ventilation for each room). Scenarii proposed by the standard are clearly in favor of a "traditional" system D: the total (supply plus exhaust) ventilation flow rate through the whole house can be two times more important for single room ventilation system than for traditional centralized system D ventilation system. In this case, the standard disadvantages the placement of single room ventilation (whose the main weakness is the generated noise) compared to centralized heat recovery ventilation.

Perspectives

The investigated device can also be adapted for tertiary building applications. It was decided to develop SRVHR unit for tertiary applications in the frame of the Bricker project (2014) aiming at retrofitting a building in Liège, Belgium. The same methodology has been used to experimentally

determine the performance map of the new unit (during the development steps and for the final characterization of the unit). Those new units are currently still under development.

The device seems particularly suitable for demand control ventilation (DCV). DCV could be practically realized by using different sensors (presence, CO_2, humidity). An investigation concerning control strategies could be realized by coupling the deterministic model of the device (performance map) with a whole building simulation model.

Coupling building and SRVHR unit model could also be used for the assessment of the saving potential resulting from the use of the device given a specific building defined by a set of parameters (defined by external wall area, U value, air tightness, etc.). Theoretical investigations about indoor air quality could also be carried out by means of this method.

References

Bricker project. 2014. http://www.bricker-project.com/

Dechesne, B., Gendebien, S., Martens, J., Gilbert, J., Lemort, V., 2014. *Designing and testing an air-PCM heat exchanger for building ventilation application coupled to energy storage.* 2014 Purdue Conferences Proceedings. http://orbi.ulg.ac.be/handle/2268/170033

NBN D50-001. *Dispositifs de ventilation dans les bâtiments d'habitation.* Institut belge de normalisation (IBN). 1991.